

SYNTHESIS AND COMPUTATIONAL METHODS FOR THE DESIGN OF EFFICIENT DISTILLATION SYSTEMS

Nikola Felbab

A thesis submitted to the Faculty of Engineering and the Built Environment,
University of the Witwatersrand, Johannesburg, in fulfilment of the require-
ments for the degree of Doctor of Philosophy.

Johannesburg, 2013



UNIVERSITY OF THE WITWATERSRAND

Faculty of Engineering and the Built Environment
School of Chemical & Metallurgical Engineering

SYNTHESIS AND COMPUTATIONAL METHODS
FOR THE DESIGN OF EFFICIENT
DISTILLATION SYSTEMS

Nikola Felbab

Supervisors

Prof. David Glasser

Prof. Diane Hildebrandt

Research partially funded by



The financial assistance of the National Research Foundation (NRF) towards this research is hereby acknowledged. Opinions expressed, and conclusions arrived at, are those of the author, and are not necessarily to be attributed to the NRF.

Abstract

The work in this thesis has been developed to facilitate understanding of limitations in distillation, as well as to aid the design of efficient distillation systems, by introducing useful methods, techniques, tools, and novel process configurations.

It is well-established that distillation is a very inefficient process (Mix et al., 1978; Humphrey, 1995; Ognisty, 1995), yet it is by far the most industrially widespread separation technique, accounting for some 90–95% of product recovery worldwide (Humphrey and Siebert, 1992; Humphrey, 1995).

There are substantial environmental and financial incentives to reduce the energy requirements of distillation systems. To this end, several different approaches have been proposed over the last few decades, including diabatic columns, complex columns, heat-pump assisted distillation, and heat-integrated distillation columns.

These solutions have not yet been widely implemented, partly owing to some practical hurdles, but also largely due to the difficulty of their design. The work in this thesis addresses several of these problems.

The major approach used in this work is to consider the process limitations in distillation systems imposed by entropy generation, pinch points, and the relationships of these phenomena to minimum reflux.

Two methods are presented for locating pinch points in non-ideal distillation systems, with one focusing on finding all pinch points in a given search space, and the other on efficiently constructing pinch point curves. The concept of finite-reflux distillation boundaries is also introduced. This, together with pinch points and pinch point curves, can be used for effective design of distillation systems using the column profile map method (Holland et al., 2004a; Tapp et al., 2004).

Heat-pump-assisted distillation is also considered, with particular emphasis on vapour recompression. A tool is derived for the rapid determination of whether or not vapour recompression is favourable to conventional dis-

tillation, and whether or not it can be implemented practically. The tool is consolidated as a single chart, and requires only the product temperatures.

Novel vapour recompression configurations are also devised, circumventing some of the major limitations of standard vapour recompression. These new configurations are applicable to light liquid feeds and heavy vapour feeds, and typically result in energy savings in the region of 50–80% compared to conventional distillation.

Declaration

I declare that this thesis is my own unaided work. It is being submitted for the degree of Doctor of Philosophy to the University of the Witwatersrand, Johannesburg. It has not been submitted before for any degree or examination to any other university.

Nikola Felbab

December 2013

Acknowledgements

This thesis is the result of thousands of hours of work, frustration, elation, and many a sleepless night, over the course of four and a half years. It has been my great honour to be associated with a number of wonderful people during this period, all of whom have contributed to the production of this thesis in one way or another.

First, my supervisors, Prof. Diane Hildebrandt and Prof. David Glasser, have my sincere thanks. Their zest for research has been inspirational, and it has been a privilege for me to be able to do my PhD with them. I thank them for having enough trust in me to allow me take my research in any direction that I wished. I value the encouragement and support they gave me throughout my postgraduate studies; I hope I have done them proud with this thesis.

I thank the Centre of Material and Process Synthesis (COMPS) for financial support during the first 18 months of my PhD studies, as well as the Department of Science and Technology, and the National Research Foundation for awarding me the Innovation Scholarship during the first half of 2010.

I am also grateful to Simon Holland and Brendon Hausberger for their encouragement to extend my postgraduate studies to PhD level. I thank them for being such supportive and accommodating employers, for allowing me time off work when I needed it, and for giving me the opportunity to financially support myself and gain practical engineering experience throughout this period.

I would like to extend my gratitude to the late Prof. Donald Williams, as well as to my high school science teacher, Mrs Nancy Fisher, both of whom encouraged and inspired my interest in chemical engineering and without whom I would never have chosen this career path.

For their part in keeping me sane, I must thank a number of my friends: first and foremost, Hein Kok for being a tremendous, patient, and understanding friend, and for all the camaraderie and great times over the last eight years; Shaun Grose for being a fantastic friend and doing his utmost to get my mind off of the work; Ronald Abbas for his help in getting me off the ground

when I first started research in the distillation group; Craig Griffiths for the great debates and programming-related discussions; and David Ming, Graham Bathgate, and Michelle Low for their friendship.

I cannot thank enough my loving and beloved parents, Ljubica and Dragan, for so many years of support and effort they selflessly invested in me to get me to where I am today. I certainly could not have done this without the amazing foundations and constant encouragement they gave me. Хвала вам за све, мили родитељи!

Lastly, and most importantly, I thank my dearest Cathleen, for her love, support, seemingly infinite patience, unwavering encouragement, and for the phenomenal times we've had over the last six years; my life would have been so much less rewarding and vibrant without her. She believed in me more than I did in myself at times, which was sometimes the only thing that kept me going. She also, extremely generously, undertook the onerous task of reading every word in this thesis, which I appreciate hugely.

Contents

Abstract	i
Declaration	iii
Acknowledgements	iv
List of Figures	x
List of Tables	xv
Nomenclature	xvi
1 Introduction	1
1.1 Background and motivation	1
1.2 Contribution of the thesis	3
1.3 Thesis outline	3
2 Entropy, Pinch Points, and Minimum Reflux	6
2.1 Introduction	7
2.2 Entropy equations	9
2.3 Important properties of the entropy equations	12
2.3.1 Path	12
2.3.2 Stationary points	12
2.4 Minimum reflux and entropy	13
2.4.1 Effect of r_{Δ} on $\delta\mathcal{S}$ in rectifying sections	14
2.4.2 Effect of r_{Δ} on $\delta\mathcal{S}$ in stripping sections	17
2.4.3 Non-sharp splits	18
2.4.4 Tangent pinches	19
2.5 New minimum reflux equation for binary separations	20
2.5.1 Examples and validation	22
2.6 Conclusion	23

3	Pinch Points in Non-Ideal Distillation Systems and Finite-Reflux Distillation Boundaries	25
3.1	Introduction	26
3.1.1	Residue curve maps	26
3.1.2	Column profile maps	27
3.1.3	Pinch point loci	30
3.1.4	The aim of this work	31
3.2	Literature survey	32
3.2.1	Pinch points	32
3.2.2	Pinch point loci	34
3.2.3	Differences between previous work and this work	35
3.3	Locating pinch points	35
3.3.1	Possible improvements	41
3.4	Pinch point loci	42
3.5	Finite-reflux distillation boundaries	45
3.6	Unifying example: distributed-feed column	49
3.7	Conclusion	56
4	An Efficient Method of Constructing Pinch Point Curves and Locating Azeotropes	59
4.1	Introduction	60
4.1.1	Difference point equation	60
4.1.2	Pinch point curves	63
4.1.3	This work	66
4.2	Literature review	67
4.2.1	Column profile and residue curve methods	67
4.2.2	Graphical methods	68
4.2.3	Non-linear root-finding methods	69
4.2.4	Differential equation methods	71
4.3	Ordinary differential equation	72
4.3.1	Brief derivation	73
4.3.2	Independent variable transform	76
4.3.3	Solution	78
4.3.4	Automatic azeotrope discovery	80
4.4	Comparison with other methods	82
4.4.1	Comparison with Poellmann and Blass's method	83
4.4.2	Comparison with other reflux-parameterised methods	86
4.4.3	Comparison with methods using PPCs implicitly	89

4.5	Examples	92
4.5.1	Software demonstration	96
4.6	Conclusion	96
5	Synthesis of Standard Vapour Recompression Distillation	99
5.1	Introduction	100
5.2	Simplifying assumptions	103
5.3	Thermodynamic analysis: conventional distillation columns	105
5.4	Thermodynamic analysis: standard vapour recompression scheme	109
5.5	Comparison of work inputs in conventional and SVRC distillation	114
5.6	Thermodynamic and practical synthesis targets	116
5.6.1	Compression ratios	117
5.6.2	Need for superheating of compressor inlet	118
5.6.3	Interpretation of Figure 5.10	118
5.7	Rigorous simulation and validation	120
5.7.1	Design methodology	121
	Example 1: 1-butene– <i>n</i> -butane	122
	Example 2: hydrogen cyanide–acrylonitrile	123
	Example 3: 1-propanol– <i>n</i> -octane	124
	Example 4: multicomponent system	125
5.8	Conclusion	126
6	Novel Feed–Product Vapour Recompression Configurations	129
6.1	Introduction	130
6.2	Developmental background	131
6.2.1	Light feed	134
6.2.2	Heavy feed	135
6.3	Novel configurations	136
6.3.1	Configuration for light feeds: FDVRC	136
6.3.2	Configuration for heavy feeds: FBVRC	138
6.4	Comparison of various configurations	139
6.4.1	Liquid feeds	141
6.4.2	Vapour feeds	143
6.5	Rigorous simulation and validation	145
6.5.1	Design methodology	146
	Example 1: light 1-heptanal–1-decanal liquid feed	147

Example 2: heavy benzene–toluene vapour feed	148
Example 3: light water–MEA–DEG liquid feed	149
Example 4: heavy <i>n</i> -pentane– <i>n</i> -hexane– <i>n</i> -heptane vapour feed	150
6.6 Conclusion	150
7 Shortcut Methods for High-Level Distillation Analysis	152
7.1 Introduction	153
7.2 Compression of saturated vapours	154
7.2.1 Isentropic and non-isentropic compression	155
7.2.2 Superheating before compression	157
7.2.3 Examples	158
7.3 Estimation of ideal binary equilibrium temperatures	159
7.3.1 Theoretical background	160
7.3.2 Standard approach	162
7.3.3 Derivation of the base equations	162
7.3.4 Correction to the base equations	165
7.3.5 Deviation from rigorous ideal VLE calculations	169
7.3.6 Extension to non-atmospheric pressures	170
7.4 Conclusion	172
8 Conclusions	174
8.1 Overview	174
8.2 Recommendations for future research	177
References	179
Appendix A	197
Appendix B	206
Appendix C	209
Appendix D	216
Appendix E	222

List of Figures

Figure

- | | | |
|------|---|----|
| 2.1 | Examples of pinch points that occur at r_{\min} for (a) a binary separation, and (b) a direct split of a ternary mixture. | 8 |
| 2.2 | Simple diagram of a generalised column section, showing flow and composition variables. | 10 |
| 2.3 | Values of $\delta\underline{S}$ as a function of the light liquid mole fraction in a rectifying section of the benzene–toluene system. | 14 |
| 2.4 | Values of $\delta\underline{S}$ as a function of the light liquid mole fraction in the benzene–toluene system, for a range of r_{Δ} values. | 16 |
| 2.5 | Comparison of r_{\min} from Underwood’s method, and coordinates corresponding to maximum $\delta\underline{S}$ in Figure 2.4. | 17 |
| 2.6 | Values of $\delta\underline{S}$ as a function of the light liquid mole fraction in a stripping section of the benzene–toluene system. | 18 |
| 2.7 | Values of $\delta\underline{S}$ as a function of the light liquid mole fraction in the benzene–toluene system, for a range of r_{Δ} values. | 18 |
| 2.8 | $\delta\underline{S}$ as a function of light mole fraction in a rectifying section, for a range of r_{Δ} at several X_{Δ} values. | 19 |
| 2.9 | McCabe–Thiele diagrams, and corresponding rectifying $\delta\underline{S}$ curves, for the benzene–ethylenediamine system at (a) feed-pinch reflux, and (b) actual minimum reflux at the tangent pinch. | 21 |
| 2.10 | Minimum reflux for the benzene–toluene system as a function of feed composition, as found by the McCabe–Thiele method, and using Eq. (2.15). | 22 |
| 2.11 | Minimum reflux for the chloroform–methanol system as a function of feed composition, as found by the McCabe–Thiele method, and using Eq. (2.15). | 23 |

2.12	Minimum reflux for the acetone–chloroform system as a function of feed composition, as found by the McCabe–Thiele method, and using Eq. (2.15).	23
3.1	Residue curve map of the acetone–benzene–chloroform system.	27
3.2	Column profile map of the ABC system.	29
3.3	Plot of an RCM and a CPM for a constant-relative-volatility system.	30
3.4	Contour map of $F^{0.25}$ values for the same system as in Fig. 3.2.	37
3.5	Flowchart representing the algorithm.	39
3.6	Plots showing (a) all of the pinch points of the CPM in Figure 3.2 found by the algorithm; (b) the focus blocks used in the algorithm; and (c) all of the points at which F -values are calculated by the algorithm.	40
3.7	(a) RCM of the ACM system; and (b) its pinch point curves.	43
3.8	Example of the constructions required by the algorithm for finding distillation boundaries.	47
3.9	Column profile resulting from a suboptimal choice of starting point z for a distillation boundary of the ABC system.	48
3.10	Demonstration that the algorithm applies to infinite reflux as well to produce traditional distillation boundaries of the ACM system.	48
3.11	Distillation boundaries found by the algorithm for the ABC system at finite reflux.	49
3.12	Distributed-feed column configuration, with pertinent flows and variables shown.	51
3.13	Non-sharp, direct split of a BXT feed in a conventional column (a) at minimum reflux; and (b) below minimum reflux.	52
3.14	Qualitative description of the desired column profile behaviour for column section 2 when it is in rectifying mode.	54
3.15	Plots of (a) PPL showing the movement of CS 2's pinch points with changing $r_{\Delta,2}$ from $r_{\Delta,1}$ to 100; (b) magnification showing intersection of the PPL and the rectifying section profile.	55
3.16	Final construction of the two-feed column, showing the end profiles, and feasible choices for the middle one.	56
4.1	CPM of the acetone–benzene–chloroform system.	62
4.2	PPC of the acetone–benzene–chloroform system.	63

4.3	Difference between this work (the PPC ODE), and the standard column profile ODE.	67
4.4	Pinch point curves of the ABC system. (a) $X_{\Delta} = (0.27, 0.28, 0.45)$; (b) $X_{\Delta} = (0.59, -0.30, 0.71)$.	94
4.5	Pinch point curves of the ACM system. (a) $X_{\Delta} = (0.22, 0.43, 0.35)$; (b) $X_{\Delta} = (0.07, -0.20, 1.13)$.	94
4.6	Pinch point curves of the BHnH system. (a) $X_{\Delta} = (0.50, 0.09, 0.41)$; (b) $X_{\Delta} = (-0.10, 0.46, 0.64)$.	94
4.7	Stereoscopic view of the pinch point curves of the BTmXC system with $X_{\Delta} = (0.23, 0.38, 0.28, 0.11)$.	95
4.8	Stereoscopic view of the pinch point curves of the ACME system with $X_{\Delta} = (0.18, 0.22, 0.30, 0.30)$.	95
4.9	Stereoscopic view of the pinch point curves of the ACMB system with $X_{\Delta} = (0.12, 0.21, 0.58, 0.09)$.	95
5.1	Schematic representations of (a) conventional distillation, (b)–(d) various heat-pump-assisted distillation configurations.	101
5.2	Schematic representation of a conventional distillation column, along with the mass, heat, and work flows in and out of the system, as well as the significant temperatures.	106
5.3	Comparison of minimum theoretical heat input and minimum practical heat input to a conventional distillation column.	108
5.4	Schematic representations of the SVRC configuration, with stream labels.	110
5.5	Qualitative pressure–enthalpy plot showing the vapour recompression process.	110
5.6	Pressure–temperature behaviour of a saturated vapour that (a) superheats on compression, and (b) condenses on compression and requires superheating.	112
5.7	Comparison of minimum theoretical and minimum practical energy inputs to the standard vapour recompression configuration.	113
5.8	Comparison of minimum theoretical and minimum practical work inputs to the conventional and standard vapour recompression configurations.	115
5.9	Plot of regions where vapour recompression is thermodynamically more efficient than conventional distillation as a function of T_C and T_R only.	117

5.10	Plot of regions of thermodynamic vapour recompression favourability, with overlays of minimum compression, and lines of zero compressor inlet superheating.	119
5.11	Flowchart representing the decision-making process with Figure 5.10.	120
5.12	Aspen Plus flowsheet for the rigorous simulation of the conventional distillation column.	121
5.13	Aspen Plus flowsheet for the rigorous simulation of the standard vapour recompression configuration.	121
6.1	Diagram of a conventional distillation column with feed preconditioning.	131
6.2	Surfaces of relative change in entropy generation when preconditioning is used, and relative change in heat input, as functions of feed condition into the system and the column.	134
6.3	Schematic drawing of the novel configuration for light, saturated liquid feeds: FDVRC.	137
6.4	Schematic drawing of the novel configuration for heavy, saturated vapour feeds: FBVRC.	139
6.5	Comparison of the minimum energy requirements, work input, entropy generation, and pressure ratio as a function of composition of the liquid feed, for conventional distillation, SVRC, and FDVRC.	142
6.6	Comparison of the minimum energy requirements, work input, entropy generation, and pressure ratio as a function composition of the saturated vapour feed, for conventional distillation, SVRC, and FBVRC.	144
6.7	Aspen Plus flowsheet for the rigorous simulation of the FDVRC configuration.	146
6.8	Aspen Plus flowsheet for the rigorous simulation of the FBVRC configuration.	146
7.1	Plot of $\ln(P_1/P_0)$ as a function of τ_1 for propylene and benzene.	157
7.2	T - x - y diagram of the benzene-toluene system.	161
7.3	Plot of $\ln(P^{\text{vap}})$ as a function of $1/T$ for a number of components.	163

7.4	Plot of $1/T$ as a function of $\ln(y_1/x_1)$ for a number of binary systems.	164
7.5	Plot of $1/T$ as a function of $\ln(y_1/x_1)$ for a number of binary systems, with T both rigorously calculated and estimated.	166
7.6	Comparison of $\ln(\alpha)$ and optimal (a) $\ln(\alpha_{\text{bubble}})$, and (b) $\ln(\alpha_{\text{dew}})$, for 4 573 binary systems.	167
7.7	T - x - y diagrams for mixtures of a binary systems with a wide range of volatilities, calculated by various methods.	168
7.8	T - x - y diagrams at 250 kPa for mixtures of a binary systems with a range of volatilities, calculated by various methods.	171
A.1	(a) McCabe–Thiele diagram showing rectifying profiles at various reflux ratios; and (b) normalised $\delta\underline{S}$ curves corresponding to the rectifying profiles for the benzene–ethylenediamine system.	203
B.1	The nomenclature required for the derivation of the relationship between $X_{\Delta,2}$ and $r_{\Delta,2}$.	206
B.2	Two envelopes around which mass balances must be performed to deduce the limiting values of $r_{\Delta,2}$.	208
E.1	FDVRC configuration with stream labels for relevant streams.	224

List of Tables

Table

3.1	Compositions and types of the ABC system pinch points at $r_{\Delta} = 6$ and $X_{\Delta} = (0.90, 0.05, 0.05)$.	40
3.2	Compositions of the ACM pinch points as found by the algorithm and their types.	44
4.1	Numerical results of various methods to calculate PPCs in Figure 7 of Krolikowski (2006).	88
4.2	Numerical results of various methods to calculate PPCs in Figure 5 of Wahnschafft and Westerberg (1992).	88
4.3	Numerical results of the original Lucia et al. algorithm and the algorithm modified using the proposed method.	91
5.1	Binary systems and simple constant properties used in high-level calculations.	108
5.2	Relationship of temperature, pressure, and phase in streams in Figure 5.4.	110
6.1	Summary of the results of the rigorous simulation examples.	147
7.1	Summary of limiting values in temperature prediction errors found across the 5 797 mixtures used in the analysis.	169
E.1	Coefficients for pure-component property models for vapour pressure, ideal gas heat capacity, liquid heat capacity, and enthalpy of vaporisation, Eqs (E-1)–(E-3).	223
E.2	Binary interaction parameters for the NRTL activity coefficient model.	224

Nomenclature

Roman letters

a, b, c	binary interaction parameter in NRTL model
B	bottoms flow rate, mol/s
c	generic constant
\hat{C}_p	specific heat capacity, J/mol·K
D	distillate flow rate, mol/s
f	vapour fraction
$f_{c,i}$	see Eq. (4.4) on p. 72
f_b	implicitly defined bubble point function
f_i	see Eq. (3.3) on p. 36
F	feed flow rate, mol/s
$F(x)$	$\sum_{i=1}^{N-1} f_i $, pinch point criterion function
$\mathcal{F}, \mathcal{H}, \mathcal{J}$	generic function
\hat{G}	specific Gibbs free energy, J/mol
\mathcal{G}_b	bubble point criterion function; see Eq. (C-6) on p. 211
\hat{H}	specific enthalpy, J/mol
i, j, k	component or iteration index
\mathbf{I}_N	$N \times N$ identity matrix
\mathbf{J}	Jacobian matrix
L	liquid flow rate, mol/s
n	continuous stage number
N	total number of components in the system
M	generic extensive property
P	pressure, Pa
P_0	ambient or atmospheric pressure, 101 325 Pa
P_i^{vap}	vapour pressure of component i , Pa
Q	heat flow, W
r	L/D , conventional reflux ratio
r_Δ	L/Δ , generalised column section reflux ratio
R	universal gas constant, 8.3144621 J/mol·K
S	V/B , reboil ratio
S_{gen}	rate of entropy generation, W/K
\hat{S}	specific entropy, J/mol·K

T	temperature, K
T_b	boiling point temperature, K
T_c	critical temperature, K
\hat{V}	specific volume, m ³ /mol
V	vapour flow rate, mol/s
w	see Eq. (7.14) on p. 158
W	work, W
W_s	mechanical shaft work, W
x_i	liquid mole fraction of component i
X_Δ	$(VY^T - LX^T)/\Delta$, difference point
y_i	vapour mole fraction of component i in equilibrium with x
Y_i	mole fraction of component i in passing vapour stream adjacent to liquid stream with composition x
z_i	overall mole fraction of component i

Greek letters

α	relative volatility
γ_i	activity coefficient of component i
δ_{ij}	Kronecker delta
δS^n	$S_{\text{liq}} - S_{\text{vap}}$ at the cross-section at stage n
Δ	$V - L$, mol/s
$\Delta \hat{G}_{\text{mix}}$	Gibbs free energy of mixing, J/mol
$\Delta \hat{G}_{\text{vap}}$	Gibbs free energy of vaporisation, J/mol
$\Delta \hat{H}_{\text{mix}}$	enthalpy of mixing, J/mol
$\Delta \hat{H}_{\text{vap}}$	latent heat/enthalpy of vaporisation, J/mol
$\Delta \hat{S}_{\text{mix}}$	entropy of mixing, J/mol·K
$\Delta \hat{S}_{\text{vap}}$	entropy of vaporisation, J/mol·K
ΔT	degrees of superheating, K
ε	tolerance in numerical algorithm
ζ_S	relative change in S_{gen} with preconditioning; see Eq. (6.1)
ζ_Q	relative change in heat input with preconditioning; see Eq. (6.2)
η	isentropic efficiency of compressor
κ_i	y_i/x_i , equilibrium constant
λ	latent heat/enthalpy of vaporisation, J/mol
Π	ratio P_{comp}/P_0
ρ^-	$r_\Delta/(r_\Delta - 1)$

ρ^+	$r_{\Delta}/(r_{\Delta} + 1)$
σ	see Eq. (7.17) on p. 158
τ	$1/T, \text{K}^{-1}$
ν	see Eq. (7.16) on p. 158
φ	root of the Underwood feed equation
ψ	$\ln(y_1/x_1)$
Ψ	see Eq. (A-34) on p. 204
ω	acentric factor

Subscripts and superscripts

bubble	relating to the bubble point
B	relating to the bottoms stream
C	relating to the condenser
col	relating to the column
comp	relating to the compressor or compression process
crit	critical
D	relating to the distillate stream
dew	relating to the dew point
E	excess property
F	relating to the feed stream
heavy	relating to the heavy key component
hex	relating to the heat exchanger
IG	relating to the ideal gas
light	relating to the light key component
liq	relating to the liquid
m	relating to stage m
min	minimum
n	relating to stage n
p	relating to a pinch point
pc	relating to the preconditioner
R	relating to the rectifying section or reboiler, depending on context
S	relating to the stripping section
sh	relating to the superheater
sys	relating to the overall system
tot	total
T	relating to the top of the column section
vap	relating to the vapour

Acronyms

ABC	acetone–benzene–chloroform
ACM	acetone–chloroform–methanol
ACMB	acetone–chloroform–methanol–benzene
ACME	acetone–chloroform–methanol–ethanol
BHnH	benzene–hexafluorobenzene– <i>n</i> -hexane
BTmXC	benzene–toluene– <i>m</i> -xylene–cyclohexane
BXT	benzene– <i>m</i> -xylene–toluene
CMO	constant molar overflow
CPM	column profile map
CRV	constant relative volatility
CS	column section
DEG	diethylene glycol
DPE	difference point equation; see Eq. (3.2) on p. 28
FBVRC	feed–bottoms vapour recompression
FDVRC	feed–distillate vapour recompression
HIDiC	heat-integrated distillation column
MEA	monoethanolamine
NaN	not a number
NRTL	non-random two-liquid (activity coefficient model)
ODE	ordinary differential equation
PECE	predict–evaluate–correct–evaluate (solver strategy)
PB	Poellmann–Blass
PP	pinch point
PPC	pinch point curve
PPL	pinch point locus
RC	residue curve
RBM	rectification body method
RCM	residue curve map
RK	Redlich–Kwong (equation of state)
SVRC	standard vapour recompression
THE	Trouton–Hildebrand–Everett
VLE	vapour–liquid equilibrium
VRC	vapour recompression

Chapter 1

Introduction

This thesis deals with a number of related topics in continuous distillation, with particular emphasis on the development of tools for the design of more effective distillation systems, and on the synthesis of new distillation arrangements, all with the aim of reducing energy and work requirements in distillation processes. The thesis is structured as six working chapters, each of which is in the form of a journal article, and is largely self-contained; the chapters can thus be read independently of one another. Although each chapter is in the form of an article, they all share common nomenclature and reference sections to avoid repetition.

In this introduction, the fundamental purpose of the work is discussed, its contribution to scientific knowledge is summarised, and a brief overview of each of the chapters that comprises the main portion of the thesis is given.

1.1 Background and motivation

Distillation is the most widely used separation technique in the process industries, accounting for approximately 90–95% of all separations (Humphrey and Siebert, 1992; Humphrey, 1995), with approximately 40 000 distillation columns in the United States alone (Humphrey and Siebert, 1992). It is also one of the most energy-intensive processes. A number of studies have provided estimates that help to contextualise the scale of energy usage in distillation processes: they account for approximately 40% of the total energy usage on chemical plants in Japan (Ohe, 2007) and in the US (Shinskey, 1977); about 10% of US industrial energy consumption (Humphrey and Siebert, 1992); and 3% of all energy used in the US (Mix et al., 1978; Humphrey, 1995; Ognisty, 1995). Mix et al. (1978) estimated that even a 10% reduction in distillation energy usage would result in savings of 100 000 bbl/d of crude

oil; since industrial production has grown significantly since that report was published in 1978, these savings would undoubtedly be even higher now.

There is clearly a strong incentive, both financially and environmentally, to reduce the energy requirements of distillation-based separations.

In order to achieve this goal, new plants, and particularly the distillation sections thereof, have to be designed more efficiently from the early design phase. Many solutions have been proposed over the last few decades, including heat-pump-assisted distillation (Null, 1976; Mészáros and Meili, 1994; Fonyó and Benkő, 1998), diabatic columns (Fonyó, 1974; Le Goff et al., 1996), complex columns (Rév et al., 2001; Hernández-Gaona et al., 2005; Agrawal, 2003; Caballero and Grossmann, 2003; Halvorsen and Skogestad, 2004; Holland et al., 2010; Caballero and Grossmann, 2013; Shenvi et al., 2013), and heat-integrated distillation columns (HIDiCs) (Glenchur and Govind, 1987; Nakaiwa et al., 2000; Olujić et al., 2003; Huang et al., 2006, 2008; Mane and Jana, 2010; Chen et al., 2010; Suphanit, 2011).

One particularly attractive solution is complex columns, which have both mass and heat integration for the separation of multicomponent mixtures. For this purpose, Tapp et al. (2004) and Holland et al. (2004a) developed the column profile map (CPM) method, which allows for the graphical design and synthesis of complex columns; this has previously been applied to the Petlyuk (Holland et al., 2010) and Kaibel (Abbas, 2011) columns. A particularly powerful feature of the CPM method is the ‘transform triangle’ (Holland et al., 2004b), which has unfortunately been applicable only to constant relative volatility systems until now. It is necessary to extend this to non-ideal systems in order to access the full potential of the CPM method to design realistic systems. This requires a fast way of finding all pinch points and pinch point curves, as well as a non-ideal analogue of transform triangles.

While they are energetically and economically attractive, diabatic columns, complex systems, and HIDiCs are held back from industrial implementation by practical hurdles. A simpler solution is heat-pump-assisted distillation. The two main disadvantages of heat-pump-assisted distillation are, first, its applicability only to close-boiling mixtures (which is a small subset of all separations), and second, the fact that heat-pump-assisted models do not generally come standard with simulation packages. Significant time and effort are therefore required to model them, and it is difficult to determine ahead of time if that effort is likely to be worthwhile.

The work in this thesis addresses many of the above problems.

1.2 Contribution of the thesis

The majority of the work in this thesis has been published in four international, peer-reviewed journals: Computers & Chemical Engineering, Industrial & Engineering Chemistry Research, Applied Thermal Engineering, and AIChE Journal. Details of these publications are given in § 1.3.

The work in this thesis (1) presents new insights into the relationship between entropy generation, pinch points, and minimum reflux; (2) provides some crucial numerical pinch-point tools to aid the design of efficient distillation columns; (3) presents a synthesis tool for assessing the thermodynamic favourability and practical feasibility of implementing standard vapour recompression entirely graphically (with no calculations whatsoever); (4) introduces two novel vapour recompression configurations for energy savings in systems where standard vapour recompression cannot be applied for practical reasons; and (5) derives shortcut methods which have proved to be useful for rapid, high-level analysis of distillation systems.

1.3 Thesis outline

Chapter 2 primarily serves as a backdrop for the rest of the thesis, as it shows the relationships between various key concepts that are developed further in the other chapters; namely, pinch points, entropy generation, and minimum reflux. A new δS function is defined for the analysis of entropy generation in a generalised column section, and a mathematical proof is given showing that the stationary points of this function correspond to pinch points. Numerical experiments are performed to verify that this is indeed the case, after which this characteristic is exploited to derive a novel minimum reflux equation for zeotropic and azeotropic binary separations, thereby demonstrating the power and usefulness of entropy generation analysis. It is especially noteworthy that the pinch points are found without VLE calculations.

Chapter 3 was published as: Felbab, N., Hildebrandt, D., Glasser, D., 2011. A new method of locating all pinch points in nonideal distillation systems, and its application to pinch point loci and distillation boundaries. *Comp. Chem. Eng.* 35 (6), 1072–1087.

This chapter presents an algorithm which can automatically find all pinch points in non-ideal distillation systems, and which can be extended to plotting pinch point curves (PPCs). This chapter also introduces a way of constructing

‘finite reflux distillation boundaries’, which are a non-ideal analogue of the ‘transform triangles’ used in the CPM method (Tapp et al., 2004; Holland et al., 2004a), allowing that feature of the CPM method to be extended beyond constant relative volatility systems. Using these three tools in conjunction with the CPM method, graphical distillation synthesis of non-ideal systems and ‘smarter’ optimisation are possible. An example of a distributed-feed column using these techniques is given. While the pinch point algorithm in Chapter 3 is effective, it is not the most efficient method presented in this thesis.

Chapter 4 was published as: Felbab, N., 2012. An efficient method of constructing pinch point curves and locating azeotropes in nonideal distillation systems. *Ind. Eng. Chem. Res.* 51 (20), 7035–7055.

In this chapter, a very efficient method is presented for the construction of PPCs. This method has the additional benefit of being able to locate azeotropes in addition to PPCs, all in a fraction of a second, thereby drastically improving on the speed of some of the work presented in Chapter 3. Even disregarding its efficiency advantage, this method is an improvement over others in that it can be implemented using tools that are readily available in all standard mathematical software packages, since it is simply an ODE-based formulation of the continuation problem; the same is not true of other PPC methods, which require specialised solvers. The proposed method is also generalised, such that it is applicable to all column sections, including those in complex configurations.

Chapter 5 was published as: Felbab, N., Patel, B., El-Halwagi, M.M., Hildebrandt, D., Glasser, D., 2013. Vapor recompression for efficient distillation. 1. A new synthesis perspective on standard configurations. *AIChE J.* 59 (8), 2977–2992.

It presents an entirely graphical method—that is, one requiring no calculations at all—to assess whether or not the standard vapour recompression (SVRC) configuration is thermodynamically favourable to conventional distillation, and if it can be implemented practically. The entire tool is presented as a single graph, and only requires the distillate and bottoms temperatures. If the ideal gas heat capacity of the overhead vapour is known, this tool can additionally estimate whether or not compressor inlet superheating is required. This approach allows for first-pass estimates to be used to discard unfavourable options immediately if there is no possible benefit to using SVRC, without the need for rigorous simulation, thereby saving considerable time and effort. Bilal Patel was responsible for the basic thermodynamic approach used

in this chapter; the rest of the work, including the thermodynamic analyses at the various levels of detail, the practical limitations, explanations of the observed behaviour, the rigorous simulation examples and validation, and the writing, are my own.

Building on the relative strengths and weaknesses of standard vapour recompression identified in Chapter 5, **Chapter 6** develops two novel feed-product vapour recompression configurations for situations where SVRC is not feasible, thereby greatly extending the range of systems to which vapour recompression can be applied. While the proposed configurations do have limitations (one configuration is designed for light liquid feeds, while the other is used for heavy vapour feeds), when they can be implemented, they invariably result in a significant reduction in energy requirements in relation to conventional distillation columns, as verified by detailed calculations and rigorous simulation.

Chapter 7 presents two useful shortcut methods for rapid, high-level analysis of distillation systems. The first of these methods is a very simple criterion to determine whether or not saturated vapours condense on compression. Should they be found to condense, this work also provides a way of making a simple estimate of the minimum required inlet superheating to avoid condensation in the compressor. This part of the chapter was published as: Felbab, N., 2013. Condensation of saturated vapours on compression and estimation of minimum suction superheating. *Appl. Therm. Eng.* 52 (2), 527–530.

The other method presented is a simple, non-iterative method of estimating the bubble- and dew-point temperatures of ideal binary mixtures, using only the pure-component boiling points, and optionally the constant relative volatility, if it is known. This approach can also be used for non-atmospheric system pressures.

Both of these methods have proven to be useful for quick calculations.

Chapter 8 gives a summary of the overall conclusions of the thesis.

Chapter 2

Entropy, Pinch Points, and Minimum Reflux

Abstract

Entropy generation, pinch points, and minimum reflux all denote limits to real operation in distillation columns. While the latter two are often considered together, neither has been investigated thoroughly in conjunction with entropy generation. This chapter serves to unify all three of these concepts by showing that all three are highly related, and not independent. This is demonstrated in two ways: first, a proof is derived showing that pinch points correspond to local minima or maxima of the entropy functions presented in this chapter; second, a novel equation is derived to determine minimum reflux in binary separations using solely entropy analysis. This chapter provides a backdrop for the remainder of this thesis, which is concerned overarchingly with pinch points and entropy generation analysis, specifically with the aim of providing tools for the design of efficient distillation systems.

2.1 Introduction

This chapter deals with three phenomena that are encountered in distillation, and thermodynamics in general: entropy generation, pinch points, and minimum reflux.

Entropy, unlike mass and energy, is a thermodynamic quantity that is not conserved: all real processes generate entropy to some extent. The second law of thermodynamics states that entropy generation must always be greater than or equal to zero. A theoretically perfect process would be reversible, i.e. it would generate no entropy; entropy consumption (negative entropy generation) is impossible, as it violates the second law. The practical implication of this is that all real processes waste a portion of the work and energy that is added to them, while reversible processes do not. As such, reversibility denotes the limit of the practical operation of any process, and a target for which all designs should strive.

More specific to distillation are the concepts of pinch points and minimum reflux. A pinch point occurs in a column when an increase in the number of stages does not lead to a change in the compositions, which mathematically amounts to the following in continuous/packed columns:

$$\frac{dx_i}{dn} = 0 \quad (2.1)$$

or in tray/plate columns:

$$x_i^{n+1} = x_i^n \quad (2.2)$$

where the superscripts ' n ' and ' $n + 1$ ' indicate stage number. If a pinch point is encountered in a distillation column, the separation cannot progress beyond that point regardless of how many stages are added, and it may become impossible to reach the required product purity specification.

Related to pinch points is the concept of minimum reflux. Lower reflux ratio is desirable because it correlates with lower energy requirements; however, a minimum reflux exists, below which operation of the column is impossible for the required product specification. In the minimum reflux state, at least one column section encounters a pinch. Moreover, a column at minimum reflux requires an infinite number of stages, and is thus clearly not practically viable. Figure 2.1*a* shows this pinch at minimum reflux for a binary separation in the form of a McCabe–Thiele plot, while Figure 2.1*b* presents the liquid column profiles for a ternary split.

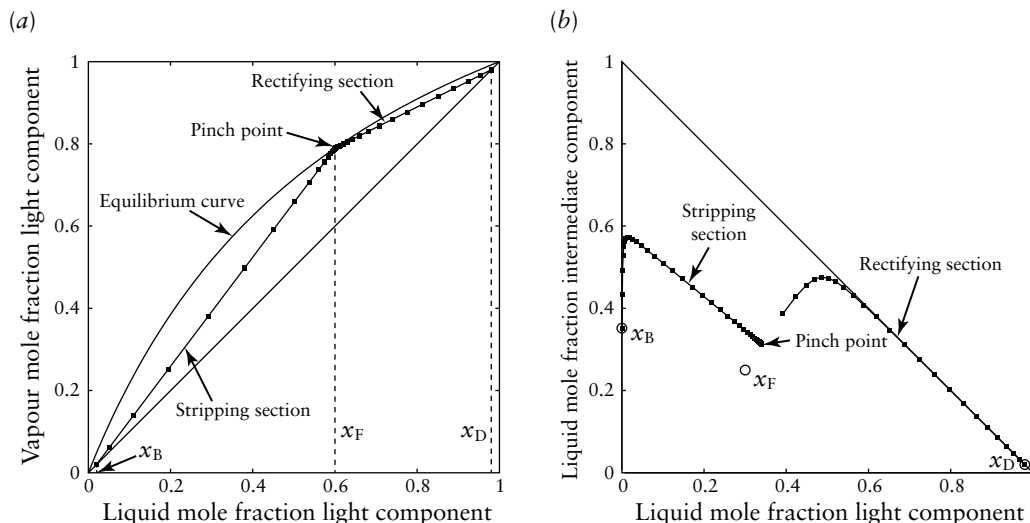


Figure 2.1 Examples of pinch points that occur at minimum reflux for (a) a binary separation, and (b) a direct split of a ternary mixture.

As such, entropy generation, pinch points, and minimum reflux all represent limits of operation.

Entropy generation has thus far been considered by a number of researchers, either in that form directly, or in the variations of exergy, availability, or lost work. Often, entropy generation is set to zero to provide a target for distillation using the reversible distillation model (e.g. Petlyuk et al., 1965; Fonyó, 1974; Koehler et al., 1991; Dhole and Linnhoff, 1993; Poellmann and Blass, 1994; Aguirre and Espinosa, 1996; Ayotte-Sauvé and Sorin, 2010).

The purposes of these studies were typically goal-driven in the sense that they were used to devise complex distillation arrangements (Petlyuk et al., 1965), minimise energy requirements using reversibility (Koehler et al., 1991; Ayotte-Sauvé and Sorin, 2010), to identify opportunities for feed preconditioning, and intermediate reboilers and condensers (Dhole and Linnhoff, 1993; Aguirre et al., 1997; Bandyopadhyay, 2002; Bandyopadhyay et al., 2003; Bandyopadhyay, 2007; Soares Pinto et al., 2011). The minimisation of entropy generation for the design of diabatic columns has also been studied (Sauar et al., 1997; Rivero, 2001; de Koeijer et al., 2002, 2004). Other work has addressed the problem on a microscopic scale, by considering entropy generation at the bubble level (Ratkje et al., 1995; Ray and Sengupta, 1996).

This chapter explores the relationship between the concepts of entropy generation, pinch points, and minimum reflux, with the goal of gaining more insight into the combined roles these phenomena play in limiting distillation. The only directly comparable work can be found in Bausa et al. (1998), in which those authors reach the same conclusion as in § 2.3 regarding station-

ary points and stability. Nevertheless, the approach taken in this chapter is different from theirs in that it is both more generalised, and delves into the topic in greater depth.

The main purpose of this chapter is to provide a backdrop for the remainder of the thesis by tying together the concepts of pinch points, reversibility, and entropy generation in distillation.

2.2 Entropy equations

In this chapter, notation from the column profile map (CPM) method will be used, as it applies to generalised column sections,¹ and does not limit interpretation to conventional rectifying and stripping sections. Details concerning the CPM method can be found in Chapters 3 and 4, and, more completely, elsewhere (Tapp et al., 2003; Holland et al., 2004a,b; Tapp et al., 2004; Holland, 2005).

A benefit of the column profile map method is that it considers all column sections (CSs), including those in complex arrangements, in exactly the same way. Several variables are defined: $\Delta = V - L$, which is the net molar flux in a CS, $r_\Delta = L/\Delta$, which is the reflux ratio of the CS, and $X_\Delta = (VY^T - Lx^T)/\Delta$, which is the difference point of the column section. The lowercase variable x is simply the liquid mole fraction vector. Uppercase Y is used to represent the mole fraction of the passing vapour stream (the vapour stream that is adjacent to the liquid stream with composition x), while lowercase y is used to indicate a stream that is in equilibrium with x .² If the common constant molar overflow (CMO) assumption is used, then X_Δ is constant throughout the CS, and can relate the compositions of the passing streams at any point; in other words, it is also true that $X_\Delta = (VY^n - Lx^n)/\Delta$ at a cross-section at an arbitrary stage n . Moreover, in column sections terminated by a reboiler or a condenser, the interpretations of Δ , r_Δ , and X_Δ are directly related to traditionally used variables: for example, it can be shown easily that in a conventional rectifying section, $\Delta = D$, $r_\Delta = r = L/D$, and $X_\Delta = x_D$, and in a conventional stripping section, $\Delta = -B$, $r_\Delta = -S - 1$, and $X_\Delta = x_B$.

1 A column section is defined as a part of the column in which there is no overall addition or removal of mass or energy.

2 Using conventional notation in staged columns, $Y^n = y^{n+1}$. Columns modelled in this chapter are continuous/packed, which means that conventional notation does not suffice, since the $(n + 1)^{\text{th}}$ stage is not related to the n^{th} stage directly by equilibrium.

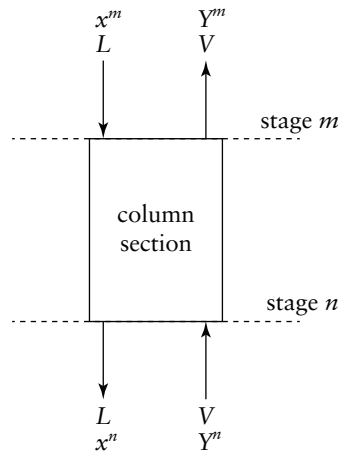


Figure 2.2
Simple diagram of a generalised column section, showing flow and composition variables.

As the thermodynamic basis, pure liquids at 298.15 K and 101 325 Pa are assigned zero enthalpy and entropy. In this chapter, the common CMO assumption is made, which stipulates that: (1) sensible heat effects are negligible in comparison with latent heat effects; (2) heat of mixing is negligible; (3) the column is adiabatic; and (4) the latent heat of each of the components is the same.

Consider the generalised column section shown in Figure 2.2, which extends from an arbitrary stage m down to stage n , with a known Δ , r_Δ , and X_Δ .

A mass balance on component i around this CS gives the following:³

$$\underbrace{Lx_i^m + VY_i^n}_{\text{Mole flow of } i \text{ in}} = \underbrace{Lx_i^n + VY_i^m}_{\text{Mole flow of } i \text{ out}}$$

$$VY_i^n - Lx_i^m = VY_i^m - Lx_i^n$$

$$\Delta X_{\Delta,i} = VY_i^n - Lx_i^n$$

$$Y_i^n = \frac{\Delta}{V} X_{\Delta,i} + \frac{L}{V} x_i^n$$

$$Y_i^n = \left(\frac{1}{1 + r_\Delta} \right) X_{\Delta,i} + \left(\frac{r_\Delta}{1 + r_\Delta} \right) x_i^n$$

$$Y_i^n = \frac{X_{\Delta,i} + r_\Delta x_i^n}{1 + r_\Delta} \quad (2.3)$$

Equation (2.3) describes the operating line of the column section, and

3 The superscripts ' m ' and ' n ' indicate stage number, and not exponentiation.

reduces to the standard operating line equations for conventional columns when the variables are transformed to their traditional counterparts.

An entropy analysis over the column section gives the following:

$$\underbrace{S_{\text{liq}}^m + S_{\text{vap}}^n}_{\text{Entropy flow in}} + \underbrace{S_{\text{gen}}}_{\text{Entropy generated}} = \underbrace{S_{\text{vap}}^m + S_{\text{liq}}^n}_{\text{Entropy flow out}}$$

$$S_{\text{gen}} = S_{\text{vap}}^m + S_{\text{liq}}^n - S_{\text{liq}}^m - S_{\text{vap}}^n$$

$$S_{\text{gen}} = (S_{\text{liq}}^n - S_{\text{vap}}^n) - (S_{\text{liq}}^m - S_{\text{vap}}^m) \quad (2.4)$$

For convenience, a new variable, δS^n , is defined as the entropy of the liquid stream minus the entropy of the passing vapour stream, at a chosen stage n . Mathematically, this definition is:

$$\delta S^n \equiv S_{\text{liq}}^n - S_{\text{vap}}^n \quad (2.5)$$

Substituting this new variable into Eq. (2.4) leads to:

$$S_{\text{gen}} = \delta S^n - \delta S^m \quad (2.6)$$

Note that in this arrangement of the entropy analysis, the entropy generation term is the δS at the top of the CS subtracted from the δS at the bottom of the CS.

In order to remove the material flux effects on the entropy generation, it is useful to divide Eq. (2.6) through by Δ , and using underbar notation to indicate a specific ‘per- Δ ’ quantity, the following is obtained:

$$\frac{S_{\text{gen}}}{\Delta} = \frac{\delta S^n}{\Delta} - \frac{\delta S^m}{\Delta}$$

$$\underline{S}_{\text{gen}} = \delta \underline{S}^n - \delta \underline{S}^m \quad (2.7)$$

Through calculations that are detailed in Appendix A.2, the expressions for the $\delta \underline{S}$ terms in Eq. (2.7) are found:

$$\delta \underline{S}^n = r_{\Delta} \Delta \hat{S}_{\text{mix,liq}}^n - \left[\lambda \sum_{i=1}^N \left(\frac{X_{\Delta,i} + r_{\Delta} x_i^n}{T_{b,i}} \right) + (1 + r_{\Delta}) \Delta \hat{S}_{\text{mix,vap}}^n \right] \quad (2.8)$$

where $\Delta \hat{S}_{\text{mix}}$ is the entropy of mixing of the stream indicated by the sub- and superscripts. Entropy of mixing is calculated as follows, assuming a vapour phase that behaves like an ideal gas:

$$\Delta \hat{S}_{\text{mix,vap}} = -R \sum_{i=1}^N Y_i \ln(Y_i) \quad (2.9)$$

$$\Delta \hat{S}_{\text{mix,liq}} = -R \sum_{i=1}^N x_i \ln(x_i \gamma_i) \quad (2.10)$$

In Eq. (2.9), Y_i is related to x_i by Eq. (2.3).

2.3 Important properties of the entropy equations

2.3.1 Path

Entropy, like enthalpy, is a state function. However, S_{gen} is not a state function, but a path function: the actual path taken is significant. The second law of thermodynamics stipulates that $S_{\text{gen}} \geq 0$ in any feasible process. Consequently, it cannot occur that $S_{\text{gen}} < 0$ in any part of the column, even if overall $S_{\text{gen}} \geq 0$. This means that not all paths for the separation are feasible, i.e. a column composition profile cannot be arbitrary; it is constrained by this S_{gen} condition. It can be deduced that if entropy must always be generated, $\delta \underline{S}^n$ is monotonic along the height of the column. The effect of this is of great importance, and will be considered later in § 2.4.

2.3.2 Stationary points

Knowledge of the maxima and minima of a function is often useful information, as it represents the limits of what values a function can assume, and where those extreme points occur.

When the derivative of Eq. (2.8) is taken with respect to n , Eq. (2.11) is obtained (see Appendix A.3 for the derivation):

$$\begin{aligned} \frac{d}{dn}(\delta \underline{S}) = & -r_{\Delta} R \sum_{i=1}^N \left[(\ln(x_i \gamma_i) + 1) \frac{dx_i}{dn} + \sum_{j=1}^{N-1} \left(\left(\frac{\partial \ln \gamma_i}{\partial x_j} \right) \frac{dx_j}{dn} \right) \right] - \\ & \lambda r_{\Delta} \sum_{i=1}^N \left[\left(\frac{1}{T_{b,i}} \right) \frac{dx_i}{dn} \right] + r_{\Delta} R \sum_{i=1}^N \left[\left(\ln \left(\frac{X_{\Delta,i} + r_{\Delta} x_i}{1 + r_{\Delta}} \right) + 1 \right) \frac{dx_i}{dn} \right] \quad (2.11) \end{aligned}$$

An interesting result is observed: each term on the right-hand side of Eq. (2.11) contains a factor of dx_i/dn . The significance of this is that when the design parameters r_{Δ} and X_{Δ} are set, and a pinch point is encountered, $dx_i/dn = 0$ for $i = 1 \dots N$, as per the definition in Eq. (2.1); therefore, at

a pinch point, $d(\delta\underline{S})/dn = 0$. In other words, exactly at a pinch point, a local maximum, local minimum, or inflection point in the $\delta\underline{S}$ function occurs. For simplicity, a constant λ has been assumed, but it can be shown that the derivative of a temperature-dependent λ also contains a dx_i/dn factor (see Appendix A.4). This is intuitive, since latent heat is a function of temperature, and temperature is a function of composition, which in turn is a function of the column stage number.

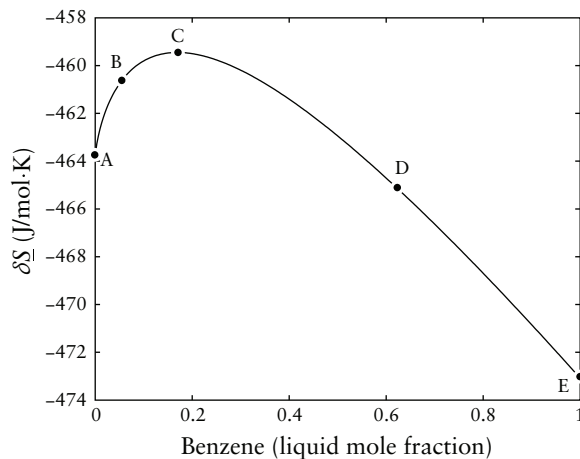
Since the difference between the δS values at the beginning and end of a path in composition space within the column section gives S_{gen} , the maximum entropy that can be generated in a column for fixed r_Δ and X_Δ occurs when the column profile runs from one pinch point to another, where one is a maximum in δS and the other a minimum.

Furthermore, according to the path argument outlined in § 2.3.1, in order to satisfy the $S_{\text{gen}} \geq 0$ condition, it cannot happen that two pinch points linked by a column profile are both at the same type of stationary point. For example, if a column profile were to go from one local maximum of δS to another local maximum, logic dictates that it must go through a local minimum between those two maxima. This, however, would lead to negative entropy generation in some part of the column, which is impossible. It is theoretically possible for a column profile to run from an unstable node, through a saddle point, and terminate at a stable node. Thus, given that the beginning and end of a column profile that connects stable and unstable nodes must be extreme points, it can be deduced that saddle points must be inflection points. If the stages are numbered from top to bottom, then stable nodes are local maxima, and unstable nodes are local minima.

Entropy generation may provide at least a partial explanation of why pinch points occur: they demarcate extremes within which a column can operate. Operating past pinch points—if it were possible—would result in a violation of the second law of thermodynamics by consuming entropy in some part of the equipment.

2.4 Minimum reflux and entropy

It is of importance that $\delta\underline{S}$, as given in Eq. (2.8), is a function of liquid composition only, once the design parameters (r_Δ and X_Δ) are set. It allows for the determination of $\delta\underline{S}$ at compositions that may not actually exist in the

**Figure 2.3**

Values of $\delta \underline{S}$ as a function of the light (benzene) liquid mole fraction in a rectifying section of the benzene–toluene system, with $r_{\Delta} = 4$ and $X_{\Delta} = (1, 0)$.

column at those chosen design parameters. Perhaps unintuitively, this provides insight into what limits compositions in the column section’s operating line.

To illustrate this, a benzene–toluene mixture can be used as an example of a near-ideal system. In the remainder of this section, the behaviour of the $\delta \underline{S}$ function is explored. First, sharp splits in rectifying and stripping sections are examined, after which non-sharp splits are treated briefly. Finally, a new minimum reflux equation is presented, based solely on entropy generation.

2.4.1 Effect of r_{Δ} on $\delta \underline{S}$ in rectifying sections

For simplicity, a sharp split is assumed in the rectifying section under consideration, i.e. $X_{\Delta} = (1, 0)$. By arbitrarily setting $r_{\Delta} = 4$, the only unspecified variable is the liquid mole fraction, x . Figure 2.3 shows the behaviour of the $\delta \underline{S}$ function as x is varied, for the fixed design parameters. On this graph, points A–E are marked, where A corresponds to pure toluene, C corresponds to the maximum of the $\delta \underline{S}$ function, and E is pure benzene; B and D are arbitrary intermediate points.

Since the horizontal axis of the graph in Figure 2.3 is the mole fraction of the light component, in the context of a distillation column, it means that the left side tends to the bottoms stream composition, and the right tends to the distillate composition. Therefore, if two compositions are arbitrarily chosen, the rightmost one in this figure would physically be located further up the column.

It is important to take cognisance of the fact that Δ in rectifying sections is positive, such that δS and $\delta \underline{S}$ have the same sign. As such, the entropy generation per Δ in the column section, $\underline{S}_{\text{gen}}$, is calculated as the difference between the $\delta \underline{S}$ value at bottom of the CS, subtracted from the $\delta \underline{S}$ at the

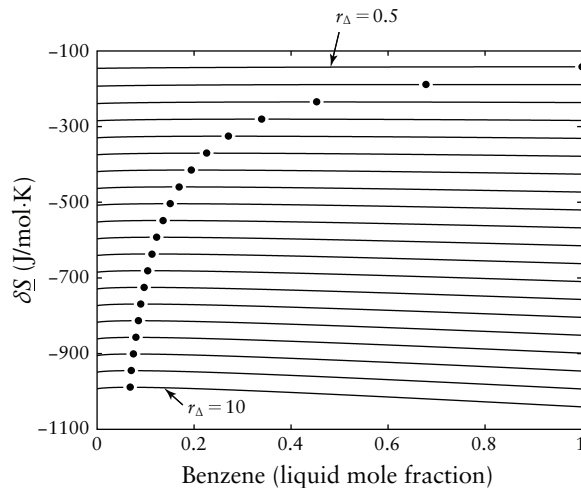
top, and in order for S_{gen} to be positive, as required by the second law of thermodynamics, $\underline{S}_{\text{gen}}$ must also be positive.

With reference to Figure 2.3, if the bottom of the column section in question had a composition at D and the top was at E, the entropy generated would be the $\delta\underline{S}$ at D ($-465.1 \text{ J/mol}\cdot\text{K}$) minus the value at E ($-473.0 \text{ J/mol}\cdot\text{K}$), which is $7.9 \text{ J/mol}\cdot\text{K}$.

Since $\underline{S}_{\text{gen}}$ cannot be negative, the paths $A \rightarrow B$, $A \rightarrow C$, and $B \rightarrow C$ are not possible. However, even though the value of $\delta\underline{S}$ at A and B is higher than that at D and E, $\delta\underline{S}$ does not decrease monotonically between B and D, but goes through a maximum at C. This means that in the part of the path $B \rightarrow C$, $\underline{S}_{\text{gen}} < 0$, which is not feasible. Therefore, even if the column section overall appears not to have negative entropy generation between A/B and D/E, those paths are not possible due to negative $\underline{S}_{\text{gen}}$. As a result of this, the only feasible paths—with respect to the five chosen points—are $C \rightarrow D$, $C \rightarrow E$, and $D \rightarrow E$, as this is where the function is monotonically decreasing.

Having specified that a sharp split is required, and assuming a conventional rectifying section, the distillate composition (the liquid composition at the top of that CS) is equal to X_{Δ} , which corresponds to point E in Figure 2.3. With the design parameters used for this graph, it can be seen that the composition at the bottom of the CS can be anywhere between points C and E, i.e. the light liquid mole fraction can range from 0.171 to 1. Note that if the light mole fraction at the bottom of the CS were any lower, the path would not be feasible. This limiting path $C \rightarrow E$ also corresponds to the maximum possible $\underline{S}_{\text{gen}}$ with those design parameters.

One of the features unique to binary distillation is that the column profiles of the rectifying and stripping sections always intersect at the feed composition when the column is at its minimum reflux, i.e. it pinches at the feed. (In multicomponent distillation, this is a special case, rather than normal behaviour.) Consequently, when considering a rectifying section in such a column, the composition at the bottom of the section is that of the feed. The implication is that for the parameters $X_{\Delta} = (1, 0)$ and $r_{\Delta} = 4$, the limit of the composition that can be fed to the column is $x_{\text{F}} = (0.171, 0.829)$. A feed composition with a lower concentration of the light material would not be feasible with those particular design parameters. This observation can also be stated in a different way: for $x_{\text{F}} = (0.171, 0.829)$ and $X_{\Delta} = (1, 0)$, the limiting (or minimum) reflux is $r_{\Delta} = 4$. Indeed, the discussion in § 2.3.2 would suggest that the composition $(0.171, 0.829)$ is a pinch point, since $\delta\underline{S}$ is at a maximum.

**Figure 2.4**

Values of $\delta\bar{S}$ as a function of the light (benzene) liquid mole fraction in the benzene–toluene system, with curves representing $r_{\Delta} = 0.5$ to $r_{\Delta} = 10$ in intervals of 0.5, at $X_{\Delta} = (1, 0)$. The dots represent the maximum $\delta\bar{S}$ on each curve.

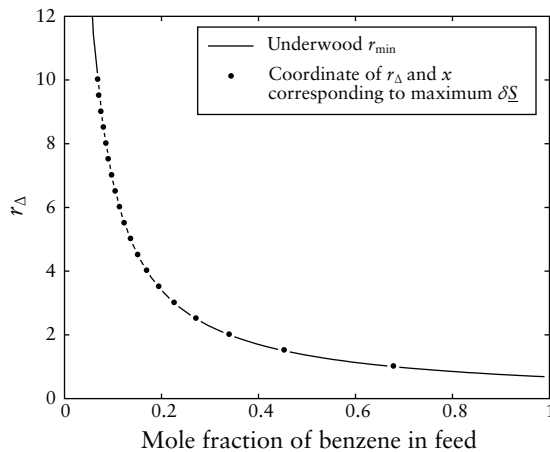
To investigate this hypothesis further, a greater number of sample points must be considered. To this end, Figure 2.4 shows similar plots to Figure 2.3, but for a range of r_{Δ} values, from 0.5 to 10 in intervals of 0.5. The maximum values are indicated by the dots for clarity. As $r_{\Delta} \rightarrow \infty$, the maximum value of $\delta\bar{S}$ tends towards the pure heavy component; conversely, as $r_{\Delta} \rightarrow 0.682$, this maximum value shifts towards the pure light component. At r_{Δ} values lower than 0.682, the composition stays at the pure light component, as that is a physical limit—a composition higher than (1, 0) is impossible. (Although the CPM method uses the information from negative compositions, entropy analysis in these regions is impossible due to the logarithm in the entropy of mixing term: negative compositions give complex values.)

Each of the maxima in Figure 2.4 has an associated composition and r_{Δ} value. These points can be plotted with composition on the horizontal axis, and r_{Δ} on the vertical axis, alongside results from the Underwood equations (Underwood, 1948), which are used to calculate minimum reflux ratio, given feed and distillate compositions, and the constant relative volatility of the system. The Underwood equations are as follows:

$$\sum_{i=1}^N \frac{\alpha_i z_{F,i}}{\alpha_i - \varphi} = 1 - q \quad (2.12)$$

$$r_{\min} + 1 = \sum_{i=1}^N \frac{\alpha_i x_{D,i}}{\alpha_i - \varphi} \quad (2.13)$$

where q is the molar liquid fraction of the feed, and φ is the Underwood root. Equation (2.12) is solved to find the root φ , which is then substituted into Eq. (2.13) to find the minimum reflux, r_{\min} . The benzene–toluene system is

**Figure 2.5**

Comparison of minimum reflux ratio from Underwood's method, and coordinates corresponding to maximum $\delta\underline{S}$ in Figure 2.4.

well-approximated with the constant relative volatility model with $\alpha = 2.47$.

The plots of r_{\min} can then be compared to verify whether or not the maxima in Figure 2.4 do indeed correspond to minimum reflux; such a comparison is made in Figure 2.5, and it confirms this hypothesis.

This work has thus far only considered a liquid feed; in order to use a vapour feed, the corresponding liquid composition in equilibrium with the feed composition must be found (by means of a dew-point calculation) for use in the $\delta\underline{S}$ equation.

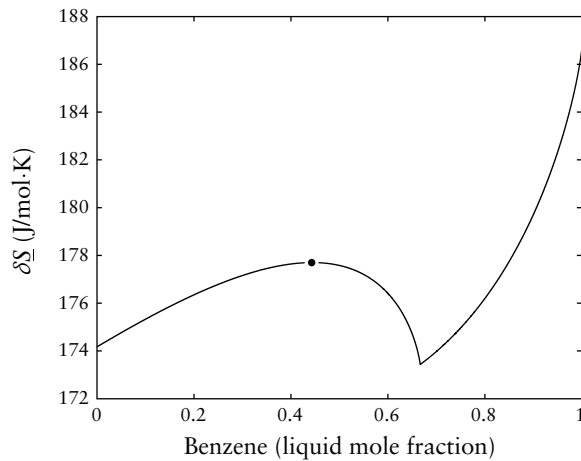
2.4.2 Effect of r_{Δ} on $\delta\underline{S}$ in stripping sections

Stripping sections can be analysed in much the same way as rectifying sections. The main difference is that stripping sections have negative Δ values; as such, for S_{gen} to be positive, $\underline{S}_{\text{gen}}$ must be negative. Also owing to the negative Δ value, stripping sections have negative r_{Δ} , and it can be shown easily that $r_{\Delta} < -1$ always.

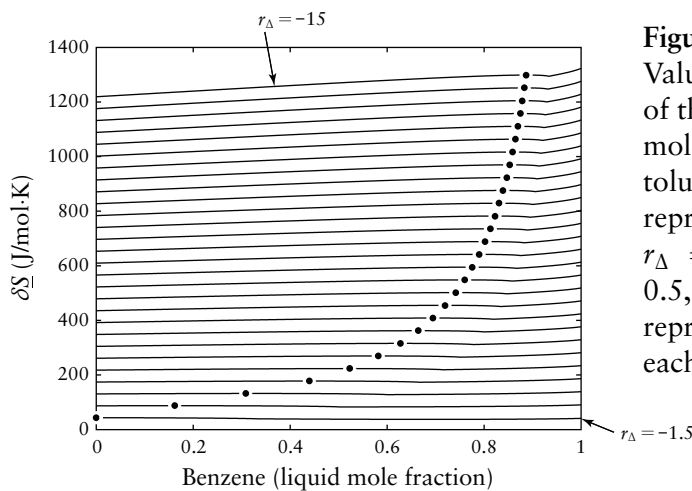
Assuming a sharp split once again, such that $X_{\Delta} = (0, 1)$, and arbitrarily designating $r_{\Delta} = -3$, a plot of $\delta\underline{S}$ can be made, as is shown in Figure 2.6. The dot indicates the local maximum that is monotonically linked to the X_{Δ} composition. For positive S_{gen} , the $\delta\underline{S}$ slope must be negative, such that valid profiles range from the leftmost part of Figure 2.6 to the local maximum shown by the dot; beyond that, negative entropy generation would occur.

Figure 2.7 shows plots of $\delta\underline{S}$ for a range of r_{Δ} values, from -15 to -1.5 in intervals of 0.5 .

In a conventional distillation column, the r_{Δ} in the stripping section can be used to calculate the corresponding r_{Δ} in the rectifying section through simple

**Figure 2.6**

Values of $\delta\underline{S}$ as a function of the light (benzene) liquid mole fraction in a stripping section of the benzene–toluene system, with $r_{\Delta} = -3$ and $X_{\Delta} = (0, 1)$. The dot represents a local maximum of $\delta\underline{S}$.

**Figure 2.7**

Values of $\delta\underline{S}$ as a function of the light (benzene) liquid mole fraction in the benzene–toluene system, with curves representing $r_{\Delta} = -15$ to $r_{\Delta} = -1.5$ in intervals of 0.5, at $X_{\Delta} = (0, 1)$. The dots represent the maximum $\delta\underline{S}$ on each curve.

mass balance. The relationship between these two r_{Δ} values is as follows, assuming CMO and a saturated liquid feed:

$$r_{\Delta,R} = (r_{\Delta,S} + 1) \left(\frac{x_{F,1} - x_{D,1}}{x_{F,1} - x_{B,1}} \right) - 1 \quad (2.14)$$

where the subscripts ‘R’ and ‘S’ denote the rectifying and stripping sections, respectively. In the sharp-split case, $x_D = X_{\Delta,R} = (1, 0)$, and $x_B = X_{\Delta,S} = (0, 1)$.

If the stripping r_{Δ} points in Figure 2.7 are transformed to rectifying r_{Δ} using Eq. (2.14), the points align with the minimum reflux in Figure 2.5.

2.4.3 Non-sharp splits

Non-sharp splits of the benzene–toluene system are briefly considered here. A non-sharp X_{Δ} could be either a rectifying section (if the compositions in the CS are heavier than the X_{Δ}) or a stripping section (if the compositions are lighter than the X_{Δ}). As such, the rectifying and stripping sections can be

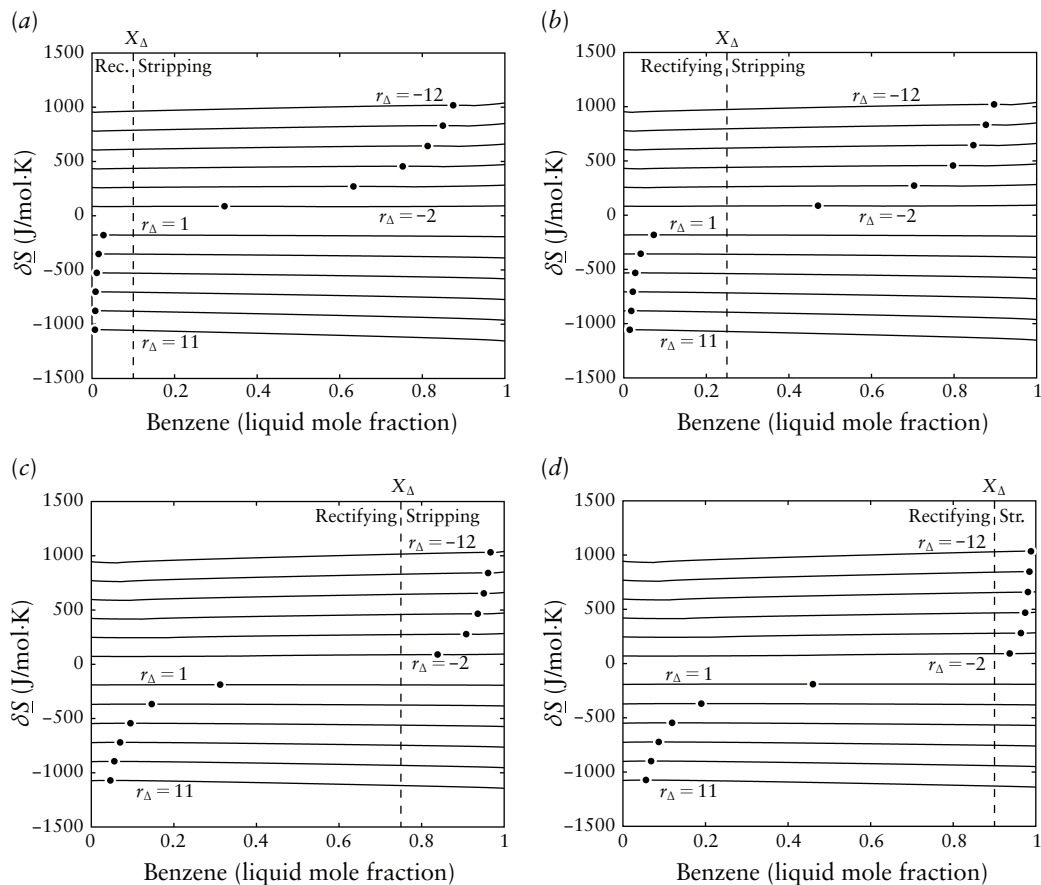


Figure 2.8 $\delta\bar{S}$ as a function of light (benzene) mole fraction, with $r_{\Delta} = 1$ to 11 for the rectifying section, and $r_{\Delta} = -2$ to -12 in the stripping section: (a) $X_{\Delta} = (0.1, 0.9)$; (b) $X_{\Delta} = (0.25, 0.75)$; (c) $X_{\Delta} = (0.75, 0.25)$; (d) $X_{\Delta} = (0.9, 0.1)$. The dots indicate local maxima in the $\delta\bar{S}$ function.

considered simultaneously on the same graphs; Figure 2.8 shows the $\delta\bar{S}$ curves for fixed X_{Δ} , and varying r_{Δ} . For the rectifying section, the r_{Δ} values range from 1 to 11 in increments of 2, and for rectifying sections, the r_{Δ} ranges from -12 to -2 in increments of 2.

The behaviour for the non-sharp splits in Figure 2.8 is qualitatively similar to the sharp splits examined in § 2.4.1 and § 2.4.2, and does not appear to exhibit any unexpected characteristics.

2.4.4 Tangent pinches

Tangent pinches can be encountered in some zeotropic and azeotropic mixtures; in such cases, minimum reflux is not determined by a pinch at the feed. As an example of a zeotropic system with a tangent pinch, consider an equimolar feed of benzene–ethylenediamine system, split into a distillate of $x_D = (0.99, 0.01)$, and a bottoms of $x_B = (0.02, 0.98)$. Figure 2.9a shows

a McCabe–Thiele diagram for this system, with reflux that gives a pinch at the feed. Because of the shape of the equilibrium curve, an operating line that pinches at the feed must cross the equilibrium curve, which is not physically possible. Therefore, the minimum reflux is determined by an operating line of the rectifying section that is tangent to the equilibrium curve; this operating line pinches at a lighter composition than the feed, and has a higher reflux than in the feed-pinch case. Figure 2.9*b* shows the true minimum reflux.

Also included in Figure 2.9 are plots of the $\delta\underline{S}$ values for the rectifying section for both of the scenarios mentioned above; it is important to note that there is a corresponding stationary point in the $\delta\underline{S}$ function at each point that the rectifying operating line intersects the equilibrium curve, as discussed in § 2.3.2. The correspondence is not exact, owing to the fact that the two approaches are inherently different in their simplifications: while the McCabe–Thiele diagram assumes CMO, and thus omits the energy balance entirely, the $\delta\underline{S}$ require values for λ and T_b , which affects the exact properties of the $\delta\underline{S}$ curves. Appendix A.5 shows the exact correspondence using rigorous thermodynamics in both.

2.5 New minimum reflux equation for binary separations

The analysis of the benzene–toluene system has shown that for a given feed, x_F , the minimum reflux ratio is the r_Δ that places a maximum in the $\delta\underline{S}$ function at the composition x_F . (The same is not true if a tangent pinch exists.)

This is an important observation that highlights the physical and practical significance of entropy in distillation columns. The knowledge that a local maximum in the $\delta\underline{S}$ function corresponds to minimum reflux means that an equation based on S_{gen} can be derived, at least for binary systems without a tangent pinch. First, the derivative of $\delta\underline{S}$ with respect to x_1 is found, which is then set to zero, i.e. $d(\delta\underline{S})/dx_1 = 0$, which defines the stationary point in $\delta\underline{S}$. Thereafter, the equation can be rearranged to make r_Δ the subject of the formula. This derivation is given in Appendix A.6, and the result is:

$$r_{\min} = \frac{(1 - x_{D,1}) \exp(\Psi) - x_{D,1}}{x_{F,1} - (1 - x_{F,1}) \exp(\Psi)} \quad (2.15)$$

where

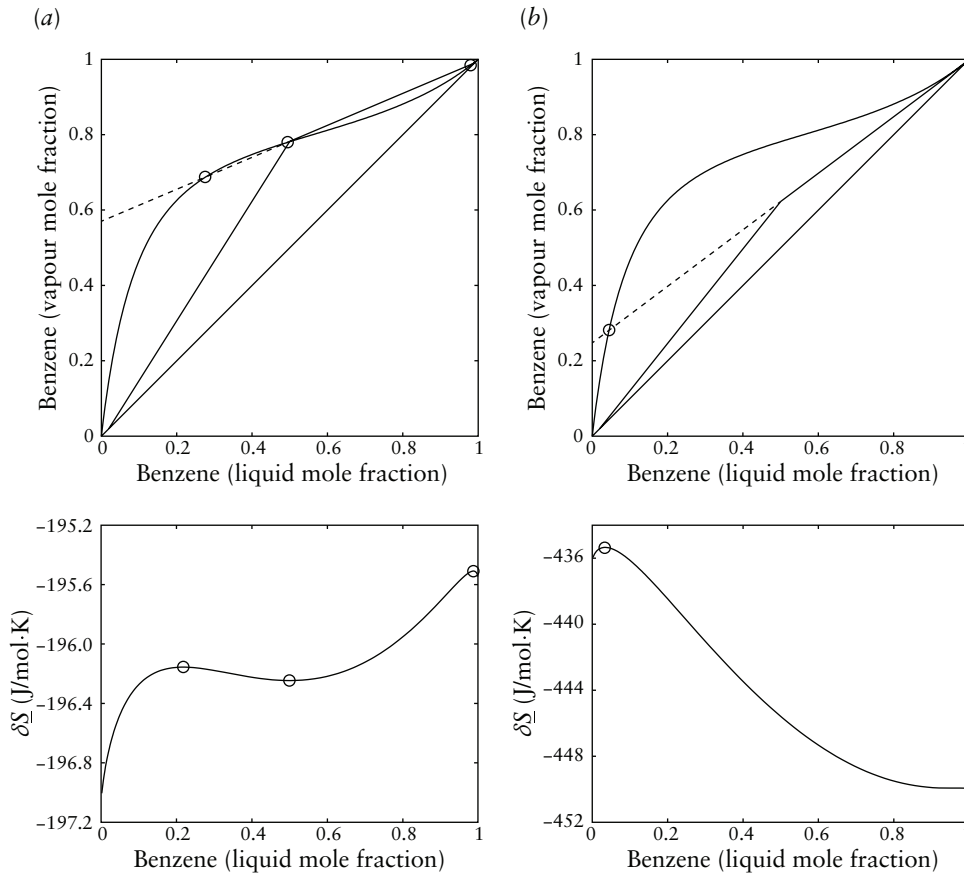


Figure 2.9 McCabe–Thiele diagrams, and corresponding rectifying δS curves, for the benzene–ethylenediamine system at (a) feed-pinch reflux, and (b) actual minimum reflux at the tangent pinch.

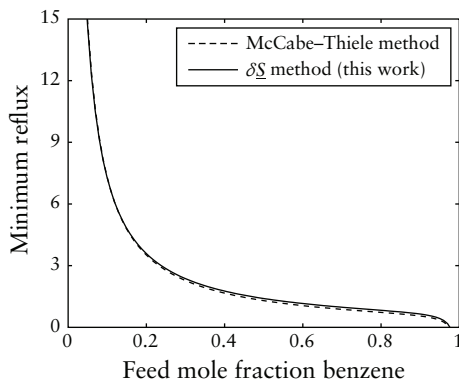
$$\Psi = \ln\left(\frac{x_{F,1}\gamma_{F,1}}{(1-x_{F,1})\gamma_{F,2}}\right) + \frac{x_{F,1}}{\gamma_{F,1}}\left(\frac{\partial\gamma_{F,1}}{\partial x_{F,1}}\right) + \frac{(1-x_{F,1})}{\gamma_{F,2}}\left(\frac{\partial\gamma_{F,2}}{\partial x_{F,1}}\right) + \frac{\lambda(T_{b,2}-T_{b,1})}{RT_{b,1}T_{b,2}}$$

The above equation is not particularly elegant, since it involves a description of the non-idealities of the system by the partial derivatives of the activity coefficient with respect to x_1 at constant T and P . These can either be calculated analytically where possible (Taylor and Kooijman, 1991), or numerically using finite differences.

For systems that exhibit ideal liquid mixing, $\gamma = 1$, such that Ψ simplifies to the following:

$$\Psi = \ln\left(\frac{x_{F,1}}{1-x_{F,1}}\right) + \frac{\lambda(T_{b,2}-T_{b,1})}{RT_{b,1}T_{b,2}}$$

As Eq. (2.15) above shows, the information required is the latent heat of the system λ , the boiling points of the pure components $T_{b,1}$ and $T_{b,2}$ at

**Figure 2.10**

Minimum reflux for the benzene–toluene system as a function of feed composition, as found by the McCabe–Thiele method, and using Eq. (2.15). Distillate composition is $x_D = (0.99, 0.01)$.

system pressure P , and the activity coefficient model (in the case of a non-ideal system).

2.5.1 Examples and validation

In order to test the Eq. (2.15), three examples without tangent pinches were used: benzene–toluene as an example of a near-ideal mixture, chloroform–methanol as an example of a minimum-boiling azeotrope (at 65.88 mol% chloroform; 326.9 K), and acetone–chloroform as an example of a maximum-boiling azeotrope (at 34.52 mol% acetone; 337.3 K).

Note that, in the case of the azeotropes, the simple distillation can take place on either side of the azeotrope. For example, in the minimum-boiling azeotrope case, the bottoms can be close to either pure component, with the distillate close to the azeotropic composition. In the maximum-boiling case, the reverse is true: the distillate can be close to the composition of the pure components, and the bottoms is close to the azeotropic composition.

Figure 2.10 shows r_{\min} as a function of feed composition for the benzene–toluene system, as found by McCabe–Thiele approach, and by Eq. (2.15). The distillate composition is $x_D = (0.99, 0.01)$.

Figures 2.11 and 2.12 show the same type of plot for chloroform–methanol and acetone–chloroform, respectively. For the former, distillate compositions on either side of the azeotrope are given: $x_D = (0.6, 0.4)$ and $x_D = (0.7, 0.3)$. Similarly, the two r_{\min} plots for acetone–chloroform are shown, for distillates of $x_D = (0.01, 0.99)$ and $x_D = (0.99, 0.01)$.

Figures 2.10–2.12 show that the r_{\min} calculations with Eq. (2.15) are very close to those using the McCabe–Thiele method. There are some slight differences, which result from differences in the two approaches, as explained in § 2.4.4. Nevertheless, the two methods do align very well, for both ideal and azeotropic systems.

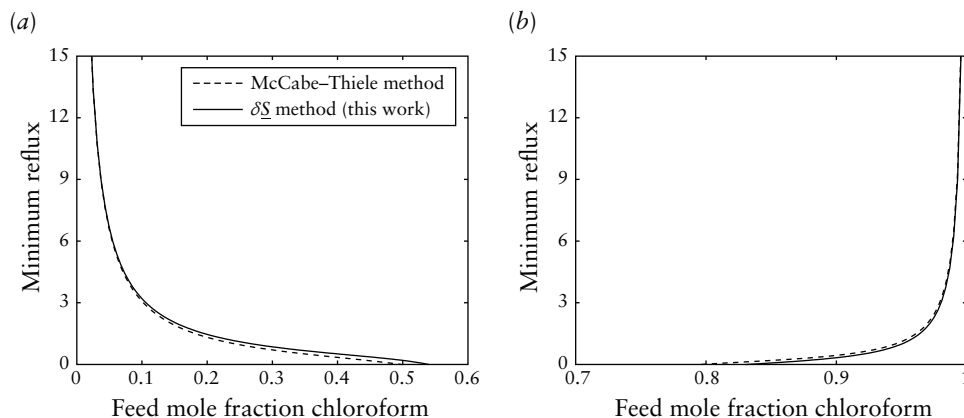


Figure 2.11 Minimum reflux for the chloroform–methanol system as a function of feed composition, as found by the McCabe–Thiele method, and using Eq. (2.15). Distillate composition is (a) $x_D = (0.6, 0.4)$; and (b) $x_D = (0.7, 0.3)$.

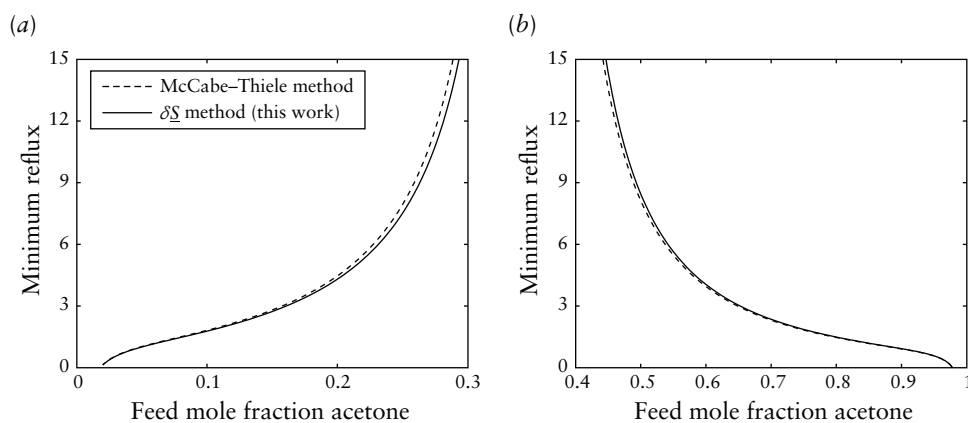


Figure 2.12 Minimum reflux for the acetone–chloroform system as a function of feed composition, as found by the McCabe–Thiele method, and using Eq. (2.15). Distillate composition is (a) $x_D = (0.01, 0.99)$; and (b) $x_D = (0.99, 0.01)$.

2.6 Conclusion

In this chapter, entropy generation in distillation column sections was examined, with equations derived for generalised column sections. Specifically, a new variable, $\delta\mathcal{S}$, was defined, which can be used to compare the difference between the entropies of the passing liquid and vapour. Entropy generation is simply the difference between $\delta\mathcal{S}$ at two points in the column sections. The behaviour of $\delta\mathcal{S}$ was then analysed, and a mathematical proof was given that the stationary points of that function correspond to traditional pinch points in distillation.

An analysis of generalised rectifying and stripping sections was then performed, and it was verified that the local extrema do indeed correspond

to pinch points. This feature, along with the knowledge that binary columns pinch at the feed, was used to derive a novel minimum reflux equation, in the form of Eq. (2.15), which is applicable to ideal or non-ideal systems without tangent pinches. Tangent pinches were found to be inflection points in the δS function.

It should be noted that Eq. (2.15) is more complicated than the McCabe–Thiele method, and is also limited to two components, since it exploits the feed pinch that occurs at minimum reflux in binary distillation. As such, it is admittedly not a practically useful tool, as it can be replaced by the McCabe–Thiele for simpler calculation of minimum reflux. However, its purpose is to demonstrate the power of entropy analysis, and the integral, often overlooked, part it plays in distillation. Using the entropy analysis, an entirely new way of finding minimum reflux was derived.

What is perhaps most remarkable, however, is the fact that entropy generation alone was used to find pinch points, without VLE calculations. It could be argued that VLE calculations are included in Eq. (2.15) implicitly through the γ terms; however for ideal systems where $\gamma = 1$, the equation still gives the correct minimum reflux, which clearly has no VLE calculation associated with it. Overall, this suggests that VLE, entropy, and hence limitations in distillation are more fundamentally linked than previously thought.

Chapter 3

Pinch Points in Non-Ideal Distillation Systems and Finite-Reflux Distillation Boundaries

The work in this chapter has been published in: Felbab, N., Hildebrandt, D., Glasser, D., 2011. A new method of locating all pinch points in nonideal distillation systems, and its application to pinch point loci and distillation boundaries. *Comp. Chem. Eng.* 35 (6), 1072–1087. This chapter is a reproduction of that publication, with some minor corrections, and changes in style and formatting for clarity. It has also been updated somewhat to reflect developments in the field since that publication. Reproduced with permission.

Copyright © 2011 Elsevier. Computers & Chemical Engineering.

Abstract

A new method for automatically finding all of the pinch points in a user-specified composition space in non-ideal distillation systems at any reflux is presented. It does not rely on the solution of ODEs, and neither knowledge of the system topology, nor rigorous simulation is required. Moreover, the method can be applied to any column section, even those within complex configurations. The method works on the principle of a systematic search over an area to find where the conditions for a pinch point are satisfied; this includes pinch points outside of the mass balance triangle, which, while physically impossible, do provide useful information. This principle is extended to reflux-parameterised pinch point loci and to finding distillation boundaries accurately. Non-idealities are modelled with the NRTL model, although any model can be used. Only ternary systems have been considered, but the method can, in principle, extend to higher-order systems.

3.1 Introduction

3.1.1 Residue curve maps

Traditionally, residue curve maps (RCMs) have been used as a graphical method to perform shortcut heuristic synthesis of multicomponent distillation systems (Fien and Liu, 1994). Residue curves are constructed mathematically by solving a system of ordinary differential equations, the general case of which is given by Eq. (3.1), for $N - 1$ components.

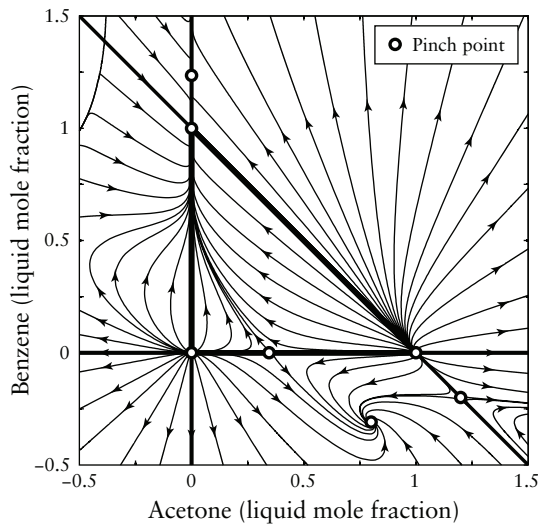
$$\frac{dx_i}{dn} = x_i - y_i \quad (3.1)$$

The above is an initial value problem, which can be solved using any combination of (x_i, \dots, x_{N-1}) that sum to unity as a starting point. When the system of equations is solved, the result is a trajectory in composition space, known as a residue curve (RC). Performing the integration with a starting point that lies on a specific RC yields that same RC. In a batch distillation system (with changing time t , rather than n , in Eq. (3.1)), the physical significance of an RC is that it shows how the composition of the liquid changes with time as it is boiled in an open system, if it had the starting composition at a known time t . Since RCs are unique, integrating Eq. (3.1) backwards from the starting point can determine what the liquid composition would have been prior to known time t .

All RCs terminate at a stable node, and originate at an unstable one, the compositions of which are at pure components or azeotropes. These compositions are referred to as stationary points. Additionally, in ternary and higher-order systems, saddle points can occur, which are simply points in the composition space past which trajectories can run, but at which they can never terminate. The above is also true of any azeotrope, which can either be a stable or unstable node, or a saddle point.

Pinch points in distillation systems occur mathematically when $dx_i/dn = 0$ in Eq. (3.1) for $N - 1$ components; since the mole fractions sum to unity, this condition is automatically met for the N^{th} component.

By plotting a number of residue curves on the same graph, an RCM is constructed, an example of which is given in Figure 3.1 for the acetone–benzene–chloroform (ABC) system. It allows for various trajectories to be considered simultaneously, which gives insight into the system behaviour. This behaviour is known as the topology of the system, which is the structure of how various stable and unstable nodes and saddle points are linked by residue

**Figure 3.1**

Residue curve map of the acetone–benzene–chloroform system.

curves. Note that in Figure 3.1, residue curves are plotted outside of the mass balance triangle (MBT) as well, which is not traditionally done. Although this is physically impossible, it is not meaningless. In his thesis, Holland (2005) showed that these residue curves outside of the MBT are mathematically and thermodynamically valid.

With regards to continuous distillation, if a distillation column is operated at infinite reflux, that is, if all of the product is returned to the column, the solution of Eq. (3.1) yields the composition profile within the column, with a known starting point at a stage n . Residue curves are identical to these column profiles, such that RCMs describe both the batch distillation case and the continuous infinite reflux one.

By using infinite reflux as a limiting case, it is possible to design separation systems, or rather to get a starting point for column sequencing or for the design of complex columns. Examples of the former can be found in Fien and Liu (1994), as well as in many modern texts on distillation.

3.1.2 Column profile maps

While RCMs do have their uses, the assumption of infinite reflux is an unrealistic and impractical one.

To circumvent this shortcoming, Van Dongen and Doherty (1985) introduced an approach to express finite-reflux column profiles in traditional rectifying and stripping sections with an ordinary differential equation analogous to Eq. (3.1). Tapp et al. (2004) built on the work of Van Dongen and Doherty by extending the latter's equation for use in generalised column sections, such as those within complex configurations like the Petlyuk column (Holland,

2005; Holland et al., 2010). Tapp et al. termed their equation the difference point equation (DPE). The DPE is given here as Eq. (3.2):

$$\frac{dx_i}{dn} = \left(1 + \frac{1}{r_\Delta}\right)(x_i - y_i) + \frac{1}{r_\Delta}(X_{\Delta,i} - x_i) \quad (3.2)$$

where $\Delta = V - L$, $r_\Delta = L/\Delta$, and $X_\Delta = (VY^T - Lx^T)/\Delta$. The last two are known as the design parameters: r_Δ is a ‘reflux ratio’ of the column section (CS), and X_Δ , the difference point, can be viewed as the pseudo-composition of the net flow in the CS. Δ is the net flux of material in the CS. In a CS terminated by a total condenser, r_Δ is the standard definition of reflux ratio, and X_Δ is the composition of the distillate. To relate the DPE to a conventional stripping section, the stages are numbered in reverse, $S = -r_\Delta - 1$ (where $r_\Delta < -1$), and X_Δ is the composition of the bottoms.

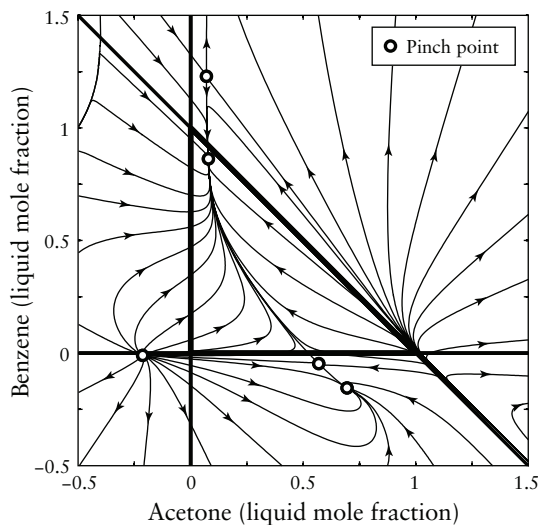
Note that constant molar overflow (CMO) is assumed for Eq. (3.2) to hold.

When these design parameters are fixed, the solution of Eq. (3.2) is a column profile, which is entirely analogous to a residue curve, at finite reflux.

Again, completely analogously to RCMs, the DPE allows for construction of column profile maps (CPMs), which are essentially RCMs, but at finite reflux. These maps trace the liquid composition profile in a generalised column section, defined as a section of the column in which there is no addition or removal of energy or mass. Since there is an X_Δ value for each component, $X_{\Delta,i}$, X_Δ can be described as a unit vector that has the same number of elements as components in the system, i.e. $X_\Delta = (X_{\Delta,1}, X_{\Delta,2}, \dots, X_{\Delta,N})$. It is noteworthy that Eq. (3.2) collapses to Eq. (3.1) as $r_\Delta \rightarrow \infty$, i.e. infinite reflux, which indicates that RCMs can be seen as a subset of CPMs. Furthermore, the mathematical conditions for a pinch point also remain the same as in RCMs: $dx_i/dn = 0$ in Eq. (3.2) for $N - 1$ components. An example of the CPM of the ABC system, with $r_\Delta = 6$ and $X_\Delta = (0.90, 0.05, 0.05)$, is given in Figure 3.2.

The relationship between CPMs and RCMs has been examined in some detail previously (Tapp et al., 2004; Holland et al., 2004a,b), but even comparing Figures 3.1 and 3.2 will give the reader some insight into this relationship. CPMs are a relatively new way of looking at distillation processes; as such, not much literature on the topic is available outside of the COMPS research group yet, although its use is becoming more widespread, e.g. see the work of Linninger and co-workers (Linninger, 2009; Kim et al., 2010), and Tian et al. (2009). Some of the more important characteristics of CPMs are reiterated below.

Although this chapter deals predominantly with non-ideal systems, it is

**Figure 3.2**

Column profile map of the ABC system with $r_{\Delta} = 6$ and $X_{\Delta} = (0.90, 0.05, 0.05)$.

convenient to first consider a system exhibiting constant relative volatility (CRV). Such a system might have, for example, relative volatility $\alpha = (2, 1, 1.5)$, such that the components are light, heavy, and intermediate, in that order.

A rectifying section terminated by a condenser has the standard interpretation of the design parameters: r_{Δ} is the reflux ratio, and the column is producing a distillate of, for example, $x_D = X_{\Delta} = (0.8, 0.1, 0.1)$. Figure 3.3 gives the RCM (i.e. CPM with $r_{\Delta} \rightarrow \infty$) of this system, as well as the CPM at $r_{\Delta} = 5$. It is important to note that the mass balance triangle has shifted at finite reflux (this phenomenon is the ‘moving triangles’ that forms the basis of Holland et al., 2004b), and the equivalence of the topology of the two triangles, regardless of their different shapes and positions. The vertices of this finite-reflux transform triangle (TT) are the pinch points. With respect to the MBT, when reflux is lowered to a finite value, the topology changes. However, with respect to the shifted or transform triangle, the topology remains unchanged. In effect, all that has changed between the two scenarios is that the pinch points have moved. Note that most of the pinch points that make up the vertices of the two TTs are outside of the real space. Although the compositions outside of the real space are physically unattainable, they are topologically important, since knowledge of their positions allows for insight into the behaviour of the column section and its structure. For example, even though a pinch point is outside of the MBT, its position influences the behaviour of column profiles within the real space, and, e.g. if it is a stable node, all profiles will run towards it, regardless of the physical impossibility of reaching it.

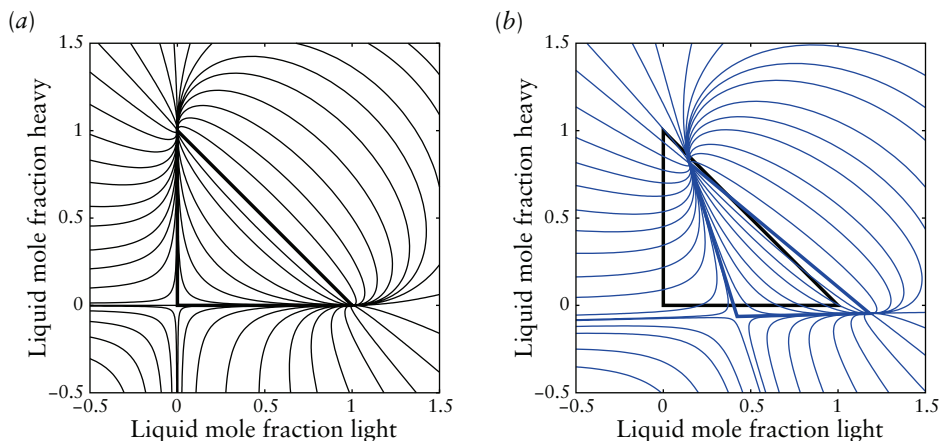


Figure 3.3 Plot of (a) RCM, and (b) CPM with $r_{\Delta} = 5$ and $X_{\Delta} = (0.8, 0.1, 0.1)$ for a constant relative volatility system with $\alpha = (2, 1, 1.5)$.

Bausa et al. (1998) and Tapp et al. (2004) both noted what has just been illustrated, i.e. that when reflux is changed, the pinch points of a system move in the composition space away from their infinite-reflux positions.

Figure 3.3 illustrates that CPMs are simply a transform of RCMs in composition space. This particular feature of the CPM method is one of its most powerful. It allows for the synthesis of columns by manipulating these triangles of known topology to achieve the behaviour that the designer requires. It departs from, and improves on, the traditional design methods which consider only one profile at a time, since the column profile map scans all possible profiles and behaviours for the chosen design parameters.

‘Unusual’ behaviour can also occur at low r_{Δ} values. For example, as the pinch points move with decreasing reflux, their stability can also change. Past a certain reflux, a stable node may suddenly become an unstable node or a saddle point, thereby dramatically changing the behaviour within the distillation column. Furthermore, as the pinch points move, they tend to move towards one another, and can ‘collide’ and merge in the composition space, thereby decreasing the number of unique pinch points. For example, if Figures 3.1 and 3.2 are compared, it can be seen that in the former (at infinite reflux) there are seven pinch points, while in the latter, only five exist. These phenomena have been examined in more detail by Beneke et al. (2011a), and mentioned by Bausa et al. (1998) and Holland et al. (2004a).

3.1.3 Pinch point loci

A pinch point locus (also known as a pinch point curve) is the locus that traces the positions of pinch points, as an independent design parameter is varied.

Usually, this parameter is r_{Δ} , but X_{Δ} could be used, depending on what is more convenient for the particular design problem. This allows for the easy determination of the parameter values that lead to the desired positioning of the pinch points, in order to achieve the required behaviour within the column.

An example, which unifies all of the discussed concepts and proposed methods into a practical application for the synthesis of a distributed-feed column, is presented at the end of this chapter.

3.1.4 The aim of this work

The position and stability of pinch points in a system determine the topology of CPMs of the various column sections that make up a column. It can be used to the designer's advantage with the CPM method, not only to synthesise a feasible column, but also to gain a better understanding of the choices that design parameters have on the final design.

Pinch points in CRV systems are straightforward to find; in fact, they can be found by software with symbolic calculation capabilities.

However, for highly non-ideal systems that can only be modelled accurately by more complicated models such as NRTL or Wilson, this problem becomes substantially more difficult: not only is it mathematically far more difficult to solve, but, as discussed earlier, pinch points have highly complex behaviour at low reflux ratios, and can merge with one another, or 'disappear' altogether, because some of the roots become imaginary. Prior to this work, unless the full CPM was plotted, it was not possible to know how many pinch points actually existed, what their locations were, and what the structure of the CPM was.

The algorithms presented here are intended as a tool to aid work with column profile maps (and especially for automation thereof), but not as a stand-alone synthesis/design technique. Tapp et al. (2004), Holland et al. (2004a), and Holland et al. (2004b, 2010) have comprehensively covered their novel design method—most of which requires pinch points—but not a way of finding pinch points or of constructing pinch point loci, which is what this chapter aims to do. Naturally, the method can be used for any other application that requires pinch points. One non-CPM example of such an application would be for use with the rectification body method (Bausa et al., 1996, 1998), which relies on pinch points.

This algorithm for finding pinch points is a 'brute-force' one, which is to say that it populates the given region with potential starting points in a

systematic manner (although only the most promising are used). While this is not computationally efficient—in fact, it is only feasible due to the computing power available nowadays—it is a requirement at this stage, as will become apparent when the algorithm is described later in § 3.3. No claims are made that it is the most efficient way to find a specific pinch point, but it is an effective method that can find all of the pinch points in a CPM automatically, given minimal information (as mentioned above, only r_{Δ} , X_{Δ} , and the bounds of the search space).

The example provided in § 3.6 serves not only to show how the concepts and methods presented here tie in with each other for the design of distillation columns, but it also provides justification for finding all of the pinch points on a CPM automatically.

3.2 Literature survey

A number of methods exist for finding the pinch points in a distillation system, usually as a step towards finding the minimum reflux for a two-section column, based on the fact that the minimum reflux is observed when the end pinch of the stripping section just touches the rectifying profile, or vice versa, depending on the type of split (Doherty and Malone, 2001). It is immediately apparent that these approaches are then limited to column configurations for which they are specifically designed, most often conventional columns.

As a brief overview, some of these methods are listed below. The reader is referred to the work of Lucia et al. (2008) and Hoffmaster and Hauan (2004) for a more detailed discussion of many of these methods.

3.2.1 Pinch points

Levy and Doherty (1986) used pinch points to determine the minimum feasible reflux ratio for a desired multicomponent split in a conventional column, modelled with non-ideal thermodynamics. They found that the end-point of the column profile is a discontinuous function of the reflux ratio; that is, when it moves past minimum reflux, it suddenly terminates at a tangent pinch, rather than running past it as it would at a higher reflux ratio. In order to find this pinch point, Levy and Doherty applied bifurcation theory and ultimately used standard root-finding techniques to solve a system of non-linear equations. However, the thermodynamic models used were the van Laar and the two-parameter Margules models, both of which are relatively simple and readily

solved by root-finding methods. More complex models, such as the NRTL model, do not lend themselves as easily to these methods.

To find the pinch points in the rectifying section of a conventional column with a specified distillate composition, Zhang and Linninger (2004) used an equation presented by Doherty and Malone (2001) with a minor modification to model vapour–liquid equilibrium (VLE) by means of an equilibrium constant. The equation can then be solved iteratively to find the pinch point composition. Doherty and Malone also gave an equation for the stripping section, which can be used in much the same way as the rectifying one, and has been implemented in the work of Lucia et al. (2008).

Koehler et al. (1991) created a hypothetically reversible distillation model (i.e. one that generates no entropy) by adding heat continuously throughout the column at zero temperature difference, along with the other appropriate assumptions that lead to reversibility. The purpose of this exercise was to find the minimum energy requirements of a conventional column, and from that to calculate the minimum reflux, based on the understanding that the two conditions correspond directly. It was found that the concentration profile of this reversible column corresponded exactly to the pinch point locus for an adiabatic column at different reflux ratios, provided that the same amount of heat is added at the end of the column section as the total heat added in the reversible case. This approach led to a new criterion for finding tangent pinches in conventional, multicomponent columns: as Koehler et al. state, ‘a tangent pinch appears in an adiabatic rectifying section if there is a local maximum in the reversible energy profile between the distillate and the computed pinch composition and if the energy demand at this maximum exceeds the energy demand of the “conventional” saddle or end pinch.’

In his thesis, Halvorsen (2001) showed how the Underwood equations for minimum energy can be used to calculate the pinch point compositions, but this is limited to constant relative volatility systems, since that is a fundamental assumption of the Underwood equations. Despite this shortcoming, Halvorsen demonstrated that this method can be applied to complex column configurations (the Petlyuk and Kaibel arrangements, specifically), unlike the other approaches discussed here.

Beneke et al. (2011b) developed a method of locating all pinch points, which is the most similar in purpose to this work. The authors state that the method is fast and robust. It operates on the principle of ‘multi-dimensional deflation’, which is a way of defining the objective function to eliminate

previously found solutions by making the function tend to infinity at previous solutions. In this way, the number of remaining solutions ‘deflates’. However, as the authors state, that alone cannot guarantee location of all pinch points. In order to locate all of them, the ‘hybrid sequential niche algorithm’ (Moon and Linninger, 2009) is employed. This is effectively a hybrid, stochastically initialised algorithm, with a genetic search component, followed by a local deterministic search. The main disadvantage of this approach, however, is that it is a complicated, non-standard algorithm, which the user needs to code from the ground up in order to use; it is thus not suitable for non-expert users.

3.2.2 Pinch point loci

Based on the reversible distillation model, Poellmann and Blass (1994) created a differential equation that satisfies the collinearity criterion between the material balance line and the equilibrium node, in order to determine the reversible profile. However, these pinch point curves are only valid for conventional column sections, and are not directly parameterised by reflux or reboil ratio, or heat duty, thereby making them useful in screening possible positions of pinch points quickly, but not the design parameters that result in those pinch points.

Pinch point loci or curves have been found by Hauan et al. (2000) by satisfying the following criterion: the mixing and separation vectors are parallel, of equal magnitude, and of opposite direction. This criterion is equivalent to $dx_i/dn = 0$ in Eq. (3.2). The same kind of approach was used by Wahnschafft et al. (1992): ‘The pinch point curve for [the distillate] can be constructed by finding the points on residue curves with their tangents passing through the product composition.’ Poellmann and Blass (1994) also show a graphical method of ‘stepping up’ from the bottoms up the column based on residue curves, while Westerberg and Wahnschafft (1996) use this same method, but to ‘step down’ from the distillate.

Pinch points are an integral part of the rectification body method of Bausa et al. (1996, 1998), and they have been found by those authors by solving plate-to-plate mass and energy balances to plot column profiles, and then find the point where $x_i^n = x_i^{n+1}$, which is the discrete form of $dx_i/dn = 0$. This method is applicable to a conventional rectifying or stripping section (including the condenser or reboiler), and it finds a specific pinch point for a specified load on the condenser or reboiler (which is the equivalent of setting the reflux ratio, but it cannot be applied to a generalised column section). Alternatively,

if the load is left as an unspecified parameter, pinch point loci can be plotted with the use of continuation methods and bifurcation; the method in general was explained by Seydel and Hlaváček (1987). Continuation methods were also used by Fidkowski et al. (1991) to track pinch points (which they refer to as ‘fixed points’, differentiated from pinch points by the fact that only the latter lie on actual column profiles) in a similar manner, to overcome shortcomings of multivariable equation solvers: ‘... many multivariable equation solvers will fail to find the fixed points unless a very good guess for [the fixed point] is provided... We have found that improved performance can be obtained using continuation methods for finding fixed points.’

3.2.3 Differences between previous work and this work

It appears that all of the existing methods for finding pinch points do not meet the goals of the proposed algorithm for one or more of the following reasons: they (1) suffer from being too restrictive with the type of column configuration to which they can be applied; (2) do not find all of the pinch points; (3) only find one specific type of pinch point (e.g. tangent pinch); (4) are too limited in the complexity of system that will allow for convergence to a solution; or (5) require more complicated hybrid solution methods than the work presented in this chapter, which largely relies on standard mathematical engineering methods.

3.3 Locating pinch points

A necessary and sufficient condition for the existence of a stationary point (node) is that the derivative in Eq. (3.2) is zero for $N - 1$ components, as has already been mentioned. In other words, in order to find a pinch point on a CPM, the liquid composition vector that satisfies the following system of equations must be found:

$$\frac{dx_1}{dn} = \left(1 + \frac{1}{r_\Delta}\right)(x_1 - y_1) + \frac{1}{r_\Delta}(X_{\Delta,1} - x_1) = 0$$

⋮

$$\frac{dx_{N-1}}{dn} = \left(1 + \frac{1}{r_\Delta}\right)(x_{N-1} - y_{N-1}) + \frac{1}{r_\Delta}(X_{\Delta,1} - x_{N-1}) = 0$$

On RCMs, there are at least three pinch points, meaning that there are three or more different compositions which satisfy this system of equations; on CPMs, the number of solutions is unknown ahead of time, making the task of finding all of the solutions difficult. In both cases, the solutions depends on the initial guesses in the numerical method used to find them. This must be done numerically with non-CRV cases, since the temperature can only be found by iteration (the procedure for bubble point calculations is well-known and need not be repeated here).

When using a model as complicated as NRTL (Renon and Prausnitz, 1968), standard non-linear root-finding algorithms tend to fail. It may not be impossible with some of these algorithms, but the computational effort required is substantial, especially if no good initial guess is available; convergence cannot be guaranteed. To reiterate Fidkowski et al. (1991), ‘... many multivariable equation solvers will fail to find the fixed points unless a very good guess for [the fixed point] is provided.’

For all work in this chapter, the total system pressure, P , was set to 101 325 Pa, and the pressure was assumed to be constant throughout the column section. Only ternary systems have been considered. The NRTL model was used in the VLE calculations throughout.

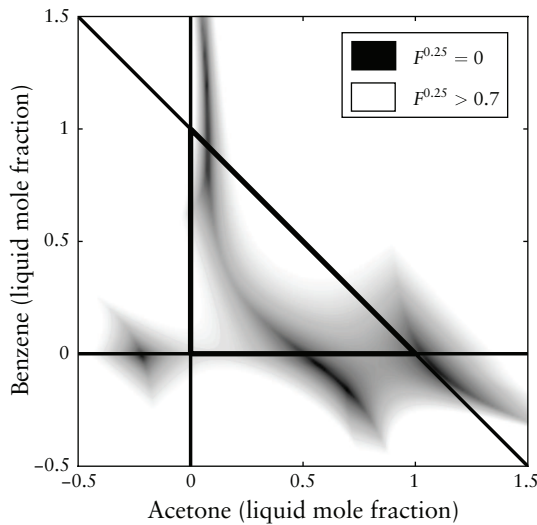
Firstly, new functions based on Eq. (3.2) are defined, as given by Eq. (3.3):

$$f_i(x_i, \dots, x_{N-1}) = \left(1 + \frac{1}{r_\Delta}\right)(x_i - y_i) + \frac{1}{r_\Delta}(X_{\Delta,i} - x_i) \quad (3.3)$$

For a ternary system, a pinch point is found at a composition for which $f_1(x_1, x_2) = f_2(x_1, x_2) = 0$, as this is equivalent to $dx_1/dn = dx_2/dn = 0$. (It was explicitly stated here that f_1 and f_2 are functions of x_1 and x_2 for emphasis. From this point on, it will be implied that this is the case.) At first glance, it may seem counterintuitive that this f_i is not a function of temperature, but of composition only; however, this arises since temperature is handled ‘internally’ within the function as it is not independent; that is, by fixing $N - 1$ liquid mole fractions and the system pressure, there are no degrees of freedom, such that T is set.

The closer an arbitrarily chosen point is to a pinch point, the closer to zero f_1 and f_2 will be. In order to find a pinch point, it is necessary that both of these functions are equal to zero.

Root-finding is most easily performed on a single function, rather than on several simultaneously. What is required is a single function whose value is

**Figure 3.4**

Contour map of $F^{0.25}$ values for the same system as in Figure 3.2. Note the correspondence between the location of the pinch points and $F^{0.25} = 0$.

zero if and only if both f_1 and f_2 are zero. A way of combining f_1 and f_2 into a single, convenient function that fulfils this criterion is shown in Eq. (3.4):

$$F(x_1, x_2) = |f_1(x_1, x_2)| + |f_2(x_1, x_2)| \quad (3.4)$$

Using Eq. (3.4), a pinch point can be described by $F(x_1, x_2) = 0$. To verify this assertion, consider the commonly used example of the ABC system. Figure 3.2 shows the CPM for this system with $X_\Delta = (0.90, 0.05, 0.05)$ and $r_\Delta = 6$, while Figure 3.4 provides a contour map of $F^{0.25}$ values with the same design parameters for visual confirmation of this notion. ($F^{0.25}$ rather than F is plotted, in order to exaggerate the contours and make them more discernible visually. It has the effect of ‘flattening’ higher values of F , but the ultimate meaning of the plot remains unchanged.) It is immediately apparent that the zero-values of F correspond exactly to the pinch points (and no other compositions) of the system. Thus, finding the compositions that give $F = 0$ will yield the location of the pinch points.

The objective is to find all of the compositions within a specified area that result in $F = 0$. All numerical methods require an initial guess, which has to be sufficiently close to the root for convergence. Moreover, without knowing the number of pinch points that a system has within the selected area, or the approximate location of the pinch points, choosing initial guesses becomes problematic. This method assumes that no information about the pinch points is available, such that the search is ‘blind’.

The procedure for the search is as follows:

- 1 Split up the area for the search into a grid of squares. For example, a square area of length 2, such as that in Figure 3.4, can be divided up into an array

of 16 square blocks of length 0.5. Each of those blocks must be checked for the presence of one or more pinch points. The purpose of the grid is to limit the number of pinch points within each block to a maximum of one or two, preferably, to decrease search time. The block being searched at any given time is referred to as the 'focus block'. Each block must be checked systematically for pinch points. To begin the search, make the first block in the main grid the focus block.

- 2 In order to look for pinch points within the focus block, an initial guess is required, but having assumed no knowledge of the topology, this guess cannot be made visually. Therefore, evaluate the F -values of, say, 300 points within the focus block; the composition that gives the smallest value of F can be used as the initial guess. In order to avoid unnecessary repetition of calculations when recursion is performed (see step 4), these points should be stored in a global database of points along with their corresponding F -values. The points can either be equally spaced, or some combination of equally spaced and randomly scattered. It is recommended to use the former, however, in order to exclude finding pinch points by chance.
- 3 With this initial guess, perform a multivariate (for x_1 and x_2 in this case) minimisation on the focus block to find the smallest value of F and the composition that corresponds to it. The multivariate minimisation algorithm used in this work was the Nelder–Mead method (Nelder and Mead, 1965). In order to limit the search to the focus block, F is introduced as a penalty function by defining it as infinity (or some very large number) for any point outside of the focus block. Alternatively, a constrained optimisation method could be used for the same purpose. The reason for using minimisation, rather than root-finding, is explained later in this section.
- 4 If the minimum F -value found in the focus block is higher than a certain tolerance ε_1 for classifying a point as a pinch point (say, $\varepsilon_1 = 1 \times 10^{-4}$), then it is considered that there is no pinch point within the focus block, and the next square on the grid becomes the focus block, for which steps 2 and 3 are carried out. If, on the other hand, the minimum value is found to be below the tolerance, a pinch point has been found. However, the fact that the algorithm converged to that pinch point does not necessarily mean it is the only one within that focus block. In order to check if this is the case, quarter the focus block itself into a new grid, and carry out steps 2 to 4 recursively on each focus block that contains a pinch point. This quartering

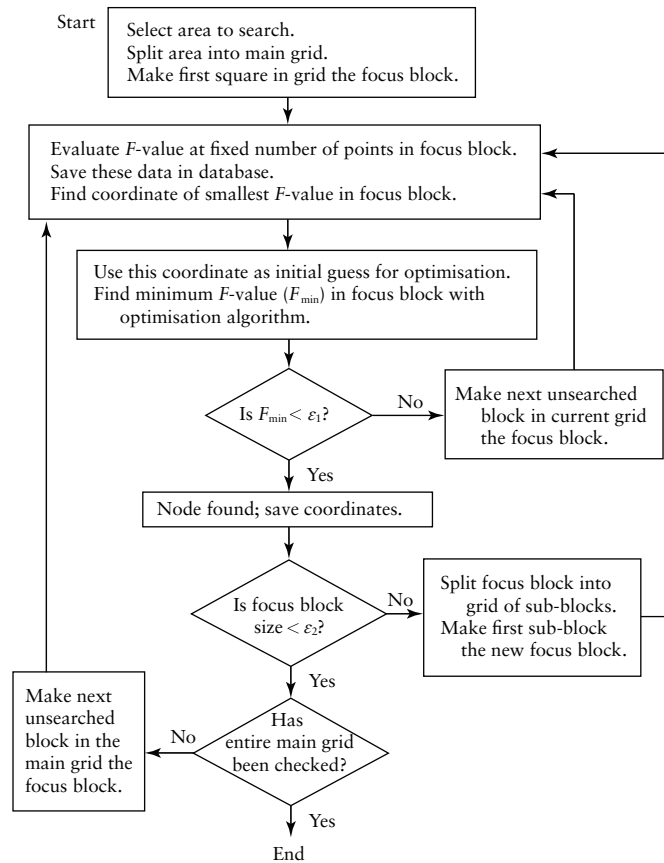


Figure 3.5 Flowchart representing the algorithm.

and searching of pinch-point-containing focus blocks is performed until some stopping criterion is fulfilled, e.g. until a focus block is smaller than a set tolerance ε_2 for the minimum allowable distance between two pinch points, say, 0.025, or some other user-specified number. Once the recursion stops, make the next unsearched block on the original grid the focus block, and repeat steps 2 to 4 until the entire area has been scanned for pinch points.

The above algorithm is represented by the flowchart in Figure 3.5. An aid for visualisation of the procedure is given in Figure 3.6, showing a comparison of the pinch point locations for the ABC system (the topology in Figure 3.2 verifies that these are all of the pinch points that exist within the shown space), the focus blocks that are used in the algorithm, and points that are evaluated as candidates for the initial guesses. A list of coordinates and pinch point types of the ABC system is given in Table 3.1. A way of determining the type of pinch point by eigenvalue methods has been described by Holland et al. (2004a), and others.

The parameters suggested above have been used in this work, but fine-tuning these values may yield more efficient location of the pinch points—for

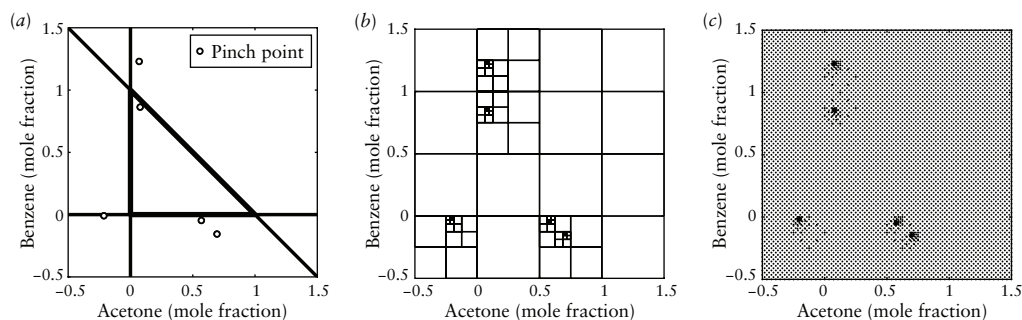


Figure 3.6 Plots showing (a) all of the pinch points of the CPM in Figure 3.2 found by the algorithm; (b) the focus blocks used in the algorithm; and (c) all of the points at which F -values are calculated by the algorithm (excluding the minimisation), as represented by the dots.

Table 3.1 Compositions and types of the ABC system pinch points at $r_{\Delta} = 6$ and $X_{\Delta} = (0.90, 0.05, 0.05)$.

No.	Composition	Type of pinch point
1	$x_p = (0.070, 1.229, -0.299)$	saddle point
2	$x_p = (0.078, 0.863, 0.059)$	stable node
3	$x_p = (-0.214, -0.009, 1.223)$	unstable node
4	$x_p = (0.569, -0.047, 0.478)$	saddle point
5	$x_p = (0.695, -0.155, 0.460)$	stable focus

example, in the recursions, only 50 or even fewer points instead of 300 can be evaluated in step 2.

There is a huge variety of computer configurations and programming languages available, both of which affect the computational time, but as an indication, it is in the order of seconds to minutes for a square area of 2×2 .

The grid of focus blocks is necessitated by the fact that for complex activity coefficient models, it has been found that using an initial guess very close to a certain pinch point can sometimes converge to a different pinch point; the grid approach forces each part of the composition space to be searched rigorously to ensure that all of the pinch points are found.

The reason that an optimisation algorithm has been chosen—rather than, perhaps more intuitively, a root-finding algorithm—is because of the nature of the search. The proposed algorithm finds all of the pinch points in a selected area, which it must do with the use of focus blocks that have few or no pinch points in them. Since there is no guarantee that there is a pinch point within a focus block—indeed, most focus blocks do not contain a pinch point—a root-finding method would have to terminate at the maximum number of iterations if the focus block has no pinch point in it. A minimisation algorithm, on the

other hand, terminates when it finds a minimum, which occurs in less than the maximum number of iterations, thereby saving computing time. Unlike, for example, the work of Drake and Manousiouthakis (2002), Burri and Manousiouthakis (2004), or Kossack et al. (2006), the optimisation used here is not for the purposes of optimising a distillation sequence/design, operation of the column, energy requirements, etc.; its actual purpose is root-finding, but in a more flexible manner than algorithms designed for that specific purpose.

One further detail which must be addressed is that sometimes the optimisation algorithm might not converge to the minimum value, but to the value of the penalty. With the F function, Nelder–Mead may fail even with the best initial guess. Counterintuitively, however, it is useful then to repeat step 3, but using the ‘second-best’ initial guess, ‘third-best’, and so on, until a satisfactory minimum is found.

Finally, once the computations have been completed, the pinch point data must also be consolidated—the search will repeatedly find the same pinch point during the recursive steps. Naturally, there will be some numerical error (the magnitude of which is determined by the optimisation algorithm’s tolerances), such that the pinch points may be described by a number of very similar, but not identical, coordinates resulting from the numerous recursions. In such a case, the coordinates with the lowest F -value in the set associated with a particular pinch point are the best approximation of the pinch point location.

This algorithm is not the most efficient way of finding the pinch points within the mass balance triangle (MBT) for the infinite reflux case: the three pure component pinch points are known *a priori*, and the binary acetone–chloroform azeotrope can be found by much simpler means, such as simple one-dimensional minimisation or root-finding method to find where $x_i - y_i = 0$. This algorithm’s true purpose becomes more apparent when (1) looking outside of the MBT (multicomponent azeotropes may exist); (2) there are multicomponent azeotropes within the MBT; or (3) the column section under consideration operates at finite reflux, and the pinch points move away from their well-known pure-component and azeotropic compositions.

3.3.1 Possible improvements

Although it has not been explored in this chapter (since absolute efficiency is not the goal), there are possible improvements that could be made to the algorithm to enhance its speed. As stated earlier, the main setback of root-

finding algorithms is that they require a good initial guess, which is why a minimisation approach was used in this work instead. However, the possibility of a hybrid algorithm exists, in which the minimisation is only used to find a good starting point using the grid approach above, and once that algorithm has found a point with a suitably low F -value, switched over to a Newton–Raphson-like algorithm to zero in on the pinch point.

3.4 Pinch point loci

When keeping X_Δ at a fixed composition (or unfixed, but with some known relationship to r_Δ) and varying the r_Δ parameter, the pinch points move in the composition space. It is possible to trace a locus of all these pinch point compositions, parameterised by r_Δ , thus providing information that is invaluable for choosing parameters in the design of columns, as is demonstrated with an example in § 3.6.

The same approach as for finding pinch points is applied, except that the full algorithm does not have to be performed, provided that a sufficiently high number of r_Δ values is used.

The procedure is as follows:

- 1 Select an area for which the pinch points are to be plotted, and find all of the pinch points at infinite reflux ($r_\Delta \rightarrow \infty$) using the pinch-point-finding algorithm described earlier for that purpose, or any other method.
- 2 Decrease the r_Δ value slightly.
- 3 Instead of repeating the first algorithm for every increment of r_Δ , which would be a lengthy process, it is far more efficient to use the previous iteration's value as a starting point for finding the pinch points of the current r_Δ , in a type of continuation method mentioned by Hoffmaster and Hauan (2004), and Fidkowski et al. (1991). This can be done provided that the r_Δ increments are sufficiently small so as to cause only minor movements in the pinch points. Thus, using the previous r_Δ value's pinch points as initial guesses, minimise the function F as given in Eq. (3.4) to find the pinch points at the current r_Δ .
- 4 Repeat steps 2 and 3 until r_Δ is nearly zero. Then, carry out steps 2 to 3 once more, but starting the algorithm with $r_\Delta \rightarrow -\infty$ (which has the same pinch points as for $r_\Delta \rightarrow \infty$, so recalculation is unnecessary) and increasing until r_Δ is almost zero.

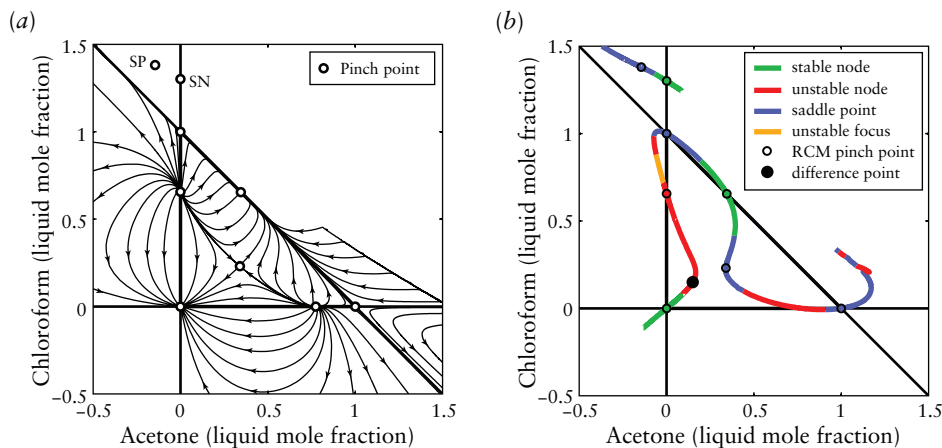


Figure 3.7 (a) RCM of the acetone–chloroform–methanol system (SP = saddle point; SN = stable node); the missing areas of the map are where the ODE solver fails; and (b) pinch point curves of the ACM system.

To test the robustness of both the pinch-point-finding algorithm (since the infinite-reflux pinch points must first be found) and the PPL algorithm, a ternary-azeotrope system will be used as an example of a highly non-ideal system. For this purpose, consider the acetone–chloroform–methanol (ACM) system, the RCM of which is given in Figure 3.7a, along with the pinch points found by the first algorithm, which are detailed in Table 3.2. The RCM has been drawn where possible, but the system exhibits several discontinuities outside of the MBT, thus limiting the areas where residue curves can be constructed, since common ODE solvers fail. The reason for these discontinuities is numerical instability in the bubble-point calculations; this is explained and discussed in general terms by Tapp et al. (2004), and Holland et al. (2004a). Note how pinch points have been found even in regions of the composition space where topological information is unavailable. One further point to address is that it may appear as though the upper part of Figure 3.7b is inconsistent in terms of topology (Fien and Liu, 1994), with a residue curve following a path from a stable node, past a saddle point, to another stable node (see pinch points 2, 3 and 5 in Table 3.2). This, however, arises because the residue curves are not continuous in that region; the discontinuities of the model cause the prediction of a pinch point’s nature to change. If the thermodynamic model did not contain discontinuities, the RCM would be topologically consistent.

For an arbitrarily chosen X_{Δ} vector of (0.15, 0.15, 0.7), the PPL is plotted in Figure 3.7b, with the node types (or stabilities) indicated by different colours. The discontinuities in the model do affect the PPL, as seen by the ‘jagged’

Table 3.2 Compositions of the ACM pinch points as found by the algorithm and their types.

No.	Composition	Type of pinch point
1	$x_p = (-0.145, 1.381, -0.236)$	saddle point
2	$x_p = (0.000, 1.302, -0.302)$	stable node
3	$x_p = (0.000, 1.000, 0.000)$	saddle point
4	$x_p = (0.000, 0.657, 0.343)$	unstable node
5	$x_p = (0.345, 0.655, 0.000)$	stable node
6	$x_p = (0.340, 0.231, 0.429)$	saddle point
7	$x_p = (0.000, 0.000, 1.000)$	stable node
8	$x_p = (0.775, 0.000, 0.225)$	unstable node
9	$x_p = (1.000, 0.000, 0.000)$	saddle point

portions of the PPL, or by points where they suddenly terminate.

The movement of the pinch points is a non-linear, but monotonic, function of r_Δ ; that is, it is relatively insensitive to changes made at high r_Δ , but very sensitive to ones made at low values of r_Δ , as it approaches zero. For example, a change of $r_\Delta = 400$ to $r_\Delta = 300$ leads to a negligible movement of the pinch points, whereas a change from $r_\Delta = 5$ to $r_\Delta = 2$ is appreciable. Thus, the spacing of the r_Δ values should not be linear, as that would result in either unnecessary calculations (and much higher computation time) if the spacing is too small, or jumps between the pinch points of consecutive r_Δ to be too large for the previous iteration's pinch points to be a good initial guess if the spacing is too large. It is difficult to say what the best distribution of r_Δ is, if indeed there exists a general optimum spacing. As a guideline, the spacing of the r_Δ values in this work was 150 logarithmically (base 10) spaced points between 300 and 1.9, and 150 linearly spaced points between 1.89 and 1×10^{-7} . The negatives of these values were used when increasing r_Δ from $-\infty$. Note that $r_\Delta = 0$ cannot be reached, as it leads to a division by zero in Eq. (3.2).

Once all of the pinch point compositions have been found, the points can be arranged and connected, if desired. The procedure for this is not entirely straightforward, but it is also not essential, nor is it an engineering problem, but a programming one; thus, it will not be detailed here.

From a plot of the PPL, the r_Δ value corresponding to a pinch point of interest can easily be calculated by letting f_i as described by Eq. (3.3) equal to zero, making r_Δ the subject of the formula, and substituting in the coordinate of the pinch point. The result is given as Eq. (3.5):

$$r_\Delta = \frac{y_i - X_{\Delta,i}}{x_i - y_i} \quad (3.5)$$

It is of significance that the r_{Δ} can be calculated by any one component i . Provided that the coordinate that is inserted into Eq. (3.5) is exact, the same r_{Δ} can be obtained with any one of the components' information (any component can serve as i in this equation, but y_i is still a function of $N - 1$ liquid mole fractions, such that the full coordinates are required). However, it is unlikely that the coordinate is known exactly from this or any other numerical method, as rounding and convergence error will be present. Consequently, Eq. (3.5) will yield slightly different r_{Δ} values, depending on which component is chosen for the calculation, and it is suggested to take the arithmetic mean of the r_{Δ} values as calculated by all N components as an attempt to mitigate these inaccuracies.

Naturally, depending on the thermodynamic model used and how well it describes the system under consideration, pinch point loci and column profiles will vary somewhat from model to model.

3.5 Finite-reflux distillation boundaries

Distillation boundaries are of great practical interest in designing distillation columns, since they represent a limit to what paths a column profile or residue curve can follow. With the knowledge of pinch point compositions, it is possible to find the distillation boundaries (at infinite or, more importantly, finite reflux) in a ternary system with a high degree of accuracy—one that is more than sufficient for design purposes. Emphasis has been placed here on finite reflux, because the traditional infinite-reflux distillation boundaries are shifted at finite reflux, allowing for a different outlook on the limits posed by distillation boundaries.

A distillation boundary is taken to mean the residue curve or column profile that originates at an unstable node, passes infinitesimally close to a saddle point, and finally terminates at a stable node.

Unlike the algorithms for finding pinch points and constructing pinch point loci, this one does rely on the simultaneous solution of the ordinary differential equations (ODEs) describing the system, given by:

$$\frac{dx_1}{dn} = \left(1 + \frac{1}{r_{\Delta}}\right)(x_1 - y_1) + \frac{1}{r_{\Delta}}(X_{\Delta,1} - x_1)$$

$$\frac{dx_2}{dn} = \left(1 + \frac{1}{r_{\Delta}}\right)(x_2 - y_2) + \frac{1}{r_{\Delta}}(X_{\Delta,2} - x_2)$$

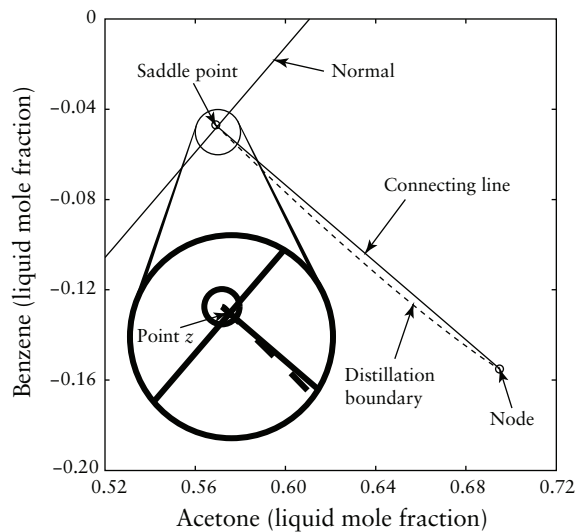
As shown by Tapp et al. (2004), the above ODEs can be integrated both backwards and forwards in n to construct a complete column section profile.

The method described here, which also assumes no prior knowledge of the system topology, centres around finding a starting point for this integration, such that the resulting profile passes sufficiently close to both a node (stable or unstable) and a saddle point to provide an accurate numerical approximation of a distillation boundary. However, in order to check that this criterion is satisfied, the location of the pinch points must first be known, which is where the pinch-point-finding algorithm is required.

Since a complete column profile will always run from an unstable node to a stable one, the main factor that distinguishes a normal column profile from a distillation boundary is its proximity to a saddle point. Given this, it may seem intuitive to use the coordinates of the saddle point as a starting point for the integration, since it is the key criterion in distinguishing that column profile as a distillation boundary. However, using any exact pinch point coordinates for this purpose is impossible, as they are stationary points; the profile would simply remain a point. Furthermore, owing to the numerical error inherent in finding the pinch point compositions in the first place, using those coordinates would repeatedly yield the same distillation boundary, which is biased by the error. Therefore, it is necessary to use a point close to the saddle point (for which knowledge of the pinch point's location—and hence the first algorithm—is needed), while making sure that it is on the same side of the boundary as the node under consideration. This is achieved by the measures taken in step 3 below.

The algorithm for finding distillation boundaries is as follows:

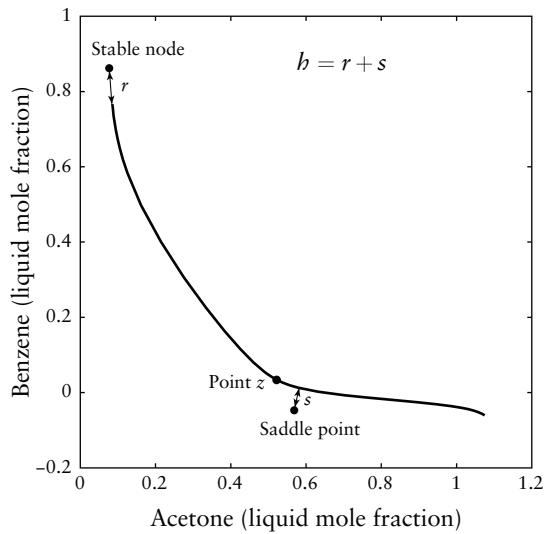
- 1 For chosen r_{Δ} and X_{Δ} parameters, find all of the pinch points, using the method presented in this chapter, or any other method. The area scanned for pinch points should be large enough to include all of the pinch points necessary to construct the distillation boundaries within the mass balance triangle, as it is in that region that distillation boundaries are of practical use. For the infinite reflux case, the area is simply that of the MBT; however, for finite reflux, it is a system- and parameter-dependent one.
- 2 Select a saddle point and node combination. The node can be stable or unstable.
- 3 Find the point z that is a small distance, say 1×10^{-3} , away from the saddle, in the direction of the node. The chosen distance must be large enough to overcome numerical errors in finding the pinch point. This ensures that the initial guess is close to the true saddle point, but still in between the saddle and

**Figure 3.8**

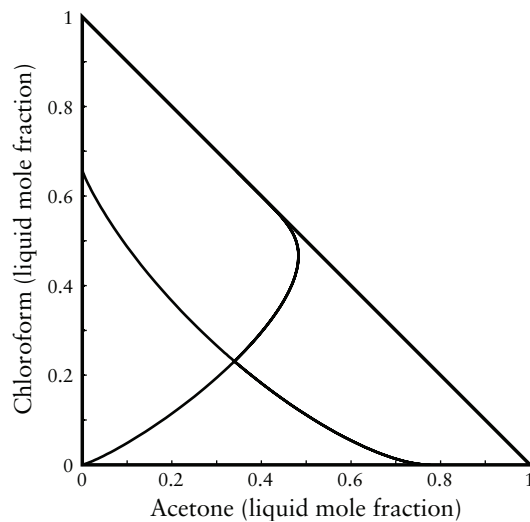
Example of the constructions required by the algorithm for finding distillation boundaries. Two of the pinch points for the ABC system at $r_{\Delta} = 6$ and $X_{\Delta} = (0.90, 0.05, 0.05)$ are shown, and a $10\times$ magnification is provided for clarity.

the node. Determine the equation of the straight line that joins the node and the saddle. Now find the equation of the normal to this line, such that the normal passes through z . See Figure 3.8 for an illustration of these constructions based on the ABC system with $r_{\Delta} = 6$ and $X_{\Delta} = (0.90, 0.05, 0.05)$.

- 4 Integrate the system of ODEs backwards and forwards for 100 (or some sufficiently high number of) stages in each direction starting from point z to obtain a curve that represents a column profile. Let r be the shortest distance between the curve and the node, and s be the shortest distance between the between the curve and the saddle point. (If calculation speed is not critical, the shortest distance between a point and a curve can be found most easily by trial-and-error, i.e. computing the distance between the point and each available coordinate that describes the curve, and then interpolating along the curve to find the minimum.) Finally, let h be the sum of r and s , i.e. $h = r + s$. (See Figure 3.9 for a graphical representation of these quantities.)
- 5 Find a starting point z for the integration that lies on the normal and minimises the function h . Again, Nelder–Mead may be used for this purpose. The starting points are restricted to the normal line because it allows the minimisation to be done on only one variable—either x_1 or x_2 —since the other variable is fixed by the equation. Moreover, the normal guarantees that there is a starting point along it, which, when minimised, will reveal a distillation boundary, if one exists.
- 6 If the minimum h that is found in step 5 is less than or equal to a certain value, say 0.02, then a distillation boundary has been found; otherwise, it is not a distillation boundary.

**Figure 3.9**

Column profile resulting from a suboptimal choice of starting point z for a distillation boundary of the ABC system at $r_{\Delta} = 6$ and $X_{\Delta} = (0.90, 0.05, 0.05)$, with integration for a small number of stages ($n = 15$) backwards and forwards from z , to allow distances r and s to be shown clearly.

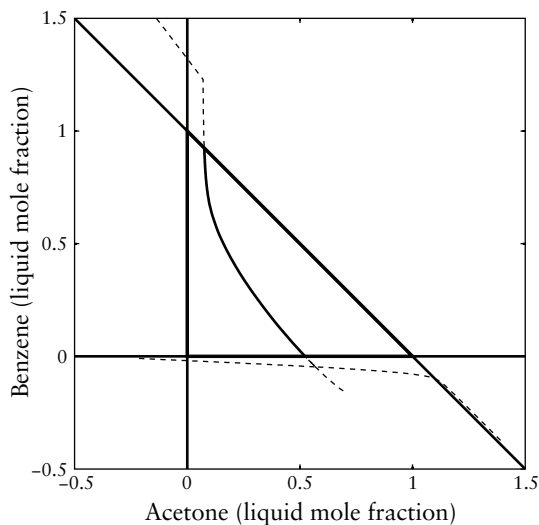
**Figure 3.10**

Demonstration that the algorithm applies to infinite reflux as well to produce traditional distillation boundaries. Pictured are the distillation boundaries of the ACM system as found by the algorithm.

- 7 Repeat steps 2 to 6 for other combinations of nodes and saddles until all of them have been checked. If the distillation boundaries within the MBT are incomplete, that is, they terminate suddenly at a point within the MBT, repeat the entire algorithm, but with an extended search area for pinch points in step 1.

In Figure 3.10, the result of the above algorithm when applied to the ACM system at infinite reflux is shown, demonstrating that it is also applicable for the construction of ‘traditional’ distillation boundaries. When compared to the RCM of the corresponding system in Figure 3.7a, it is clear that the distillation boundaries found correspond accurately to the ones observed in the RCM.

As an example of finite-reflux distillation boundaries (FRDBs), Figure 3.11 shows the distillation boundaries for the ABC system with parameters $r_{\Delta} = 6$ and $X_{\Delta} = (0.90, 0.05, 0.05)$. Figure 3.2 gives the CPM of this system, and can be used for the purposes of verification and comparison; its pinch point

**Figure 3.11**

Distillation boundaries found by the algorithm for the ABC system at $r_{\Delta} = 6$ and $X_{\Delta} = (0.90, 0.05, 0.05)$ (dashed line = boundary outside MBT; solid line = boundary inside MBT).

compositions and types were provided in Table 3.1 earlier. There is only one continuous boundary within the MBT, and it is this one that is of interest. The finite reflux case also highlights the necessity of finding nodes outside of the real space. Within the MBT, there is only one pinch point. This pinch point alone can provide no information about the distillation boundaries; the ones outside of the real space that are linked to it are required as well to allow the boundary to be found.

A few further points must be addressed. First, given that in systems with more than three components a distillation boundary is an $(N-1)$ -dimensional surface, a simple curve cannot describe it; thus, this approach is limited to ternary systems. Second, depending on the parameters chosen when finite reflux is considered, pinch points required to provide a complete construction of the distillation boundaries within the MBT may be significantly far away from the MBT, which may require a large search area and thus be computationally expensive. Third, with certain parameters, a specific pinch point required to find the distillation boundary may be positioned behind a discontinuity, thereby rendering the above algorithm impossible for the part of the boundary that requires knowledge of that pinch point and continuity between the PPs.

3.6 Unifying example: distributed-feed column

An example is presented here to unify the concepts and methods discussed in this chapter, i.e. column profile maps, pinch points, pinch point loci, X_{Δ} points outside of the real space, and finite-reflux distillation boundaries, with application to a practical problem.

The CPM method does not have any particular advantages over traditional methods for the design of simple columns, i.e. those with one feed stream, a distillate and a bottoms stream, a condenser and a reboiler, and two column sections. For more complex columns, however, it proves to be very useful. Perhaps the simplest complex column is a distributed-feed column, and, as such, it will be used for this example. An entire chapter is dedicated to distributed-feed columns with CRV systems in Holland's thesis (2005) with any number of feeds; here, a simple non-CRV example is presented, where the feed is split into only two streams, and is present as a saturated vapour. A vapour feed is used in this example because, with that feed condition, the mass balance dictates that the liquid profiles must intersect, thus simplifying visualisation of the problem. Figure 3.12 shows a schematic diagram of such a distributed-feed column. According to Holland, for sharp splits, distributed-feed columns have no advantage over single-feed columns; however, for non-sharp splits, it is possible in certain cases to obtain a reduction in reflux ratio (and hence in energy requirements), and/or a reduction in the total number of stages.

The design procedure by CPMs is the same for non-ideal systems as for CRV systems, except for one aspect: real systems do not have transform triangles as ideal systems do. With CRV systems, the lines linking the vertices of the TT (stable node, unstable node, and saddle point), are straight; for real systems, this is not true, since there is curvature in the boundaries linking the pinch points. The boundaries that link the nodes to the saddle point are simply the finite-reflux distillation boundaries discussed earlier, and account for two of the three boundaries required for a non-ideal TT. However, at this point in time, it is impossible to determine which profile that links the unstable node to the stable node represents the third boundary; as a surrogate for non-CRV transform triangles, the FRDB can be used. This, although not a complete TT, is sufficient for design purposes, as it demarcates the critical boundary.

Holland (2005) showed that distributed-feed columns are feasible in CRV systems if the top and bottom sections' transform triangles overlap (although the actual profiles themselves need not). The real system equivalent of this observation is that the FRDBs of the top and bottom sections must intersect.

This example will consider the benzene-*m*-xylene-toluene (BXT) system. It should be noted that this system is very nearly an ideal one, whereas this chapter deals with non-ideal systems. The reasoning behind this decision is as follows: the previous sections have already demonstrated that the proposed

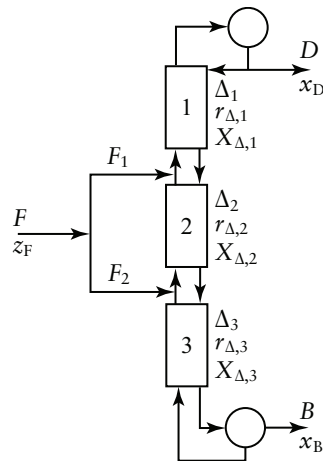


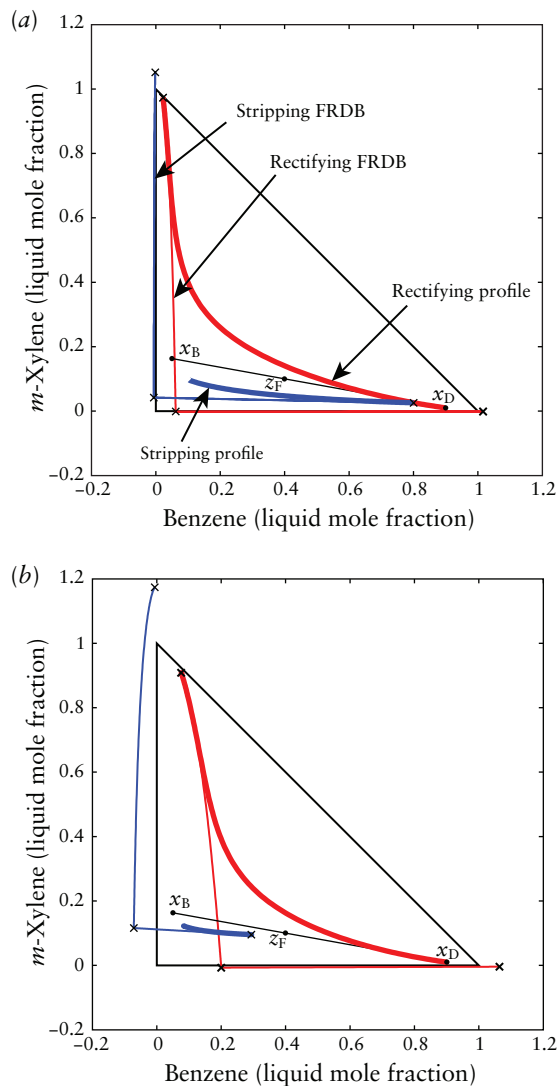
Figure 3.12
Distributed-feed column configuration, with pertinent flows and variables shown.

methods work with non-ideal systems; this example, on the other hand, is provided to demonstrate the use of finding all the pinch points, PPL, and finite-reflux distillation boundaries in the context of the CPM design method. By using a near-ideal system, the example is kept as concise as possible and avoids complications that might otherwise obscure the fundamental purpose of the example.

A saturated vapour feed with composition $z_F = (0.40, 0.10, 0.50)$ is assumed, being split into a distillate of $x_D = (0.90, 0.01, 0.09)$, and a bottoms of $x_B = (0.050, 0.163, 0.787)$; because of linear mixing rules, all three of these points lie on a straight line. Typically, product specifications are given as inequalities based on maximum allowable impurities; here, the problem is simplified somewhat and exact compositions are chosen, in order to eliminate the degrees of freedom associated with ‘looser’ product specification constraints. Assuming a feed $F = 100$ mol/s, it is easy to show by way of mass balance that $D = 41.18$ mol/s and $B = 58.82$ mol/s.

The aim is to synthesise a distributed-feed column with a lower reflux ratio than that of a conventional column performing the same split. See Figure 3.12 for an illustration of the column arrangement, and as a guide to the nomenclature.

Minimum reflux for the above split and feed in a simple distillation column is observed when the stripping profile just touches the rectifying profile, as shown in Figure 3.13a. This occurs at a reflux ratio of 10.7, i.e. $r_{\Delta,1} = 10.7$. Note that although CPMs contain all possible profiles for the chosen design parameters, only a single column profiles for each section has been shown; this is because the column profiles of sections terminated by a reboiler or condenser must go through their respective X_{Δ} points, and there exists only one such profile for each of these sections. FRDBs have been included for two

**Figure 3.13**

Split of the BXT system from $z_F = (0.50, 0.20, 0.30)$ into $x_D = (0.90, 0.01, 0.09)$ and $x_B = (0.05, 0.163, 0.787)$ in a conventional column (a) at minimum reflux ($r_{\Delta,1} = 10.7$); and (b) below minimum reflux ($r_{\Delta,1} = 3$). The crosses denote pinch points, and the FRDBs are included.

reasons: first, they give an indication of how the topology has shifted from the RCM; and second, they allow the feasibility of the distributed-feed column to be assessed by verifying intersections of the FRDBs, before any further calculations are performed. (Note that there is a jump between the start of the stripping profile and the bottoms composition, x_B . This occurs because the bottom product composition and the composition at the bottom of the stripping section are not equal; they are related by equilibrium and the mass balance around the partial reboiler. This is not true for the rectifying section, where the total condenser ensures that the distillate composition is the same as that of the reflux.)

The aim is to design the distributed-feed column to operate at a significantly lower reflux ratio than the minimum, say, $r_{\Delta,1} = 3$. Figure 3.13b shows the column section profiles of a simple column at this reflux ratio; it is clear that the profiles do not intersect, and thus the simple column is not feasible. With

the middle section (column section 2 in Figure 3.12), the goal is to create a ‘bridge’ between these separate profiles.

First, the mass balance constraints must be applied. According to the problem statement, $X_{\Delta,1}$, $X_{\Delta,3}$, and $r_{\Delta,1}$ have been specified as x_D , x_B , and 3, respectively. Furthermore, it is known that $\Delta_1 = D$ and $\Delta_3 = -B$. Since the feed is saturated vapour, and CMO is assumed, the liquid flows throughout the column are the same, i.e. $L_1 = L_2 = L_3$. From $r_{\Delta,1} \equiv L_1/\Delta_1$, it is evident that $L_1 = \Delta_1 r_{\Delta,1}$. Consequently,

$$r_{\Delta,3} \equiv \frac{L_3}{\Delta_3} = \frac{L_1}{\Delta_3} = \left(\frac{\Delta_1}{\Delta_3}\right)r_{\Delta,1}$$

such that $r_{\Delta,3}$ is also fixed. For this problem, setting $r_{\Delta,1} = 3$ as required results in $r_{\Delta,3} = -2.1$.

Therefore, the only parameters that still remain unfixed are those of the middle section, $r_{\Delta,2}$ and $X_{\Delta,2}$. However, these two parameters are not independent, as shown in Appendix B.1. The relationship between them is:

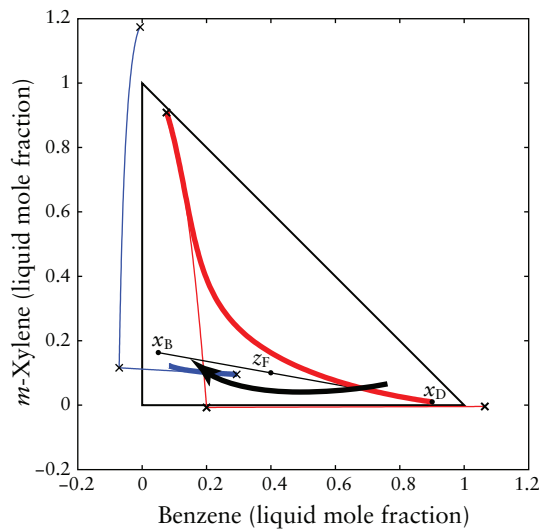
$$X_{\Delta,2} = \left(\frac{\Delta_3}{\Delta_1}\right)\left(\frac{r_{\Delta,2}}{r_{\Delta,1}}\right)(X_{\Delta,3} - z_F) + z_F \quad (3.6)$$

As such, the system has only one degree of freedom: either $r_{\Delta,2}$ or $X_{\Delta,2}$. Although either could be chosen as the independent variable, it is somewhat simpler to use $r_{\Delta,2}$, since it is a scalar, whereas $X_{\Delta,2}$ is a vector.

Having chosen $r_{\Delta,2}$ as the parameter to manipulate, it is important to determine the range of values that $r_{\Delta,2}$ is allowed to assume. CS 2 can either operate in ‘rectifying mode’ or in ‘stripping mode’. For the former, $\Delta_2 > 0$, such that the net flux of material in the CS is upwards; for the stripping mode, the opposite is true, i.e. $\Delta_2 < 0$. With mass balances around the feed points, it can be deduced that $r_{\Delta,2} \geq r_{\Delta,1}$ when CS 2 is in rectifying mode, and $r_{\Delta,2} \leq r_{\Delta,3}$ when it is in stripping mode. The proof of this given in Appendix B.2.

In order to bridge the gap between the rectifying and stripping profiles, one option is to set CS 2 to rectifying mode, and place an unstable node to the right of the rectifying profile, such that there will be at least one column profile that runs through the rectifying profile. CS 2 will be set to rectifying mode arbitrarily. Figure 3.14 is provided as a qualitative description of the desired profile behaviour of CS 2, represented as the thick black line.

The question of how to find the value or values of $r_{\Delta,2}$ that can produce the required behaviour remains. To address this question, pinch point loci can be used. For the two-distributed-feeds case, it has been shown that only one

**Figure 3.14**

Qualitative description of the desired column profile behaviour for column section 2 when it is in rectifying mode, shown by the thick black line.

independent parameter exists, which has been chosen here to be $r_{\Delta,2}$. Thus, when the $r_{\Delta,2}$ -parameterised PPL is constructed (and the stability at each point noted), all of the pinch points can be examined to see if there is a value or range of values of $r_{\Delta,2}$ that satisfy the desired behaviour in Figure 3.14; that is, an $r_{\Delta,2}$ that places an unstable node to the right of the rectifying profile.

Figure 3.15a shows a pinch point locus (indicated by the thickest lines) for $r_{\Delta,2}$ ranging from $r_{\Delta,1}$ to 100, which is applicable to CS 2 when it is in rectifying mode. The different colours of the PPL indicate the stability of the nodes, where the colours have the same meanings as in Figure 3.7b; the column profiles are black, rather than coloured, for clarity.

As established earlier, it is necessary for an unstable node of the middle column section be placed on the right of the rectifying profile. For this, the limiting reflux occurs when the unstable branch of the PPL intersects the rectifying profile at $r_{\Delta,2} \approx 9.07$, as shown in Figure 3.15a. There is a change in the stable branch (as indicated by the change from green to lime) in that the stable node becomes a stable focus as reflux is increased. Since both of these are stable, however, it does not impact on the behaviour of the profiles under consideration. The saddle point of the CPM must be roughly to the left of the stripping section's end-pinch, in order to ensure that the middle profile will intersect both end profiles; the PPL shows that saddle point moves up and slightly to the left, which is acceptable. As such, $3 < r_{\Delta,2} < 9.07$ for a feasible, non-pinch column.

Finally, a value for $r_{\Delta,2}$ must be set, which is greater than 3, and less than 9.07, but close to the latter, such as $r_{\Delta,2} = 7$; for this reflux ratio, Eq. (3.6) gives $X_{\Delta,2} = (1.5667, -0.1100, -0.4567)$, which is outside of the MBT, yet still a

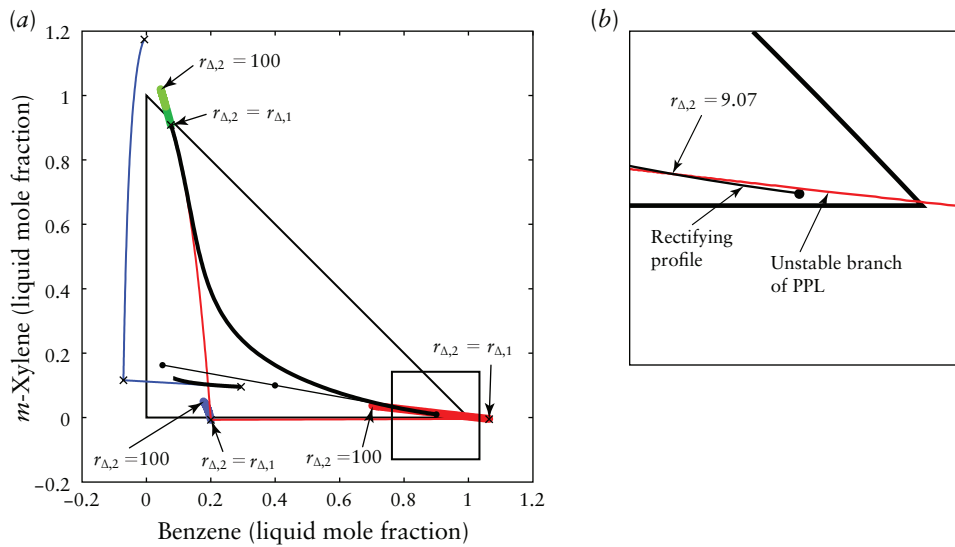
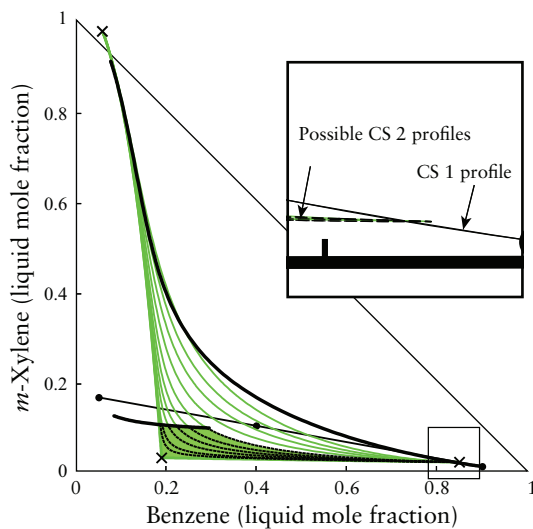


Figure 3.15 Plots of (a) pinch point loci showing the movement of CS 2's pinch points with changing $r_{\Delta,2}$ from $r_{\Delta,1}$ to 100, along with end profiles; (b) magnification showing intersection of the pinch point locus and the rectifying section profile.

perfectly valid choice. Figure 3.16 shows the two end profiles, and the CPM for the middle section for this chosen $r_{\Delta,2}$. It can be seen from the CPM which profiles are feasible; a few of these are shown as dotted profiles, but, naturally, this represents only a subset of infinite possible profiles within the shaded region. Once CS 2's parameters are chosen, a mass balance can be performed around either feed to determine the required split ratio of the original feed: in this case, $F_1 = 0.235 F$ and $F_2 = 0.765 F$. A specific profile in the CPM can be chosen for CS 2 by changing where in the column the feeds are placed (which also has an impact on the total number of stages required).

Thus, with the same feed and products, the reflux ratio has been reduced from 10.7 (the minimum reflux in a simple column) to 3, which is substantially lower, and would result in considerable energy savings. Moreover, the simple column operating at its minimum reflux requires an infinite number of stages, whereas the one produced in this example does not pinch, and thus has a finite number of stages.

A distributed-feed column has been synthesised, and it has been shown how it can reduce the reflux ratio of the column substantially. More importantly, this example illustrates the principle of the CPM design method, the significance of pinch points, pinch point loci, their effect on the topology of the CPMs, and their usefulness in the synthesis of complex columns. This example is a relatively simple one; the synthesis of Petlyuk columns with the CPM method is more involved, and has been shown by Holland et al. (2010).

**Figure 3.16**

Final construction of the two-feed column, showing the end profiles, and feasible choices for the middle one. The parameters are given in-text. A magnification is provided to show clearly how all of the possible profiles for the middle section cross the rectifying profile.

The above example gives one set of solutions to the problem, but it does not give the optimal solution: it cannot find the ‘best’, designer-specified compromise between capital and operating costs, and if, for example, an inequality is set for the product compositions, as is usually done, there are a great number of solutions to the problem.

Obviously, manual trial-and-error attempts to find the optimum would be futile. A more realistic option is optimisation using a computer; however, even for a ternary system, the number of parameters in the search space is large. Ideally, insight into the system behaviour should be gained using the CPM method in order to limit the range of parameters (recall the $r_{\Delta,2} < 9.07$ limit that was found in this example, which would change if the product specifications, feed composition, or $r_{\Delta,1}$ changed), and then apply the computerised optimisation, leading to a ‘smarter’ optimisation approach.

Such an optimisation is not dealt with in this work; however, it is clear that in order to optimise a complex column by a procedure such as the one above with the use of a computer, an automatic method is required. One of the greatest hurdles to overcome in this situation is finding all of the non-ideal pinch points without human intervention; the proposed algorithm solves this problem.

3.7 Conclusion

A new algorithm for locating nodes in generalised column sections has been proposed. It has been demonstrated to locate all of the pinch points in highly non-ideal systems successfully. An extension of the method was made to con-

struct pinch point loci, which can give valuable insight into what nodes exist in a system, even outside of the mass balance triangle, and how they can be manipulated under finite reflux conditions, and moved into or out of the positive space in the MBT.

The approach is versatile in that it can make use of any activity coefficient model (as simple or as complicated as the designer deems necessary), and in that it is applicable to any column section, which it owes to the difference point equation. Moreover, no knowledge of the topology of the system is required. No claims are made that the proposed algorithm is the most efficient way of finding nodes in certain circumstances, such as within the mass balance triangle at infinite reflux, or when the knowledge of only a single, specific pinch point is required, but it is designed to be versatile and automated; that is, it finds all of the pinch points at any reflux, for any generalised column section, inside or out of the MBT, and without the need for human intervention in achieving its goals once the design parameters are chosen. Furthermore, it can largely be implemented using widely available numerical methods, e.g. Nelder–Mead simplex minimisation.

While any method could be used to find pinch points, and a large number of starting points could be used in an attempt to find all of them with that given method as well, a critical issue remains: since the total number of pinch points at finite reflux is unknown ahead of time, it is not possible to know if all of them have been found. To address this, the proposed method introduces the focus block grid, as well as the internal subdivision and recursion within these blocks, in order to make sure that all of the pinch points are found. Indeed, the method is not efficient, but it is thorough in its search.

Finally, it was shown how the knowledge of pinch point compositions can be used to find finite-reflux distillation boundaries in ternary systems. Furthermore, it strengthens the argument for searching for pinch points outside of the mass balance triangle; at finite reflux, knowledge of the nodes outside of the triangle is necessary in order to find distillation boundaries. The method works for all infinite reflux cases, but the movement of pinch points in the composition space at finite reflux can prove to be problematic if the pinch points required to find the boundary are far from the mass balance triangle, or if they lie behind a discontinuity in the thermodynamic model.

In this chapter, only ternary systems have been considered, but in principle, the method can be extended to higher dimensions; it would simply involve looking for pinch points in $N - 1$ dimensions, and using the generalised form

of Eq. (3.4), as given by Eq. (3.7):

$$F(x_1, \dots, x_{N-1}) = \sum_{i=1}^{N-1} |f_i(x_1, \dots, x_{N-1})| \quad (3.7)$$

Naturally, PPL of these higher-order systems can also be found, although not graphically represented for systems of more than four components.

However, the number of calculations required by this method increases exponentially with each added component (and hence dimension) and may prove to be too intensive computationally for a large number of components to be practical with readily available technology at this point in time, but the principle still holds in all cases.

While this chapter has provided several useful concepts and tools, Chapter 4 presents an improved approach to finding pinch points and pinch point curves, which is more robust and orders of magnitude faster. Nevertheless, it does not completely replace this work, nor does it render the work in this chapter invalid, as many of the concepts that were developed here carry over to that work.

Chapter 4

An Efficient Method of Constructing Pinch Point Curves and Locating Azeotropes

The work in this chapter has been published in: Felbab, N., 2012. An efficient method of constructing pinch point curves and locating azeotropes in nonideal distillation systems. *Ind. Eng. Chem. Res.* 51 (20), 7035–7055. This chapter is a reproduction of that publication, with some minor corrections, and changes in style and formatting for clarity. Reproduced with permission.

Copyright © 2012 American Chemical Society. Industrial & Engineering Chemistry Research.

Abstract

An efficient, robust, ODE-based formulation of the continuation problem is presented for the automatic construction of all branches of the pinch point curves in any homogeneous distillation system (even highly non-ideal ones) that can be represented using an activity coefficient model, with any number of components, and for any adiabatic, non-reactive column configuration. Constant molar overflow is assumed. The curve is parameterised by reflux ratio, making it particularly applicable to distillation design and synthesis. Naturally, it can be used to find pinch point locations at a given finite reflux, as this is simply a subset of the pinch point curve. The method presented in this chapter can also automatically locate all N -component azeotropes very efficiently, orders of magnitude faster than commercial process simulators. It has the additional advantage of being solvable using tools already available in typical mathematical software packages. A computer implementation of the proposed method is available.

4.1 Introduction

Distillation columns are one of the chemical process industry's most prevalent separation units, and also one of the most energy-intensive. Successful design of efficient columns hinges both on the understanding of their behaviour, and on the ability to model and predict their operation sufficiently well. One particularly important phenomenon is the pinch point. Pinch points are compositions which remain constant with an increasing number of stages in the column; that is, if they are reached, no more separation is possible within that column. They denote limits of operation for a given set of design parameters.

The above criterion for a pinch point is expressed mathematically, for all i , as:

$$\frac{dx_i}{dn} = 0 \quad (4.1)$$

or, in its discrete form, as:

$$x_i^{n+1} = x_i^n \quad (4.2)$$

Stability theory identifies different types of pinch points (Fien and Liu, 1994), such as stable and unstable nodes, saddle points, and a few other peculiarities that seem to exist only outside of the mass balance triangle (MBT) (Holland et al., 2004a). All of these are described equally by Eq. (4.1).

There are effectively two main classes of column profile modelling: continuous methods, which model packed distillation columns; and discrete methods, which model tray columns. However, as long as a consistent set of assumptions is used, the choice of modelling approach does not impact on the location of the pinch points (Levy et al., 1985; Julka and Doherty, 1990; Poellmann and Blass, 1994). Even the inclusion of mass transfer resistance does not affect the pinch point locations (Baur et al., 2005).

4.1.1 Difference point equation (DPE)

The continuous modelling approach is used in this work, for reasons discussed in § 4.3.1. This approach was pioneered almost a century ago (Lewis, 1922), used by several workers throughout the early- to mid-20th century (Dodge and Huffman, 1937; Tiller and Tour, 1944; Acrivos and Amundson, 1955), and much later brought into its more popular, modern form by Van Dongen and Doherty (1985), who presented an ordinary differential equation to describe

the column profile in the rectifying or stripping sections of a conventional column. Tapp et al. (2004) and Holland et al. (2004a) then extended this equation to a form that describes a profile inside a generalised column section (CS);¹ that is, within any column configuration, regardless of complexity (Holland, 2005; Holland et al., 2010; Felbab et al., 2011). They termed this equation the difference point equation (DPE), as given in Eq. (3.2):

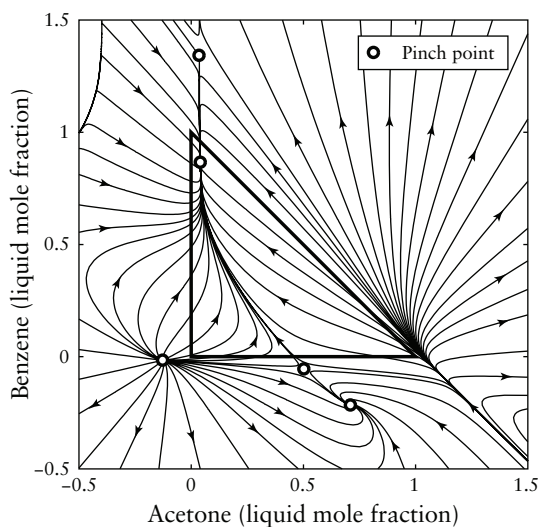
$$\frac{dx_i}{dn} = \underbrace{\left(1 + \frac{1}{r_\Delta}\right)}_{\text{separation vector}} (x_i - y_i) - \underbrace{\frac{1}{r_\Delta} (X_{\Delta,i} - x_i)}_{\text{mixing vector}} \quad (4.3)$$

where $X_{\Delta,i} = (VY_i^T - Lx_i^T)/\Delta$ (the difference point, which is effectively a pseudo-composition of the CS), $r_\Delta = L/\Delta$ (the ‘reflux ratio’ of the column section), and $\Delta = V - L$ (the net molar flux in the column section). X_Δ and r_Δ are design parameters, and (along with knowledge of how the column section fits into the overall column configuration) they are sufficient to specify a CS. Furthermore, X_Δ is a unit vector with the same number of elements as components in the system. Note that the DPE assumes constant molar overflow (CMO) and constant pressure in a CS, and is thus not appropriate for systems and configurations for which these assumptions cannot be justified.

The result of integrating Eq. (4.3) from $n = 0$ to an arbitrary stage n is the column profile in a CS with the specified design parameters. For a conventional column, or any CS terminated by a reboiler or condenser, the interpretation of the design parameters is straightforward: X_Δ is the product composition (typically denoted as x_D or x_B), and r_Δ is the reflux ratio. For a stripping section, it can easily be shown that reboil ratio is $S = -r_\Delta - 1$ (where $r_\Delta < -1$). The variable Δ , as explained earlier, is the net flux of material in the CS, and a positive value denotes a net flux upwards in the column section (i.e. $V > L$), while the converse is true for a negative value. As such, a rectifying section has $\Delta > 0$ and a stripping section has $\Delta < 0$ in any column configuration.

When a series of profiles based on Eq. (4.3) is plotted on the same graph, the result is a column profile map (CPM) (Tapp et al., 2004). Figure 4.1 is an illustration of such a map for the acetone–benzene–chloroform (ABC) system with arbitrarily chosen $X_\Delta = (0.72, 0.13, 0.15)$ and $r_\Delta = 9$. Note the pinch points on the figure. In the limit of $r_\Delta \rightarrow \infty$, it is evident that Eq. (4.3) breaks down to $dx_i/dn = x_i - y_i$, which is the well-known residue curve equation. As such, a CPM at infinite reflux is equivalent to a residue curve map (RCM).

1 A column section is defined as a section of the column in which there is no overall addition or removal of mass or energy.

**Figure 4.1**

CPM of acetone–benzene–chloroform with $r_{\Delta} = 9$ and $X_{\Delta} = (0.72, 0.13, 0.15)$.

As the reflux ratio is lowered at a constant X_{Δ} , the pinch points move in the composition space. At low enough values of r_{Δ} , these pinch points tend to ‘collide’ with one another and merge, resulting in fewer pinch points (Bausa et al., 1998; Holland et al., 2004a; Beneke et al., 2011a). For a given X_{Δ} , each pinch point has a critical r_{Δ} , past which the pinch point no longer exists. This reflux ratio will be denoted in this chapter as $r_{\Delta, \text{crit}}$, and is the reflux ratio that corresponds to the turning point as described by Fidkowski et al. (1991). For non-ideal systems, it is not possible to know the number of pinch points that exist at a certain reflux ratio *a priori* (Felbab et al., 2011).

It should be stressed that CPMs are typically plotted both within the mass balance triangle and outside of it, as in Figure 4.1. These negative compositions are physically impossible, but the information that they provide has been used extensively in the CPM design method (Holland et al., 2004b; Holland, 2005; Holland et al., 2010; Tapp et al., 2004; Holland et al., 2004a; Felbab et al., 2011). Moreover, negative compositions have been shown to be mathematically and thermodynamically consistent (Holland, 2005). Ample justification for considering negative compositions has been provided in the cited works and in Chapter 3; in summary, although a pinch point in the negative composition space can never be reached, it does influence the behaviour of the column profiles within the MBT, exactly as a pinch point within the non-negative space would. Thus, for example, if a stable node lies outside of the MBT, the profiles within the MBT will still tend towards that pinch composition, regardless of the impossibility of reaching it.

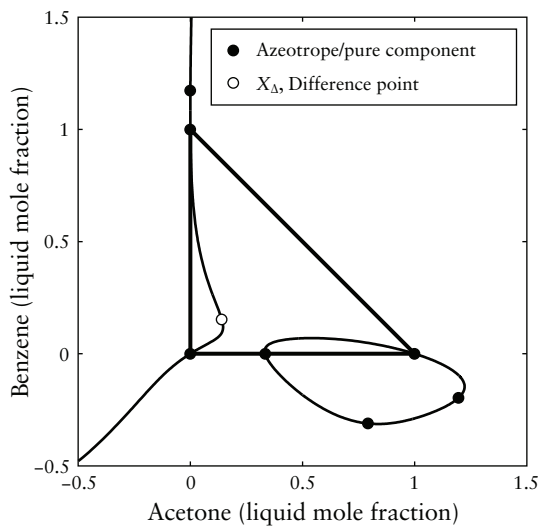


Figure 4.2
Pinch point curve of the acetone–benzene–chloroform system.

4.1.2 Pinch point curves (PPCs)

For a given set of the r_{Δ} and X_{Δ} parameters, certain pinch points exist. Their exact locations, naturally, depend on the chemical system under consideration, the chosen design parameters, and the thermodynamic model used to predict the system's behaviour. As r_{Δ} is varied, with all other factors remaining the same, the pinch points (PPs) move in the composition space in a continuous manner. This movement of PPs can be traced as a locus, or curve, known as the pinch point curve (PPC). Other terms for the PPC mentioned in the literature include pinch point locus, pinch point trajectory and pinch point branch. Given the equivalence of the residue curve equation and Eq. (4.3) at infinite reflux, the PPC must pass (at infinite reflux) through the pinch points on an RCM; that is, the pure components, as well as any azeotropes that the system contains. There are usually multiple branches of PPCs, and highly non-ideal systems (i.e. those exhibiting azeotropy) tend to have even greater complexity, and therefore even more branches. An example of highly non-ideal PPCs is given in Figure 4.2.

The locus of pinch points must terminate when it reaches $r_{\Delta, \text{crit}}$, thereby describing a 'PPC section', which spans from $r_{\Delta} \rightarrow \infty$ to $r_{\Delta, \text{crit}}$. Crucially, the adjoining PPC section terminates at the same point.

In this chapter, a new ordinary differential equation (ODE)-based method of constructing all of the branches of pinch point curves in any system—ideal to highly non-ideal—is presented.

Pinch point curves have been used for a number of applications in distillation design and analysis over the last few decades. There are three main categories of application: (1) determination of feasible regions/compositions,

(2) distillation system synthesis, and (3) reversible distillation. These applications are discussed in more detail below, highlighting the importance and usefulness of pinch point curves. The methods of calculating PPCs, which are the primary focus of this chapter, are covered in the literature review in § 4.2.

4.1.2.1 Determination of feasible regions

The impact of design variables on the possible operation of a distillation column is undoubtedly an important consideration. Other researchers have done extensive work on operating leaves (sometimes also called distillation regions in the literature), on ways of extending or manipulating them, and on applying them to systematic column sequencing (Wahnschafft et al., 1992; Wahnschafft and Westerberg, 1992; Wahnschafft et al., 1994; Castillo et al., 1998a,b; Hoffmaster and Hauan, 2002; Tapp et al., 2003; Modise et al., 2005; Krolikowski, 2006; Tian et al., 2009). The principle of operating leaves can be explained simply as follows: for a fixed product composition in a ternary system, there are two boundaries that demarcate which compositions can be attained within a column section. One is at infinite reflux, and the other is where the column pinches; both are at opposite ideal extremes of operation. In other words, one boundary is the residue curve—or the distillation line in staged columns (Castillo et al., 1998a)—that passes through the product composition, and the other is the pinch point curve, which also passes through the product composition. For relatively ideal systems, these two curves also intersect at another composition and create a leaf-shaped region in the composition space, hence the name ‘operating leaf’. Highly non-ideal systems can exhibit more complex behaviour (Hoffmaster and Hauan, 2002).

4.1.2.2 Distillation synthesis and design

Broadly, pinch point curves have been used for distillation synthesis by scanning the possible locations of all pinch points, and, if they are parameterised by a variable that is useful for design, using that knowledge to change the system behaviour as required.

An example of this is the rectification body method (RBM) of Bausa et al. (1996, 1998). A rectification body is a manifold of all possible profiles for a given column section that are contained between two related pinch points (stable node, unstable node, and/or saddle point) and the product composition in ternary systems. Systems not modelled with constant relative volatility (CRV) have curved boundaries between these pinch points. The authors

approximate these with straight lines, leading to triangular rectification bodies in ternary systems, and irregular tetrahedral ones in quaternary systems. Minimum reflux for sharp splits, for example, is found when one rectification body just touches another. The use of pinch point curves (which the authors parameterise with condenser duty and link to reboiler duty by energy balance) allows the designer to find the variables which lead to adjoining of the rectification bodies. Brüggemann and Marquardt (2004) used PPCs for the synthesis of extractive configurations in conjunction with the RBM.

The trajectory bundle theory that Serafimov et al. (1973a,b) introduced and Petlyuk and Danilov (Petlyuk and Danilov, 2001a,b, 2002; Petlyuk et al., 2007, 2008, 2009) developed further bears similarities to the RBM, but with the ability to handle non-ideal systems and their curved boundaries. It therefore relies heavily on pinch points: for example, the PPC is used to find the minimum reflux for multicomponent separations with trajectory bundle theory (Petlyuk and Danilov, 2002).

Pinch point curves are also integral to the concept of shortest stripping lines developed by Lucia and Amale (2006): their observation was that minimum energy designs are found when the reboil ratio is selected such that the length of the stripping profile from the bottoms composition to the stripping pinch point curve is minimised. PPCs were also used by Amale and Lucia (2008) to make the observation that non-pinch minimum energy solutions exist when, amongst other criteria, the system contains a stripping PPC with unstable branches.

The CPM method uses PPCs to find which reflux ratios correspond to desired pinch point locations, as shown in Chapter 3.

4.1.2.3 Reversible distillation profiles

A reversible column (that is, one that generates no entropy) can theoretically be achieved in an infinitely long column by the continuous addition or removal of heat at the correct temperature (zero temperature difference with the environment) and the elimination of other process variable gradients, e.g. pressure. It is well-established that a reversible column profile is identical to an adiabatic pinch point curve (Koehler et al., 1991; Poellmann and Blass, 1994; Petlyuk et al., 2008; Ayotte-Sauvé and Sorin, 2010). A column that pinches at every point has zero driving force for separation due to vapour–liquid equilibrium at every cross-section in the column, resulting in reversibility (Petlyuk, 2004; Ayotte-Sauvé and Sorin, 2010).

4.1.3 This work

This chapter proposes a new method of constructing pinch point curves: a continuation method formulated as an ordinary differential equation. The integration of this ODE results in the pinch point curve directly: a section of the pinch point curve is constructed from a single integration of the ODE. The proposed method uses the column section reflux ratio, r_{Δ} , as the independent variable. No other ODE-based method which is parameterised by the reflux ratio (or another distillation design variable) to construct PPCs has been presented in the open scientific literature.

A novel transform is also suggested for the proposed ODE, which gives a substantial increase in performance.

The advantages of the ODE approach over other methods are discussed in § 4.6.

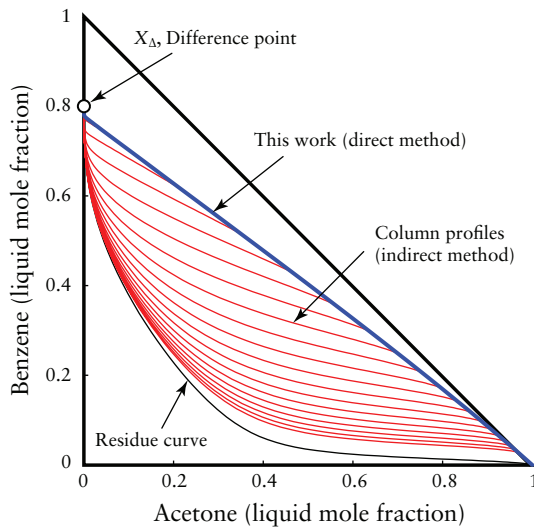
The approach proposed here is not a standalone design or synthesis method, but rather is designed to be an efficient and reliable way of obtaining the PPCs for use with other methods which require them, some of which have been mentioned in § 4.1.2.1–4.1.2.3.

There is only one other ODE-based method from which PPCs result directly (Poellmann and Blass, 1994), which, unlike the proposed ODE, is parameterised by temperature. This is discussed further in § 4.2.4.

Note that the integration of the ODE defined in Eq. (4.3), which uses stage number, n , as its independent variable, produces column profiles that can be used to find stable and unstable pinch points by driving them towards these pinch points at a high number of stages, as explained later in § 4.2.1. However, this is an indirect ODE-based way of locating pinch points, and computational effort is required to generate information (the non-pinched parts of the profile) which may be unnecessary for the problem under consideration. The difference between the direct and indirect ODE approaches is illustrated in Figure 4.3, in which the separate column profiles are plotted over a range of r_{Δ} values, each integration terminating at a discrete point on the PPC. In this figure, the blue line shows the pinch point curve resulting from one integration of the proposed ODE, unlike the several integrations required using column profiles.

The method of Poellmann and Blass (1994) has shown greater efficiency and simplicity than other approaches, according to the authors.

The method proposed in this chapter, however, is even simpler and less computationally intensive than Poellmann and Blass's, while being more robust and arguably more convenient for design purposes. This claim is sup-

**Figure 4.3**

Difference between this work (the pinch point curve ODE), and the standard column profile ODE in Eq. (3.2), illustrated with an example using the ABC system. The blue line gives the pinch point curve, which is the goal of the proposed method.

ported by a comparison of the proposed method and other major approaches, which is given in § 4.4.1 and 4.4.2.

Throughout this work, the NRTL activity coefficient model was used, unless otherwise specified, and system pressure was set to be uniform at $P = 101\,325$ Pa. The vapour phase was treated as an ideal gas.

In this chapter, § 4.2 provides a review of existing methods for finding pinch point curves; § 4.3 describes the method proposed in this work; § 4.4 provides a comparison of the proposed method with some existing ones; and § 4.5 gives examples of results using the proposed method.

4.2 Literature review

A number of methods for constructing pinch point curves can be found in the literature, all of which solve some formulation of $dx_i/dn = 0$ in Eq. (4.3), and many of which have common features. One of these features, parametric continuation, is discussed in § 4.2.3. The methods detailed here can be divided into four broad categories: (1) column profile and residue curve methods, (2) graphical methods, (3) non-linear root-finding methods, and (4) differential equations.

4.2.1 Column profile and residue curve methods

Column profiles (or residue curves, at infinite reflux) can be applied to find pinch points. From an appropriate starting point in the column section, the column profile is constructed—either by integrating Eq. (4.3), or by

performing tray-to-tray calculations—to a large number of stages, which causes the profile to approach a stable pinch point. Alternatively, negative integration, or the equivalent ‘backward’ calculation of a trayed column, can be used to approach an unstable pinch point. This principle was explained graphically in Figure 4.3. The same idea applies to residue curves, which are equivalent to a collapsed version of Eq. (4.3) at $r_{\Delta} \rightarrow \infty$, i.e. $dx_i/dn = x_i - y_i$.

This approach has been used by Lucia and Taylor (2006), who presented an algorithm to construct distillation boundaries in azeotropic systems. It is an optimisation-based method that determines the longest local residue curve (maximum line integral) joining a selected pair of stable and unstable nodes, as long as they are in the same distillation region. As a consequence of this procedure, saddle nodes can also be discovered, as they must lie on at least one distillation boundary.

The above method has been extended to finding four-component separation boundaries by Bellows and Lucia (2007). In four-component cases, the separation boundary is determined by the local maximum surface area (as determined by triangulation), with the added constraint of Levi–Civita parallelism. Bellows and Lucia stated that stable nodes were located by integrating the residue curve equation ($dx_i/dn = x_i - y_i$) using Euler’s forward method with a fixed step size of $h = 0.01$ for 30 000 steps. The method can extend to any number of components, and can also be used for finite-reflux applications. Moreover, because the method of Bellows and Lucia generates distillation boundaries, it follows that azeotropes are found as well.

Lucia et al. (2008) generalised these methods to find energy-efficient column designs by a two-stage optimisation technique. The first of these stages is a non-linear programming problem, which finds the shortest stripping line in order to calculate the minimum reboil ratio. This optimisation can result in the location of both a feed pinch and a saddle pinch, as shown in Figure 5 of Lucia et al. (2008). The fact that the optimisation algorithm must try numerous reboil ratios in its search for the shortest stripping line means that the natural course of Lucia et al.’s method will implicitly find a stable section of the PPC.

4.2.2 Graphical methods

The criterion for a pinch point is satisfied when the tangent to the residue curve at that point passes through the product composition (Wahnschafft and Westerberg, 1992; Wahnschafft et al., 1994; Poellmann and Blass, 1994;

Westerberg and Wahnschafft, 1996; Petlyuk, 2004). The simplest—although least accurate and least efficient—method of constructing pinch point curves is a graphical implementation of this principle, as was used by, e.g. Wahnschafft et al. (1994), and Westerberg and Wahnschafft (1996). For this method, a residue curve map is plotted, and points demarcated where the tangent to a residue curve passes through the product composition (the proof is straightforward, and can be obtained by setting $dx_i/dn = 0$ in Eq. (4.3) and rearranging the result). When these points are linked in the correct order, the result is a locus of pinch points, i.e. a pinch point curve. A further disadvantage of this approach is the limitation in the number of components that can be considered: systems of more than four components cannot be represented graphically.

4.2.3 Non-linear root-finding methods

Non-linear root-finding methods for PPCs effectively all have two things in common: the roots of the pinch equations are found, and continuation is used. The pinch equations that are typically used are Eq. (3.2) with $dx_i/dn = 0$, but in a less general form, e.g. specified only for the rectifying section.

Parametric continuation—or simply ‘continuation’—in the context of pinch point curves is a means of solving the pinch equation by starting at a known solution and gradually changing the value of the variable that parameterises the PPC. In this case, the starting point is most often the pure components and azeotropes, which correspond exactly to the pinch points in a column at infinite reflux. Continuation then uses the $(k - 1)^{\text{th}}$ solution as a starting point for computing the k^{th} solution, with incremental changes in the parameter of interest.

Pinch equations have been used to find pinch points and construct PPCs (Bausa et al., 1998). Details of how these solutions were found are not provided in the cited paper, but since pinch equations are given, the reader is led to assume that some sort of non-linear root-finding technique was applied. The PPCs as considered by Bausa et al. are parameterised by reboiler or condenser duty. While this does have specific applicability in design, it is limited to column sections terminated by a reboiler or condenser; in many complex configurations, there are column sections without any heat addition or removal. For example, the Petlyuk column has six column sections, four of which have no reboiler or condenser (Petlyuk et al., 1965; Halvorsen and Skogestad, 2004; Holland et al., 2010); a PPC parameterised by reboiler

or condenser duty is thus not applicable to such column sections. To circumvent this, von Watzdorf et al. (1999) parameterised the PPC in complex configurations with, for example, the sidestream flow rate in a column with a sidestream; again, however, this lacks generality.

Krolikowski (2006) also applied a non-linear root-finding method, along with continuation, but no specifics are given about the algorithm.

Lucia et al. (2008) advocated the use of the pinch equations to find pinch points, which are useful in the interpretation of their shortest stripping line optimisation procedure, discussed in § 4.2.1.

More information is provided by Fidkowski et al. (1991), who solved the pinch equations along with an arc length equation. Effectively, this allowed the authors to overcome the issue that a curve parameterised by reflux ratio (or rather, inverse reflux/reboil ratio as used in the cited paper) has a singular Jacobian at the turning point of the parameter. By adding the arc length equation, the inverse reflux ratio becomes an unknown, and arc length of the PPC becomes the parameter, which—unlike inverse reflux ratio—is monotonic. Fidkowski et al. applied a Newton–Raphson method (with optimisation of the Newton step length) to solve the pinch and arc length equations. They also state that, ‘... many multivariable equation solvers will fail to find the fixed points unless a very good guess for [the pinch point] is provided.’

Aguirre and Espinosa (1996) developed a different method to solve reversible profiles. They echo the above statements that Newton’s method requires very good initial guesses in order to be convergent and that the near-singularity of the Jacobian in the vicinity of turning points can cause failure. For constructing reversible profiles, they presented an improved, more robust version of the algorithm given by Koehler et al. (1991). Because of the shortcomings of Newton-type methods, Aguirre and Espinosa opted for a derivative-free predictor–corrector method, where the prediction is done with a secant of the last two points while the correction uses the improved algorithm to compute the exact solution. PPCs resulting from this method are parameterised by the liquid mole fraction of the heavy component.

Based on the reversible column model, a non-linear programming optimisation formulation was presented by Barttfeld and Aguirre (2002) for the solution of the PPC, which is solved as a two-step process to guarantee the optimal solution.

Hoffmaster and Hauan (2002) have reported the use of the software pack-

age AUTO97² (Doedel et al., 1998) (software for continuation and bifurcation analysis of ODEs) to solve the collinearity criterion for pinch points. The collinearity criterion is exactly equivalent to solving for $dx_i/dn = 0$ in Eq. (4.3), since it simply means that the mixing vector and separation vector sum to zero.

A computerised algorithm of the graphical method discussed earlier has been implemented by Castillo et al. (1998a). A circle in composition space with a fixed radius, and with a known pinch point at its centre, is constructed mathematically. A search is then performed on a part of this circle to find a composition which satisfies the appropriate interpretation of the collinearity criterion, i.e. the condition that the pinch point and its equilibrium vapour composition, as well as the product composition, all lie on a common straight line.

An iterative, Underwood-like method was proposed by Terranova and Westerberg (1989) for plotting pinch point temperature against condenser duty in non-ideal distillation systems, implicit in which is the determination of the pinch point location with varying reflux ratio, i.e. pinch point curves. As with all such direct-iteration methods, it is simple to implement, but requires a good initial guess and may not converge quickly.

Felbab et al. (2011) proposed a grid-search type method for automatically locating all pinch points in non-ideal distillation systems by minimising a function which represents the pinch condition. Using continuation, pinch point curves can be plotted readily. Although the search is thorough, it is not particularly efficient, and extension to more than three components may prove to be infeasible due to the computational effort required.

4.2.4 Differential equation methods

Poellmann and Blass (1994) presented an ODE that satisfies the collinearity criterion in order to determine reversible profiles. The appeal of an ODE for the purposes of constructing PPCs is that continuation is handled automatically by the very nature of the ODE algorithm when the parameterising variable is used as the independent variable in the ODE. In the cited work, the ODE was solved using the Runge–Kutta–Fehlberg technique. It has a number of advantages over other methods: for example, the method of Fidkowski et al. (1991) is more complicated than theirs, and the methods of Petlyuk et al. (1981) and

² AUTO is currently in its 2007 incarnation, known as AUTO-07p.

Köhler (1991) have solutions that jump between branches of the PPCs that are close together, whereas the ODE does not.

While the ODE method of Poellmann and Blass is indeed preferable in many ways to other methods, it does have some drawbacks: it is parameterised by pinch point temperature, which is a variable that is not particularly useful for design. Furthermore, because of the formulation of their equation, integration cannot be initiated exactly at the product composition; this problem is overcome by shifting the starting point of the integration off the product composition in the direction of the equilibrium node instead. Using products (essentially X_Δ) on the MBT boundary requires that the integration be initiated at a pinch point that is not on the same boundary as the product composition. The authors also state that the integration cannot be initiated at product compositions outside of the MBT.

Poellmann and Blass based their ODE on the function f_c , which represents the collinearity criterion, and is defined as follows:³

$$f_{c,i} = \kappa_N x_N (x_i - X_{\Delta,i}) - \kappa_i x_i (x_N - X_{\Delta,N}) + x_N X_{\Delta,i} - x_i X_{\Delta,N} = 0 \quad (i = 1 \dots N - 1) \quad (4.4)$$

Implicitly differentiating Eq. (4.4) with respect to T yields a non-homogeneous system of linear equations with dx_i/dT as the vector of unknowns. The coefficient matrix comprises partial derivatives of $f_{c,i}$ with respect to x_j , and the non-homogeneity is the partial derivative of \vec{f}_c with respect to T .

The method of Poellmann and Blass is the most obviously comparable to the work presented in this chapter, and a detailed comparison will be made later in § 4.4.1.

4.3 Ordinary differential equation

The ordinary differential equation that forms the basis of this chapter is detailed below. A brief derivation is provided in the main text, although a complete one can be found in Appendix A.4. The integration of the system of ODEs using a single starting point yields a partial branch of the pinch point curve; performing the integration numerous times using the appropriate starting points—as discussed below—enables the complete branches of the PPCs to be constructed.

³ Note that superficial modifications have been made to Poellmann and Blass's equation to conform with the notation in this thesis.

The minimum information required is the thermodynamic properties of the system, specifically vapour pressure and binary interaction parameters for the activity coefficient model of choice. Knowledge of azeotropic compositions also aids the calculation, and can be a once-off computation for each system. A number of other techniques are available for finding azeotropes (Maier et al., 1988; Bossen et al., 1993; Chapman and Goodwin, 1993; Fidkowski et al., 1993; Maranas et al., 1996; Harding et al., 1997; Wasylkiewicz et al., 1999; Gani and Bek-Pedersen, 2000; Bonilla-Petriciolet et al., 2009; Felbab et al., 2011), or the proposed method itself can be extended to find azeotropes.

A selection of practical considerations for the implementation of the method are listed in Appendix C.3.

4.3.1 Brief derivation

As with all other methods, the definition of a pinch point is the criterion used as the basis for the proposed method, i.e. at a pinch point, $x_i = x_{p,i}$, and from Eq. (4.3), the following is true:

$$\left(1 + \frac{1}{r_\Delta}\right)(x_{p,i} - y_{p,i}) + \frac{1}{r_\Delta}(X_{\Delta,i} - x_{p,i}) = 0 \quad (4.5)$$

Equation (4.5), in some form or other, is the basis for effectively every PPC algorithm.

It is important to note the dependencies of the variables. By fixing values of r_Δ and X_Δ , and assuming a fixed system pressure, all of the pinch points on a CPM are defined (Tapp et al., 2004); by fixing those design parameters, the liquid compositions corresponding to pinch points, $x_{p,i}$, are set. In other words, $x_{p,i}$ is a function of r_Δ and X_Δ only. In this brief derivation, X_Δ is taken to be constant; however, this is not the case in complex configurations, such as distributed-feed columns (Felbab et al., 2011). The full derivation allowing for variable X_Δ is included in Appendix A.4. $x_{p,i}$ is the dependent variable, and r_Δ is the independent variable. $y_{p,i}$ is the vapour mole fraction of component i in equilibrium with the liquid mixture at the pinch point, $x_{p,i}$, and it is a function of $x_{p,1}, \dots, x_{p,N-1}$ only, as dictated by the bubble point calculation for a set system pressure P .

By differentiating Eq. (4.5) with respect to r_Δ and rearranging, the following is obtained:

$$\frac{dx_{p,i}}{dr_\Delta} - \left(1 + \frac{1}{r_\Delta}\right) \frac{dy_{p,i}}{dr_\Delta} = \frac{1}{r_\Delta^2}(X_{\Delta,i} - y_{p,i}) \quad (4.6)$$

In Eq. (4.6), the derivative $dy_{p,i}/dr_\Delta$ can be arranged into a convenient form by taking the total derivative of $y_{p,i}$ and dividing through by dr_Δ , such that:

$$\frac{dy_{p,i}}{dr_\Delta} = \sum_{j=1}^{N-1} \left(\frac{\partial y_{p,i}}{\partial x_{p,j}} \right) \frac{dx_{p,j}}{dr_\Delta} \quad (4.7)$$

Upon substitution of Eq. (4.7) into Eq. (4.6):

$$\frac{dx_{p,i}}{dr_\Delta} - \left(1 + \frac{1}{r_\Delta} \right) \left[\sum_{j=1}^{N-1} \left(\frac{\partial y_{p,i}}{\partial x_{p,j}} \right) \frac{dx_{p,j}}{dr_\Delta} \right] = \frac{1}{r_\Delta^2} (X_{\Delta,i} - y_{p,i}) \quad (4.8)$$

Equation (4.8) cannot be rearranged to make $dx_{p,i}/dr_\Delta$ the subject of the formula explicitly.

In order to better understand Eq. (4.8), it is useful to first consider a system of three components, i.e. $N = 3$. For this case,

$$\begin{aligned} \frac{dx_{p,1}}{dr_\Delta} - \left(1 + \frac{1}{r_\Delta} \right) \left[\left(\frac{\partial y_{p,1}}{\partial x_{p,1}} \right) \frac{dx_{p,1}}{dr_\Delta} + \left(\frac{\partial y_{p,1}}{\partial x_{p,2}} \right) \frac{dx_{p,2}}{dr_\Delta} \right] &= \frac{1}{r_\Delta^2} (X_{\Delta,1} - y_{p,1}) \\ \frac{dx_{p,2}}{dr_\Delta} - \left(1 + \frac{1}{r_\Delta} \right) \left[\left(\frac{\partial y_{p,2}}{\partial x_{p,1}} \right) \frac{dx_{p,1}}{dr_\Delta} + \left(\frac{\partial y_{p,2}}{\partial x_{p,2}} \right) \frac{dx_{p,2}}{dr_\Delta} \right] &= \frac{1}{r_\Delta^2} (X_{\Delta,2} - y_{p,2}) \end{aligned}$$

The above system is simply a system of linear equations in $dx_{p,1}/dr_\Delta$ and $dx_{p,2}/dr_\Delta$. To make this more evident, it can be written as:

$$\begin{aligned} \left[1 - \left(1 + \frac{1}{r_\Delta} \right) \left(\frac{\partial y_{p,1}}{\partial x_{p,1}} \right) \right] \frac{dx_{p,1}}{dr_\Delta} - \left(1 + \frac{1}{r_\Delta} \right) \left(\frac{\partial y_{p,1}}{\partial x_{p,2}} \right) \frac{dx_{p,2}}{dr_\Delta} \\ = \frac{1}{r_\Delta^2} (X_{\Delta,1} - y_{p,1}) \\ - \left(1 + \frac{1}{r_\Delta} \right) \left(\frac{\partial y_{p,2}}{\partial x_{p,1}} \right) \frac{dx_{p,1}}{dr_\Delta} + \left[1 - \left(1 + \frac{1}{r_\Delta} \right) \left(\frac{\partial y_{p,2}}{\partial x_{p,2}} \right) \right] \frac{dx_{p,2}}{dr_\Delta} \\ = \frac{1}{r_\Delta^2} (X_{\Delta,2} - y_{p,2}) \end{aligned}$$

The general case of this linear system—for N components—can most easily be expressed in matrix notation:

$$A\vec{d} = \vec{b} \quad (4.9)$$

where

$$\mathbf{A} = \mathbf{I}_{N-1} - \left(1 + \frac{1}{r_\Delta}\right)\mathbf{J} \quad (4.10)$$

$$\mathbf{J} = \begin{bmatrix} \frac{\partial y_{p,1}}{\partial x_{p,1}} & \frac{\partial y_{p,1}}{\partial x_{p,2}} & \cdots & \frac{\partial y_{p,1}}{\partial x_{p,N-1}} \\ \frac{\partial y_{p,2}}{\partial x_{p,1}} & \frac{\partial y_{p,2}}{\partial x_{p,2}} & \cdots & \frac{\partial y_{p,2}}{\partial x_{p,N-1}} \\ \vdots & \vdots & \ddots & \vdots \\ \frac{\partial y_{p,N-1}}{\partial x_{p,1}} & \frac{\partial y_{p,N-1}}{\partial x_{p,2}} & \cdots & \frac{\partial y_{p,N-1}}{\partial x_{p,N-1}} \end{bmatrix} \quad (4.11)$$

$$\mathbf{I}_{N-1} = \begin{bmatrix} 1 & 0 & \cdots & 0 \\ 0 & 1 & \cdots & 0 \\ \vdots & \vdots & \ddots & \vdots \\ 0 & 0 & \cdots & 1 \end{bmatrix} \quad (4.12)$$

$$\vec{d} = \begin{bmatrix} \frac{dx_{p,1}}{dr_\Delta} \\ \frac{dx_{p,2}}{dr_\Delta} \\ \vdots \\ \frac{dx_{p,N-1}}{dr_\Delta} \end{bmatrix} \quad (4.13)$$

$$\vec{b} = \frac{1}{r_\Delta^2} \begin{bmatrix} X_{\Delta,1} - y_{p,1} \\ X_{\Delta,2} - y_{p,2} \\ \vdots \\ X_{\Delta,N-1} - y_{p,N-1} \end{bmatrix} \quad (4.14)$$

The solution vector \vec{d} of Eq. (4.9) gives the definition of the proposed ODE. The practical meaning of this statement is the following: ODE solvers used to solve equations of the form $dy/dt = f(t, y)$ operate on functions of the general form $dydt=ode(t, y)$. In this context, the t argument is r_Δ , and the y argument is the vector of pinch points \vec{x}_p that corresponds to the given r_Δ . On each call to this ode function, the arguments r_Δ and \vec{x}_p are used to solve the linear system given by Eq. (4.9), to produce the vector \vec{d} , which is the required output $dydt$.

Any activity coefficient model that satisfactorily describes the system can

be used. The Jacobian matrix \mathbf{J} can be evaluated either by using numerical derivatives directly with $N - 1$ bubble point calculations, or preferably, by using the non-iterative method described in Appendix C.2, which yields much higher efficiency than the former. For constant relative volatility, (somewhat lengthy) algebraic expressions can be obtained for the above.

If X_Δ is not constant, but rather has a known relationship to r_Δ , as is encountered in complex columns (Holland, 2005; Felbab et al., 2011), then the vector \vec{b} is defined as follows, the proof of which can be found in Appendix A.4:

$$\vec{b} = \frac{1}{r_\Delta} \begin{bmatrix} \frac{1}{r_\Delta}(X_{\Delta,1} - y_{p,1}) - \frac{dX_{\Delta,1}}{dr_\Delta} \\ \frac{1}{r_\Delta}(X_{\Delta,2} - y_{p,2}) - \frac{dX_{\Delta,2}}{dr_\Delta} \\ \vdots \\ \frac{1}{r_\Delta}(X_{\Delta,N-1} - y_{p,N-1}) - \frac{dX_{\Delta,N-1}}{dr_\Delta} \end{bmatrix} \quad (4.15)$$

4.3.2 Independent variable transform

Solving the ODE as defined above provides the correct result with good efficiency.

However, the effect of r_Δ on $x_{p,i}$ is highly non-linear (Felbab et al., 2011), where at high $|r_\Delta|$, a large change in r_Δ will have a very small effect on $x_{p,i}$, but at low $|r_\Delta|$, tiny changes can lead to large movements in the pinch points. This non-linearity leads to unnecessary solutions of the ODE at high $|r_\Delta|$ where pinch point movement is negligible.

A way of circumventing this is proposed here, by the introduction of a new variable:

$$\rho^+ \equiv \frac{r_\Delta}{r_\Delta + 1} \quad (r_\Delta \geq 0) \quad (4.16)$$

The reason for the superscript ‘+’ in Eq. (4.16) will become apparent shortly. Note the behaviour of the variable ρ^+ : as $r_\Delta \rightarrow \infty$, $\rho^+ \rightarrow 1$, and as $r_\Delta \rightarrow 0$, $\rho^+ \rightarrow 0$. This has the effect of limiting the variable ρ^+ to the range $(0, 1)$ instead of r_Δ 's range of $(0, \infty)$. Furthermore at high ρ^+ , a small change in that variable leads to a large change in r_Δ , which in turn moves the pinch points by a small amount. As a result, $x_{p,i}$ is far more linearly dependent on

ρ^+ , and the latter would serve much better as the independent variable to the proposed ODE.

Unfortunately, however, a plot of ρ^+ against r_Δ reveals that the behaviour of ρ^+ is not symmetrical for positive and negative r_Δ values, and indeed approaches ∞ as r_Δ tends to -1 .

To achieve symmetrical behaviour, negative r_Δ values must be transformed with a different, although very similar, variable:

$$\rho^- \equiv \frac{r_\Delta}{r_\Delta - 1} \quad (r_\Delta \leq 0) \quad (4.17)$$

Indeed, numerical experiments have shown that using ρ^+ and ρ^- as the independent variables in the proposed ODE results in a speed increase of approximately 40–60% compared to using r_Δ as the independent variable.

In order to implement these new variables in the ODE, the matrix \mathbf{A} and vectors \vec{d} and \vec{b} , given in Eqs (4.10), (4.13), and (4.14), respectively, are redefined, as shown below in § 4.3.2.1 and 4.3.2.2. The ODE is still defined by the solution of Eq. (4.9), but using these new definitions of \mathbf{A} , \vec{d} , and \vec{b} .

ρ^\pm will be taken to mean either ρ^+ or ρ^- , whichever is appropriate to the context.

4.3.2.1 Transform of ODE for rectifying sections (positive r_Δ)

For $r_\Delta > 0$, Eq. (4.9) is solved for \vec{d} using the following definitions:

$$\mathbf{A} = (\rho^+ - 1)^2 \left(\mathbf{I} - \frac{1}{\rho^+} \mathbf{J} \right)$$

$$\vec{d} = \begin{bmatrix} \frac{dx_{p,1}}{d\rho^+} \\ \frac{dx_{p,2}}{d\rho^+} \\ \vdots \\ \frac{dx_{p,N-1}}{d\rho^+} \end{bmatrix}$$

$$\vec{b} = \left(\frac{1 - \rho^+}{\rho^+} \right)^2 \begin{bmatrix} (X_{\Delta,1} - y_{p,1}) \\ (X_{\Delta,2} - y_{p,2}) \\ \vdots \\ (X_{\Delta,N-1} - y_{p,N-1}) \end{bmatrix}$$

4.3.2.2 Transform of ODE for stripping sections (negative r_Δ)

For $r_\Delta < 0$, Eq. (4.9) is solved for \vec{d} using the following definitions:

$$\mathbf{A} = -(\rho^- - 1)^2 \left[\mathbf{I} - \left(2 - \frac{1}{\rho^-} \right) \mathbf{J} \right]$$

$$\vec{d} = \begin{bmatrix} \frac{dx_{p,1}}{d\rho^-} \\ \frac{dx_{p,2}}{d\rho^-} \\ \vdots \\ \frac{dx_{p,N-1}}{d\rho^-} \end{bmatrix}$$

$$\vec{b} = \left(\frac{1 - \rho^-}{\rho^-} \right)^2 \begin{bmatrix} (X_{\Delta,1} - y_{p,1}) \\ (X_{\Delta,2} - y_{p,2}) \\ \vdots \\ (X_{\Delta,N-1} - y_{p,N-1}) \end{bmatrix}$$

Note that the transform to ρ^\pm that has just been proposed should be used in favour of the approach in § 4.3.1 for improved efficiency. The remainder of the text, however, discusses r_Δ values, for more intuitive interpretation. In order to use those values with the ρ^\pm transform, the r_Δ values must first be transformed to the appropriate ρ^\pm values using Eqs (4.16) and (4.17). The solution of the ODE will return a vector of ρ^\pm values, which can be converted back to r_Δ using the reverse operation.

4.3.3 Solution

In this section, it is assumed that all of the azeotropes are known; pure components are known *a priori*. The problem can also be extended quite easily to use only the pure components as starting points, and to discover the azeotropes, if any exist, during the course of the integration; this is discussed later in the text in § 4.3.4.

4.3.3.1 Starting point

The above system of ODEs can be integrated from the appropriate initial value, which can be any known pinch point position at a known r_Δ . The most

convenient strategy is to use the knowledge that as $r_{\Delta} \rightarrow \pm\infty$, the pinch points are located at pure components and azeotropes. (Note that the azeotropes must correspond exactly to the activity coefficient model used, i.e. predictions of azeotropes using one model should not be used with another model.) Using these starting points has two main advantages: firstly, the information is usually readily available or calculable, and secondly, as explained earlier in this chapter, as $|r_{\Delta}|$ is decreased, a given pinch point tends to ‘disappear’ or ‘merge’ with another pinch point below a certain critical reflux ratio for that pinch point (Bausa et al., 1998; Holland et al., 2004a; Beneke et al., 2011a); as such, at infinite reflux, the maximum possible number of pinch points exists, which means that the most information is available to construct the entire PPC.

Initiating the integration directly from infinity is not numerically possible. However, at high $|r_{\Delta}|$, the locations of pinch points are highly insensitive to changes in r_{Δ} (Felbab et al., 2011), such that a sufficient approximation typically is to initiate the integration at $|r_{\Delta}| = 1 \times 10^{14}$. Therefore, when considering stripping sections where the r_{Δ} values are negative, the $r_{\Delta} \rightarrow -\infty$ starting point can be replaced with $r_{\Delta} = -1 \times 10^{14}$.

A better starting point, however, is to set $|r_{\Delta}| = 1 \times 10^{14}$, but then to calculate the pinch point at that r_{Δ} value using Newton’s method. The offset from the pure component or azeotrope is truly minuscule at such a high r_{Δ} , meaning that convergence of Newton’s method is practically guaranteed and requires one or two iterations at most, but the increase in accuracy of the proposed method is noticeable. As such, this offset starting point is suggested in favour of the exact pure component or azeotrope, although it is not strictly required.

4.3.3.2 Termination point

If the entire PPC is required, the integration should stop at $r_{\Delta} \rightarrow 0$, or at the smallest value of r_{Δ} for which the pinch point still exists. The limit ($r_{\Delta} \rightarrow 0$), rather than the equality ($r_{\Delta} = 0$) is used, since division by zero would be encountered with the latter in the ODE. A sufficient numerical approximation is to use $r_{\Delta} = \pm 1 \times 10^{-14}$.

Recall that there is a critical reflux ratio, $r_{\Delta, \text{crit}}$, for a pinch point before it ‘disappears’. If the end-point r_{Δ} is set such that a pinch point can never reach it, the ODE solver—depending on its design—may enter an infinite loop trying to progress beyond that point. This phenomenon is the ‘turning point’

mentioned in the literature (Fidkowski et al., 1991; Aguirre and Espinosa, 1996). A special provision must be made for this in the ODE solver routine: if two successful successive steps are spaced sufficiently close together—that is, if the relative difference between the two successive r_Δ values is less than a set tolerance—the integration must be terminated.

Therefore, integration for the full PPC is carried out from $r_\Delta = 1 \times 10^{14}$ to $r_\Delta = \max\{1 \times 10^{-14}, r_{\Delta,\text{crit}}\}$ and from $r_\Delta = -1 \times 10^{14}$ to $r_\Delta = \min\{-1 \times 10^{-14}, r_{\Delta,\text{crit}}\}$. Note that the signs of the integration bounds must be the same for a given integration; also note that $r_{\Delta,\text{crit}}$ cannot be known beforehand, such that the zero approximation ($\pm 1 \times 10^{-14}$) is only ever specified by the user. As such, the ODE algorithm must have provision to exit at $r_{\Delta,\text{crit}}$ when it is detected, as described above.

If only pinch points at a specific r_Δ are required, the integration can be terminated at the specified value. The final composition reached at the end of the integration gives the pinch point, with one caveat: the same potential issue as with PPC exists in that the chosen reflux may be beyond the critical reflux of a given pinch point section, and the integration—using the abovementioned provision—will terminate at the critical reflux ratio, as it cannot reach the desired one.

Inherent in the ODE algorithm's output is information about the independent variable, r_Δ , values corresponding to each of the liquid compositions that describes the PPC; if the final r_Δ is not the one that was set as the end-point of the integration, it means that the integration terminated at $r_{\Delta,\text{crit}}$, and the pinch point can be disregarded, as it does not correspond to the selected r_Δ .

4.3.4 Automatic azeotrope discovery

If azeotrope information is not available, the proposed method can easily be extended to find the azeotropes automatically.

As explained earlier, integration from infinity stops at $r_{\Delta,\text{crit}}$, at which matrix **A** becomes singular and a 'turning point' is reached. In order to 'jump' over this turning point onto the adjoining PPC section, a simple arc length extrapolation can be performed.

The arc length is computed for the PPC from the infinite-reflux pinch point (pure component or azeotrope) to the $r_{\Delta,\text{crit}}$, which is then extended by a small calculated or fixed value, such as 1×10^{-3} , by means of non-linear extrapolation. This provides a liquid composition which is on the adjoining

section of the PPC, beyond the threshold of the turning point. Since the extrapolation amount is so small, it is a very reliable approximation.

The r_Δ corresponding to this extrapolated composition on the adjoining PPC section can be calculated. In order to do this, Eq. (4.5) is rearranged to make r_Δ the subject of the formula, resulting in the following:

$$r_\Delta = \frac{X_{\Delta,i} - y_{p,i}}{y_{p,i} - x_{p,i}} \quad (4.18)$$

With a known pinch point liquid composition, x_p , and the vapour in equilibrium with it, y_p , any component i can be used in Eq. (4.18). For the exact pinch point, any component used as i will give the same r_Δ . Because of the inherent numerical error in both the integration and the extrapolation, however, there will always be a slight difference between the r_Δ calculated using different components as i ; in effect, N slightly different r_Δ values can be obtained using each of the N components as i . The best approach for choosing the optimal r_Δ from the available selection of values is to use the F function of Felbab et al. (2011), defined as follows:

$$F(x_1, \dots, x_{N-1}, r_\Delta, X_\Delta) = \sum_{i=1}^{N-1} |f_i(x_1, \dots, x_{N-1}, r_\Delta, X_\Delta)| \quad (4.19)$$

where

$$f_i(x_1, \dots, x_{N-1}, r_\Delta, X_\Delta) = \left(1 + \frac{1}{r_\Delta}\right)(x_i - y_i) + \frac{1}{r_\Delta}(X_{\Delta,i} - x_i) \quad (4.20)$$

For a pinch point, $f_i = 0$ for all i . The function F is formulated such that it can only be zero if, and only if, all f_i are zero. With this information—along with the known values of x_i , y_i and X_Δ —each candidate r_Δ can be tried in Eq. (4.19); the one resulting in the smallest F is the most accurate r_Δ .

Alternatively, since x_i , y_i , and X_Δ are fixed, a simple one-dimensional minimisation in r_Δ can be performed on Eq. (4.19) to find the optimal r_Δ ; Eq. (4.18) provides an excellent initial guess for this minimisation. Both approaches are computationally inexpensive.

Finally, integrating from this new point at its calculated r_Δ to infinity, or rather, the $r_\Delta = \pm 1 \times 10^7$ approximation of infinity, ends at an azeotrope or pure component. If this technique is used after integration has been performed from all of the pure components, and if redundant calculation of PPC sections is avoided, then this will only yield azeotropes.

It is suggested to refine the located azeotrope using Newton's method,

which should converge in very few iterations, as the end-point of the integration is a very good approximation of the actual azeotrope.

Note that in highly non-ideal systems—which may have azeotropes both inside and outside the MBT—there may be branches of the PPC which do not pass through the pure components at all, depending on the choice of X_{Δ} . Consequently, discovery of those azeotropes, and indeed, the associated PPC branches, cannot be guaranteed with this method, although these branches are unlikely to have any practical use in conjunction with the selected X_{Δ} .

The use of a variety of X_{Δ} locations, and logging a database of the found azeotropes, however, is likely to yield most or all of the azeotropes outside of the MBT eventually.

4.4 Comparison with other methods

This section details how the proposed method compares with other methods for constructing pinch point curves, as well as how it performs in methods which use pinch points implicitly. The example used for the latter is the minimum energy algorithm of Lucia et al. (2008).

Details are provided in the text below, but the results can be summarised as follows:

- The proposed method is faster than the ODE of Poellmann and Blass (1994), as well as more numerically robust, and is in a form that is more applicable to distillation design.
- In comparison with traditional continuation methods, the proposed method offers somewhat (10–30%)⁴ better performance, is not susceptible to branch switching like the former, and is more readily solved with standard mathematical software packages.
- Use of the proposed method in conjunction with Lucia et al.'s (2008) algorithm leads to appreciably faster computation of the minimum reboil ratio than the original, but has the drawback that the results are only reliable for packed stripping sections; for staged stripping sections—in some cases—too low a reboil ratio leads to instability which is not observed in packed column. As a result, only a subset of the full PPC is applicable to staged columns, and there is no *a priori* way of determining this subset. Therefore, the use of the

⁴ These numbers are dependent on the algorithms used in either case, and should be considered as indicative, not conclusive.

proposed algorithm does not give the correct answer in all cases for a staged stripping section, and the original method of Lucia et al. should be utilised in that context.

4.4.1 Comparison with Poellmann and Blass's method

As briefly described earlier, Poellmann and Blass (1994) presented an ODE-based method for constructing PPCs which was superior to others. Since it is the only other ODE-based method for this purpose, it serves as the most apt subject for comparison with the proposed method.

By differentiating the $f_{c,i}$ function, defined by Eq. (4.4), implicitly with respect to T , Poellmann and Blass obtained a non-homogeneous system of linear equations—similarly to the proposed method—except with the ODE defined in terms of the derivative dx_i/dT . This system of linear equations is defined as follows:

$$\left(\frac{\partial f_{c,i}}{\partial x_j}\right)\left(\frac{dx_i}{dT}\right) = -\left(\frac{\partial f_{c,i}}{\partial T}\right) \quad (4.21)$$

for i and $j = 1 \dots N - 1$.

Mole fraction summation to one is ensured in the $(\partial f_{c,i}/\partial x_j)$ matrix as well as in (dx_i/dT) .

Poellmann and Blass expanded all of the partial derivatives in Eq. (4.21) to expressions involving partial derivatives of κ , P^{vap} , γ , and x_i with respect to T and x_j , all of which can be evaluated analytically. The exact expressions are fairly complicated, and can be found in § 3.8, Appendix A of Poellmann and Blass (1994).

One of the most significant differences in the derivation of the proposed method and the Poellmann–Blass (PB) method is that the latter obtained a constant c that relates the two vectors required for the collinearity criterion, $x - X_\Delta$ and $y - x$. They then cancelled out this c by using components i and k , where $i \neq k$, and equating the two expressions. This work, on the other hand, recognises that the constant c is, in fact, $-(r_\Delta + 1)$ —which can be proved by simple manipulation of Eq. (4.5)—and does not attempt to remove it from the calculation. As such, it is then possible to use r_Δ (or its simple transform to ρ^\pm) as the integration variable.

These two different approaches lead to ODEs with very different characteristics. A practical comparison of the proposed method and the PB method is given below.

Note that Poellmann and Blass obtained analytical expressions for their entire calculation; this requires compositional and temperature derivatives of the activity coefficient model ($\partial\gamma_i/\partial x_j$ and $\partial\gamma_i/\partial T$, respectively), as well as temperature derivatives of the vapour pressure model (dP_i^{vap}/dT). While using analytical expressions does increase numerical stability in the calculations, it requires the user to have not only the chosen models available, but also their various derivatives, which are often not easy to obtain for the more complicated activity coefficient models (Taylor and Kooijman, 1991). Moreover, it introduces an additional potential source of error, both in the mathematics and in the programming. To avoid this, both methods are compared on the basis of the abovementioned derivatives being evaluated numerically by forward differences, thereby requiring the user to define only the appropriate models.

4.4.1.1 Parameterising variable

The parameterising variable used by Poellmann and Blass is temperature, which has both inherent advantages and disadvantages. The most significant advantage of having T as an independent variable is that it avoids bubble point calculations altogether, because T never has to be calculated. On the other hand, although the pinch point curves are obtained, the information that is directly available from the ODE solution is the pinch point temperatures along the PPC, which has only minor usefulness for design purposes.

The proposed method uses the ρ^\pm variable (which is directly related to the generalised column section reflux ratio, r_Δ) for the parameterisation, which is arguably more pertinent to design. Furthermore, the method presented in this chapter need only use the pure components as starting points, whereas that of Poellmann and Blass must be initiated at the pure components and azeotropes, as well as at X_Δ . Even if arc length extrapolation were to be used in conjunction with the Poellmann–Blass method, azeotropes cannot be identified using temperature, whereas the same is not true of reflux ratio, for which $r_\Delta \rightarrow \pm\infty$ (or equivalently, $\rho^\pm \rightarrow 1$) demarcates an infinite-reflux pinch point, and therefore an azeotrope.

4.4.1.2 Calculations

For the evaluation of the vector \vec{b} , given by Eq. (4.14), one bubble point calculation is required at every step of the integration. This adds some computational effort in comparison with the PB method—which requires none—but the result of the integration can, in this case, contain both the

r_{Δ} and the T at every point describing the PPC. If the Jacobian matrix J is evaluated using numerical differentiation directly, then an additional $N - 1$ bubble point calculations are required (one bubble point calculation for each column of the Jacobian). These additional bubble point calculations, however, can be avoided altogether by using the method in Appendix C.2, such that only one such computation is required at every step. Both approaches are described in Appendix C.2.

Since the movements in composition space between successive steps during the integration are quite small, the temperature does not change markedly from step to step; consequently, except for the initial point, the previous step's temperature can be used as a very good starting estimate for the current step's temperature, requiring very few iterations in the bubble point calculation even for a low convergence tolerance.

4.4.1.3 Practical implementation

The proposed method can be integrated successfully with a number of ODE solvers, but perhaps the simplest one that yields good results with reasonable efficiency is the 3(2) Runge–Kutta pair due to Bogacki and Shampine (1989), which performs well at moderate to high integration tolerances.

The PB method, however, appears to give satisfactory results only at lower tolerances, meaning that a more advanced ODE solver is needed for efficient calculation: for example, Poellmann and Blass used the Runge–Kutta–Fehlberg method. As such, while computational efficiency is gained by the PB method in that it does not require bubble point calculations, some is lost in the requirement of low integration tolerance.

The implication is that the proposed method is more numerically robust than the PB method, which may suggest that the latter is not particularly amenable to the use of numerical derivatives.

4.4.1.4 Performance

A direct performance comparison of the methods is not entirely straightforward, but endeavours have been made to compare the two as fairly as possible.

The performance of the methods was compared using the same ODE solver with the same integration tolerance, and with step sizes in the various numerical derivatives manually optimised for the best performance in each case. Ideally, several stiff and non-stiff ODE solvers should be trialled; unfortunately, however, few ODE solvers seem to perform reasonably with both the

PB ODE and the proposed one. A solver that meets this criterion is the Adams–Bashforth–Moulton PECE method (Shampine and Gordon, 1975), which was implemented for this comparison.

The ABC system served as the subject of the analysis, and a number of different X_{Δ} points were used.

All integration was started from the pure components and azeotropes (inside and outside of the MBT), meaning that the arc length extrapolation described earlier was not used in the comparison. Owing to the different parameterising variables in the two cases, the ‘distance’ from the MBT that the methods can reach before terminating is different, and usually longer for the proposed method, with the consequence that its computation time is somewhat lengthened as it integrates further.

One way of somewhat lessening the effects of different integration ‘distances’ is to compare the two methods not on a direct computation time basis, but on an adjusted computation time, defined here as computation time per arc length.

Finally, the two methods were compared using the best configuration of solver, tolerance, etc. for each.

Using the same configuration (solver and tolerance), the proposed method was approximately 10–15% faster than the PB method, despite the former’s lack of bubble point calculations; the reason for this is likely that proposed formulation is more numerically robust. When the two methods were compared at their respective optimal configurations, the proposed method was found to be 45–55% faster.

4.4.1.5 Flexibility

The proposed method is able to accommodate both a fixed X_{Δ} , as well as one that varies with r_{Δ} , which is an important feature for complex column design (Holland, 2005; Felbab et al., 2011). The PB method, however, does not allow for this approach, as the authors focused their attention on conventional columns only. The proposed method therefore has wider applicability than does the PB method.

4.4.2 Comparison with other reflux-parameterised methods

The proposed method was also compared with continuation methods.

Computation time is provided to give an indication of the performance; the time pertains to Fortran 2003 code compiled to MATLAB executables (mex files), running under Microsoft Windows 7 Professional 32-bit on an Intel Core i5 430M (2533 MHz) with 3 GB of DDR3-1333 SDRAM. Parallel processing was not used.

All calculations for the proposed method and the continuation algorithms were started at pure components and azeotropes, and in both cases, the range $|r_{\Delta}| = 1\,000$ to $|r_{\Delta}| = 0.01$ was used.

A few points should be made clear prior to considering the results: continuation algorithms are a relatively specialised class of solvers, and are thus not widely available. No major mathematical software package appears to come with a built-in version of any continuation algorithm, and only a handful of third-party tools are available for this purpose. Even in Fortran, which probably has the greatest number of available algorithms, only a few appropriate professional options are available: AUTO (Doedel et al., 1998), PITCON (Rheinboldt and Burkardt, 1983), and ABCON (Lundberg and Poore, 1991). The latter is only available as a single-precision routine, which can only return as values the final point in the continuation; it is thus unsuitable for this purpose. AUTO, on the other hand, is a well-known standalone tool, but it is only available in a form that is not particularly amenable to incorporation into a user's own project without a great deal of effort. The only remaining option, thus, is PITCON.

In light of this lack of real choice, a user may be forced to write his or her own continuation algorithm if they wish to use continuation to find PPCs. As such, a custom continuation algorithm was devised to see how a user-made algorithm might compare with the proposed method. It is summarised in Appendix C.4.

PITCON was parameterised by $\lambda = 1/r_{\Delta}$ (as suggested by Fidkowski et al., 1991) and ρ^{\pm} , while the custom continuation algorithm was parameterised by r_{Δ} and ρ^{\pm} .

The proposed ODE was solved with the Adams–Bashforth–Moulton multistep PECE method.

In all of the cases above, all endeavours were made to minimise the computational effort in order to make a fair assessment. For example, the previously calculated temperature was used as the initial guess for the next step in order to accelerate the bubble point calculations. Moreover, all common subroutines (bubble point calculations, Jacobian evaluations, etc.) were the same for all

Table 4.1 Numerical results of various methods to calculate PPCs in Figure 7 of Krolkowski (2006).

Method	Parameter	No. Points	Time (s)	Maximum F
This work	ρ^\pm	106	0.007028	4.6308×10^{-4}
Continuation: PITCON	λ	2094	0.050993	4.7832×10^{-3}
Continuation: PITCON	ρ^\pm	1176	0.033645	3.5577×10^{-3}
Continuation: Custom	r_Δ	143	0.009083	6.2063×10^{-5}
Continuation: Custom	ρ^\pm	137	0.007639	2.4472×10^{-4}

Table 4.2 Numerical results of various methods to calculate PPCs in Figure 5 of Wahnschafft and Westerberg (1992).

Method	Parameter	No. Points	Time (s)	Maximum F
This work	ρ^\pm	122	0.008272	6.2000×10^{-5}
Continuation: PITCON	λ	130 ^a	0.028243	6.7764×10^{-3}
Continuation: PITCON	ρ^\pm	392 ^a	0.169078	6.9027×10^{-3}
Continuation: Custom	r_Δ	138	0.009960	2.1684×10^{-4}
Continuation: Custom	ρ^\pm	152	0.010372	2.0868×10^{-4}

^a Some PPC branches were incomplete; the algorithm returned NaNs at some point.

methods where applicable.

The computation times presented here are the average values of 50 consecutive runs of each method, where the first run was disregarded to exclude additional time required to load the function into memory.

Finally, in order to assess the accuracy of each method, the maximum value of F in Eq. (4.19) along the calculated PPC is reported. This is effectively the same as the L_1 -norm of Eq. (4.5). The lower the F , the more accurate the pinch points, but in most cases, $F \leq 1 \times 10^{-3}$ is sufficiently accurate for design purposes.

For these numerical tests, two examples from the open literature were recreated: (1) the PPCs for the ABC system in Figure 7 of Krolkowski (2006), the results of which are reported in Table 4.1; and (2) the PPCs for the ethylene glycol–isopropanol–water (EGIW) system in Figure 5 of Wahnschafft and Westerberg (1992), the results of which are reported in Table 4.2. Note that Wahnschafft and Westerberg do not provide written values for the required compositions, such that some error in reading from the graph must inevitably be incurred. The X_Δ was estimated to be $(-1.893, 2.372, 0.5205)$.

The results in Tables 4.1 and 4.2 indicate that the proposed method is the fastest, followed relatively closely by the custom continuation algorithm, which is approximately 10–30% slower. The accuracy of the two methods is

roughly equivalent, and not significantly different to have a practical impact; neither method is consistently more accurate than the other.

The performance of PITCON is somewhat unexpected: it generates a large number of points, and its efficiency suffers as a result. Adjustment of its parameters to try and improve performance led to larger steps initially, followed by rapidly diminishing step sizes, which ultimately gave noticeably incomplete PPCs. It took several times longer than the proposed ODE, and produced PPCs that in some parts were too inaccurate. In the second test, two of the PPC sections terminated prematurely because the algorithm returned NaNs. It can, therefore, be concluded that PITCON is not well-suited to the PPC problem.

While the ρ^\pm transform has a universal beneficial effect on the proposed ODE, its effect on the performance of continuation algorithms is not as uniform: in some cases it is beneficial, and in others not.

4.4.3 Comparison with methods using PPCs implicitly

The proposed method was intended for use with other design methodologies, and tests were performed to see how it would fare in a method that uses PPCs only implicitly.

The method of Lucia et al. (2008) was briefly introduced in § 4.2.1. It is a two-step global optimisation algorithm, the first step of which is a non-linear programming problem used to find the minimum energy requirements for a given distillation problem. The algorithm requires the following inputs: feed composition, feed condition, the desired distillate compositions, the bottoms compositions in a conventional column, and an initial reboil ratio. A purity constraint is set on the distillate composition.

At a given reboil ratio, the stripping section is constructed, starting from the bottoms composition and proceeding upwards, for a large number of stages ($n \geq 300$), such that it effectively pinches, i.e. terminates at a stable pinch point. Lucia et al. considered staged columns, the mathematical construction of which amounts to solving Eq. (4.3) using Euler's forward method for $\Delta n = 1$. The resulting stripping line has a piecewise length in the composition space. Once the stripping section has been described, the rectifying section— if present—is constructed, starting from the stripping section pinch point and again proceeding upwards. The construction of the rectifying section continues until it converges to a point, or leaves the mass balance triangle.

An optimisation algorithm is applied to the above procedure to find the reboil ratio that minimises the length of the stripping line, with the constraint that the end of the rectifying section (distillate) must satisfy the specified minimum product purity. The reboil ratio that satisfies these criteria is the minimum reboil ratio, and therefore corresponds to the minimum energy requirements.

The construction of the stripping section, as described above, finds the stable pinch point from which the rectifying section is to be constructed, and it also provides a convenient objective function for the minimisation. However, the drawback to this is that it requires a large number of bubble point calculations, which are the most computationally expensive parts of distillation calculations.

The proposed ODE method can find the same pinch points as used in Lucia et al.'s algorithm; however, without the stripping line being computed, the same objective function cannot be used. A modification to Lucia et al.'s algorithm to incorporate the proposed method is described as follows:

Before the optimisation procedure commences, the proposed method is used to determine the pinch point curve associated with the bottoms composition. This results in composition and reboil ratio information along the PPC. The PPC also has an associated arc length, and at a given arc length, the reboil ratio and pinch composition are known (interpolation is required for intermediate values not present in the output of the ODE solver). In turn, once the reboil ratio and pinch composition are known, the rectifying section can be constructed exactly as in the original algorithm.

An optimisation algorithm can be applied to this modified procedure in order to find the arc length along the PPC that minimises reboil ratio without violating the distillate purity constraint.

To summarise the difference between the two approaches, if the objective function to be minimised is expressed as $f = \text{objfun}(x)$, then Lucia et al.'s original algorithm has f defined as stripping line length, and x as reboil ratio, while the version modified with the proposed method has f as reboil ratio, and x as arc length along the PPC. The constraints are the same.

A comparison using the original algorithm and the modified one was performed using two examples from Lucia et al. (2008). The first of these is from § 6.6 of Lucia et al.: the ABC system modelled with UNIQUAC, with $x_F = (0.17, 0.72, 0.72)$, $x_D = (0.9900, 0.0093, 6.666 \times 10^{-4})$, and $x_B = (1 \times 10^{-10}, 0.86734, 0.13266)$. The column is considered feasible if $x_{D,1} \geq 0.99$.

Table 4.3 Numerical results of the original Lucia et al. algorithm and the algorithm modified using the proposed method; parameters given in text.

Algorithm	Pinch Point Refining	Minimiser	Min. Reboil Ratio	Time (s)
Original	–	DIRECT	1.16082	0.464
Proposed	None	DIRECT	1.16109	0.163
Proposed	10 Euler steps	DIRECT	1.16084	0.167
Proposed	Variable no. Euler steps	DIRECT	1.16082	0.217
Original	–	Nelder–Mead	1.16082	0.311
Proposed	None	Nelder–Mead	1.16106	0.094
Proposed	10 Euler steps	Nelder–Mead	1.16084	0.121
Proposed	Variable no. Euler steps	Nelder–Mead	1.16082	0.186

Two minimisation algorithms were tried: the DIRECT algorithm, due to Jones et al. (1993), and a bracketing scheme with bound-constrained Nelder–Mead (Nelder and Mead, 1965) as the local minimiser.

For each test, 1 000 runs were performed; each time, a random value of reboil ratio, S , between 5 and 20 was generated. This value was used as the upper bound in the DIRECT algorithm (with the lower bound at $S = 0.1$), and as the initial guess for the Nelder–Mead-based scheme. In all cases, the search was limited to the interval $[0.1, 20]$. For the modified version, the initial value of S was translated to an arc length along the PPC. The solution always converged to the same value within six significant figures.

As observed in § 4.4.2, there is some small numerical error in the PPC generated with either the proposed method or standard continuation methods. These pinch compositions can be refined by driving them closer to the true pinch points using a few Euler steps of the stripping section; the modified algorithm was tested with no refining, with ten Euler steps, and with a variable number of Euler steps that matched the accuracy of Lucia et al.’s original version.

Table 4.3 summarises the results of the tests, where the computing times are averaged over the 1 000 runs. The same computing configuration as described in § 4.4.2 was used.

The minimum reboil value found—and verified—in this test was 1.16082, which differs slightly from Lucia et al.'s published value of 1.159295. Although the same UNIQUAC binary interaction parameters and vapour pressure constants were used, the difference could potentially be caused by different UNIQUAC structural parameters, different system pressures, or round-off error in the set distillate and/or bottoms compositions. Nevertheless, this small discrepancy does not impact on the present comparison.

Table 4.3 shows that in all cases, the modified version is faster; even using pinch point refining to achieve the same accuracy as the original algorithm, it is approximately twice as fast. If slight error in the minimum reboil is tolerable, then the unrefined modified algorithm yields significantly better performance. These observations can be explained by the fact that by not generating the stripping section at each step in the minimisation procedure, the proposed modification avoids a great number of bubble point calculations.

The second test performed was another example taken from Lucia et al. (2008): in § 6.12 of that paper, a split of ABC modelled with UNIQUAC is described, with $x_F = (0.0330, 0.5275, 0.4395)$, $x_D = (0.033, 0.022, 0.945)$, and $x_B = (0.0330, 0.6373, 0.3297)$. Unfortunately, the modified algorithm gives an incorrect value that is lower than the one found by the original algorithm. The reason for this is that staged column modelling is equivalent to Euler forward integration with step size 1, which is not always a stable solution scheme. At low values of reboil ratio, a packed column section modelled using robust integration of Eq. (4.3) is numerically stable, but a staged one is not, and its trajectory diverges and tends to another pinch point. As a result, the staged column's feasible pinch points are a subset of the continuous column's, and the proposed method has no way of accounting for this.

Consequently, the modified method—though faster when it does work—does not give reliable results for staged columns; in this case, the original method is preferred.

4.5 Examples

Some examples of the PPCs obtained by the algorithm are presented here for ternary and quaternary systems. The computation times given here are for the same computer configuration described in § 4.4.2.

Only pure components were used as starting points, such that azeotropes

were discovered automatically by the method. For each example, the computation time for the entire procedure is given in the caption.

In order to assess the capabilities of the proposed method, the examples below include some extremely complicated systems with interesting behaviour, such as benzene–hexafluorobenzene–*n*-hexane (BHnH), and acetone–chloroform–methanol–benzene (ACMB). Despite being a ternary system, BHnH has four binary azeotropes (within the MBT): two normal binary azeotropes, and the well-known double binary azeotropes between benzene and hexafluorobenzene. ACMB on the other hand, has six azeotropes (within the MBT): four binary, one ternary, and one quaternary.

The quaternary systems are given as parallel stereoscopic figures for three-dimensional viewing. A brief guide on how to view these images is provided in Appendix C.5.

Blue pinch points curves signify $r_{\Delta} > 0$, while red indicates $r_{\Delta} < 0$. The order of the components of the X_{Δ} vector corresponds to the acronym of the system given in the caption.

Figure 4.4 shows the ABC system, while Figure 4.5 gives examples using the acetone–chloroform–methanol (ACM) system. The last ternary example given here is the aforementioned BHnH system in Figure 4.6.

One particularly noteworthy aspect is a comparison with the self-explanatory ‘azeotrope search’ feature in AspenTech’s Aspen Plus (Aspen Technology, Inc., 2007). To find all of the six real azeotropes of the ACMB system, Aspen Plus takes 33.1 seconds; on the same machine, in the same computing environment, and using the same activity coefficient model, the proposed algorithm finds all of those azeotropes—as well as some outside of the real space—and all the branches of the pinch point curves, in 0.329 seconds. For the BHnH system, Aspen Plus manages to find only two of the four real azeotropes, taking 32.8 seconds to do so. The proposed algorithm, however, successfully locates all of the real azeotropes, along with the PPCs and azeotropes outside of the MBT, in less than 0.117 seconds.

Although no examples of non-constant X_{Δ} are given here—in order to avoid a full column synthesis example, which would be required to give context to the non-constant X_{Δ} —it has been confirmed to work by recreating Figure 3.15.

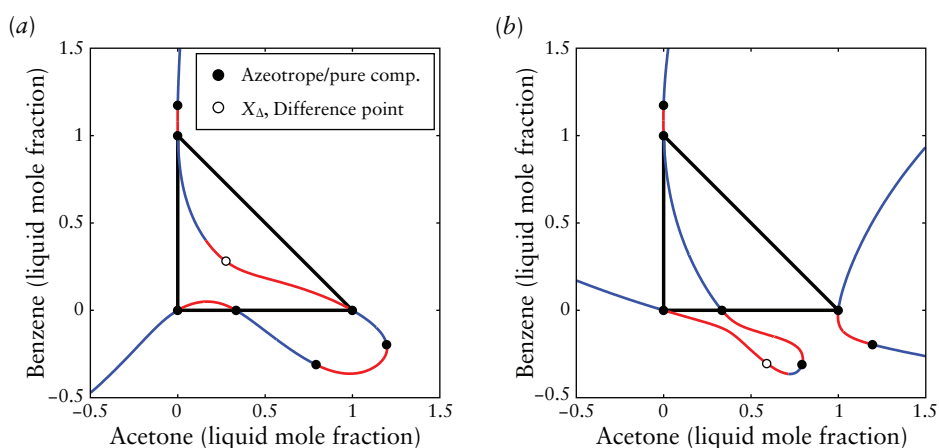


Figure 4.4 Pinch point curves of the ABC system. (a) $X_{\Delta} = (0.27, 0.28, 0.45)$; time: 0.084 s. (b) $X_{\Delta} = (0.59, -0.30, 0.71)$; time: 0.081 s.

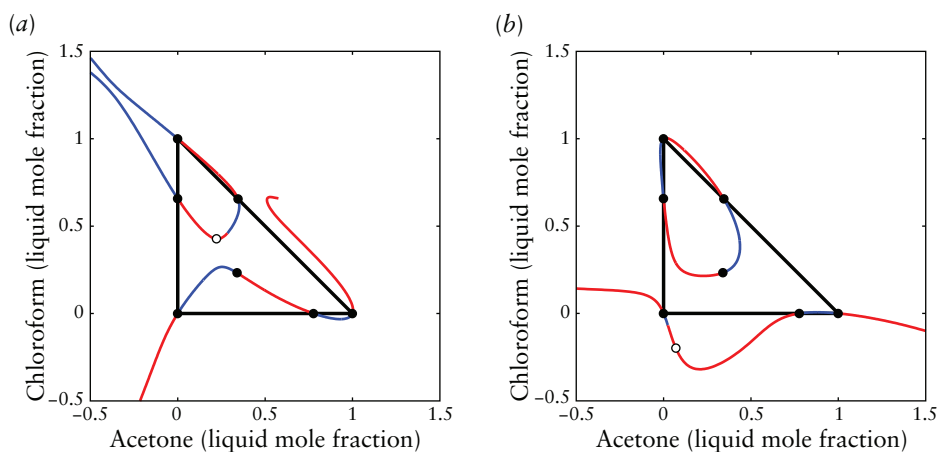


Figure 4.5 Pinch point curves of the ACM system. (a) $X_{\Delta} = (0.22, 0.43, 0.35)$; time: 0.089 s. (b) $X_{\Delta} = (0.07, -0.20, 1.13)$; time: 0.090 s.

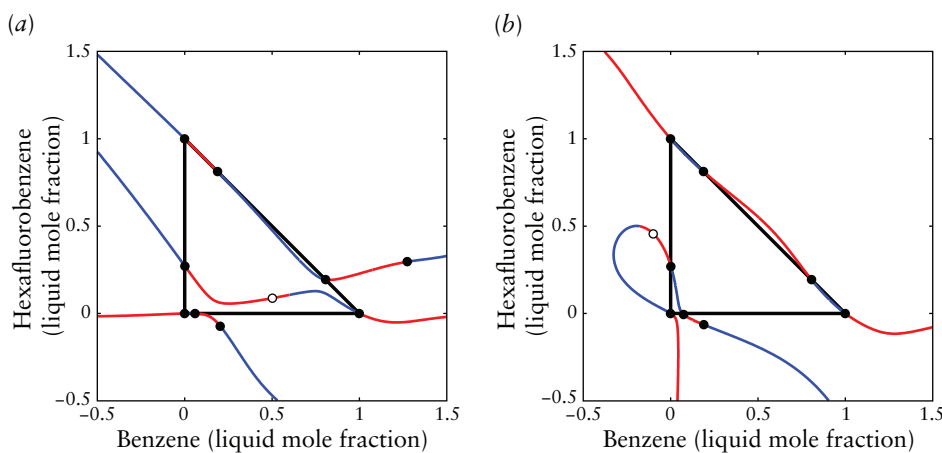


Figure 4.6 Pinch point curves of the BHnH system. (a) $X_{\Delta} = (0.50, 0.09, 0.41)$; time: 0.117 s. (b) $X_{\Delta} = (-0.10, 0.46, 0.64)$; time: 0.109 s.

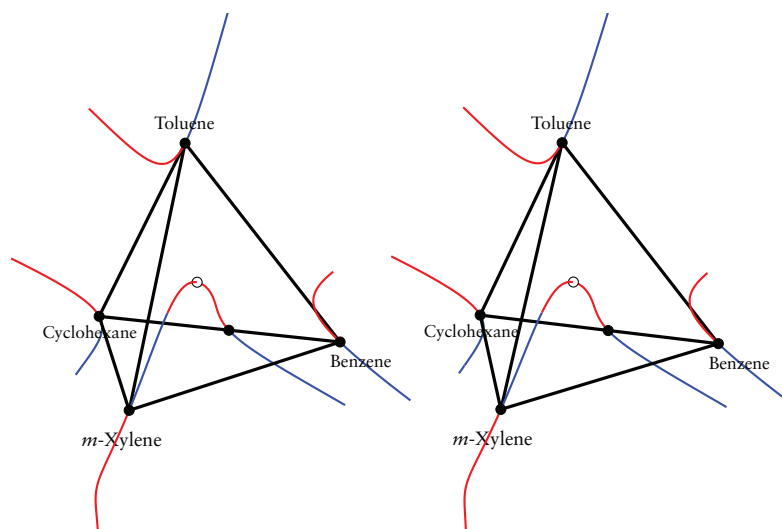


Figure 4.7 Parallel stereoscopic view of the pinch point curves of the BTmXC system with $X_{\Delta} = (0.23, 0.38, 0.28, 0.11)$; time: 0.083 s

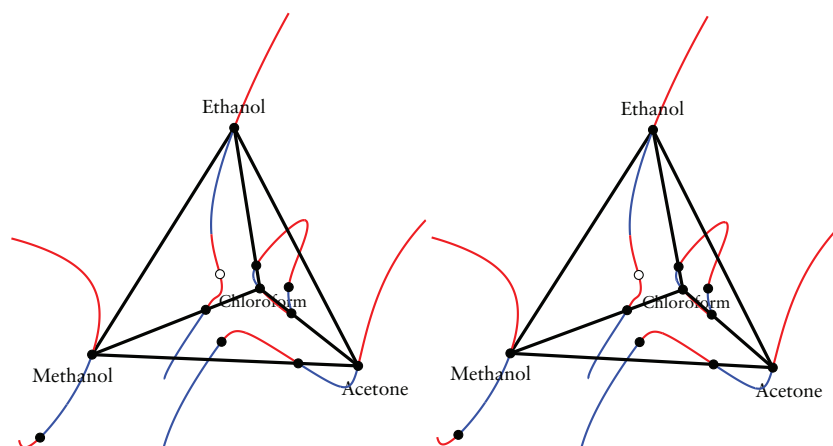


Figure 4.8 Parallel stereoscopic view of the pinch point curves of the ACME system with $X_{\Delta} = (0.18, 0.22, 0.30, 0.30)$; time: 0.254 s

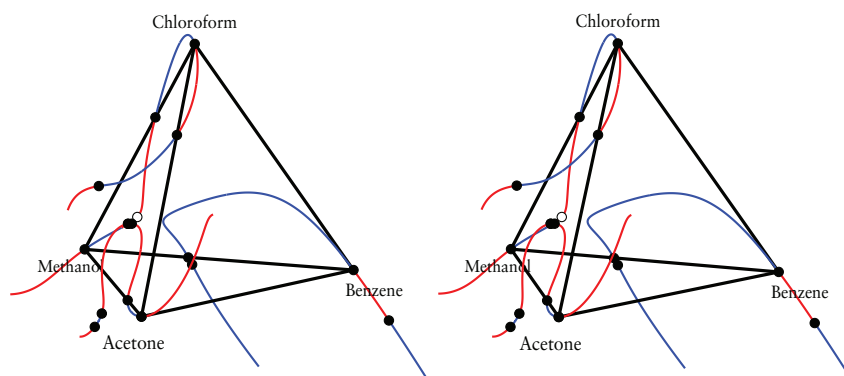


Figure 4.9 Parallel stereoscopic view of the pinch point curves of the ACMB system with $X_{\Delta} = (0.12, 0.21, 0.58, 0.09)$; time: 0.329 s

4.5.1 Software demonstration

Software demonstrating the work presented in this chapter can be obtained freely from me. To obtain the software, simply send an email, blank or otherwise, with the title *PPC Software Request* to Nik.Felbab@gmail.com, and a URL for the download will automatically be sent in return.

4.6 Conclusion

This chapter has presented a new method of constructing all branches of the pinch point curves in homogeneous, non-ideal (or ideal) multicomponent systems. It takes the form of a non-stiff ordinary differential equation, the solution of which is a partial branch of the pinch point curves. Initiating the integration at the appropriate starting points (pure components and azeotropes) leads to the complete pinch point curves. In effect, this is a continuation method formulated as an ODE. Although the method has the ability to construct the full PPC, it does not need to; if a user requires only a specific subset, integration can be carried out from a known pinch point to a specific reflux/reboil ratio, to generate only the part of the PPC that is of interest.

The method requires only the activity coefficient model and vapour pressure model for the input of a new system, although it can make use of azeotrope data, if available.

Novel variables, ρ^+ and ρ^- , which are simple transforms of r_Δ , were introduced. The use of these variables, instead of r_Δ , linearises the PPC problem somewhat, which has a significant influence on the efficiency of the proposed ODE: when ρ^\pm is used as the independent variable or parameter, it results in a 40–60% speed increase compared to r_Δ .

The choice of ODE solver is up to the user; all non-stiff ODE solvers that were trialled worked with the proposed formulation.

In comparison with the ODE of Poellmann and Blass (1994), (the PB method), the proposed ODE has the following advantages:

- 1 It is parameterised by reflux ratio, rather than temperature, making it more applicable to design;
- 2 It is based on the difference point equation, allowing for use in any generalised column section (including in complex columns);
- 3 Unlike the PB method, it allows for a non-constant X_Δ , which is often encountered in complex columns;

- 4 It is simpler, faster and more numerically robust than the PB method (using numerical derivatives of γ and P^{vap}); and
- 5 It can locate azeotropes if required (marked by $r_{\Delta} \rightarrow \infty$), whereas the PB method has no way of identifying azeotropes.

In comparison with continuation methods, the proposed ODE has the following advantages:

- 1 In the numerical experiments performed in this chapter, the proposed ODE was found to be 10–30% faster. This, however, is not inherent to the approach, and it is conceivable that a continuation algorithm with a better predictor and step-size control than the one used here could outperform the proposed method; however,
- 2 ODE solvers are significantly more prevalent than continuation algorithms (this is an important point which is expanded on below); and
- 3 Continuation algorithms suffer from branch-switching when two branches of the PPC are close to one another. This was noticed in this work, as well as by Poellmann and Blass (1994). ODEs, however, do not have this drawback.

The proposed method is the only method that formulates the PPC problem as an ODE parameterised by the column section reflux ratio, or indeed, any design variable. The significance of the parameter is that it is arguably more useful for design than the ODE of Poellmann and Blass.

Continuation methods are also typically parameterised by reflux ratio, or by a simple transform of reflux ratio (such as $\lambda = 1/r_{\Delta}$), but there is one significant, albeit subtle, advantage to the ODE approach: continuation methods are a relatively specialised class of solvers. Currently, their use is not nearly as widespread as that of ODEs, and compared to ODE solvers, relatively few professional continuation solvers exist, none of which is available ‘out-of-the-box’ with typical mathematical software packages. The integration of ODEs, on the other hand, is a standard, everyday engineering problem. An important consequence of this is that to generate pinch point curves efficiently with the proposed method, practising, non-expert engineers can easily use tools with which they are familiar, and which are available in every major mathematical software package (ODE solvers, linear system solvers, and, optionally, interpolation routines). The convenience of this brings efficient and reliable PPC construction to a much wider audience using the proposed method than with standard numerical continuation.

The proposed algorithm was also tested in conjunction with the algorithm of Lucia et al. (2008) that, in its first phase, finds the pinched, minimum energy solution to a given distillation problem. The use of the PPC generated by the proposed method as a modification to Lucia et al.'s original algorithm was found to yield significant speed benefits. However, when using staged—rather than packed—columns, the proposed method has no way of discerning the subset of the PPC that is applicable to staged columns; as such, its reliability is not guaranteed, and Lucia et al.'s original method must be used in this context.

Optionally, the proposed method can be extended to find azeotropes, which it does more reliably and much faster than Aspen Plus, with the caveat that for thermodynamic models that do not allow negative mole fractions, several X_{Δ} points must be tried to find all of the azeotropes.

The proposed method has a number of important advantages over other methods intended for the same purpose, and can be utilised in the design and synthesis of distillation columns—in conjunction with methodologies that require the use of pinch point curves or that are based on the reversible distillation model—or, more broadly, in any application that requires the efficient location of azeotropes in an N -component system at a given pressure.

Chapter 5

Synthesis of Standard Vapour Recompression Distillation

The work in this chapter has been published in: Felbab, N., Patel, B., El-Halwagi, M.M., Hildebrandt, D., Glasser, D., 2013. Vapor recompression for efficient distillation. 1. A new synthesis perspective on standard configurations. *AIChE J.* 59 (8), 2977–2992. This chapter is a reproduction of that publication, with some minor corrections, and changes in style and formatting for clarity. Reproduced with permission. This work is my own, except for the thermodynamic derivation leading to Eq. (5.23), which was done by Bilal Patel.

Copyright © 2013 American Institute of Chemical Engineers. AIChE Journal.

Abstract

The vapour recompression distillation scheme is examined and compared with conventional distillation in an analysis spanning fundamental thermodynamics, high-level calculations, and rigorous simulation. The purpose of this chapter is threefold: first, it provides greater insight into vapour recompression distillation. Second, it provides a process synthesis tool to rapidly assess whether vapour recompression is likely to be more thermodynamically favourable than conventional distillation for a given split. Third, it may be used to determine if vapour recompression can be implemented practically. The tool presented in the chapter is consolidated in the form of a single chart, for which only the top and bottom product temperatures are required in order to determine the outcome. Using this chart, first-pass estimates can be obtained with no calculations whatsoever. The tool, which appears to be the first of its kind in this context, is validated with examples and rigorous simulation.

5.1 Introduction

Despite the well-established fact that distillation is an energetically inefficient process (Freshwater, 1951; Flower and Jackson, 1964; King, 1980), it has seen widespread industrial application for the separation of mixtures over the last century: by Humphrey's (1995) estimate, up to 90% of all product recovery. Conventional, or simple, distillation columns (those with one feed, a distillate, a bottoms, a condenser, and a reboiler; see Figure 5.1a) are the most prevalent, even though they are often not the most efficient distillation configuration.

Improvements in the energy efficiency of distillation remain a challenge for industry, especially due to the rising costs of energy and growing environmental concerns. In an attempt to mitigate this, a large number of increasingly complex modifications to, and departures from, conventional distillation have been devised over the last few decades. These include:

- 1 Complex distillation arrangements/column coupling (Rév et al., 2001; Hernández-Gaona et al., 2005; Agrawal, 2003; Caballero and Grossmann, 2003, 2013; Shenvi et al., 2013), e.g. Petlyuk (Petlyuk et al., 1965; Halvorsen and Skogestad, 2004, 2011; Holland et al., 2010), multi-effect (Al-Elg and Palazoglu, 1989; Agrawal, 2000; Engelen and Skogestad, 2005), and distributed-feed columns (Soave and Feliu, 2002; Holland, 2005; Felbab et al., 2011);
- 2 Diabatic columns (Fonyó, 1974; Le Goff et al., 1996), in which heat is added or removed on several or all stages, allowing the column to operate more reversibly;
- 3 Heat-pumping techniques (Fonyó and Benkő, 1998), e.g. vapour recompression, and absorption heat pumps;
- 4 Heat-integrated distillation columns (HIDiCs) (Nakaiwa et al., 2000; Olujić et al., 2003; Huang et al., 2006, 2008; Mane and Jana, 2010; Chen et al., 2010; Suphanit, 2011), in which the rectifying section is compressed and transfers heat to the stripping section, utilising a combination of the first three modifications;

The literature covering these topics is vast (which is indicative of the urgency to find energy savings in distillation processes); thorough reviews and comparisons can be found in Rév et al. (2001), Nakaiwa et al. (2003), and Jana (2010).

Research related to energy efficient columns is on a trajectory of increasing complexity, with simpler systems thought to be well-understood. One such

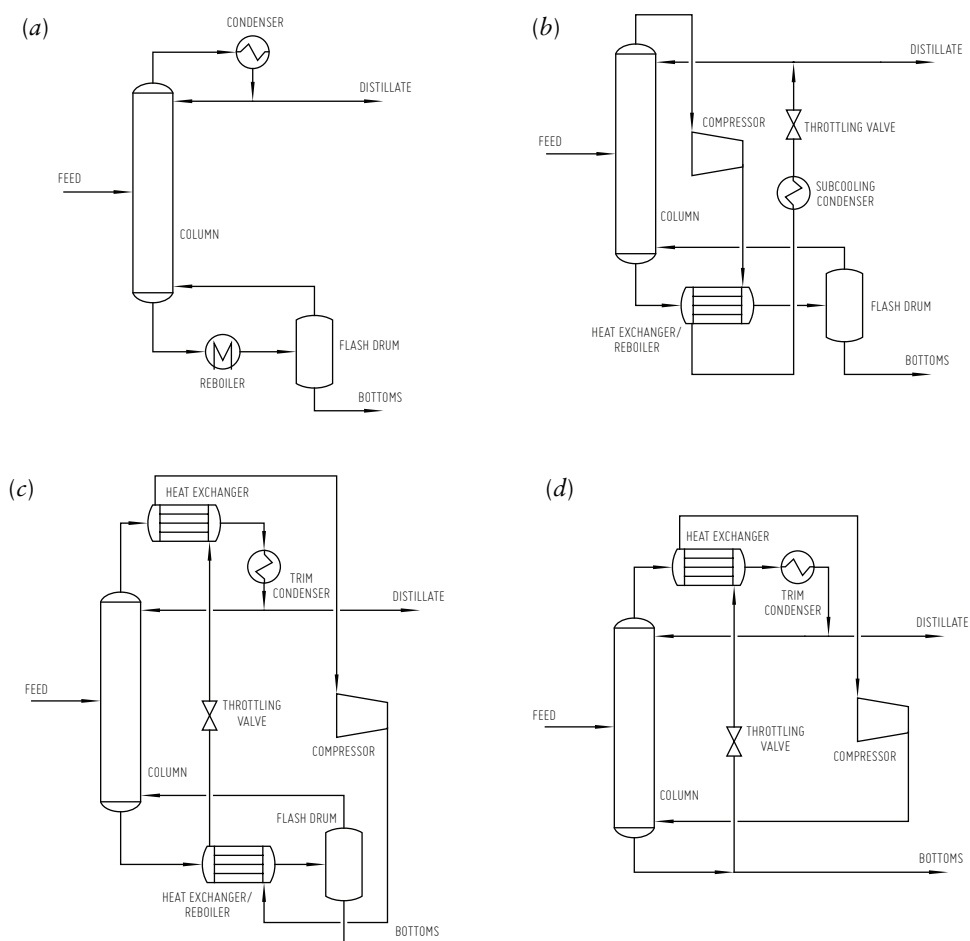


Figure 5.1 Schematic representations of (a) conventional distillation, (b) vapour recompression, (c) heat-pump-assisted distillation with an external working fluid, and (d) bottoms flashing.

class of ‘simple’ systems is heat-pump-assisted distillation, of which there are three typically used variants: vapour recompression (VRC); the closed-cycle process, which involves the use of an external working fluid; and bottoms flashing (Ferré et al., 1985; Mészáros and Fonyó, 1986; Annakou and Mizsey, 1995; Demirel, 2004). Figures 5.1*b–d* show the general schematics of these configurations, respectively. Of these three alternatives, vapour recompression has been found to be the most advantageous and economical (Null, 1976; Mészáros and Meili, 1994; Fonyó and Benkő, 1998).

The application of vapour recompression to distillation has been studied extensively (Null, 1976; Quadri, 1981a,b; Carta et al., 1982; Omideyi et al., 1984; Brousse et al., 1985; Flores et al., 1984; Ferré et al., 1985; Meili and Stuecheli, 1987; Muhrer et al., 1990; Mészáros and Meili, 1994; Annakou and Mizsey, 1995; Fonyó and Benkő, 1998). The literature to date has focused mainly on the detailed analysis and simulation of various systems,

on the economic optimisation of these systems and their operating conditions, and on controllability. Many of these studies have found—for the various systems studied—that vapour recompression is most beneficial for close-boiling mixtures, systems which require high heat loads, small column pressure drops, and low process temperatures (Carta et al., 1982; Cheng and Luyben, 1985).

Previous research has dealt with simulation or optimisation of standard vapour recompression (SVRC), but has not considered a generalised process synthesis approach. It is this gap in the literature that this chapter is aiming to bridge; the main goal of this chapter is to develop a tool that can rapidly provide insight into the operation of SVRC prior to rigorous simulation. This tool can assess whether or not SVRC is inherently more efficient for a given split than conventional distillation at the most fundamental thermodynamic level, and whether or not it is likely that SVRC could be implemented practically. In this way, rigorous calculation, simulation, and optimisation effort—which can be substantial—need not be wasted if there is no possible benefit to using SVRC for a given problem. The presented methodology can be used to discard clearly unfavourable alternatives immediately; unlike optimisation, its purpose is not to find the best possible alternative.

Previously, thermodynamic analyses utilising the first (Freshwater, 1951; Flower and Jackson, 1964; King, 1980) and second (Fonyó, 1974; Fitzmorris and Mah, 1980; Itoh et al., 1980; Kaiser and Gourlia, 1985; Le Goff et al., 1996; Taprap and Ishida, 1996; Hernández-Gaona et al., 2005) laws have been performed on conventional distillation columns. A review of the application of thermodynamic analyses to separation systems—and conventional distillation in particular—can be found in Demirel (2004).

In this chapter, fundamental thermodynamic principles are applied to SVRC. The main innovation of this work is the presentation of the resulting process synthesis tool as a single chart (see Figure 5.10), for which only the distillate and bottoms temperatures are required. Using solely these two temperatures, estimates can be made of whether or not SVRC is inherently thermodynamically more efficient than conventional distillation, and the minimum compression ratio (a technical deciding factor for practical implementation) can be determined. Moreover, if the ideal gas heat capacity of the overhead vapour is known, it is possible to estimate whether superheating of the compressor inlet is necessary to avoid condensation on compression. Using this tool, the applicability of vapour recompression can be assessed completely

graphically; that is, with no calculations at all. This appears to be the first approach of its kind for SVRC; previously, no general guidelines for rapidly determining if vapour recompression is worthwhile have been presented in the open scientific literature. In this era, in which energy savings are becoming more and more crucial, it is useful to have simple guidelines to aid the engineer in the decision-making process; this applies equally to greenfield projects and to retrofitting.

In the sections that follow, a thermodynamic analysis of conventional columns is first presented in § 5.3. This then provides a basis for comparison with standard vapour recompression, which considers energy flows, as well as work flows in § 5.4. Thereafter, a general thermodynamic criterion for the rapid determination of the efficiency of SVRC compared to conventional distillation is presented in § 5.6. Additional indicators for two key variables—compression ratio and compressor inlet superheating—are incorporated in § 5.6; these dictate whether or not it might be possible to implement the SVRC practically. All of this information is consolidated in Figure 5.10, which allows for entirely graphical estimation of whether or not SVRC is likely to be favourable and feasible for a given problem. The results are confirmed with a number of rigorous simulations in § 5.7.

Throughout this work, ambient pressure, P_0 , and temperature, T_0 , are taken to be 101 325 Pa and 298.15 K, respectively. As the thermodynamic basis, pure liquids are taken to have zero enthalpy and entropy at ambient conditions. vapours are treated as ideal gases, since the pressures used in vapour recompression are sufficiently low to make effects of non-ideality negligible. As a convention, component indices in a mixture are arranged in order of volatility, with ‘1’ being the most volatile, e.g. $x_{F,2}$ refers to the liquid mole fraction of the second-lightest component in the feed.

5.2 Simplifying assumptions

The rigorous simulation and comparison of conventional columns and SVRC can be a time-consuming endeavour, and a potentially wasted one if SVRC proves not to be advantageous or even technically feasible. To reduce this wasted effort, the main aim of this work is to derive a tool that gives a preliminary indication as to whether SVRC might have benefits over conventional distillation; rigorous simulation is then only undertaken when this preliminary indication shows evidence of potential benefits. With this goal in

mind, it is clear that the synthesis tool should be fast, simple, and analytical (as opposed to computational). For the purposes of arriving at simple, high-level calculations for easy analysis, a number of assumptions are made in this chapter:

- 1 The reboiler adds work as a reversible heat pump, and the condenser removes work as a reversible heat engine. As will be seen later, the purpose of the thermodynamic analysis in this chapter is to compare the best inherent performance of the conventional and SVRC configurations; this reversibility represents the limit of operation for these pieces of equipment, and is thus an appropriate assumption;
- 2 The feed and products are liquid. This is a common scenario in distillation, and here it serves the purpose of removing a degree of freedom, thereby reducing the number of variables to one amenable to high-level analysis;
- 3 The feed mixture is a binary, ideal mixture. The fact that it is binary allows for pure-component products in the configurations considered in this chapter (see the next point). Its ideality removes the complexity associated with non-ideal mixtures, which would require iterative computations, and would thus render the analytical equations derived in this chapter impossible; instead, the simple constant relative volatility (CRV) model can be used;
- 4 The feed mixture is split into pure components, with the pure light component recovered in the distillate, and the pure heavy component recovered in the bottoms. The purpose of this complete separation is threefold: first, it represents the limit of operation in terms of degree of separation, and is also a reasonable approximation of the most typical separation problems, in which quite pure products are sought; second, it removes degrees of freedom, and allows the analysis to focus on more important variables; and finally, it allows for easier analysis, since the product vapour and liquid saturation temperatures are simply the pure-component boiling points, eliminating the need for iterative bubble- or dew-point calculations, and additional property information;
- 5 The distillation column adheres to constant molar overflow (CMO): sensible heat effects are negligible in comparison with latent heat, heat of mixing is zero, all components have the same latent heat, and the column is adiabatic. This is a very common simplification that is generally quite accurate for ideal and near-ideal mixtures.

The examples presented later in § 5.7 each deviate from one or more of the above assumptions, and it would appear that the applicability of the proposed approach does not diminish appreciably as a result of these simplifying assumptions. Note that the assumption of a binary mixture in point 3, and of pure-component products in point 4 above, are not strictly necessary for the novel methodology proposed in this chapter, as long as the product temperatures are known; these assumptions merely simplify the analysis in this chapter.

5.3 Thermodynamic analysis: conventional distillation columns

In this section, a brief, high-level thermodynamic analysis of conventional distillation is performed. The foundation of this work is well-known (Kayihan, 1980; Henley and Seader, 1981; Gomez-Munoz and Seader, 1985; Glinos and Malone, 1989; Skogestad, 2009), but it is included here to serve as a basis for comparison with the standard vapour recompression scheme.

Conventional distillation columns can be thought of as a coupled heat pump and heat engine, where the former adds work to the column (reboiler), and the latter removes it (condenser). The input work is greater than the output work, such that there is net addition of work to the column, part of which is used to perform the separation, and the remainder of which contributes to entropy generation. This is a well-established understanding of the fundamental work flows in distillation columns: they extract work from heat flows by degrading the quality of the heat (Terranova and Westerberg, 1989; Chiang and Luyben, 1983; Mullins and Berry, 1984; Smith et al., 2010).

In order to improve overall process efficiency, the work flow that is removed from the column can, in some cases, be reused in another part of the process, as long as that part of the process can accept lower-quality heat (Linnhoff et al., 1983). This is the preferred approach; however, in the absence of the overall process context, this chapter will consider the distillation system in isolation.

Work addition and removal in distillation columns

Figure 5.2 shows a schematic representation of the work inputs and outputs, and also serves as a reference for the nomenclature used in this section. As-

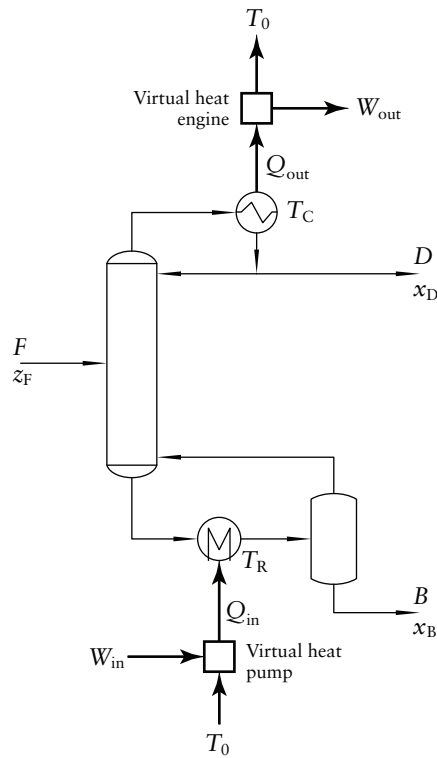


Figure 5.2
Schematic representation of a conventional distillation column, along with the mass, heat, and work flows in and out of the system, as well as the significant temperatures.

suming a reversible heat pump, the work input is expressed mathematically as:

$$W_{\text{in}} = Q_{\text{in}} \left(1 - \frac{T_0}{T_R} \right) \quad (5.1)$$

The work removed from the column by a reversible heat engine is:

$$W_{\text{out}} = Q_{\text{out}} \left(1 - \frac{T_0}{T_C} \right) \quad (5.2)$$

Minimum theoretical energy input to effect separation (reversible distillation model)

An entropy analysis over the column gives:

$$F\hat{S}_F + \frac{Q_{\text{in}}}{T_R} + S_{\text{gen}} = D\hat{S}_D + B\hat{S}_B + \frac{Q_{\text{out}}}{T_C} \quad (5.3)$$

The temperatures of heat input and output are taken at the limit of performance; that is, countercurrent heat exchangers with infinite heat transfer area are assumed, such that the heating medium enters at the temperature of the process stream outlet, and the cooling medium leaves at the process stream inlet temperature. In other words, heat is added at the process stream outlet temperature, and it is removed at the process stream inlet temperature.

A reversible column is one that generates no entropy, i.e. $S_{\text{gen}} = 0 \text{ W/K}$. This is the ideal case, in that no work is wasted, and it demarcates the theoretical limit of performance: no distillation column could be more efficient than a completely reversible one. Consequently, a reversible column represents the minimum theoretical heat requirement of a distillation column to perform a given separation.

Assuming a column that generates no entropy ($S_{\text{gen}} = 0 \text{ W/K}$), and separates the feed mixture into pure liquid components ($\hat{S}_{\text{D}} = \hat{S}_{\text{B}} = 0$), Eq. (5.3) becomes:

$$F\Delta\hat{S}_{\text{mix}} + \frac{Q_{\text{in}}}{T_{\text{R}}} = \frac{Q_{\text{out}}}{T_{\text{C}}} \quad (5.4)$$

The assumptions made in this section also give an energy balance of $Q_{\text{in}} = Q_{\text{out}}$, hence:

$$\Delta\hat{S}_{\text{mix}} = \frac{Q_{\text{in}}}{F} \left(\frac{1}{T_{\text{C}}} - \frac{1}{T_{\text{R}}} \right) \quad (5.5)$$

Rearranging Eq. (5.5) and recognising that $\Delta\hat{S}_{\text{mix}} = -R \sum x_i \ln x_i$ for ideal mixtures, the following is obtained:

$$Q_{\text{in,sep}} = -\frac{FR \sum x_{\text{F},i} \ln x_{\text{F},i}}{\frac{1}{T_{\text{C}}} - \frac{1}{T_{\text{R}}}} \quad (5.6)$$

Equation (5.6) represents the minimum theoretical heat input required to perform the separation.

Furthermore, Eq. (5.5) can be substituted into Eq. (5.1) to give:

$$F\Delta\hat{S}_{\text{mix}} = \frac{W_{\text{in,sep}}}{T_{\text{C}}} \left(\frac{T_{\text{R}} - T_{\text{C}}}{T_{\text{R}} - T_0} \right) \quad (5.7)$$

The relationship in Eq. (5.7) will be useful later in § 5.6.

Minimum practical energy input

In practice, distillation columns have a minimum heat input that is different from Eq. (5.6) owing to their internal configuration, with the minimum heat requirement corresponding to minimum reflux. Using a simple derivation (which is given in Appendix D.1), with minimum reflux estimated by Underwood's method (1948), the following equation gives the minimum practical heat input into a distillation column:

$$Q_{\text{in,min}} = F\lambda \left(\frac{1}{\alpha - 1} + x_{\text{F},1} \right) \quad (5.8)$$

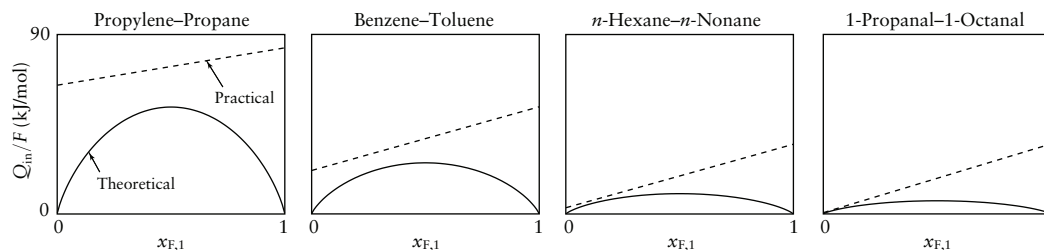


Figure 5.3 Comparison of minimum theoretical heat input and minimum practical heat input to a conventional distillation column for a sharp split as a function of mole fraction of the light component in the feed.

Table 5.1 Binary systems and simple constant properties used in high-level calculations.

Light (1)	Heavy (2)	α	λ (kJ/mol)	$\hat{C}_{p,1}^{\text{IG}}$ (J/mol·K)	T_C (K)	T_R (K)
propylene	propane	1.29	18.73	53.4	225.5	231.1
acetonitrile	nitromethane	1.84	32.32	58.3	354.8	374.4
benzene	toluene	2.47	31.98	104.9	353.3	383.8
<i>n</i> -hexane	<i>n</i> -nonane	11.21	31.84	175.6	341.9	424.0
1-propanal	1-octanal	58.47	34.46	174.1	321.1	447.3

Comparison of theoretical and practical minimum energy

It is now possible to compare the practical minimum heat input, Eq. (5.8), with the theoretical minimum, Eq. (5.6). To do this, Q_{in}/F for the practical and theoretical minima is plotted as a function of feed composition in Figure 5.3; the systems considered and their (constant) properties are given in Table 5.1. The chosen systems cover a wide range of relative volatilities (or differences in reboiler and condenser temperatures, which are related) in order to assess why some are amenable to vapour recompression, and others not.

Figure 5.3 not only shows that the separation of wider-boiling mixtures requires less energy than that of narrow-boiling ones, but also that these systems can operate closer to their theoretical minima using the conventional distillation column. However, the most important insight that this figure offers is that conventional distillation becomes less and less efficient as the feed tends to higher purity in either direction. This is intuitive, since theoretically, little work addition is required to effect a small degree of separation. In reality, however, the operation of a distillation column requires vaporisation in the reboiler, which does not necessarily contribute to the separation process itself; indeed, a feed with an infinitesimal amount of impurity requires effectively no work of separation, yet vaporisation must still take place. This vaporisation is not proportional to the degree of impurity in the feed.

5.4 Thermodynamic analysis: standard vapour recompression scheme

A simple diagram of the SVRC scheme is given in Figure 5.1*b*. vapour leaving the top of the column is compressed isentropically, causing an increase in both pressure and temperature. The purpose of the compression is twofold: first, it elevates the temperature of the overhead vapour in order to provide a driving force for heat transfer to the bottom liquid; second, it elevates the dew point of the overhead vapour, allowing its latent heat to be used at a higher temperature. This overhead vapour stream—the temperature of which exceeds that of the bottoms—is heat exchanged with the liquid leaving the bottom of the column, partially vaporising the latter; in other words, the overhead vapour stream uses its latent heat to vaporise the liquid, and in the process, it itself condenses. This partially condensed stream is then subcooled in the condenser to such a point that when its pressure is dropped back down to the column pressure, it does not vaporise (ideally, it should be a saturated liquid). Part of this liquid stream is refluxed to the column, and the remainder is drawn off as the distillate. Overall, energy is only added to the compressor, and it is removed in the condenser.

Figure 5.4 shows a schematic representation of the mass and energy flows in the SVRC configuration; it also provides stream labels for the important streams. Table 5.2 gives the relationship of T , P , and phase for these streams, assuming complete separation of the binary feed. To aid understanding further, a qualitative pressure–enthalpy plot relating to the process is given in Figure 5.5. Note that while Figure 5.1*b* does not include a superheater prior to compression, Figure 5.4 does, because some saturated vapours condense on isentropic compression, which must strictly be avoided in a compressor Meili and Stuecheli (1987); Patwardhan (1987); Gmehling et al. (2012). This is discussed at greater length later in this section.

Minimum theoretical energy input to effect separation in SVRC (reversible model)

The use of the superheater may be necessary for some fluids, but will be disregarded for the present, high-level analysis, i.e. $Q_{\text{sh}} = 0 \text{ W}$, as it is not a set feature of SVRC. Using the same assumptions as before, the energy balance

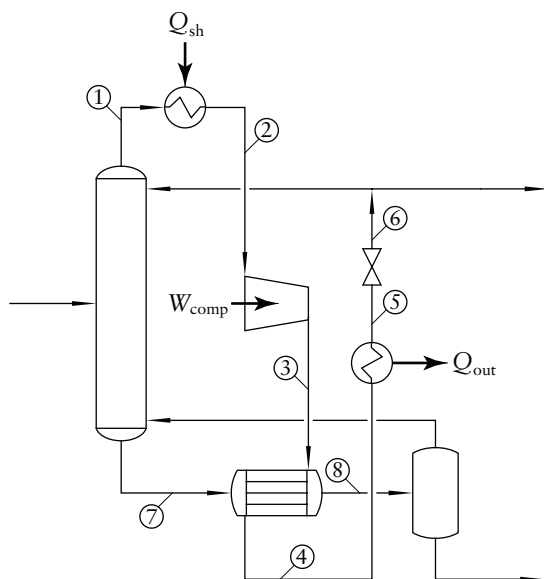


Figure 5.4
Schematic representations of the SVRC configuration, with stream labels. See Table 5.2 for stream information.

Table 5.2 Relationship of temperature, pressure, and phase in streams in Figure 5.4, assuming complete separation of the binary feed.

Stream	T	P	Phase
1	T_C	P_0	saturated vapour
2	$T_2(> T_C)$	P_0	superheated vapour
3	$T_3(> T_2)$	P_{comp}	superheated or saturated vapour
4	$T_4(> T_R)$	P_{comp}	saturated vapour and liquid
5	T_C	P_{comp}	subcooled liquid
6	T_C	P_0	saturated liquid
7	T_R	P_0	saturated liquid
8	T_R	P_0	saturated vapour and liquid

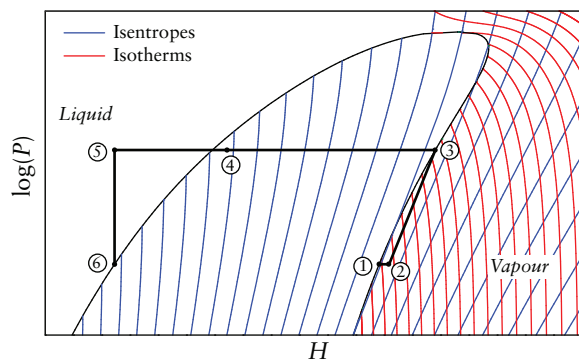


Figure 5.5
Qualitative pressure–enthalpy plot showing the vapour recompression process relating to Figure 5.4, and assuming minimum compressor inlet superheating.

around the system reduces to:

$$W_{\text{comp}} = Q_{\text{out}} \quad (5.9)$$

The compression is performed isentropically, which, by definition, means that the compression step itself generates no entropy. As in the case of the conventional distillation model, heat is removed at the temperature of the process stream inlet to the heat exchanger, which in this case is T_4 . Consequently, the entropy analysis (assuming reversibility) is:

$$F\Delta\hat{S}_{\text{mix}} = \frac{Q_{\text{out}}}{T_4} \quad (5.10)$$

On substitution of Eq. (5.9) into Eq. (5.10), the following relationship is obtained:

$$F\Delta\hat{S}_{\text{mix}} = \frac{W_{\text{comp}}}{T_4} \quad (5.11)$$

The left-hand side of Eq. (5.11) is fixed by the problem specification, but the value of T_4 is less obvious. Indeed, T_4 can be manipulated using different design parameters. In order to provide a driving force for the heat exchange, $T_4 > T_R$; however, the limit of operation occurs in a heat exchanger with infinite heat exchange area, in which case, $T_4 = T_R$. The latter also minimises W_{comp} according to Eq. (5.11). Consequently, the following interpretation is used:

$$F\Delta\hat{S}_{\text{mix}} = \frac{W_{\text{comp}}}{T_R} \quad (5.12)$$

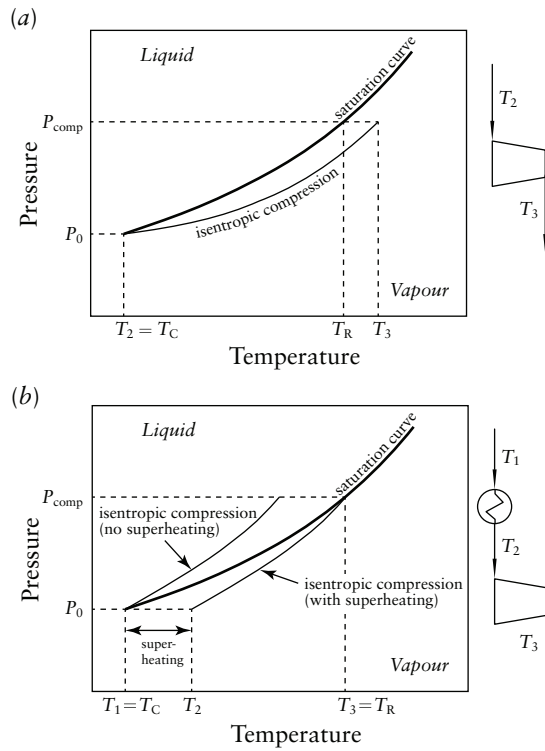
The minimum theoretical energy (and work) addition using a perfect compressor, therefore, is given by:

$$W_{\text{comp,sep}} = T_R F\Delta\hat{S}_{\text{mix}} \quad (5.13)$$

$$W_{\text{comp,sep}} = -FRT_R \sum x_{F,i} \ln x_{F,i} \quad (5.14)$$

Minimum practical energy input in SVRC

As with the conventional column, the mass balance and minimum reflux ratio impose limitations on the minimum energy that is practically required to operate the SVRC configuration. In this section, an idealised SVRC model is derived, but with the inclusion of fundamental mass balance constraints that are inherent to the operation of distillation columns.


Figure 5.6

Pressure–temperature behaviour of a saturated vapour that (a) superheats on compression, and (b) condenses on compression and requires superheating. Note that the isentropic compression curves assume vapour compression; if this line enters the liquid region, that assumption is incorrect, and some liquid is formed, in which case, the true compression profile simply follows the saturation curve.

An important point to take into consideration is that the saturated vapours of some fluids become superheated on isentropic compression, while others condense. The following criterion can determine which of those two outcomes occurs (Felbab, 2013):

$$\hat{C}_{p,1}^{\text{IG}} T_C < \lambda \text{ (superheated)} \quad \hat{C}_{p,1}^{\text{IG}} T_C > \lambda \text{ (partially condensed)} \quad (5.15)$$

Besides the practical issue of liquid formation in the condenser, if some of the fluid condenses within the compressor, the stream's full latent heat is not available to perform the reboil duty. If the fluid condenses, a superheater is used prior to compression in order to avoid condensation. Figure 5.6 best illustrates the P – T behaviour in these instances, and the application of superheating. Minimum superheating results in a saturated vapour at the compressor outlet.

In either case, the pressure must be raised to a point where the condensing temperature is greater than T_R , or, in the limit, equal to T_R . Since the minimum energy input is sought in this section, this limit will be used.

If the saturated vapour superheats on compression, then, as derived in Appendix D.1, the energy/work input in the compressor is given by:

$$W_{\text{comp,min}} = F \hat{C}_{p,1}^{\text{IG}} T_C \left(\frac{1}{\alpha - 1} + x_{F,1} \right) \left[\exp \left(\frac{\lambda}{\hat{C}_{p,1}^{\text{IG}}} \left(\frac{1}{T_C} - \frac{1}{T_R} \right) \right) - 1 \right] \quad (5.16)$$

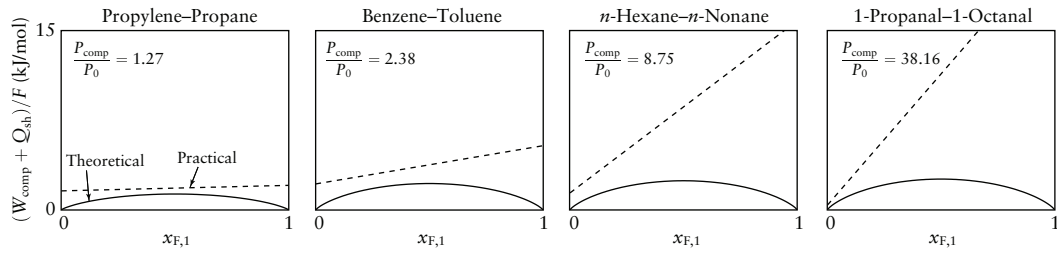


Figure 5.7 Comparison of minimum theoretical and minimum practical energy inputs to the standard vapour recompression configuration for a sharp split as a function of mole fraction of the light component in the feed. The minimum compression ratios are indicated.

The total energy (and work) input into the system in this case is simply equal to $W_{\text{comp,min}}$.

If the saturated vapour condenses, then superheating is required. The minimum energy input to the superheater is, as shown in Appendix D.1:

$$Q_{\text{sh,min}} = F \hat{C}_{p,1}^{\text{IG}} \left(\frac{1}{\alpha - 1} + x_{F,1} \right) \left[T_{\text{R}} \exp \left(\frac{\lambda}{\hat{C}_{p,1}^{\text{IG}}} \left(\frac{1}{T_{\text{R}}} - \frac{1}{T_{\text{C}}} \right) \right) - T_{\text{C}} \right] \quad (5.17)$$

After the superheater, compression takes place, the energy input of which is given by the following:

$$W_{\text{comp,min}} = F \hat{C}_{p,1}^{\text{IG}} T_{\text{R}} \left(\frac{1}{\alpha - 1} + x_{F,1} \right) \left[1 - \exp \left(\frac{\lambda}{\hat{C}_{p,1}^{\text{IG}}} \left(\frac{1}{T_{\text{R}}} - \frac{1}{T_{\text{C}}} \right) \right) \right] \quad (5.18)$$

The derivation for Eq. (5.18) is given in Appendix D.1. In the case of the saturated vapour condensing on compression, the total energy input into the system is the sum of Eqs (5.17) and (5.18).

Comparison of theoretical and practical minimum energy input

Using the above equations, it is possible to compare the minimum theoretical energy input—Eq. (5.14)—with the practical minimum, for the same systems as in Figure 5.3. For saturated vapours that superheat on isentropic compression, the minimum practical energy input is given by Eq. (5.16); for fluids that condense, it is the sum of Eqs (5.17) and (5.18). This comparison is shown in Figure 5.7, with the minimum compression ratios indicated for each system.

Note that the range of the vertical axis is much smaller in Figure 5.7 than in Figure 5.3. This illustrates that SVRC is more energy-efficient in all of the examined systems, even when compressor inlet superheating is required. (There is a cross-over point with very wide-boiling systems, for which conventional distillation is more efficient than SVRC; this is examined later in § 5.6.)

It is also noteworthy that the observed trend using SVRC is the opposite of that in conventional columns: wider-boiling mixtures require more energy to separate fully, and cannot operate as close to the theoretical minimum as close-boiling separations can.

5.5 Comparison of work inputs in conventional and SVRC distillation

When comparing the same process with different parameters, as has been done above, energy is a sufficient indicator of efficiency. However, the comparison of work input into different processes is more instructive than energy input, as it correlates with actual resource consumption (coal, natural gas, etc.), and takes the quality of heat into account. For example, a process could require a large heat load that needs to be supplied at ambient temperature, in which case that energy is effectively ‘free’; a process with a smaller heat load that requires heat at 800 K would need to consume resources to obtain that high-quality heat.

The equations for work input can be deduced easily, as shown below.

Minimum theoretical work input in conventional distillation columns

$\Delta\hat{S}_{\text{mix}} = -R \sum x_i \ln x_i$ can be substituted into Eq. (5.7) and the result rearranged to obtain the minimum theoretical work input into a conventional distillation column:

$$W_{\text{in,sep}} = -FRT_C \left(\frac{T_R - T_0}{T_R - T_C} \right) \sum x_{F,i} \ln x_{F,i} \quad (5.19)$$

Minimum practical work input in conventional distillation columns

The practical minimum work input is found by substituting Eq. (5.8) into Eq. (5.1) to obtain:

$$W_{\text{in,min}} = F\lambda \left(\frac{1}{\alpha - 1} + x_{F,1} \right) \left(1 - \frac{T_0}{T_R} \right) \quad (5.20)$$

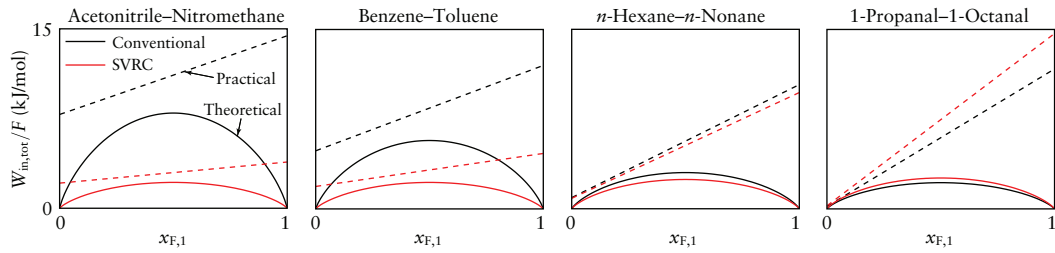


Figure 5.8 Comparison of minimum theoretical and minimum practical work inputs to the conventional and standard vapour recompression configurations for a sharp split as a function of mole fraction of the light component in the feed.

Minimum theoretical work input in SVRC

In the SVRC scheme, the energy and work inputs in the compressor are equivalent. Therefore, the minimum theoretical work input into the SVRC—assuming no compressor inlet superheating—is given by Eq. (5.14).

Minimum practical work input in SVRC

For the SVRC when no superheating is necessary, the practical minimum work input is given by Eq. (5.16).

If compressor superheating is necessary, the virtual work associated with the heat in the superheater is obtained by substituting Eq. (5.17) into Eq. (5.1), noting that the heat is added not at T_R but at T_2 (the expression for which is given in Appendix D.1 as Eq. (D-10)):

$$W_{\text{sh,min}} = F \hat{C}_{p,1}^{\text{IG}} \left(\frac{1}{\alpha - 1} + x_{F,1} \right) \left[T_R \exp \left(\frac{\lambda}{\hat{C}_{p,1}^{\text{IG}}} \left(\frac{1}{T_R} - \frac{1}{T_C} \right) \right) - T_C \right] \left[1 - \frac{T_0}{T_R} \exp \left(\frac{\lambda}{\hat{C}_{p,1}^{\text{IG}}} \left(\frac{1}{T_C} - \frac{1}{T_R} \right) \right) \right] \quad (5.21)$$

In this case, the work input in the compressor is simply Eq. (5.18), such that the total work input, when superheating is required, is the sum of Eqs (5.21) and (5.18).

Using the above equations, plots of the minimum theoretical and practical work inputs for conventional and SVRC distillation as a function of feed composition are made in Figure 5.8. The same mixtures as in Figures 5.3 and 5.7 are used, with the exception of the propylene–propane system, which has normal boiling points below ambient temperature and thus requires elevated pressures or a refrigeration system.

Figure 5.8 shows that the scale of work input into the two configurations is much more comparable than that of energy input. This can largely be attributed to the fact that the energy input in a compressor is ‘pure’ work, while only a temperature-dependent fraction of heat input is virtual work, in accordance with Eq. (5.1). The qualitative behaviour of minimum theoretical and practical work as a function of feed composition is the same as with energy input. In systems with small temperature differences between the distillate and bottoms, the expected result is seen: SVRC is better than conventional distillation. However, there is a cross-over point, where the work input in the two cases is equivalent (see, for example, the *n*-hexane–*n*-nonane split, where the two configurations are nearly the same). For wide-boiling mixtures, such as 1-propanal–1-octanal, the SVRC is worse than conventional distillation.

A quantitative description of this cross-over point is derived in § 5.6.

5.6 Thermodynamic and practical synthesis targets

For a fixed feed, $F\Delta\hat{S}_{\text{mix}}$ is fixed, and is the same in the conventional distillation case, Eq. (5.7), and in the SVRC case, Eq. (5.12). Thus, $F\Delta\hat{S}_{\text{mix}}$ in the two cases can be equated to obtain:

$$\frac{W_{\text{in}}}{T_{\text{C}}}\left(\frac{T_{\text{R}} - T_{\text{C}}}{T_{\text{R}} - T_0}\right) = \frac{W_{\text{comp}}}{T_{\text{R}}} \quad (5.22)$$

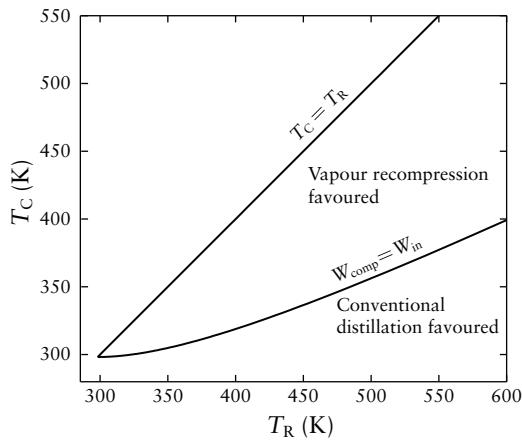
In order to find the region where SVRC is better than conventional distillation, a boundary must be defined where the work input in the two cases is the same, i.e. $W_{\text{in}} = W_{\text{comp}}$. Applying this to Eq. (5.22) and rearranging the result leads to the following equation:

$$T_{\text{C}} = \frac{T_{\text{R}}^2}{2T_{\text{R}} - T_0} \quad (5.23)$$

Equation (5.23) describes the relationship between T_{R} and T_{C} where the work input into the conventional column and SVRC configuration is the same, at a fundamental thermodynamic level.

Figure 5.9 shows a plot that demarcates the region where SVRC is more thermodynamically efficient than conventional distillation as a function of the reboiler and condenser temperatures (boiling points of the feed mixture’s constituent components, in the sharp-split case).

While this chapter focuses on SVRC, the same analysis can be performed on the other configurations in Figure 5.1, that is, heat-pump-assisted distillation

**Figure 5.9**

Plot of regions where vapour recompression is thermodynamically more efficient than conventional distillation as a function of T_C and T_R only.

with an external working fluid, and bottoms flashing. A brief analysis of these configurations can be found in Appendix D.2.

5.6.1 Compression ratios

Despite the fact that the SVRC region in Figure 5.9 is quite large, vapour recompression is used relatively seldom. This can be explained by the practical consideration mentioned earlier: large differences between T_C and T_R require a large increase in temperature in the compressor, which in turn translates to a high compression ratio. Compressors with high compression ratios are uneconomical and inefficient (Boyce, 2011). Consequently, it is useful to represent this practical limitation alongside the fundamental thermodynamic one.

Unfortunately, at least four variables need to be specified for a system: T_C , T_R , $\hat{C}_{p,1}^{IG}$, and λ , yet not all four can be represented independently on a two-dimensional plot. One way of overcoming this restriction is to use an approximation for λ in the form of the Trouton–Hildebrand–Everett rule (Everett, 1960; Nash, 1984), which gives good estimates for non-polar hydrocarbons:

$$\frac{\lambda}{RT_C} = 4.0 + \ln(T_C/\text{K}) \quad (5.24)$$

It can be shown, as has been done in Appendix D.1, that the minimum pressure ratio can be estimated using the following equation:

$$\frac{P_{\text{comp}}}{P_0} = \exp\left([4.0 + \ln(T_C/\text{K})] \left(1 - \frac{T_C}{T_R}\right)\right) \quad (5.25)$$

Equation (5.25) can be used to plot contours of specific P_{comp}/P_0 values in the T_R – T_C space. These have been included in Figure 5.10. It is important to note that the practical compression ratios (say, $P_{\text{comp}}/P_0 < 3$) are almost

entirely within the vapour recompression region. The implication of this is that in almost all cases where vapour recompression can practically be applied, that configuration is more efficient thermodynamically than conventional distillation.

5.6.2 Need for superheating of compressor inlet

It is also useful to determine whether or not superheating of the compressor inlet is required.

The vapour enters the superheater at T_C and is heated to T_2 , the expression for which is available in Appendix D.1. No superheating is required when $T_2 = T_C$. The equation for zero superheating is derived in Appendix D.1; the result is given here as:

$$T_C = T_R \exp\left(\frac{R[4.0 + \ln(T_C/K)]}{\hat{C}_{p,1}^{\text{IG}}}\left(\frac{T_C}{T_R} - 1\right)\right) \quad (5.26)$$

For a specified value of $\hat{C}_{p,1}^{\text{IG}}/R$, Eq. (5.26) can be solved numerically to plot lines of zero superheating in the T_R - T_C space, which have also been shown in Figure 5.10. This allows for rapid assessment of whether or not the inclusion of a superheater before the compressor is likely to be required, if the \hat{C}_p^{IG} of the overhead vapour is known.

5.6.3 Interpretation of Figure 5.10

To use Figure 5.10, the T_R - T_C coordinate is first located on the chart. If this point is within the vapour recompression region (see Figure 5.9), it means that SVRC will likely be more thermodynamically efficient than conventional distillation for that system. However, even if it is thermodynamically favourable, it does not necessarily mean that SVRC can be practically implemented. To address this issue, the P_{comp}/P_0 ratio corresponding to the T_R - T_C coordinate is located on the appropriate isobar on the chart. This value represents an estimate of the minimum pressure ratio that is required in the compressor; if this is lower than a practical maximum (around 3, as a guideline), then it is likely that the SVRC could be implemented practically, and rigorous simulation should be used to verify this estimate. Note that if the T_R - T_C coordinate is close to the $W_{\text{comp}} = W_{\text{in}}$ line, and the pressure ratio is reasonable, rigorous simulation should be performed, since estimates using Figure 5.10 are likely to be inconclusive in this case.

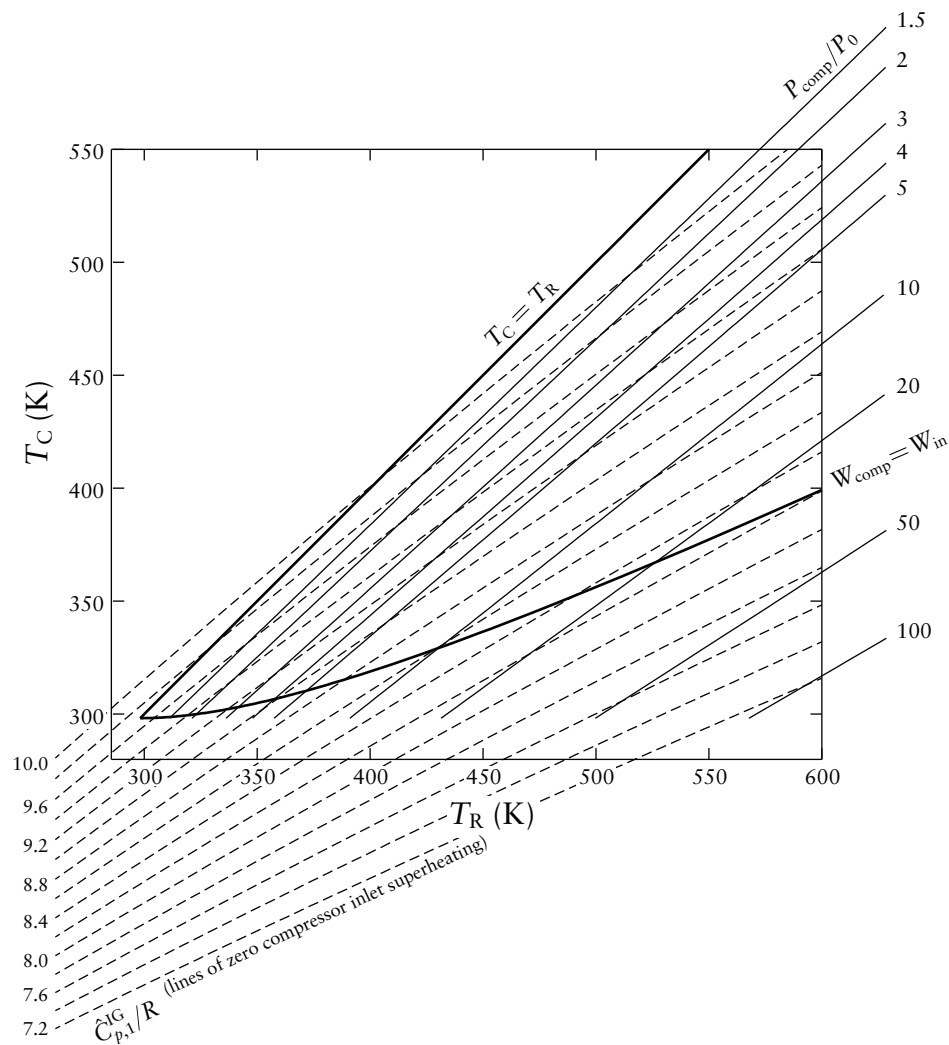


Figure 5.10 Plot of regions where vapour recompression is thermodynamically more efficient than conventional distillation as a function of T_C and T_R , with overlays of minimum required compression ratios, and lines of zero compressor inlet superheating for various $\hat{C}_{p,1}^{IG}/R$ values.

The above decision process is summarised in the flowchart given in Figure 5.11.

Additionally, the T_R – T_C coordinate will also have a $\hat{C}_{p,1}^{IG}/R$ value associated with it, which is located on the appropriate dashed line. If the actual value of $\hat{C}_{p,1}^{IG}/R$ is lower than the one corresponding to the T_R – T_C coordinate, the vapour superheats on isentropic compression; otherwise, it partially condenses, and a superheater is required before to the compressor inlet. While this is informative, it cannot provide information about the exact amount of superheating required; as such, it is not necessarily part of the decision-making process.

It should be reiterated that these are estimates only, since a number of

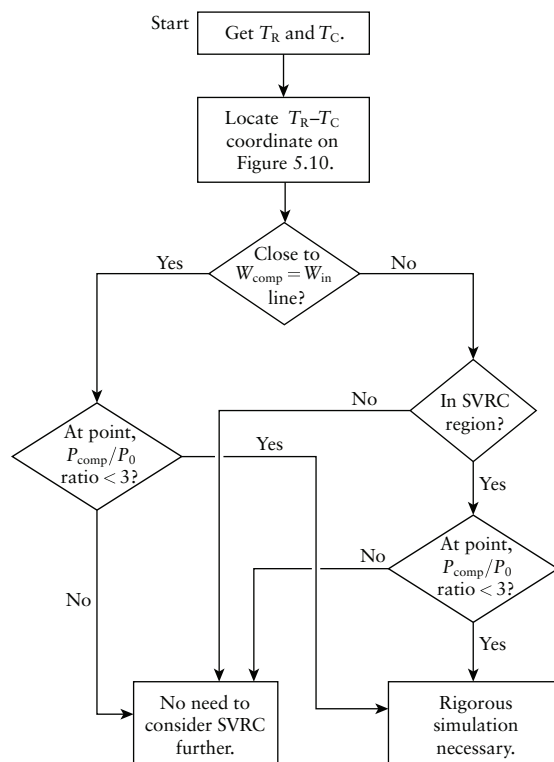


Figure 5.11
Flowchart representing the decision-making process with Figure 5.10.

simplifications must be made to arrive at this entirely graphical, generalised result. Consequently, it is used to assess whether SVRC is likely to be better than conventional distillation, and whether it could be implemented, but the result is not definitive.

5.7 Rigorous simulation and validation

The usefulness of Figure 5.10 is tested here by means of a number of examples, and validated using rigorous simulation in AspenTech's Aspen Plus (Aspen Technology, Inc., 2007). Figure 5.10 is intended only for rough, high-level estimates due to its numerous simplifying assumptions. The examples also serve to demonstrate how the results using Figure 5.10 should be interpreted.

Note that the compression ratio lines and the zero-superheating lines are most accurate close to the $T_C = T_R$ line, since the constant properties assumed in the defining equations lose accuracy over wide temperature ranges. Additionally, the use of Eq. (5.24) makes the results less reliable when the light component is highly polar, e.g. contains H-bonds. The examples here include systems that do not adhere to these restrictions.

The general connectivity of the simulated flowsheets is given for the conventional case in Figure 5.12, and in Figure 5.13 for the SVRC. The NRTL

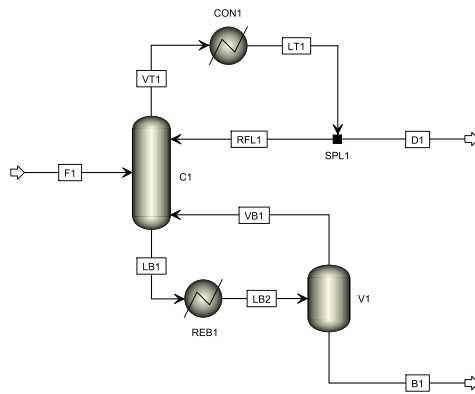


Figure 5.12
Aspen Plus flowsheet for the rigorous simulation of the conventional distillation column.

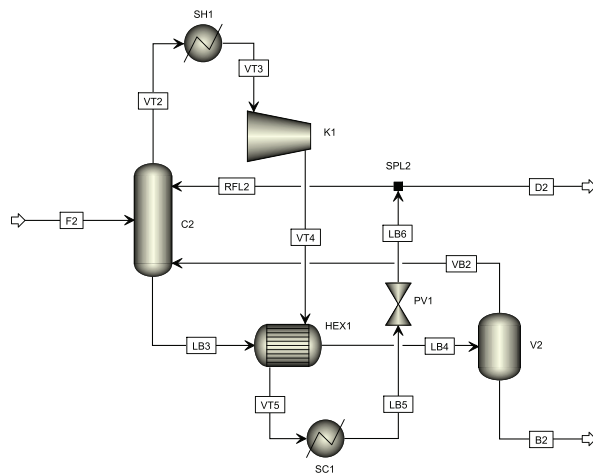


Figure 5.13
Aspen Plus flowsheet for the rigorous simulation of the standard vapour recompression configuration.

activity coefficient model (Renon and Prausnitz, 1968) was used for the VLE calculations. The column was modelled using the RADFRAC block, and the compressor was modelled as completely isentropic.

For each example, the simulation settings are given in Appendix D.3.

5.7.1 Design methodology

It is important to note that the purpose of these simulations was not to determine the optimal design, but rather to compare a conventional column with the SVRC, both of which have the same parameters (reflux ratio, product compositions, number of stages, feed stage, etc.). The design methodology for the Aspen Plus simulations was partially one of trial-and-error, using starting estimates for some of the key parameters.

The conventional column was simulated first. Once the feed and product compositions had been chosen, the Aspen Plus shortcut distillation model, DSTWU, was used to estimate the minimum reflux ratio, r_{\min} . Thereafter, the reflux ratio was chosen as $r = 1.5 r_{\min}$. Through simple mass balance, using this reflux ratio and the desired product compositions, the required split at

SPL1, and the vapour fraction in REB1 (see Figure 5.12 for nomenclature) can be estimated. The column (C1) was simulated using the RADFRAC model, which initially had 10 stages. The feed stage was found to have little effect in these simulations, and was thus set to half-way up the column in each case, thereby eliminating a degree of freedom; had the optimal configuration been sought, greater care would have been taken regarding the feed stage. The simulation was run, and if—after some manual adjustment of the SPL1 and REB1 settings—the approximate product compositions were not achieved, the number of stages was increased, and the process repeated.

Once the conventional column had been simulated successfully, the SVRC simulation (as shown in Figure 5.13) was set up such that the RADFRAC column (C2) had exactly the same specification as in the conventional case. Similarly, SPL2 had the same split fraction as SPL1, and the cold stream outlet vapour fraction from HEX1 was the same as the vapour fraction in REB1. These parameters ensured that the column internals, and thus the product compositions, would be identical in both configurations. The compression ratio in K1 and the superheating in SH1 were estimated initially using a shortcut method (Felbab, 2013), and then adjusted simultaneously, until both were at a (rough) minimum which allowed the SVRC system to work, but resulted in no condensation in the compressor.

Example 1: 1-butene–*n*-butane

The normal boiling point of 1-butene is 266.91 K, and that of *n*-butane is 272.65 K, both of which are below the assumed ambient temperature of 298.15 K. In order to avoid the use of an external refrigeration system to remove heat at a sub-ambient temperature, it is simpler to run the system at a higher pressure, thereby raising the boiling points.

At a pressure of 400 kPa, 1-butene has a boiling point of 307.56 K, while *n*-butane has 315.09 K, both of which can readily be serviced using steam and cooling water. Consequently, the feed and column are set to this pressure. The average \hat{C}_p^{IG} of 1-butene at these two temperatures is 88.73 J/mol·K.

First, the point at $T_R = 315.09$ K and $T_C = 307.56$ K is located on Figure 5.10. This is well within the vapour recompression zone, indicating that vapour recompression should be thermodynamically preferable to conventional distillation for this split. The isobaric lines indicate that the minimum compression ratio of a bit less than 1.5—approximately 1.3—is required, which can be readily achieved in a compressor, meaning that vapour

recompression should be practically feasible. For this system, the value of \hat{C}_p^{IG}/R is 10.67. The point for this system lies between the zero-superheating lines for \hat{C}_p^{IG}/R of 9.6 and 9.8. Since the actual \hat{C}_p^{IG}/R value of 10.67 is clearly higher than either of these, it is expected that superheating of the compressor inlet is required.

For the rigorous simulation, a feed of 1 kmol/h of a mixture with 63 mol% 1-butene and 37 mol% *n*-butane was sent into both columns, each with a reflux ratio of 14.38. The lowest compression ratio that could be used in the compressor successfully was 1.43, which was estimated reasonably well with Figure 5.10.

The simulation gave a distillate with $x_D = (0.9989, 0.0011)$ and a bottoms with $x_B = (0.0041, 0.9959)$.

For the conventional column, the only energy input is at the reboiler, which was found to have a load of 52.754 kW. From Eq. (5.1), the virtual work input associated with this heat can be estimated at 2.830 kW.

The SVRC had a work/energy input in the compressor of 2.597 kW, and a heat input in the superheater of 2.880 kW. The virtual work associated with the latter was estimated at 0.193 kW. The total energy input, therefore, was 5.477 kW, and the total work input was 2.790 kW.

The energy requirements of the SVRC were approximately ten times smaller than for the conventional distillation column, with slightly lower overall work input, the latter being crudely approximated.

Example 2: hydrogen cyanide–acrylonitrile

There is a small region in Figure 5.10 where the compression ratio is practically implementable, but is in the region expected to be thermodynamically unfavourable with vapour recompression. This example is intended to determine whether this is indeed the case.

Hydrogen cyanide has a normal boiling point of 298.85 K, while that of acrylonitrile is 350.50 K.

At this T_R – T_C coordinate on Figure 5.10, the required compression ratio is at least 4, which is relatively high, although it may be possible to achieve the necessary compression in a single-case compressor. As mentioned above, this system was chosen to lie in the region where vapour recompression is unfavourable.

For hydrogen cyanide at its boiling point, $\hat{C}_p^{\text{IG}}/R = 4.309$. The zero-superheating line corresponding to the coordinate for this system is at a value

of approximately $\hat{C}_p^{\text{IG}}/R = 9.0$; since the actual value is significantly lower, it is highly unlikely that compressor inlet superheating is required.

The rigorous simulation was performed with a feed of 1 kmol/h having a composition of 71 mol% hydrogen cyanide and the balance acrylonitrile. The entire system was isobaric at 100 kPa. The minimum compression ratio was found to be 6.42, which is not lower than the estimated minimum. Moreover, as estimated, compressor superheating was not necessary.

In both configurations, the reflux ratio was set to 0.46, resulting in product compositions of $x_D = (0.9996, 0.0004)$ and $x_B = (0.0001, 0.9999)$.

In the conventional column, the heat input was 8.140 kW (associated virtual work input: 1.213 kW). The SVRC had work/energy input of 1.649 kW. Consequently, while the SVRC has lower energy requirements, its work input is higher than the conventional column's, as predicted with Figure 5.10.

Example 3: 1-propanol–*n*-octane

This example deviates from three of the assumptions in Figure 5.10: first, it is highly non-ideal and contains an azeotrope; second, the overhead vapour includes an H-bond, such that Eq. (5.24) is less accurate; and finally, the split is not sharp.

The normal boiling point of 1-propanol is 370.35 K, and that of *n*-octane is 398.83 K. The azeotrope—as predicted with NRTL—occurs at 74.37 mol% 1-propanol, and has a temperature of 367.10 K.

A feed of 1 kmol/h of 23 mol% 1-propanol and the balance *n*-octane is to be separated into >70 mol% 1-propanol in the distillate, and >90 mol% *n*-octane in the bottoms. Prior to simulation, the exact temperatures of the distillate and bottoms are unknown, such that some assumptions must be made about these temperatures; it will be assumed that the distillate is at the temperature of the azeotrope (367.10 K) and the bottoms is at the temperature of the heavy key component (398.83 K).

Using this T_R-T_C coordinate on Figure 5.10, it is expected that SVRC should be more thermodynamically efficient than conventional distillation, and that the compression ratio should be at least 2.5, approximately. The mole-fraction-weighted \hat{C}_p^{IG}/R of the overhead vapour at 367.10 K is 15.97; the zero-superheating $\hat{C}_{p,1}^{\text{IG}}/R$ corresponding to the coordinate for this system is 9.4. As the actual value is higher, it is expected that superheating will be required.

The simulation was performed using a reflux ratio of 0.547 in both the SVRC configuration and the conventional distillation. The resulting distillate had a composition of $x_D = (0.7189, 0.2811)$ and $x_B = (0.0088, 0.9912)$.

In the conventional case, the heat input was 6.567 kW, which has an associated work input of 1.585 kW.

In the SVRC case, as predicted with Figure 5.10, superheating was required. Since a fair amount of superheating is required, and since the amount of superheating required is not independent of the compression ratio, the minimum compression ratio is not straightforward; indeed, an optimisation could be performed to minimise the work input. (Optimisation is not the objective here; all that needs to be shown is whether or not the SVRC can be designed to have lower work input than conventional distillation, as was estimated.) The superheater was set to heat the overhead vapour by 65 K; the corresponding compression ratio could be no lower than 2.6.

The heat duty of the superheater was 1.266 kW, with an associated virtual work input of 0.392 kW. The compressor had energy/work input of 0.471 kW. Thus, the total work input was 0.863 kW, which is approximately half of the work input in the conventional case.

The prediction with Figure 5.10 was again good, despite departures from its inherent assumptions.

Example 4: multicomponent system

The final example deviates from the base assumptions by having more than two components, and not performing a sharp split. The feed in this problem is a quaternary mixture of methanol, 2-propanol, 2,6,8-trimethyl-4-nonanone, 1-undecanal with a flow of 1 kmol/h and composition $x_F = (0.13, 0.22, 0.24, 0.41)$.

A rigorous simulation of a conventional distillation column with a reflux ratio of 0.429 resulted in a distillate of $x_D = (0.371, 0.628, 7.4 \times 10^{-8}, 2.3 \times 10^{-10})$, which has temperature 345.78 K, and bottoms $x_B = (6.7 \times 10^{-5}, 9.0 \times 10^{-4}, 0.369, 0.630)$ at temperature 497.64 K. The activity coefficients were modelled using UNIFAC.

The heat load obtained from the simulation is 15.431 kW, which has an associated virtual work input of 6.186 kW.

The question to be answered is whether this split would benefit from a vapour recompression system, and if such a system could realistically be implemented. On Figure 5.10, the relevant point for this system is at $T_C = 345.78$ K

and $T_R = 497.64\text{K}$. At this coordinate, the system is in the region where conventional distillation is more efficient, such that no gains are expected using vapour recompression. Moreover, the minimum compression ratio is estimated at higher than 20, meaning that practical implementation is clearly not feasible.

A rigorous simulation of the SVRC was not possible without excessive settings (several hundred degrees of superheating and compression ratios in excess of 100). A comparison of work inputs in the two configurations was thus not possible; however, Figure 5.10 correctly identified that the minimum compression ratio was much too high for practical implementation of the SVRC scheme.

5.8 Conclusion

The rigorous simulation, and subsequent comparison, of conventional distillation and standard vapour recompression (SVRC) can be a time-consuming exercise; without knowing ahead of time if there is potential benefit to SVRC, this effort may be wasted. It is useful for the engineer to be able to gain insight into whether SVRC is a realistic candidate for a given separation problem prior to performing rigorous simulation. Previously, there were no general guidelines or rapid estimation methods for determining the potential applicability of SVRC available in the open scientific literature. The work in this chapter bridges this gap: a novel, consolidated graphical process synthesis tool was presented to estimate whether vapour recompression is likely to be thermodynamically favourable to conventional distillation, and if so, whether it can be implemented practically. This tool requires minimal information, namely distillate and bottoms temperatures, and optionally the overhead vapour heat capacity. It is entirely calculation-free, which makes it particularly useful for first-pass estimates during conceptual design and process synthesis.

A thermodynamic analysis and comparison was conducted on conventional distillation columns and the standard vapour recompression configuration. When considering only the energy inputs to the systems, the energy requirements for vapour recompression were found to be significantly lower with narrow-boiling mixtures, and somewhat lower in much wider-boiling ones.

However, a more thermodynamically accurate comparison using work flows—rather than simply energy flows—revealed that the quality of heat

has a marked impact on the true efficiency of the two configurations. The thermodynamic benefits of vapour recompression were found to be less clear on this basis than when comparing energy loads directly.

A very simple quantitative description of the region where SVRC is thermodynamically favourable to conventional distillation was given in Figure 5.9 as a function of distillate and bottoms temperatures only. This chart serves as a generalised, graphical estimate of the region in which SVRC is thermodynamically preferred.

This chart also provides additional insight: the SVRC region is broad enough to include many systems which have not had vapour recompression applied to them in practice. The reason for this breadth is that some key factors limit practical implementation of vapour recompression, despite thermodynamic favourability. The most significant of these is the required compressor pressure ratio, which in practice should typically be less than about 3 or 4. A less significant factor is the need for superheating of the compressor to avoid condensation that many saturated vapours undergo upon compression.

To address the first of these concerns, an overlay of estimated minimum compression ratio was added to Figure 5.9 to produce Figure 5.10. This shows that the region where the compression ratio is reasonable is almost entirely a subset of the SVRC-preferred region, resulting in a relatively narrow band on Figure 5.10. The implication of this is that in almost all cases where the compression ratio is low enough to be applied practically, vapour recompression is thermodynamically favourable to conventional distillation.

If the ideal gas heat capacity of the overhead vapour is known, an estimate can be made as to whether compressor inlet superheating is required. Lines of zero superheating for various heat capacities are also overlaid on Figure 5.10 to estimate whether or not a superheater before the compressor is necessary to avoid condensation in the compressor.

The usefulness of the presented process synthesis tool was tested using a number of examples, each of which extended the application beyond the initial set of assumptions used in deriving Figure 5.10. These examples were validated using rigorous simulation with Aspen Plus.

While the key technical issues have been dealt with in this chapter, one important practical consideration, which, unfortunately, cannot be easily generalised, and which has thus not been dealt with in this chapter, is the economic impact of vapour recompression on the total capital expenditure. Specifically, the compressor tends to be an expensive piece of equipment, which benefits

from the economy of scale. Thus, once the technical viability has been established, the economics surrounding its implementation must be considered on a case-by-case basis; these costs are harder to quantify in advance. However, as energy costs continue to rise, the benefits of resource savings will begin to outweigh the setbacks of higher capital costs.

Chapter 6

Novel Feed–Product Vapour Recompression Configurations

Abstract

Two novel vapour recompression configurations that can have significant energy-saving benefits are presented. These vapour recompression configurations differ in their range of applicability from standard vapour recompression: where the latter is practically applicable only to the separation of close-boiling mixtures, the proposed configurations benefit wider-boiling systems. For a given system, the proposed configurations always have lower compression ratios than standard vapour recompression. However, the energy-saving advantage of the proposed configurations is limited to certain feed types: one configuration is developed for liquid feeds that are close in composition to the distillate, and the other for vapour feeds that are near the bottoms composition. The novel configurations are verified and compared to conventional and standard vapour recompression distillation using rigorous analysis and simulation.

6.1 Introduction

In Chapter 5, standard vapour recompression (SVRC) was examined in some detail, and a general comparison was made with conventional distillation columns. A process synthesis tool was developed for rapid assessment of the thermodynamic performance of those two configurations. It was found that for a wide range of systems, SVRC is thermodynamically favourable to conventional columns; however, only a very small subset of these systems can use SVRC in practice, due to the limiting factor of compression ratio: typical single-stage compressors in the petrochemical industry are limited to pressure ratios of about 3.5 (Boyce, 2011).

SVRC is attractive not only for its benefits in terms of energy efficiency, but also because of its comparative simplicity: the trend in research is one of growing complexity, from diabatic (Fonyó, 1974; Le Goff et al., 1996), to complex (Rév et al., 2001; Hernández-Gaona et al., 2005; Agrawal, 2003; Caballero and Grossmann, 2003, 2013; Shenvi et al., 2013), to heat-integrated distillation columns (Glenchur and Govind, 1987; Nakaiwa et al., 2000; Olujić et al., 2003; Huang et al., 2006, 2008; Mane and Jana, 2010; Chen et al., 2010; Suphanit, 2011). Moreover, the SVRC configuration has the advantage of being constructed using industry-standard units, while the same cannot be said of all of the aforementioned complex modifications, e.g. the concentric column of Glenchur and Govind (1987).

The aim of the work in this chapter is to bring the relative simplicity and energy-saving capabilities of vapour recompression to a wider range of systems than SVRC allows. The resulting configurations meet this goal, and are applicable to systems far outside of the reach of SVRC. However, while SVRC can accept feeds of any type, but is limited to close-boiling systems, the novel configurations presented in this chapter are applicable to a much greater range of systems. One of the novel configurations is limited to light liquid feeds, and the other to heavy vapour feeds. Nevertheless, in situations where the appropriate feed is available, the proposed configurations often yield significant advantages in comparison to conventional distillation and SVRC.

It appears that the type of vapour recompression between products and the feed that is proposed in this work has not previously been investigated.

The point of departure for this work is a parametric study of the effects of feed preconditioning on the entropy generation and total heat input in a conventional distillation column, which is shown in § 6.2. Thereafter, the results of the preconditioning investigation are used to identify possible targets for

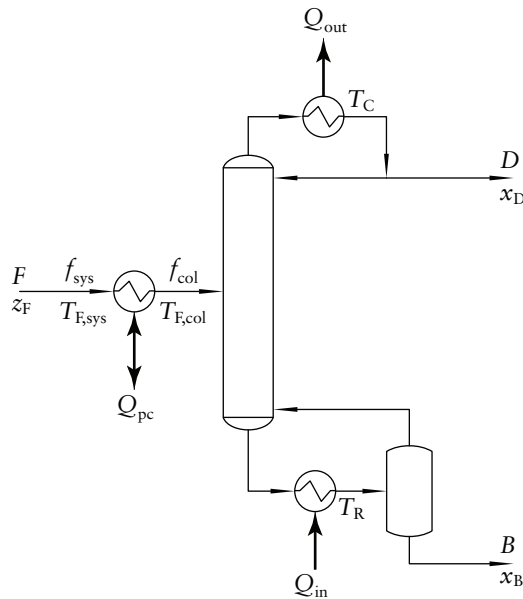


Figure 6.1
Diagram of a conventional distillation column with feed preconditioning.

vapour recompression, which are then developed to produce the novel configurations in § 6.3. By way of numerical experiments, a comparative analysis is performed on conventional columns, SVRC, and the proposed configurations, to examine the lowest possible energy input, work input, entropy generation, and compression ratios, under pinched conditions; this can be found in § 6.4. Finally, rigorous simulations are used to demonstrate and validate the use of the novel configurations in four examples in § 6.5.

6.2 Developmental background

The point of departure for the novel configurations is a parametric study of the effects on entropy generation, S_{gen} , and total heat input, $Q_{\text{in,tot}}$, that result from changing the feed condition (preconditioning) in a conventional column, while adjusting the column to be at minimum reflux in all cases (which is a function of feed condition to the column). This is achieved by placing a preconditioner on the feed stream, which is a heat exchanger that can either add or remove energy to effect the condition change. A schematic drawing of this arrangement is given in Figure 6.1, with the relevant variables labelled.

Preconditioning, and especially preheating, has previously been studied by a number of researchers (Agrawal and Herron, 1997, 1998; Soave and Feliu, 2002; Bandyopadhyay, 2002; Bandyopadhyay et al., 2003; Deshmukh et al., 2005; Bandyopadhyay, 2007; Huang et al., 2008). However, none of these studies has thoroughly investigated the effects of feed preconditioning on entropy generation (or related quantities, such as exergy) alongside energy

requirements in conventional columns, while accounting for the changing minimum reflux that results from the preconditioning. Previous research has considered preheating in two-feed columns (Wankat and Kessler, 1993; Agrawal and Herron, 1997, 1998; Soave and Feliu, 2002; Deshmukh et al., 2005), feed preheating and controllability of heat-integrated distillation columns (Huang et al., 2008), or have focused on column internals (Bandyopadhyay, 2002; Bandyopadhyay et al., 2003; Bandyopadhyay, 2007). As such, none of these previous studies has considered preconditioning in exactly the same way as is required in this chapter.

The limit of thermodynamic efficiency is zero entropy generation. Real processes, however, generate entropy to varying degrees, with lower entropy generation being favourable for efficiency.

As a way of investigating the impact of preconditioning, a simple numerical experiment was set up: a continuous column was rigorously modelled to separate a feed mixture into products with 99.9 mol% purity. The feed composition was fixed, after which a feed condition was selected by defining the vapour fraction of the feed entering the system, f_{sys} . For each f_{sys} , an f_{col} was also selected; the latter is simply the vapour fraction of the feed entering the column, after the preconditioner. Therefore, if $f_{\text{sys}} > f_{\text{col}}$, the preconditioner is removing heat, i.e. cooling; conversely, if $f_{\text{sys}} < f_{\text{col}}$, the preconditioner must be a heater.

For each combination of f_{sys} and f_{col} , it is possible to determine the effect on entropy generation, as well as on total heat input. For this purpose, two new variables are defined. To evaluate the relative change in entropy generation between cases with and without a preconditioner, the following variable is used:

$$\zeta_S \equiv \frac{S_{\text{gen}} (\text{with preconditioner}) - S_{\text{gen}} (\text{no preconditioner})}{S_{\text{gen}} (\text{no preconditioner})} \quad (6.1)$$

To evaluate the effects on total heat input, $Q_{\text{in,tot}}$, the following variable is defined similarly to ζ_S :

$$\zeta_Q \equiv \frac{Q_{\text{in,tot}} (\text{with preconditioner}) - Q_{\text{in,tot}} (\text{no preconditioner})}{Q_{\text{in,tot}} (\text{no preconditioner})} \quad (6.2)$$

The symbol Q_{pc} will be used to denote the energy transferred by the preconditioner. If the preconditioner is cooling, then $Q_{\text{pc}} < 0$, and the only heat input into the system is at the reboiler, such that $Q_{\text{in,tot}} = Q_{\text{in}}$. If, on the other hand, the preconditioner is adding energy, then $Q_{\text{pc}} > 0$, and energy is

added at two points in the system (at the reboiler, and at the preconditioner), in which case $Q_{\text{in,tot}} = Q_{\text{in}} + Q_{\text{pc}}$. The above conditions can be generalised as follows:

$$Q_{\text{in,tot}} = Q_{\text{in}} + \max\{Q_{\text{pc}}, 0\} \quad (6.3)$$

The values of Q_{in} and Q_{pc} can be determined from the mass and energy balances around the configuration in Figure 6.1, while S_{gen} can be calculated using an additional entropy analysis:

$$F\hat{S}_F + \frac{Q_{\text{pc}}}{T_{\text{F,col}}} + \frac{Q_{\text{in}}}{T_{\text{R}}} + S_{\text{gen}} = D\hat{S}_D + B\hat{S}_B + \frac{Q_{\text{out}}}{T_{\text{C}}} \quad (6.4)$$

In Eq. (6.4), Q_{in} and Q_{out} are assumed to be positive values, with the direction of heat transfer set by the side of the equation on which they reside; Q_{pc} , however, can be positive or negative, depending on its duty. While the exact temperatures of heat input and rejection are seldom clear, they are chosen in Eq. (6.4) so as to maximise the entropy generation, i.e. to consider the conservative or worst-case scenario.

Further information on the energy and entropy balances can be found in Appendix E.1.

For the purposes of this investigation, the well-known, near-ideal mixture of benzene–toluene was used. Three feed compositions were considered: a light feed with $z_{\text{F}} = (0.95, 0.05)$, an equimolar feed, and a heavy feed of $z_{\text{F}} = (0.05, 0.95)$. In all cases, the distillate composition was $x_{\text{D}} = (0.999, 0.001)$ and the bottoms composition was $x_{\text{B}} = (0.001, 0.999)$. The properties used in this model are given in Appendix E.1.

It is obvious, but important to note, that the temperature of the light feed is close to that of the distillate, and the temperature of the heavy feed is close to that of the bottoms.

For each of the feed cases, the ζ_{S} and ζ_{Q} surfaces were plotted as functions of f_{sys} and f_{col} , where the column is operated at minimum reflux corresponding to z_{F} and f_{col} . The plots for the light, equimolar, and heavy feeds are given in Figures 6.2*a*, *b*, and *c*, respectively.

Wherever $f_{\text{sys}} = f_{\text{col}}$, the feed remains unchanged; as such, ζ_{S} and ζ_{Q} are zero along this line in all of the plots.

Figure 6.2*b* shows the ζ_{S} and ζ_{Q} surface for the equimolar feed; it is observed that some slight reduction in entropy generation can be achieved using preconditioning, but it is accompanied by quite a high increase in total heat input. Opportunities for new configurations do not appear forthcoming

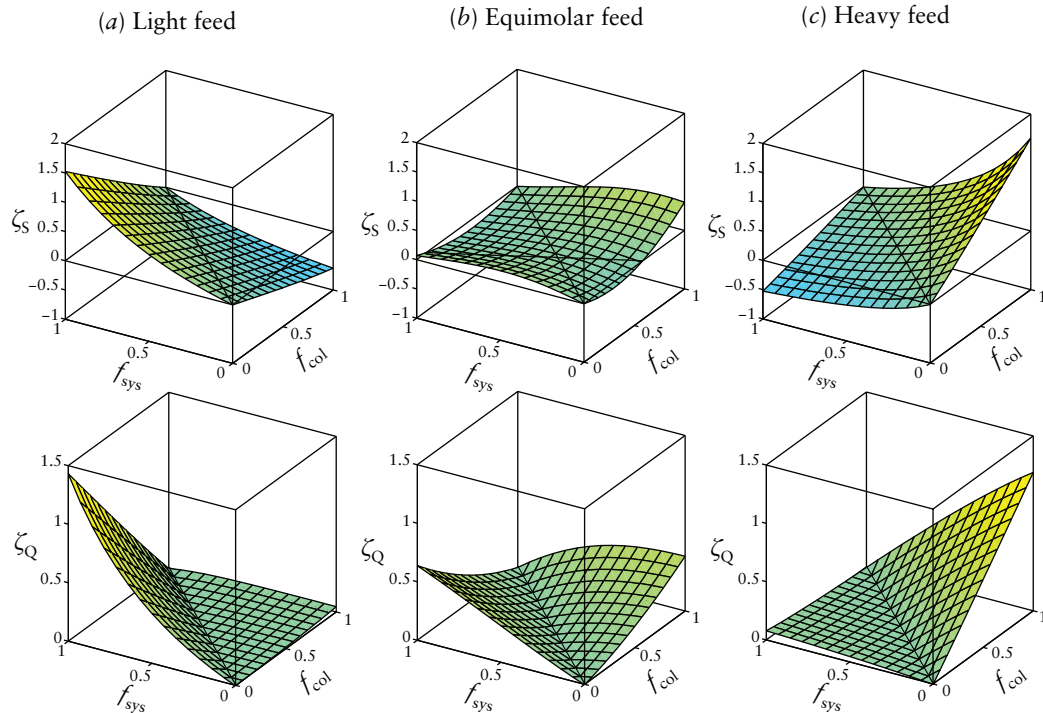


Figure 6.2 Surfaces of relative change in entropy generation when preconditioning is used, ζ_S , and relative change in heat input, ζ_Q , as functions of the feed vapour fraction into the system, f_{sys} , and the vapour fraction into the column, f_{col} . Plots are shown for a benzene–toluene feed of (a) $z_F = (0.95, 0.05)$, (b) $z_F = (0.50, 0.50)$, and (c) $z_F = (0.05, 0.95)$. The column is always at minimum reflux.

for this case, and it will be disregarded from this point forth; nonetheless, it is included here for completeness, and to indicate that possible benefits are only marginal.

6.2.1 Light feed

In the case with the light feed (Figure 6.2a), if the feed is condensed to any extent ($f_{\text{col}} < f_{\text{sys}}$), the total heat input increases ($\zeta_Q > 0$), as does the entropy generation ($\zeta_S > 0$). However, it is seen that if the light feed is vaporised, there is a slight increase in heat input, along with a large decrease in entropy generation; i.e. at the expense of some additional heat input, the column operates more reversibly. This effect is most pronounced when the light, saturated liquid feed is vaporised completely, and it is this scenario that will be of interest for the light feed in the rest of this chapter.

A light feed flow rate of $F = 1$ mol/s is assumed. Without vaporisation of the light feed ($f_{\text{sys}} = 0 = f_{\text{col}}$), the minimum reflux is $r_{\text{min}} = 0.6568$, total heat input into the system is $Q_{\text{in,tot}} = 48.995$ kW, and entropy generation is $S_{\text{gen}} = 9.367$ W/K. However, when the feed is vaporised completely ($f_{\text{sys}} = 1, f_{\text{col}} = 1$),

$r_{\min} = 0.7399$, $Q_{\text{in,tot}} = 51.444 \text{ kW}$, and $S_{\text{gen}} = 3.493 \text{ W/K}$. As Figure 6.2a shows, there is a 62.7% decrease in entropy generation, accompanied by an increase in total heat input of 5.0%.

If the internal flows in the column were kept identical in the two cases, then the energy balance would dictate that the overall heat input would remain the same: there would be a reduction in reboiler duty equal to the vaporisation duty on the feed. However, vaporising the feed leads to an increase in the minimum reflux ratio in the column from 0.6568 to 0.7399, which increases the overall heat input slightly. Nevertheless, a significant portion of this heat is supplied to the system at a much lower temperature (that of the feed, which is close to the temperature of the distillate in the case of the light feed). Thus, instead of supplying a given amount of heat without preconditioning at the higher bottoms temperature, slightly more heat is added when preconditioning is used, but a large portion of it is introduced at a temperature near the (lower) distillate temperature, which results in lower entropy generation, i.e. more reversible operation.

6.2.2 Heavy feed

In the case of the heavy feed (Figure 6.2c), the trend observed is opposite to that of the light feed: if the feed is vaporised to any extent, there is a sharp increase in both heat input and entropy generation, but if it is condensed to any extent, there is a relatively small increase in heat input, and a large decrease in entropy generation. The greatest reduction in entropy generation for the heavy feed occurs when a saturated vapour feed is condensed completely; this will be the point of interest with the heavy feed for the remainder of this chapter.

As with the light feed, a feed flow rate of $F = 1 \text{ mol/s}$ is assumed. Without condensation of the feed ($f_{\text{sys}} = 1 = f_{\text{col}}$), $r_{\min} = 37.589$, $Q_{\text{in,tot}} = 24.819 \text{ kW}$, and $S_{\text{gen}} = 12.713 \text{ W/K}$. When the heavy, saturated vapour feed is fully condensed prior to entering the column ($f_{\text{sys}} = 1$, $f_{\text{col}} = 0$), $r_{\min} = 16.545$, $Q_{\text{in,tot}} = 26.894 \text{ kW}$, and $S_{\text{gen}} = 6.046 \text{ W/K}$. This amounts to a decrease in entropy generation of 52.4%, and an increase in total heat input of 8.4%.

While the results for the light and heavy feeds are almost the same—albeit at ‘inverse’ conditions—the reason for the decrease in entropy generation and the slight increase in heat input is very different.

In the case of the heavy feed, heat is removed from the feed stream. If the internal flows in the column were to remain the same in the preconditioned and non-preconditioned cases, the overall energy balance would stipulate that the

reboiler duty would increase by the same amount as the heat load removed from the feed. Overall, the heat input would be much greater. However, condensing the heavy vapour feed results in a significant reduction in the minimum reflux ratio: from 37.589 to 16.545, which has the effect of reducing the heat load. In essence, there are two competing factors: an increase in the reboiler heat input due to the offset of duty from the feed stream, and a decrease due to the reduction in minimum reflux; the net result is that the overall heat input is slightly increased. Despite this, there is a reduction in entropy generation, since a fair portion of the overall heat rejection takes place at a higher temperature (that of the feed, which, in the heavy-feed case, is close to the bottoms temperature), compared to when no preconditioning is done. In the case without a preconditioner, all of the heat is rejected at the lowest possible temperature, i.e. that of the distillate.

6.3 Novel configurations

It was shown in the previous section that, at least for the benzene–toluene system, vaporising a light saturated liquid feed, or condensing a heavy saturated vapour feed, resulted in more reversible operation, as long as the reflux ratio was adjusted to be proportional to minimum reflux in each case. However, this preconditioning also resulted in somewhat increased heat input. The significant (>50%) reduction in entropy generation is promising, but to make the modification truly compelling, a reasonable reduction in energy requirements is also necessary.

The approach to achieving a simultaneous reduction of entropy generation and heat input is discussed in this section. While the general principle for the light and heavy feeds is quite similar, the resulting configurations are different, and will thus be treated separately.

6.3.1 Configuration for light feeds: FDVRC

The analysis of preconditioning has shown that it is desirable to vaporise a light feed before it enters the column, at the expense of additional energy input. Rather than including an additional external heat input, it would be preferable to transfer the required energy to the feed stream from within the system, thus conserving energy. The best candidate for this is the overhead vapour, which has a large latent heat load that could be used for this purpose. Thus, in the process of transferring energy, the feed would vaporise completely, and the

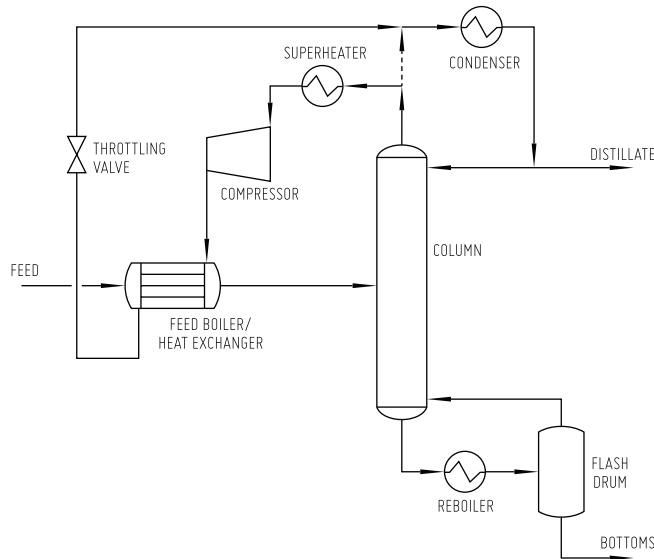


Figure 6.3
Schematic drawing of the novel configuration for light, saturated liquid feeds: FDVRC. The dashed line is an optional partial bypass stream.

overhead vapour would condense partially. (The uncondensed portion of the overhead vapour would then be condensed fully in a conventional condenser.)

However, it is unfortunately not possible to transfer this energy by direct heat exchange, since the overhead vapour is at a lower temperature than the feed, i.e. the energy transfer would take place in the wrong direction. One way of overcoming this problem is by introducing a heat pump to transfer heat from the lower temperature to the higher one. For ease of interpretation, a diagram of the proposed novel configuration is given in Figure 6.3, which is explained below.

The heat pump system is achieved by compressing the overhead vapour, thereby raising its temperature, and also lifting the dew point of the overhead vapour, such that it will condense at a higher temperature than the feed, allowing the vapour's energy to be transferred to the feed. Since the feed flow is smaller than the overhead vapour flow, there is sometimes no need to compress the entire overhead vapour stream; it is more efficient to use only a portion of the overhead vapour stream to vaporise the feed. This partial bypass is shown as the dashed stream in Figure 6.3.

After the heat exchange, the pressure of the partially condensed overhead vapour is dropped back down to column pressure, after which it joins with the bypassed overhead vapour; the combined overhead stream is then condensed in the condenser. Finally, part of the liquid overhead product is refluxed back to the column, and the remainder drawn off as distillate, as in a conventional column. This new configuration is dubbed Feed–Distillate Vapour Recompression (FDVRC).

Note that the configuration in Figure 6.3 also contains a superheater be-

fore the compressor. As explained in some detail in Chapter 5, the reason for this superheating is that some saturated vapours—depending on their properties—condense on compression (Patwardhan, 1987; Felbab, 2013); liquid formation, however, must be strictly avoided in compressors to prevent erosion (Meili and Stuecheli, 1987; Patwardhan, 1987; Gmehling et al., 2012). To circumvent this problem, a superheater can be used prior to compression, allowing the compressor outlet to remain uncondensed. The superheater does introduce an additional heat input to the overall system, and must be taken into account when considering the total energy input. Moreover, if the latent heat of the overhead vapour is insufficient to vaporise the feed stream, then the full overhead stream is needed (i.e. no partial bypass), and the energy deficit is added using the superheater.

6.3.2 Configuration for heavy feeds: FBVRC

The use of heat pumps to transfer energy from one part of the system to another is not limited to light feeds. In § 6.2.2, it was found that if a heavy saturated vapour feed of benzene–toluene was fed into the system, and condensed fully prior to entering the column, there was a significant reduction in entropy generation, accompanied by a small increase in total heat input. It would be advantageous if the benefit of lower entropy generation could be retained, while reducing the heat input.

Since energy needs to be removed from the feed stream in order to condense it, it would be most efficient to use that energy in another part of the system where energy input is required. The most obvious candidate for this energy transfer is the reboiler. Since the feed is at a lower temperature than the bottom liquid from the column, energy can only be transferred from the former to the latter by means of a heat pump. This concept leads to the novel configuration shown in Figure 6.4, which is dubbed Feed–Bottoms Vapour Recompression (FBVRC).

The saturated vapour feed may need to be superheated to avoid condensation on compression, as mentioned earlier. It is then compressed in order to raise its temperature, along with its dew point; in this way, the feed can condense at a higher temperature than the bottoms in order to transfer energy to the latter in the reboiling heat exchanger. The liquid from the bottom of the column is saturated, such that this addition of heat in the heat exchanger causes it to partially vaporise. If the latent heat of the condensing feed is insufficient to provide the required reboil rate, additional energy can be added

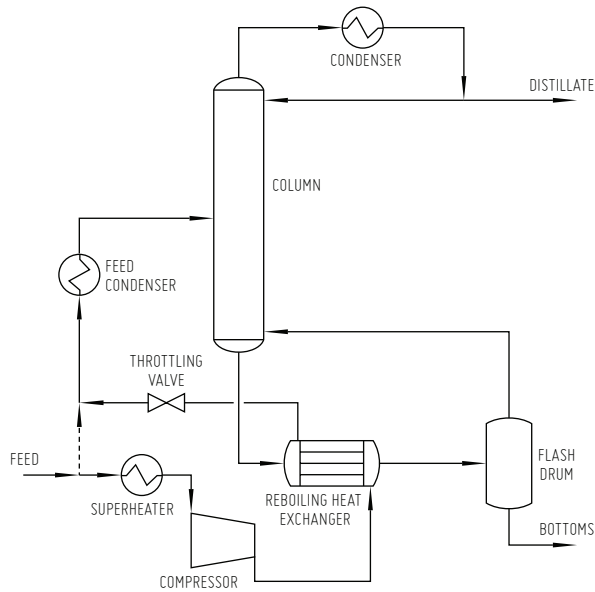


Figure 6.4
Schematic drawing of the novel configuration for heavy, saturated vapour feeds: FBVRC. The dashed line is an optional partial bypass stream.

using the superheater. If, on the other hand, the vapour feed can provide more energy than necessary for the reboil duty, energy can be saved by using only a part of the feed; the rest can be bypassed to the feed condenser, as indicated by the dashed stream in Figure 6.4. The compressed feed leaves the heat exchanger as a partially or totally condensed stream, which is then brought down to column pressure using a throttling valve, and then combined with the bypass stream. This combined feed stream is then fully condensed, and fed to the column. The rest of the column is operated like a conventional column.

6.4 Comparison of various configurations

In Chapter 5, high-level thermodynamic analyses were performed on conventional columns and SVRC using simple equations, based on a number of simplifications. Only a small number of constant properties are needed in that approach. Using those equations, it is possible to gain a general understanding of the behaviour of the configurations, and to assess different systems for which simple properties are available. The same sort of approach can be used for the FDVRC configuration proposed in this chapter; unfortunately, however, that sort of high-level analysis is impractical for FBVRC, which requires compression and condensation of mixtures (as opposed to pure components) and renders the high-level analysis counterproductively complex. As such, in order to carry out the comparison in this section on a consistent basis, the analyses of conventional, SVRC, FDVRC, and FBVRC use detailed, rigorous calculations, rather than the high-level approach from

Chapter 5. The properties used for these models are given in Appendix E.1. The relevant equations for the high-level analysis of the FDVRC can be found in Appendix E.2.

As in Chapter 5, the aim here is to determine the behaviour of the various configurations under the best theoretical circumstances in each case, from a process point of view. Liquid and vapour feeds are treated separately, since the FDVRC and FBVRC configurations are applicable to different feed conditions.

In order to limit the number of variables being assessed, two conditions are fixed: only binary systems are considered, and the distillate and bottoms in each case are set to 99.9 mol% purity of light and heavy component, respectively.

The parameter that is varied is the feed composition. For each feed composition—given the above fixed conditions—a fully pinched, idealised design is calculated, which entails the following:

- 1 The column is pinched, i.e. at minimum reflux, which is calculated rigorously using mass and energy balances. This not only gives the minimum energy requirement, but it also requires an infinite number of stages, thereby eliminating another variable from the analysis;
- 2 The compressor pressure ratio is set to the minimum value at which the full latent heat of the hot stream can be transferred to the cold stream, while giving at least one temperature pinch in the heat exchanger. The heating and cooling curves are calculated to ensure that this condition is met, and that there is no temperature cross-over at any point in the heat exchanger; and
- 3 The compressor has an isentropic efficiency of 100%.

There is a degree of freedom in how much energy is added via the superheater, and how much via the compressor. For example, it is theoretically possible, though undesirable, to add the entire required boil-up duty via the superheater, which entirely defeats the energy-saving capabilities of these configurations. As such, the chosen design philosophy is to use the minimum compression ratio that allows the compressed stream to deliver its full latent heat load to the cold stream; the superheater is used in only two situations: to avoid condensation in the compressor, and to add additional energy when the latent heat is insufficient to provide the required heat duty.

Four near-ideal binary systems are examined using the above methodology. For the purposes of this analysis, azeotropic systems were not considered, as

they add additional complications. The systems were chosen to represent a wide range of relative volatilities, which is the main characteristic that defines zeotropic separation problems; these systems are: acetonitrile–nitromethane ($\alpha \approx 1.84$), benzene–toluene ($\alpha \approx 2.47$), 1-heptanal–1-decanal ($\alpha \approx 4.96$), and *n*-hexane–*n*-nonane ($\alpha \approx 11.21$).

The performance and efficiency of the different configurations is determined using several metrics: the minimum energy input and its associated work input, the entropy generation, and the minimum required compression ratio (which is not applicable to the conventional column). The first three are given as values per unit feed flow, for generality. As discussed in Chapter 5, all heat flows have associated virtual work input. Work is a useful metric because it takes into account the quality of the heat, not just the quantity. If the best-case scenario is considered, it is assumed that the virtual work is added using a reversible heat pump. Therefore, the reversible work input, W_{in} , associated with a heat input, Q_{in} , at temperature T is estimated as follows:

$$W_{\text{in}} = Q_{\text{in}} \left(1 - \frac{T_0}{T} \right) \quad (6.5)$$

For each calculation, thorough checks were carried out to ensure that mass and energy were in balance, that entropy generation in each part of the process was positive, and that the direction of heat transfer was correct in all cases.

6.4.1 Liquid feeds

For liquid feeds, the conventional, SVRC, and FDVRC configurations are applicable. The plots of energy input, work input, entropy generation, and compression ratio for these configurations are given in Figure 6.5. Note that the plots for SVRC in the *n*-hexane–*n*-nonane system are not shown for the full feed composition range; points which required supercritical temperatures in the compressor were omitted.

In comparison with conventional distillation, it is seen in Figure 6.5 that for light feeds—the intended area of application of the proposed configuration—FDVRC is indeed more efficient than conventional distillation, regardless of the metric used: energy input, work input, and entropy generation are all lower for the FDVRC.

The motivation behind the FDVRC configuration was an attempt to retain the entropy generation advantages of preconditioning, while simultaneously reducing the energy requirements. From the plots for the benzene–toluene

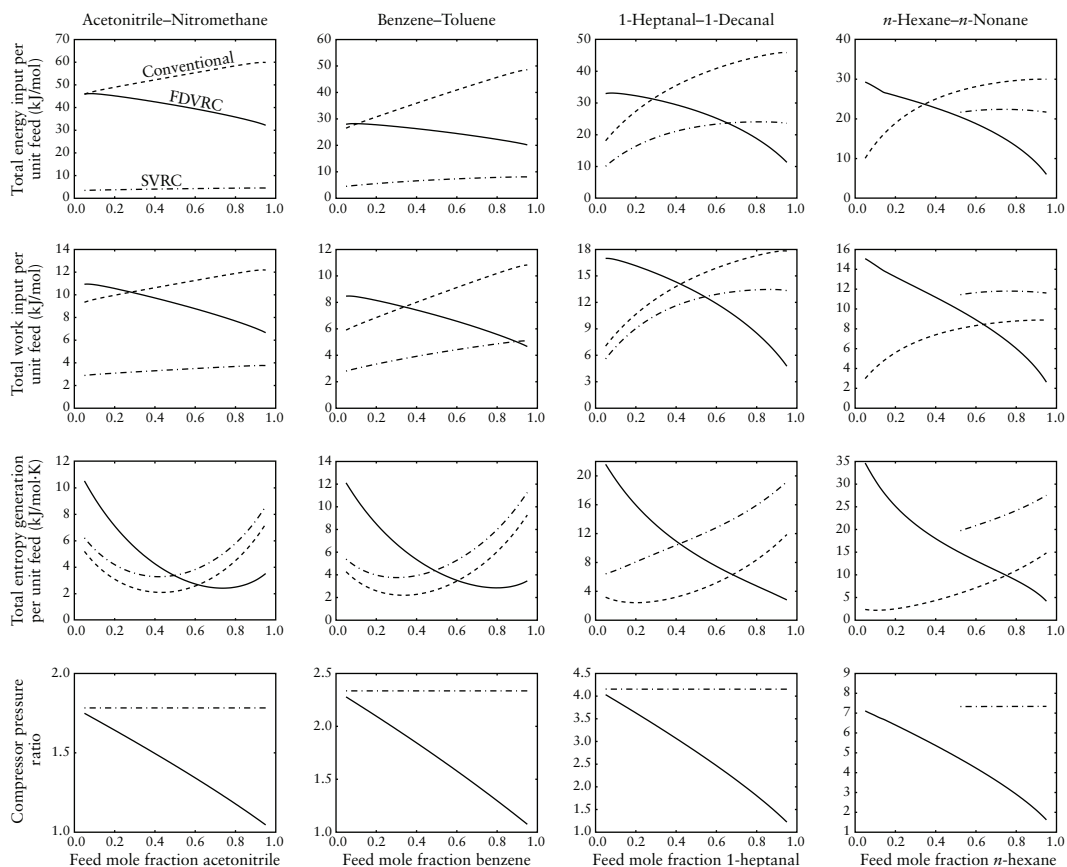


Figure 6.5 Detailed comparison of the minimum energy requirements, associated work input, entropy generation, and pressure ratio as a function of composition of the saturated liquid feed, for conventional distillation (dashed line), SVRC (dot-dashed line), and FDVRC (solid line). Plots are shown for various near-ideal binary systems, in order of increasing relative volatility from left to right. Product purities of 99.9 mol% are fixed in each case.

system in Figure 6.5, it is seen that the 95-mol%-benzene feed undergoes a reduction in entropy generation of 62.6% compared with conventional distillation, and a reduction in energy requirements of 58.5%. The FDVRC scheme has thus been successful in its purpose.

It is clear that, in all cases, light feeds benefit from FDVRC compared to conventional distillation. The approximate trend that is apparent in Figure 6.5 is that lower relative volatility systems benefit less from FDVRC than do higher relative volatility systems.

Compared to SVRC, FDVRC is not as efficient for systems with low relative volatilities; indeed, those are the systems for which SVRC excels, both thermodynamically and practically, as shown in Chapter 5. However, when systems with higher relative volatilities are considered, the advantage of FDVRC for light feeds becomes obvious.

One crucially important advantage that FDVRC has over SVRC is that of compression ratios. For practical implementation, a single-case compressor is generally limited to a pressure ratio of 3.5 Boyce (2011); in many systems, this is the deciding factor for implementation of vapour recompression. Moreover, higher pressure ratios have a negative impact on the process economics, along with a decrease in the compressor efficiency (Boyce, 2011). While SVRC has a fixed minimum pressure ratio for a given system, the pressure ratio for FDVRC tends to unity as the feed composition tends to that of the distillate. Consequently, in systems where the practical implementation of SVRC is limited by the pressure ratio, FDVRC can still be used successfully, at least for light feeds.

It is thus obvious that FDVRC is applicable to a range of distillation problems beyond the reach of SVRC, where it can yield significant efficiency benefits.

6.4.2 Vapour feeds

Unlike FDVRC, FBVRC is designed for heavy vapour feeds. As such, conventional distillation, SVRC, and FBVRC are compared in Figure 6.6. The FBVRC line is absent from the acetonitrile–nitromethane system because, in all cases, it requires a supercritical gas in the compressor to provide the required reboil duty, and has thus been omitted. Another feature that should be addressed is the sudden change in gradient in some plots for the FBVRC. This occurs due to a change in the heat transfer regime, brought on by the feed vapour not having sufficient latent heat to provide the reboil duty beyond a certain composition, which thus requires additional energy input in the superheater.

The conclusions that can be drawn about FBVRC from Figure 6.6 are more straightforward than for the previous analysis concerning FDVRC. First, it is noted that for the acetonitrile–nitromethane system, for which SVRC excels, FBVRC is not applicable at all. This can be attributed in part to the fact that the mixture is close-boiling, and thus has a large reflux ratio, leading to quite a high reboil rate. The problem is compounded by the fact that both components have a very low ideal gas heat capacity, and thus superheat rapidly on compression. Consequently, when the additional energy for reboil is added in the superheater, the temperature rises rapidly, and becomes supercritical when compression is performed. Moreover, as the temperature increases, the latent heat decreases, and ultimately results in a lack of subcritical solution for the configuration.

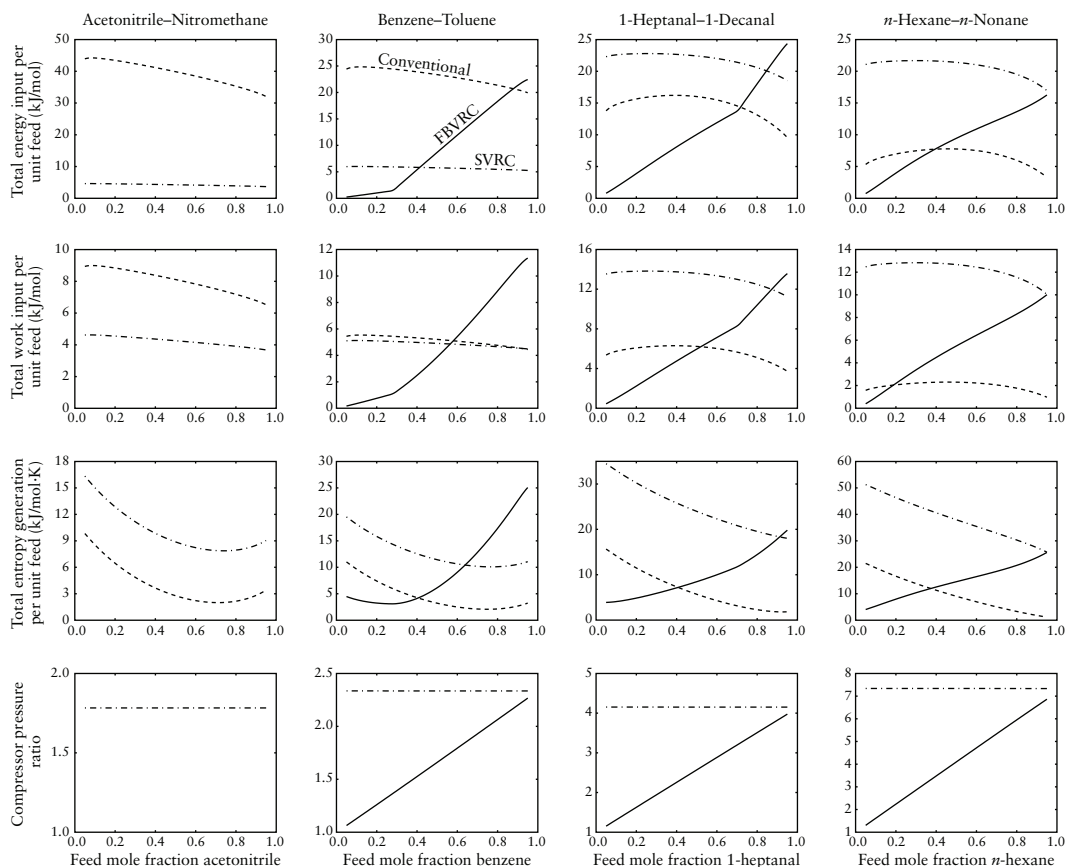


Figure 6.6 Detailed comparison of the minimum energy requirements, associated work input, entropy generation, and pressure ratio as a function composition of the saturated vapour feed, for conventional distillation (dashed line), SVRC (dot-dashed line), and FBVRC (solid line). Plots are shown for various near-ideal binary systems, in order of increasing relative volatility from left to right. Product purities of 99.9 mol% are fixed in each case.

Isentropic compression of saturated vapours in the other three systems leads to partial condensation, which—counterintuitively—is favourable, in order to avoid the problem of uncontrollable, excessive superheating on compression that the acetonitrile–nitromethane system experiences. These other systems use the superheater to ensure that no condensation takes place in the compressor, and to add the additional heat for reboil.

In the cases where supercritical temperatures are not a concern, it is abundantly clear that FBVRC is significantly better for heavy feeds than conventional or SVRC distillation, as measured by any of the metrics.

The motivation leading to the FBVRC scheme was an attempt to obtain similar entropy generation reduction benefits as preconditioning heavy vapour feeds, but accompanied by a suitable reduction in energy input. It is seen that the FBVRC configuration is exceptionally effective in achieving this goal. For

example, with a 5-mol%-benzene feed in the benzene–toluene case, using FBVRC instead of conventional distillation yields a decrease of 59.4% in entropy generation, and a staggering reduction in energy requirements of 99.1%.

Moreover, not only is FBVRC more efficient than SVRC for the heavy vapour feeds, but it also requires much lower compressor pressure ratios than SVRC in that feed composition region. Similarly to FDVRC, as the feed composition tends to that of the bottoms, the minimum pressure ratio tends to unity. FBVRC is applicable to systems for which the SVRC's pressure ratio is prohibitive of practical implementation.

6.5 Rigorous simulation and validation

The previous section considered the minimum-energy case, and was useful for identifying the relative strengths and weaknesses of FDVRC and FBVRC compared to conventional and SVRC distillation. However, these minimum-energy designs are not practically achievable, as they require an infinite number of stages, and infinite heat transfer area in the heat exchangers. It is thus important to investigate whether the benefits of the proposed configurations carry over to more realistic scenarios, by means of rigorous simulation with a commercial process simulation package. The software used for this purpose was Aspen Plus (Aspen Technology, Inc., 2007). Vapour–liquid equilibrium (VLE) was modelled using its NRTL-RK property method: the NRTL model for the liquid (Renon and Prausnitz, 1968), and the Redlich–Kwong equation of state for the vapour (Redlich and Kwong, 1949). The flowsheets and associated nomenclature for the conventional and SVRC simulations can be found in Figures 5.12 and 5.13, respectively. Figures 6.7 and 6.8 give the flowsheets and nomenclature for the FDVRC and FBVRC configurations, respectively.

The examples were chosen to validate some of the scenarios in which FDVRC and FBVRC were advantageous in Figures 6.5 and 6.6, and to investigate the application of the novel configurations to multicomponent systems. Note that the examples in this section were specifically chosen for scenarios in which FDVRC and FBVRC are expected to perform well; the novel configurations are not applicable and advantageous in all problems. Azeotropic systems are not considered, as they tend to require high boilup rates, which significantly reduces the benefits of the proposed configurations.

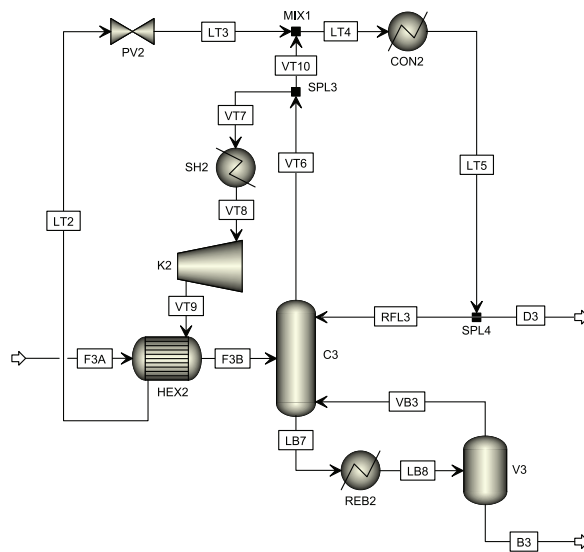


Figure 6.7
Aspen Plus flowsheet for the rigorous simulation of the FDVRC configuration.

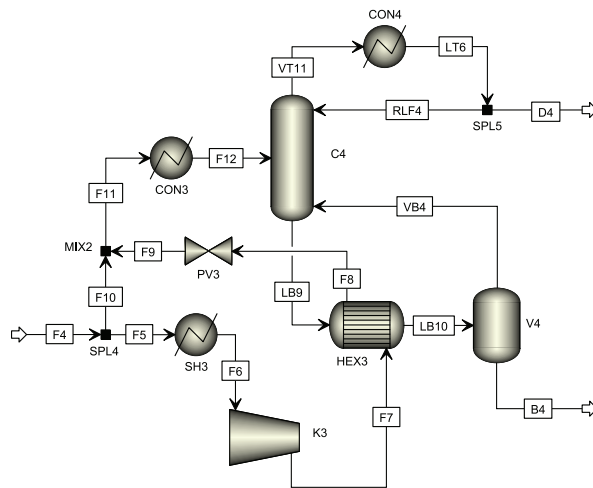


Figure 6.8
Aspen Plus flowsheet for the rigorous simulation of the FBVRC configuration.

The settings for the simulations are provided in Appendix E.3, and the results of the four examples are summarised in Table 6.1.

6.5.1 Design methodology

First, the feed composition and condition, and desired product compositions were set.

For the binary separation examples, the minimum reflux, r_{\min} , was rigorously calculated by means of mass and energy balances; the reflux ratio was set to $r = 1.5 r_{\min}$. In order to determine the number of stages required, and to identify the feed stage, a ‘rigorous McCabe–Thiele’ approach was used: that is, having specified the feed, products, and reflux ratio, mass and energy balances were used to ‘step down’ from the top of the column, stage by stage, until the

Table 6.1 Summary of the results of the rigorous simulation examples, showing the energy and work input for all of the configurations, as well as the compression ratio, where applicable.

Ex.	Conventional		SVRC			FDVRC			FBVRC		
	E_{in}	W_{in}	E_{in}	W_{in}	Π	E_{in}	W_{in}	Π	E_{in}	W_{in}	Π
1	13.02	5.05	7.73	4.49	4.56	6.55	2.80	1.55	–	–	–
2	14.28	3.17	3.10	2.71	2.67	–	–	–	2.06	0.83	1.30
3	12.15	4.72	4.66	4.66	23.53	5.26	2.32	3.50	–	–	–
4	11.48	2.25	5.59	3.74	4.20	–	–	–	1.42	0.57	1.35

Total energy input, E_{in} , and total work input, W_{in} , have units of kW.

$\Pi \equiv P_{comp}/P_0$.

liquid composition at the bottom of the column met the bottoms composition criterion. This also provided a value for the required reboiler vapour fraction.

For the multicomponent examples, ChemSep (Kooijman and Taylor, 2013) was used to estimate minimum reflux (using fixed product specifications and 300 stages). Thereafter, the reflux ratio was chosen as $r = 1.5 r_{min}$, and the minimum number of stages was found by trial and error such that the product specifications were met using the chosen reflux ratio.

This preliminary simulation provided initial guesses for the Aspen Plus input parameters. As a safety factor, one extra stage was added to the rectifying section, and one to the stripping section in the Aspen Plus simulations. A minimum approach temperature of 5 K was specified in the heat exchangers.

Example 1: light 1-heptanal–1-decanal liquid feed

It is seen in Figure 6.5 that FDVRC appears to be thermodynamically superior to conventional and SVRC distillation for light liquid feeds of 1-heptanal–1-decanal; it also has the advantage of requiring a much lower compression ratio than SVRC for these light feeds.

To test this by means of rigorous simulation, a 1 kmol/h saturated liquid feed of 90 mol% 1-heptanal was selected, to be split into a distillate of >99.5 mol% 1-heptanal, and a bottoms of >99.5 mol% 1-decanal.

Because both the conventional column and the column SVRC are fed with direct liquid feed, they are able to produce exactly the same products. For these configurations, the final simulation produced a distillate with 99.55 mol% 1-heptanal, and a bottoms with 99.91 mol% 1-decanal, both of which meet the required purity specifications. The FDVRC column is fed with a vaporised

feed, which can thus not result in exactly the same products as the previous two configurations. For the FDVRC, the simulation gave a distillate of 99.51 mol% 1-heptanal, with a bottoms of 99.82 mol% 1-decanal.

The total energy input, total work input—as simply estimated using Eq. (6.5)—and compression ratio for the SVRC and FDVRC are given in Table 6.1. The result shows that FDVRC has 49.7% lower energy input than conventional distillation, and 15.3% lower than SVRC. Work input is also lowest in the FDVRC, with a 44.6% reduction compared to the conventional case, and 37.6% lower compared to SVRC.

While the thermodynamic improvements of FDVRC over SVRC are less pronounced than over conventional columns, a key differentiator is the required pressure ratio. The SVRC requires a compressor ratio of 4.56, which is too high to be implemented practically in a single-case compressor; the FDVRC, however, needs only a low ratio of 1.55, which is easily achievable in practice.

Consequently, not only is FDVRC the best of the three configurations for this problem, but it can also be implemented practically, whereas SVRC cannot.

Example 2: heavy benzene–toluene vapour feed

Figure 6.6 indicated that for a heavy vapour feed in the benzene–toluene system, significant improvements over conventional and SVRC could be achieved using FBVRC.

For the purposes of this rigorous simulation, a saturated vapour feed of 9 mol% benzene was chosen, with the aim of separating it into products with >99.5 mol% purity.

The conventional column and SVRC can produce exactly the same products; for these configurations, the simulation produced a distillate of 99.80 mol% benzene, and a bottoms of 99.78 mol% toluene. The FBVRC simulation gave a distillate of 99.72 mol% benzene, and a bottoms of 99.65 mol% toluene.

As for Example 1, the results are given in Table 6.1.

It is seen that FBVRC is significantly better than either the conventional column and SVRC: in terms of energy requirements, FBVRC is better than conventional distillation by 85.6%, and better than SVRC by 33.5%. The reduction in work input is 73.9% compared to the conventional case, and 69.4% compared to SVRC.

The thermodynamic benefits are not as extreme as in Figure 6.6, which can be attributed to the imposition of practical limitations: the specified approach temperature requires the condensing temperature to be raised, leading to a higher compression requirement, and consequently more superheating of the compressor feed. Moreover, because the feed flow is fixed, yet the reboil rate changes with reflux, the advantage of FBVRC decreases as reflux increases. Thus, by using $r = 1.5 r_{\min}$, along with the other factors, energy/work load in the FBVRC is increased compared to the minimum shown in Figure 6.6.

In this example, the SVRC scheme's compression ratio is 2.67, which could be practically implemented; nevertheless, FBVRC requires less than half of that compression ratio.

As a result, it has been shown in this rigorous simulation that FBVRC was significantly better than the other two configurations, both thermodynamically and practically.

Example 3: light water–monoethanolamine–diethylene glycol liquid feed

A 1 kmol/h saturated liquid feed mixture of water, monoethanolamine, and diethylene glycol is to be split into a nearly pure water distillate of >99.999 mol% water, and a bottoms with <0.00001 mol% water.

The simulations of the conventional and SVRC configurations gave a distillate of $x_D = (0.99999, 8.8861 \times 10^{-6}, 1.7454 \times 10^{-30})$, and a bottoms of $x_B = (2.7137 \times 10^{-9}, 0.27268, 0.72733)$. The FDVRC simulation produced a distillate of $x_D = (0.99999, 6.6312 \times 10^{-6}, 6.032 \times 10^{-17})$, and a bottoms of $x_B = (1.1954 \times 10^{-6}, 0.27269, 0.72731)$.

Table 6.1 summarises the results of these simulations. In terms of energy requirements, FDVRC is 56.7% better than the conventional column, but 12.8% worse than the SVRC. If work input is considered, the FDVRC is better than the other two schemes: it has 50.7% lower work input than the conventional case, and 50.2% lower than SVRC.

Even though FDVRC requires slightly more energy than SVRC, the latter's practical implementation is clearly prevented by its very high pressure ratio of 23.53. The pressure ratio for the FDVRC is 3.50, which, although at the limit of practicable single-case compression, could still be implemented.

Example 4: heavy *n*-pentane–*n*-hexane–*n*-heptane vapour feed

A 1 kmol/h saturated vapour feed of *n*-pentane–*n*-hexane–*n*-heptane with composition $z_F = (0.05, 0.05, 0.90)$ is to undergo an indirect split to a bottoms of >99.5 mol% *n*-heptane, and a distillate with <1 mol% *n*-heptane.

The conventional and SVRC simulations produced a distillate of $x_D = (0.52305, 0.47634, 6.1495 \times 10^{-4})$, and a bottoms of $x_B = (4.2735 \times 10^{-7}, 4.93354 \times 10^{-3}, 0.99507)$, both of which meet the specification. The simulation of the FBVRC configuration resulted in a distillate of $x_D = (0.52219, 0.47506, 2.7469 \times 10^{-3})$, and a bottoms of $x_B = (8.1726 \times 10^{-7}, 4.9911 \times 10^{-3}, 0.99500)$, which also meets the product specification.

The results are summarised in Table 6.1, and it is seen that the energy requirements of FBVRC are 87.7% lower than conventional distillation, and 74.7% lower than SVRC. In terms of work input, a decrease of 74.9% is observed using FBVRC instead of conventional distillation, and a decrease of 84.9% compared to SVRC.

Furthermore, the SVRC's minimum compression ratio of 4.20 is prohibitive of practical implementation, whereas FBVRC requires a low pressure ratio of 1.35. Consequently, not only does the FBVRC configuration require significantly less energy and work input than the other two options, but it can be applied in practice, while SVRC cannot.

6.6 Conclusion

Through the use of entropy generation analysis, potential targets for improvement in conventional distillation were identified, which ultimately led to two novel feed–product vapour recompression configurations: Feed–Distillate Vapour Recompression (FDVRC), and Feed–Bottoms Vapour Recompression (FBVRC). These novel configurations are intended for situations in which standard vapour recompression (SVRC) cannot be applied, due to either thermodynamic or practical reasons.

In Chapter 5, it was shown that although SVRC is thermodynamically favoured over conventional distillation for a wide range of systems, it is practically limited to a narrow subset of these, where compression ratios are small enough to be practically implemented in a single-stage compressor. It was also identified in the Chapter 5 that distillation is least efficient (i.e. furthest from its theoretical minimum) when feed composition is close to that of a product.

FDVRC is designed for feeds in the liquid phase, where the feed composition is close to that of the distillate; the closer these two compositions, the better the energy efficiency and the lower the required compression ratio in FDVRC. Similar behaviour is exhibited by FBVRC, except that it is intended for vapour feeds that are close in composition to the bottoms. For both of these arrangements, the required compression ratio is always lower than that of SVRC; when the novel configurations are used with their intended feeds, the compression ratio is significantly lower than in SVRC.

While SVRC can accept all feeds but is limited in the systems it can benefit, FDVRC and FBVRC are applicable to a much wider range of systems, but can only accept specific feeds: light liquid feeds, or heavy vapour feeds.

Through rigorous calculations for a range of binary systems, as well as rigorous simulation for some binary and ternary separations, it was shown in this chapter that the novel configurations are always better than conventional distillation (for the appropriate feeds) in terms of energy and work requirements. For situations where SVRC is practically applicable, it was seen that SVRC is usually better than the novel configurations; however, the range of systems to which SVRC can be applied is very limited due to the required compression ratios, as explained above. In these cases where SVRC is not a feasible option, if the feed is a light liquid or a heavy vapour, one of the novel configurations can usually be used, yielding significant energy and work requirement benefits over conventional distillation. (Note that if the feed condition is not already fixed by an upstream unit operation, such as a reactor, changing the feed condition in order to use it with the proposed configurations is not beneficial.)

As such, for the appropriate feeds, the novel configurations can greatly expand the region in which vapour recompression can be implemented for energy savings, beyond the very limited range of SVRC.

While the major process portion of the proposed configurations has been examined in this chapter, a number of aspects remain to be examined in future work: simple, general guidelines or rules-of-thumb for when FDVRC or FBVRC are better than SVRC need to be developed; the controllability and start-up of the novel configurations must be assessed; and an industrial case study of the economics surrounding the novel configurations should be performed, showing how they compare to SVRC and conventional columns, and whether the energy savings over the lifetime of the plant are worth the additional capital expenditure.

Chapter 7

Shortcut Methods for High-Level Distillation Analysis

The first part of the work in this chapter, § 7.2, was published as: Felbab, N., 2013. Condensation of saturated vapours on compression and estimation of minimum suction superheating. *Appl. Therm. Eng.* 52 (2), 527–530. This paper has been reproduced with permission in this chapter, along with some minor corrections, and changes in style and formatting for clarity.

Copyright © 2013 Elsevier. Applied Thermal Engineering.

Abstract

This chapter presents two simple shortcut (estimation) methods, which were developed because comparable methods available in the literature were unsatisfactory. One of the methods presented is used to determine whether saturated vapours will condense or become superheated on compression. A simple way of estimating minimum compressor inlet superheating to avoid condensation is given. The other problem that is addressed is the non-iterative estimation of bubble- and dew-point temperatures of ideal binary mixtures using only the pure-component boiling points and the constant relative volatility. Although both methods assume that vapours behave as ideal gases with constant properties, such simplifications are often sufficient for initial analysis of distillation systems, and have been used successfully in Chapter 5 and in the high-level analysis of the FDVRC configuration in Appendix E.2.

7.1 Introduction

In the initial stages of solving distillation problems, it is often useful to be able to make quick, non-iterative estimates of values, in favour of detailed—often iterative—calculations. Even for detailed calculations, it is useful to have a simple way of obtaining good, convergent initial guesses for the iterations. This chapter presents two new methods that were developed during the course of the work in this thesis, in order to fill gaps where methods in the literature were unsatisfactory, for reasons discussed below.

The first of these methods allows for the determination of whether a saturated vapour will condense or become superheated on compression (taking into account the compressor's isentropic efficiency), and, if it condenses, what the minimum superheating of the compressor inlet must be in order to avoid condensation within the compressor. It appears that there is only one previous work on this topic in the open scientific literature (Patwardhan, 1987), which was found to be inadequate for the purposes of the work in this thesis for a number of reasons:

- 1 It relies on liquid heat capacity, as well as temperature-dependent latent heat (or critical temperature and acentric factor for use with a correlation that Patwardhan suggests). Instead, it is preferred in this work to perform high-level calculations using constant ideal gas heat capacity, and constant latent heat;
- 2 Patwardhan (1987) does not provide a way of estimating the minimum suction superheating that is required to prevent condensation;
- 3 It assumes 100% isentropic compression, whereas the presented method allows for the inclusion of the compressor's isentropic efficiency. Although this is not strictly necessary for this work, it still has more flexibility than Patwardhan's method.

The second method presented addresses the issue of non-iterative (i.e. temperature-explicit) estimation of bubble- and dew-point temperatures of ideal binary mixtures. In essence, the goal is to obtain a good estimate of the equilibrium temperatures that would result from calculations with Raoult's law and temperature-dependent vapour pressure, assuming ideal liquid behaviour, i.e. $\gamma = 1$ for both components. For the proposed method, only the pure-component boiling points and constant relative volatility are required. The only other method that was found in the literature for achieving this was that

given by Halvorsen (Halvorsen, 2001; Halvorsen and Skogestad, 2000), which lacks a theoretical basis; the proposed work does not. More importantly, as a result of its more theoretical basis, the proposed work has higher accuracy than Halvorsen's. However, Halvorsen's approach has the advantage of extending to multicomponent systems, whereas the work here is limited to binary systems. Therefore, the proposed work is preferred for binary systems, while Halvorsen's should be used for multicomponent mixtures.

7.2 Compression of saturated vapours

When a saturated vapour is compressed isentropically, it may become superheated, or it may partially condense; which of these two outcomes will occur depends on the properties of the fluid being compressed and—to a lesser degree—on the compressor efficiency (Holland et al., 1982; McLinden and Radermacher, 1987; Patwardhan, 1987; Gopichand et al., 1988; Srinivasan, 1991; Granryd, 2001; Radermacher and Hwang, 2005; Gmehling et al., 2012). It is imperative to avoid any condensation, as liquid formation in the compressor can rapidly damage the equipment by erosion (Meili and Stuecheli, 1987; Patwardhan, 1987; Gmehling et al., 2012).

One major use of compressors is in heat pumps, which have a wide range of industrial uses, typically in energy-saving configurations, and in refrigeration cycles. In refrigeration cycles, or in other heat-pumping techniques with closed loops, the working fluid is independent from the main process itself, and there is a wide range of fluids that can be chosen to best suit the process requirements in terms of physical properties and economic considerations (Holland et al., 1982; Durandet, 1983; Radermacher and Hwang, 2005).

However, in heat pump applications such as vapour recompression distillation (Carta et al., 1982; Flores et al., 1984; Gopichand et al., 1988; Fonyó and Benkő, 1998), or in heat-integrated distillation columns (Nakaiwa et al., 2000; Jana, 2010), the fluid to be compressed cannot be independently chosen; moreover, the compressed fluid is a saturated vapour in these applications, and it is invaluable to know whether condensation will occur, and if so, how much superheating of the compressor suction vapour is required to avoid this.

To answer the first question, Patwardhan (1987) developed a criterion to determine whether isentropic compression will lead to superheating or partial condensation. This criterion requires the saturated inlet compressor temperature, the fluid's liquid heat capacity, and its latent heat as a function of

temperature. Patwardhan also proposed replacing the latter with a correlation requiring the acentric factor and the critical temperature. With the assumption of liquid incompressibility, the criterion is as follows:

$$\frac{\hat{C}_p^{\text{liq}}}{R} < \beta \text{ (superheated)} \quad \frac{\hat{C}_p^{\text{liq}}}{R} > \beta \text{ (partially condensed)} \quad (7.1)$$

where

$$\beta = -\frac{T_0}{R} \frac{d}{dT} \left(\frac{\lambda(T)}{T} \right)_{T=T_0} \quad (7.2)$$

Equation (7.1) requires the liquid heat capacity, \hat{C}_p^{liq} , while Eq. (7.2) requires the saturated compressor suction temperature, T_0 , and the temperature-dependent latent heat, λ .

Patwardhan suggested the use of a correlation in (Reid et al., 1977) to obtain β as a function of acentric factor, ω , and critical temperature, T_c :

$$\beta = 7.08 \left(1 - \frac{T}{T_c} \right)^{-0.646} \left(-0.646 + \frac{T_c}{T} \right) + 10.95 \omega \left(1 - \frac{T}{T_c} \right)^{-0.544} \left(-0.544 + \frac{T_c}{T} \right) \quad (7.3)$$

This work proposes an alternative to Patwardhan's (1987) method; it uses only the ideal gas heat capacity and latent heat, both evaluated at T_0 . Therefore, neither the temperature dependence of λ , nor ω , nor T_c is required. It also allows for the inclusion of the effects of the compressor's isentropic efficiency. Lastly, equations are derived for the estimation of suction superheat required to ensure no condensation takes place in the compressor.

7.2.1 Isentropic and non-isentropic compression

An ideal gas, when compressed isentropically from pressure P_0 to P_1 , experiences an increase in temperature from T_0 to some temperature $T_{1,\text{isentropic}}$; the relationship between these temperatures and pressures can easily be deduced, assuming constant \hat{C}_p^{IG} :

$$\frac{P_1}{P_0} = \left(\frac{T_{1,\text{isentropic}}}{T_0} \right)^{\hat{C}_p^{\text{IG}}/R} \quad (7.4)$$

If the compressor is not perfectly isentropic, its efficiency, η , can be taken into account, again assuming constant \hat{C}_p^{IG} :

$$\eta \equiv \frac{W_{s,\text{isentropic}}}{W_{s,\text{actual}}} = \frac{H_{1,\text{isentropic}} - H_0}{H_{1,\text{actual}} - H_0} = \frac{T_{1,\text{isentropic}} - T_0}{T_1 - T_0} \quad (7.5)$$

$$T_{1,\text{isentropic}} = \eta(T_1 - T_0) + T_0 \quad (7.6)$$

where T_1 is the actual exit temperature from the compressor. Substituting Eq. (7.6) into Eq. (7.4):

$$\frac{P_1}{P_0} = \left(\eta \left(\frac{T_1}{T_0} - 1 \right) + 1 \right)^{\hat{C}_p^{\text{IG}}/R} \quad (7.7)$$

The vapour pressure curve describes the pressures and temperatures at which a substance is saturated; if, at a given pressure, the fluid's temperature exceeds the saturation temperature, the fluid is superheated. The Clausius–Clapeyron equation is useful for relating a known point on the saturation curve to one at a similar temperature assuming constant λ :

$$\ln\left(\frac{P_1}{P_0}\right) = -\frac{\lambda}{R}\left(\frac{1}{T_1} - \frac{1}{T_0}\right) \quad (7.8)$$

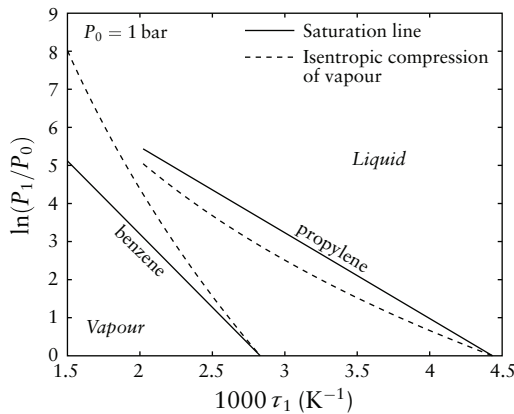
If a new variable is defined as $\tau_1 = 1/T_1$, and the logarithm of Eq. (7.7) is taken, the following is obtained:

$$\ln\left(\frac{P_1}{P_0}\right) = -\frac{\hat{C}_{p,1}^{\text{IG}}}{R} \ln\left(\frac{\tau_1 T_0}{\eta - \tau_1 T_0(\eta - 1)}\right) \quad (7.9)$$

and using τ in Eq. (7.8) gives:

$$\ln\left(\frac{P_1}{P_0}\right) = -\frac{\lambda}{R}\left(\tau_1 - \frac{1}{T_0}\right) \quad (7.10)$$

First, the assumption is made that the saturated vapour becomes superheated on compression. If, for a given compressor pressure ratio (P_1/P_0), τ_1 in Eq. (7.9) is lower than the τ_1 in Eq. (7.10), the assumption was correct, and the compressed vapour will indeed be superheated. Otherwise, if the opposite is found to be true, then the compressed fluid must be condensed. This is represented graphically in Figure 7.1, for benzene (partially condensed) and propylene (superheated), with plots of Eqs (7.9) and (7.10). Note that in the case of condensation, the actual compression profile runs along the saturation line; the representation of isentropic compression in Figure 7.1 assumes that only vapour exists. If it enters the liquid region, it means that the assumption is incorrect. Furthermore, propylene was included in this plot, and treated as an ideal gas for illustrative purposes; in reality, it does not approximate an ideal gas at these conditions.

**Figure 7.1**

Plot of $\ln(P_1/P_0)$ as a function of τ_1 for propylene (superheated on isentropic compression) and benzene (condensed on isentropic compression).

Since both equations pass through T_0 and P_0 , it is sufficient to compare their gradients at that point to determine whether condensation will occur. Equation (7.10) is a straight line, and its gradient is already known to be $-\lambda/R$. For Eq. (7.9), the gradient can be found by taking the derivative of $\ln(P_1/P_0)$ with respect to τ_1 to obtain $-\hat{C}_p^{\text{IG}} T_0 \eta / R$. Therefore, the proposed criterion is, very simply:

$$\hat{C}_p^{\text{IG}} T_0 \eta < \lambda \text{ (superheated)} \quad \hat{C}_p^{\text{IG}} T_0 \eta > \lambda \text{ (partially condensed)} \quad (7.11)$$

Because only the gradient at T_0 is considered, and \hat{C}_p^{IG} and λ are evaluated at that temperature, it can be shown that the only assumptions in Eq. (7.11) are that the gas is ideal and that the specific volume of the saturated liquid is negligible in comparison with the specific volume of the saturated vapour. Both of these are reasonable assumptions far from the critical point.

Durandet (1983) implicitly presented a similar criterion to Eq. (7.11), but the derivation is based solely on the fluid properties and can therefore not take into account the compressor's efficiency.

7.2.2 Superheating before compression

If it is found that the saturated vapour condenses on compression, the problem can be circumvented by superheating the inlet to the compressor by some ΔT . In some cases, even if the fluid does not condense at small pressure ratios, it may condense prior to reaching the required pressure ratio. It is useful to be able estimate the minimum ΔT required for this superheating (which should produce a saturated vapour at the outlet of the compressor). The superheated inlet temperature to the compressor, therefore, is $T_{0,\text{superheated}} = T_{0,\text{saturated}} + \Delta T$,

which makes Eq. (7.9):

$$\ln\left(\frac{P_1}{P_0}\right) = -\frac{\hat{C}_p^{\text{IG}}}{R} \ln\left(\frac{\tau_1(T_0 + \Delta T)}{\eta - \tau_1(T_0 + \Delta T)(\eta - 1)}\right) \quad (7.12)$$

The vapour pressure expression, Eq. (7.10), remains unchanged, as it is a function of the fluid only, and not of the process. Therefore, equating Eqs (7.10) and (7.12) and solving for ΔT gives:

$$\Delta T = \frac{\eta(T_1 - T_0) + wT_0}{\eta - w} \quad (7.13)$$

where

$$w = 1 - \exp\left(\frac{\lambda(T_1 - T_0)}{\hat{C}_p^{\text{IG}}T_0T_1}\right) \quad (7.14)$$

The form of Eq. (7.13) makes it suitable for problems where the compression is used to increase the temperature to a specified T_1 . With typical process simulators (which do not allow specification of a compressor outlet temperature) this problem is, in fact, a relatively difficult multivariate optimisation problem.

For applications where the compressor pressure ratio is specified, the following form can be used:

$$\Delta T = \frac{T_0\left[\frac{\eta v}{\lambda - v} + \sigma\right]}{\eta - \sigma} \quad (7.15)$$

where

$$v = RT_0 \ln\left(\frac{P_1}{P_0}\right) \quad (7.16)$$

$$\sigma = 1 - \left(\frac{P_1}{P_0}\right)^{R/\hat{C}_p^{\text{IG}}} \quad (7.17)$$

If $\Delta T \leq 0$, no inlet superheating is required.

The estimates from Eqs (7.13) and (7.15) can be used as initial guesses for the iterations required to obtain these numbers rigorously.

7.2.3 Examples

In all of the following examples, rigorous simulation was performed with AspenTech's Aspen Plus using the SR-POLAR (Schwartzentruber–Renon equation of state) property method.

Example 1

Compressing saturated benzene vapour at 0.75 bar ($P_0 = 0.75$ bar, $T_0 = 344.0$ K, $\hat{C}_p^{\text{IG}} = 96.81$ J/mol·K, $\lambda = 31263.32$ J/mol) in a perfect compressor ($\eta = 1$) results in partial condensation according to Eq. (7.11). However, the same feed in a compressor with $\eta = 0.78$ gives a superheated gas. Rigorous simulation confirmed these results.

Example 2

Saturated 1-heptanol vapour at 1 bar ($P_0 = 1$ bar, $T_0 = 449.4$ K) needs to be compressed to $P_1 = 1.6$ bar in an ideal compressor ($\eta = 1$). Its properties at T_0 are $\hat{C}_p^{\text{IG}} = 249.05$ J/mol·K and $\lambda = 46355.86$ J/mol. From Eq. (7.11), $\hat{C}_p^{\text{IG}} T_0 \eta = 111923.07$ J/mol $> \lambda$, which means that isentropic compression leads to condensation. The minimum degrees of inlet superheating required, as estimated with Eq. (7.15), are $\Delta T = 10.42$ K. Rigorous simulation gave 9.38 K.

Example 3

A vapour recompression system requires saturated *n*-octane vapour at 0.7 bar ($P_0 = 0.7$ bar, $T_0 = 386.14$ K) to be compressed until it reaches temperature $T_1 = 410.0$ K. At T_0 , $\hat{C}_p^{\text{IG}} = 233.91$ J/mol·K, and $\lambda = 36113.82$ J/mol. The compressor is not perfect, and has $\eta = 0.82$. From Eq. (7.11), $\hat{C}_p^{\text{IG}} T_0 \eta = 74064.05$ J/mol $> \lambda$, which means that compression leads to partial condensation. The minimum ΔT according to Eq. (7.13) is 12.42 K; rigorous simulation gave this value as 11.80 K.

7.3 Estimation of ideal binary equilibrium temperatures

For high-level or shortcut distillation calculations, such as at early stages of process synthesis or conceptual design when broad screening of alternatives is performed, information that is typically available is the normal boiling points of the pure components, T_b , and their constant relative volatility, α . If temperature is a significant variable, it is useful to be able to estimate the bubble- or dew-point temperatures quickly using the available information, without performing the iterative calculations that are required for the accurate

computation of vapour–liquid equilibrium (which also requires additional information, such as vapour pressure as a function of temperature). There appears to be only one comparable method that satisfies the same criteria; it is described in § 7.3.2, and a comparison with the proposed method is performed later in § 7.3.5.

The equations presented here allow for the estimation of equilibrium temperatures as a function of liquid or vapour composition, with the use of only the normal boiling points of the pure components and a constant value for the relative volatility. They are given as Eqs (7.38) and (7.39). The fact that the proposed method is non-iterative makes it particularly useful for spreadsheeting applications, and for the direct inclusion of bubble- or dew-point temperatures as a function of composition in other equations.

The proposed method with normal boiling points can only be used to estimate equilibrium temperatures at atmospheric pressure (101 325 Pa); at different pressures, pure-component boiling points would be required at the system pressure. An extension of the proposed method to other pressures is given in § 7.3.6.

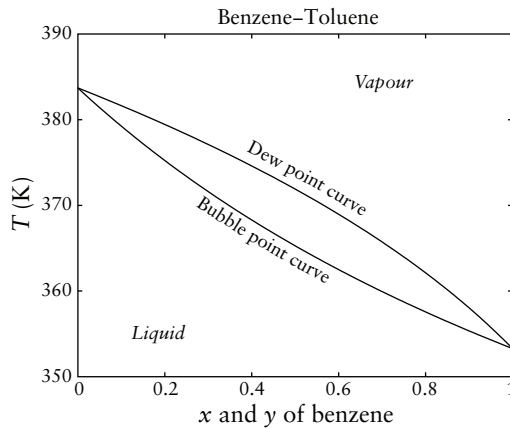
7.3.1 Theoretical background

Perfectly ideal mixtures obey Raoult’s law exactly:

$$y_i P = x_i P_i^{\text{vap}}(T) \quad (7.18)$$

where $P^{\text{vap}}(T)$ is the vapour pressure at temperature T , and P is the system pressure; x_i is the liquid mole fraction of component i , and y_i denotes the vapour mole fraction of component i in equilibrium with x .

For a given liquid composition, the bubble point is the temperature that results in $\sum y_i = 1$ using Eq. (7.18); conversely, for a given vapour composition, the dew point is located by finding the temperature that satisfies $\sum x_i = 1$. In order to find these temperatures, an iterative approach is required, since vapour pressure equations are typically pressure-explicit, and cannot be rearranged into temperature-explicit form. The details of these calculations are well-known, and can be found in most thermodynamics textbooks (Smith et al., 2001; Sandler, 2006; Prausnitz et al., 1980). A typical, near-ideal phase envelope is shown in Figure 7.2 in the form of a T – x – y diagram for the classic benzene–toluene system. The fact that the bubble and dew point curves are ‘anchored’ at either end by the boiling points of the pure components means that the curves are, in a sense, special interpolations

**Figure 7.2**

T - x - y diagram of the benzene-toluene system.

between those two anchor points. Roughly, the relative volatility dictates the width of the phase envelope.

Note that using only the vapour pressures, any two substances can be treated as an ‘ideal’ mixture with Raoult’s law; however, this does not mean that the result corresponds to the real behaviour of the mixture, because the activity coefficient (γ_i) must be taken into account. It is the engineer’s task to understand when $\gamma_i \approx 1$ in order to be able to reliably approximate the mixture as ideal.

Relative volatility for an ideal mixture is given by:

$$\alpha_{12}(T) = \frac{P_1^{\text{vap}}(T)}{P_2^{\text{vap}}(T)}$$

where $P_i^{\text{vap}}(T)$ is the vapour pressure of component i at temperature T ; ‘1’ refers to the light component and ‘2’ to the heavy component.

In this work, the subscripts associated with α will be dropped, and the meaning of α will be taken to be the above. In the absence of α or P^{vap} data, it is possible to obtain relatively good estimates of α from the normal boiling points of a mixture’s constituent components using correlations (Melpolder and Headington, 1947).

For high-level calculations, constant relative volatility (CRV) is typically assumed, i.e. α is a constant. This is sufficient to get a relatively good idea of the separability, or x - y relationship, of the mixture, if its behaviour is close to ideal.

For a binary mixture,

$$y_1 = \frac{\alpha x_1}{\alpha x_1 + 1 - x_1} \quad (7.19)$$

where x_1 is the liquid mole fraction of the light component, and y_1 is the vapour mole fraction of the light component in equilibrium with the liquid.

Equation (7.19) can be rearranged to give:

$$x_1 = \frac{y_1}{y_1 + \alpha - \alpha y_1} \quad (7.20)$$

The CRV model can give an idea of equilibrium compositions, but it can provide no information about the bubble- and dew-point temperatures.

7.3.2 Standard approach

Halvorsen and Skogestad (2000) described a method of estimating the equilibrium temperatures using only the pure component boiling points and their constant relative volatility. The simplest possible approach is to use simple weighting of pure-component boiling points by mole fraction. If weighting is done with the liquid mole fraction, i.e. $T \approx \sum x_i T_{b,i}$, the temperatures are over-predicted. If the weighting is done on the basis of the vapour mole fraction, i.e. $T \approx \sum y_i T_{b,i}$, the opposite is observed: the temperatures are under-predicted. Consequently, by using the arithmetic mean of x and y , a more accurate estimate of T is obtained:

$$T = \sum \left(\frac{x_i + y_i}{2} \right) T_{b,i} \quad (7.21)$$

Equilibrium temperatures can be approximated using Eq. (7.21). For two components, with y_1 in Eq. (7.21) replaced with Eq. (7.19), the bubble point is estimated as follows:

$$T_{\text{bubble}} = \frac{x_1}{2} (T_{b,1} - T_{b,2}) \left(1 + \frac{\alpha}{\alpha x_1 + 1 - x_1} \right) + T_{b,2} \quad (7.22)$$

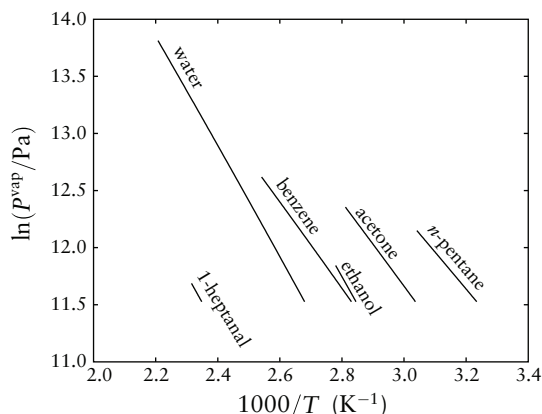
Similarly, an equation for estimating the dew point in binary mixtures can be derived by replacing x_1 in Eq. (7.21) with Eq. (7.20):

$$T_{\text{dew}} = \frac{y_1}{2} (T_{b,1} - T_{b,2}) \left(1 + \frac{1}{y_1 + \alpha - \alpha y_1} \right) + T_{b,2} \quad (7.23)$$

Equations (7.22) and (7.23) can be used to estimate the bubble and dew points, respectively, given α , $T_{b,1}$, and $T_{b,2}$. In this chapter, these will be referred to as the ‘standard equations’.

7.3.3 Derivation of the base equations

The proposed equations are derived in a very different way to the standard equations, with somewhat more of a theoretical foundation.

**Figure 7.3**

Plot of $\ln(P^{\text{vap}})$ as a function of $1/T$ for a number of components.

The logarithm of vapour pressure, $\ln(P^{\text{vap}})$, is most linear in reciprocal temperature, $1/T$, especially over relatively small temperature ranges (Poling et al., 2001), far from the critical temperature (both of which are the case in many distillation problems). This attribute has been exploited for accelerated convergence of bubble and dew point calculations (Prausnitz et al., 1980), and has been used to provide an initial guess of P^{vap} for P^{vap} calculations using equations of state, when the critical and normal boiling points are known (Sandler, 2006). The near-linearity has also been demonstrated in many other cases, often for the graphical validation of predicted values against experimental data points (Kudchadker and Zwolinski, 1966; Macknick and Prausnitz, 1979; Campanella, 1997; Emami et al., 2008). More information on this linear relationship can be found in (Poling et al., 2001).

Figure 7.3 shows plots of $\ln(P^{\text{vap}})$ as a function of $1/T$, in the temperature range T_b to $0.7 T_c$, for a number of organic compounds, which confirms the near-linearity of this relationship. P^{vap} data for all of the work in this chapter was obtained from (Liley et al., 1997).

For a set system pressure P , rigorous VLE calculations result in corresponding x , y , and T at equilibrium using Raoult's law, as explained earlier. If Raoult's law, Eq. (7.18), is rearranged and the natural logarithm is taken on both sides, the following is obtained:

$$\frac{y_i}{x_i} = \frac{P_i^{\text{vap}}}{P} \quad (7.24)$$

$$\ln\left(\frac{y_i}{x_i}\right) = \ln\left(\frac{P_i^{\text{vap}}}{P}\right) \quad (7.25)$$

$1/P$ on the right-hand side of Eq. (7.25) is simply a constant multiplier. The implication of Eq. (7.25) is that the behaviour of $\ln(y_i/x_i)$ is directly proportional to $\ln(P_i^{\text{vap}})$, which in turn makes it quite linear in $1/T$. Conversely,

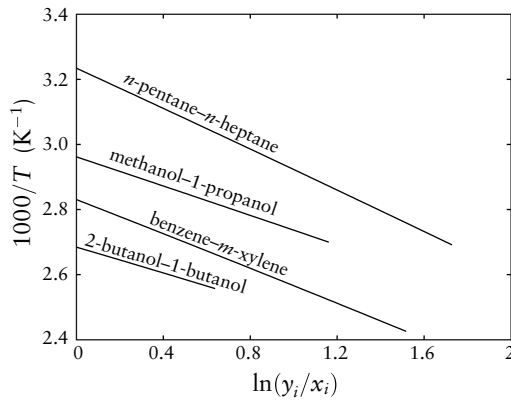


Figure 7.4
Plot of $1/T$ as a function of $\ln(y_1/x_1)$ for a number of binary systems.

$1/T$ is expected to be quite linear in $\ln(y_i/x_i)$. Figure 7.4 confirms this using a plot of $1/T$ as function of $\ln(y_1/x_1)$ for a variety of ideal binary systems, in the composition range (0, 1). The vapour compositions were calculated using Raoult's law, Eq. (7.18).

The linear relationship between these two variables in Figure 7.4 can be represented by:

$$\tau = m\psi + c \quad (7.26)$$

where

$$\tau \equiv \frac{1}{T} \quad (7.27)$$

$$\psi \equiv \ln\left(\frac{y_1}{x_1}\right) \quad (7.28)$$

with m as the gradient, and c as the intercept.

ψ can be approximated as a function of x_1 and α by substituting Eq. (7.19) into Eq. (7.28) to obtain:

$$\psi = \ln\left(\frac{\alpha}{\alpha x_1 + 1 - x_1}\right) \quad (7.29)$$

In Eq. (7.26), m and c are unknown; however, there are two pieces of information that can be used to estimate them: the two pure-component boiling points. At $x_1 = 1$, it is known that $T = T_{b,1}$, which leads to $\psi = \ln(1) = 0$ and $\tau = 1/T_{b,1}$. Substituting these last two expressions into Eq. (7.26) gives:

$$c = \frac{1}{T_{b,1}} \quad (7.30)$$

At $x_1 = 0$, it is known that $T = T_{b,2}$, or, transformed to the relevant

variables, $\psi = \ln(\alpha)$ and $\tau = 1/T_{b,2}$. Using this information, along with Eq. (7.30), in Eq. (7.26) gives:

$$m = \frac{\frac{1}{T_{b,2}} - \frac{1}{T_{b,1}}}{\ln(\alpha)} \quad (7.31)$$

Finally, the bubble point as a function of liquid composition can be estimated by substituting Eqs (7.27), (7.29), (7.30), and (7.31) into Eq. (7.26):

$$T_{\text{bubble}} = \left[\left(\frac{\frac{1}{T_{b,2}} - \frac{1}{T_{b,1}}}{\ln(\alpha)} \right) \ln \left(\frac{\alpha}{\alpha x_1 + 1 - x_1} \right) + \frac{1}{T_{b,1}} \right]^{-1} \quad (7.32)$$

For the dew point as a function of vapour composition, Eq. (7.20) can be substituted into Eq. (7.32) to give:

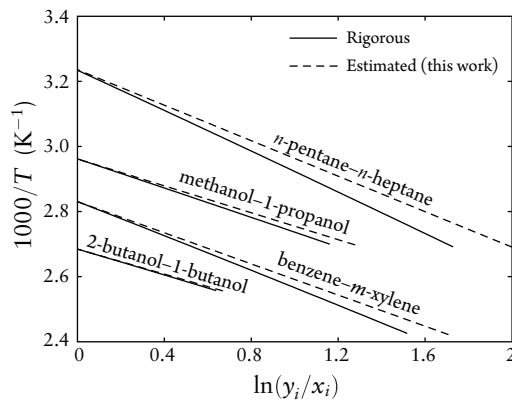
$$T_{\text{dew}} = \left[\left(\frac{\frac{1}{T_{b,2}} - \frac{1}{T_{b,1}}}{\ln(\alpha)} \right) \ln(y_1 + \alpha(1 - y_1)) + \frac{1}{T_{b,1}} \right]^{-1} \quad (7.33)$$

In Eqs (7.32) and (7.33), the values of $T_{b,1}$ and $T_{b,2}$ are unambiguous; the value for a constant α is less so. The approach traditionally used in shortcut distillation calculations is to determine the α at the top and bottom of the column, and to use the geometric mean of the two, $\alpha_{\text{mean}} = \sqrt{\alpha_{\text{top}} \alpha_{\text{bottom}}}$, as the constant α value (Halvorsen and Skogestad, 2000). For separation into pure components, α_{top} is evaluated at $T_{b,1}$, and α_{bottom} is evaluated at $T_{b,2}$; this is the value of α adopted in this work, as it is the average α for the entire composition range.

7.3.4 Correction to the base equations

On analysis of the temperature estimations by Eqs (7.32) and (7.33) for a large number of systems, a trend was observed: as α increases, the deviation of the prediction from the rigorous values increases, even when the CRV model fits the x - y data very well. (The appropriateness of the CRV model for the x - y relationship was measured by comparing rigorous results to CRV-model predictions, and finding the coefficient of determination of R_{xy}^2 for the fit, where the subscript 'xy' indicates that the value corresponds to the x - y relationship only.)

Moreover, the deviation in temperature prediction was found to be almost always negative, indicating that Eqs (7.32) and (7.33) exhibit systematic error; in other words, the CRV model on its own is not ideally suited for the prediction of bubble- and dew-point temperatures using the proposed approach.

**Figure 7.5**

Plot of $1/T$ as a function of $\ln(y_1/x_1)$ for a number of binary systems, with T both rigorously calculated and estimated.

To examine the nature of the error, Figure 7.5 compares $1/T$ as a function of $\ln(y_1/x_1)$ for both the values obtained using Raoult's law and those obtained with Eqs (7.32) and (7.33). The most noticeable observation in this plot is that the estimated lines have the correct intercept on the $1/T$ axis, but the gradient of these lines differs from the correct value of the rigorous calculations. The gradient of the predicted lines is determined by the α value used in the proposed equations; from this, it can be inferred that there must exist an 'optimal' α that gives the correct gradient, which is different from α_{mean} .

For each binary system, this optimal α can be found by non-linear regression to most closely match the rigorous data. In this work, 4 573 binary mixtures were considered, all of which had $\alpha \leq 30$, and $R_{xy}^2 \geq 0.98$. The latter constraint ensured that the x - y behaviour of these mixtures was approximated reasonably well by the CRV model. This limitation was imposed because the proposed equations are intended for use in circumstances where the CRV model is appropriate, and they cannot be expected to work well in cases where this is not true.

It was found that the bubble point equation and the dew point equation have different optimal α values: α_{bubble} gives the best prediction of T_{bubble} in Eq. (7.32), and α_{dew} gives the best prediction of T_{dew} in Eq. (7.33).

The relationship between the natural logarithms of α and α_{bubble} for the 4 573 mixtures is shown in Figure 7.6a; for the logarithms of α and α_{dew} , it can be seen in Figure 7.6b. The logarithms of these variables—rather than the variables directly—are shown, as they were found to have a remarkably linear relationship. Moreover, these linear fits almost exactly pass through the origin, and, as such, the model that will be used for the fitting is simply of the $y = mx$ variety. Regression for the two cases provides $\ln(\alpha_{\text{bubble}})$ and $\ln(\alpha_{\text{dew}})$ as functions of $\ln(\alpha)$ gives:

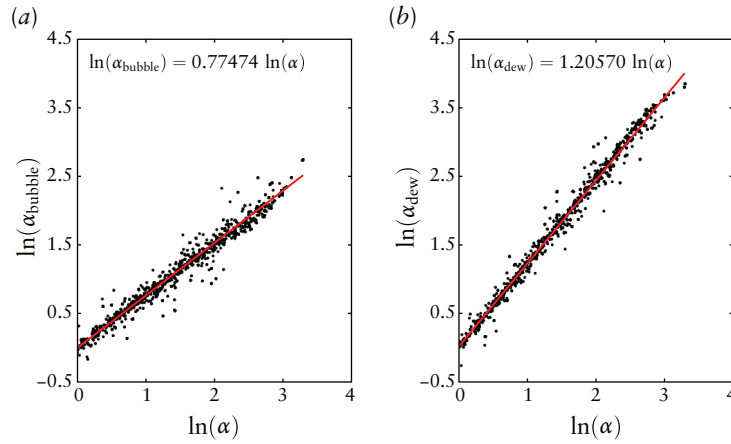


Figure 7.6 Comparison of $\ln(\alpha)$ and optimal (a) $\ln(\alpha_{\text{bubble}})$, and (b) $\ln(\alpha_{\text{dew}})$, for 4 573 binary systems, along with linear fits to the data, passing through the origin.

$$\ln(\alpha_{\text{bubble}}) = 0.77474 \ln(\alpha) \quad (7.34)$$

$$\ln(\alpha_{\text{dew}}) = 1.20570 \ln(\alpha) \quad (7.35)$$

If exponents are taken on both sides of Eqs (7.34) and (7.35), the following is obtained:

$$\alpha_{\text{bubble}} = \alpha^{0.77474} \quad (7.36)$$

$$\alpha_{\text{dew}} = \alpha^{1.20570} \quad (7.37)$$

To apply the above correction, α in Eqs (7.32) and (7.33) is replaced with α_{bubble} and α_{dew} , respectively, to obtain:

$$T_{\text{bubble}} = \left[\left(\frac{\frac{1}{T_{b,2}} - \frac{1}{T_{b,1}}}{\ln(\alpha^{-0.775})} \right) \ln(x_1 + \alpha^{-0.775}(1 - x_1)) + \frac{1}{T_{b,1}} \right]^{-1} \quad (7.38)$$

$$T_{\text{dew}} = \left[\left(\frac{\frac{1}{T_{b,2}} - \frac{1}{T_{b,1}}}{\ln(\alpha^{1.206})} \right) \ln(y_1 + \alpha^{1.206}(1 - y_1)) + \frac{1}{T_{b,1}} \right]^{-1} \quad (7.39)$$

T - x - y diagrams can be constructed with the standard equations, and with the proposed equations. Figure 7.7 shows these for a number of mixtures, along with the rigorously calculated values for comparison.

For the benzene–toluene mixture ($\alpha = 2.47$; $T_{b,1} = 353.3$ K; $T_{b,2} = 383.7$ K), both the standard equations and the proposed ones give very good agreement with the rigorous calculations, with the former incurring a maximum absolute error of 0.38 K, and the latter 0.048 K.

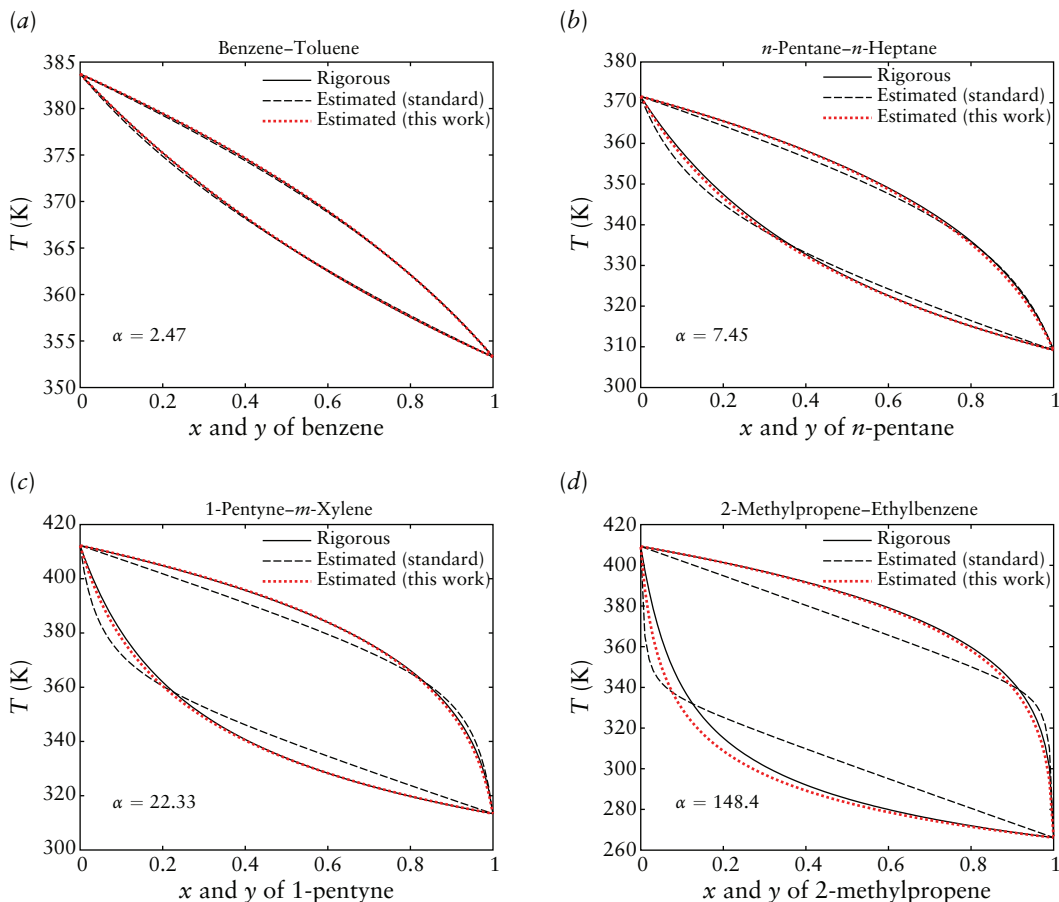


Figure 7.7 T - x - y diagrams for mixtures of (a) benzene-toluene; (b) n -pentane- n -heptane; (c) 1-pentyne- m -xylene; (d) 2-methylpropene-ethylbenzene; showing rigorously calculated temperatures, and estimates using the standard and proposed equations.

The differences between the two approaches start to become more evident when α is increased. In the n -pentane- n -heptane mixture ($\alpha = 7.45$; $T_{b,1} = 309.2$ K; $T_{b,2} = 371.5$ K), predictions with the standard equations show a maximum absolute error of 3.60 K, while the proposed equations give a lower 1.12 K.

When the two sets of equations are applied to an even higher α , in this case for the 1-pentyne- m -xylene mixture ($\alpha = 22.33$; $T_{b,1} = 313.4$ K; $T_{b,2} = 412.3$ K), the standard equations incur a maximum error of 10.79 K, while the proposed equations have this value at 2.77 K.

An example of an extreme case, which has an α value far outside of the regressed range for the proposed equations, is the 2-methylpropene-ethylbenzene mixture ($\alpha = 148.4$; $T_{b,1} = 266.1$ K; $T_{b,2} = 409.3$ K). For this mixture, the maximum error with the standard equations is 33.57 K; this number is much lower for the proposed equations at 14.43 K.

Table 7.1 Summary of limiting values in temperature prediction errors found across the 5 797 mixtures used in the analysis.

Equations	AAE (K)	ARE	MAE (K)	MRE
Standard	<5.59	<1.46%	<18.16	<4.30%
Proposed (this work)	<2.95	<0.81%	<9.43	<2.46%

AAE = average absolute error; ARE = average relative error; MAE = maximum absolute error; MRE = maximum relative error

In all of the examples provided here, the proposed equations give more accurate estimates of the equilibrium temperatures than do the standard ones. It appears that the accuracy of the proposed equations is also considerably less sensitive to α , and therefore provides considerably better estimates even at high α values. The errors of both methods are considered in more detail in § 7.3.5.

A trend that is noticed—and best exemplified in Figure 7.7*d*—is that the standard equations inherently have a shape that is qualitatively ‘wrong’ for the description of the phase envelopes. The effects of this are not obvious—and are indeed of little practical concern—at low α values, but become very prominent at high ones. The proposed equations, however, having more of a theoretical foundation, are in a form that is more suitable for the description of the phase envelopes, both quantitatively and qualitatively.

7.3.5 Deviation from rigorous ideal VLE calculations

In this section, the deviations from rigorously calculated values of the proposed equations, Eqs (7.38) and (7.39), and the standard equations, Eqs (7.22) and (7.23), are considered in more detail. The analysis was performed on 5 797 mixtures, with $\alpha \leq 30$, and with no limitation on the appropriateness of the CRV model, in order to determine the range of error that can be expected from the proposed equations, even when the CRV model does not predict the x - y behaviour well.

In this analysis, for each mixture, the absolute errors (maximum and average), and the relative errors (maximum and average) are examined. Moreover, the bubble- and dew-point temperatures were considered together, such that only the worst error of both (across the entire composition range), is reported.

The limiting values of these errors are summarised in Table 7.1. Overall, the proposed equations incur approximately half of the error of the standard equations.

7.3.6 Extension to non-atmospheric pressures

If the normal boiling points of the pure components are known, it is possible to approximate the boiling points at different, albeit similar, pressures. This affects the pure-component ‘anchor’ points in the T - x - y diagram, as well as the α . In other words, the known values are the atmospheric pressure P_0 (101 325 Pa) and the normal boiling points, $T_{b,1}$ and $T_{b,2}$; at a pressure of P_1 , the boiling points change to $T'_{b,1}$ and $T'_{b,2}$.

Two simplifying models are employed: the Clausius–Clapeyron equation, along with the Trouton–Hildebrand–Everett (THE) rule (Everett, 1960; Nash, 1984), both of which apply to pure components. The former was given as Eq. (7.8), and with the present notation, is:

$$\ln\left(\frac{P_1}{P_0}\right) = -\frac{\lambda_i}{R}\left(\frac{1}{T'_{b,i}} - \frac{1}{T_{b,i}}\right) \quad (7.40)$$

The THE rule was given as Eq. (5.24), and is expressed as follows with the present notation:

$$\lambda_i = RT_{b,i}[4.0 + \ln(T_{b,i}/\text{K})] \quad (7.41)$$

Equation (7.41) estimates the latent heat of component i at its normal boiling point; if $T_{b,i}$ were replaced with $T'_{b,i}$, it would be impossible to calculate $T'_{b,i}$ explicitly in the next step. A compromise that yields significantly better results for the estimation of $T'_{b,i}$ is the following minor change to Eq. (7.41):

$$\lambda_i = RT'_{b,i}[4.0 + \ln(T_{b,i}/\text{K})] \quad (7.42)$$

When Eqs (7.40) and (7.42) are combined and rearranged to make $T'_{b,i}$ the subject of the formula, the following is obtained:

$$T'_{b,i} = T_{b,i}\left(1 + \frac{\ln(P_1/P_0)}{[4.0 + \ln(T_{b,i}/\text{K})]}\right) \quad (7.43)$$

The α value also changes at different pressures; for this, it is possible to use the correlation of Melpolder and Headington (1947), which can be expressed as follows using the notation in this chapter:

$$\alpha(T) = \exp\left(\frac{T'_{b,2} - T'_{b,1}}{T}\left[22.44 - 1.15 \ln(P_1/\text{Pa}) + \frac{T}{33.76 \ln(P_1/\text{Pa}) - 165.19}\right]\right) \quad (7.44)$$

where T is in K.

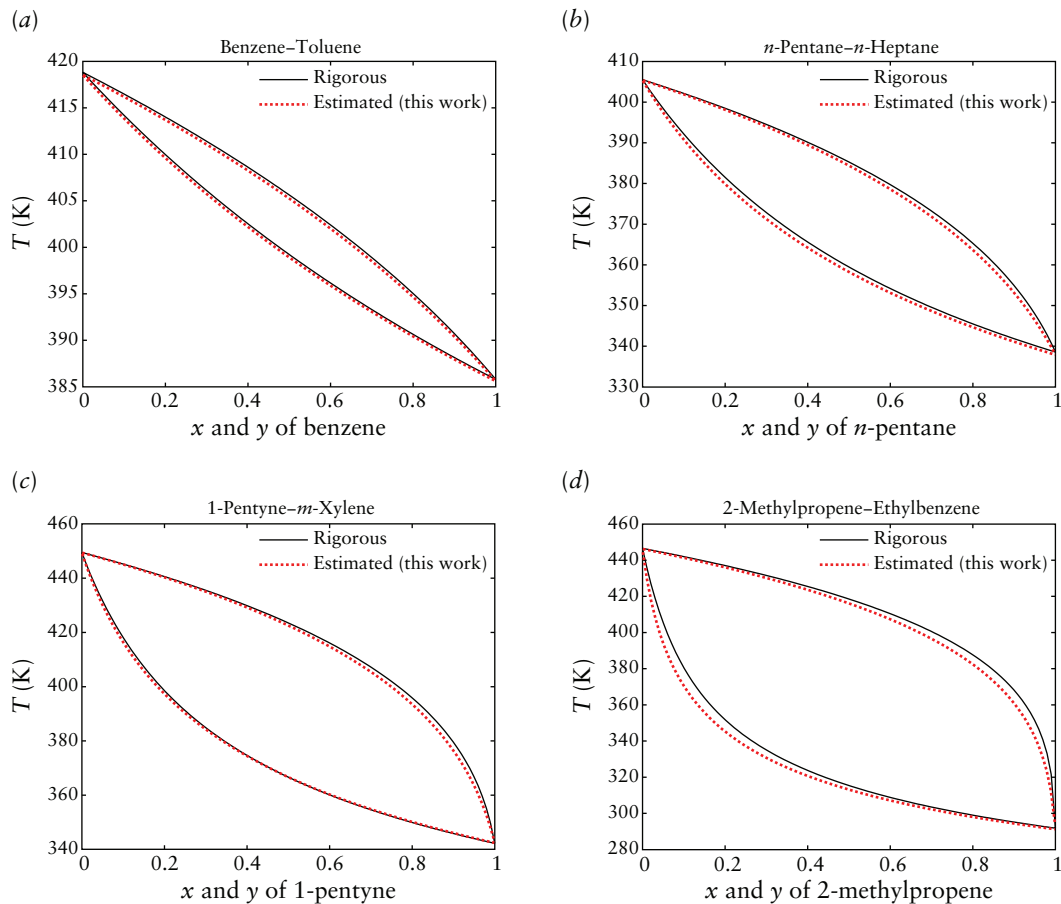


Figure 7.8 T - x - y diagrams at system pressure of 250 kPa for mixtures of (a) benzene–toluene; (b) n -pentane– n -heptane; (c) 1-pentyne– m -xylene; (d) 2-methylpropene–ethylbenzene; showing rigorously calculated temperatures, and estimates using the proposed equations.

The geometric mean α , as used in this work (and shown as α' here, to indicate that it is at the non-atmospheric pressure, P_1), is obtained as:

$$\alpha' = \sqrt{\alpha(T'_{b,1}) \alpha(T'_{b,2})} \quad (7.45)$$

where $T'_{b,1}$ and $T'_{b,2}$ are obtained using Eq. (7.43), while $\alpha(T'_{b,1})$ and $\alpha(T'_{b,2})$ are obtained from Eq. (7.44).

In order to test Eqs (7.38) and (7.39) with non-atmospheric pressure using the method described in this section, the T - x - y diagrams in Figure 7.7 were recreated, but at a system pressure of 250 kPa. These higher-pressure T - x - y diagrams are given in Figure 7.8. It is seen that the proposed method works approximately as well at the higher pressure as it does at atmospheric pressure.

7.4 Conclusion

For preliminary investigations of distillation systems, shortcut methods are a useful approach to gain insight into the behaviour of these systems. This class of shortcut tool is typically simple and non-iterative, which tends to be particularly useful for obtaining analytical solutions, or for spreadsheeting applications. One well-known example of such a shortcut method is the constant relative volatility model for describing VLE.

In this chapter, two methods were presented, which were developed to fill gaps in the literature, where the methods that existed were either not suitable, or not theoretically sound.

The first of these methods was a very simple criterion for determining whether a saturated vapour will condense or be superheated when compressed; it is particularly suitable for easy memorisation and ‘back-of-the-envelope’ calculations. The proposed criterion is simpler than Patwardhan’s (Patwardhan, 1987) approach, requires fewer fluid properties, and needs no temperature dependence information. Furthermore, it allows for the inclusion of compressor efficiency information, which Patwardhan’s (Patwardhan, 1987) method does not. The proposed criterion works well when temperature and pressure are well below the critical point, approximating an ideal gas. However, it must be stressed that—as a rough guideline—the criterion should not be used for $T_0/T_c > 0.6$. Moreover, if $\hat{C}_p^{\text{IG}} T_0 \eta / \lambda$ is close to unity, caution should be exercised by using a rigorous simulation instead, since the ideal gas assumption will seldom be exact.

Additionally, equations were derived for the estimation of minimum compressor inlet superheating required to avoid condensation. The results were validated through rigorous simulation, and the estimates found to be sufficiently good to be useful for modest compressor pressure ratios. The values obtained are not exact since the equations do not account for the temperature dependence of fluid properties, or for departures from ideal gas behaviour. As with the criterion, these equations should not be applied when $T_0/T_c > 0.6$.

The second development in this chapter was novel, temperature-explicit equations for the estimation of bubble and dew points of ideal binary mixtures—given as Eqs (7.38) and (7.39)—using only the boiling points of the mixtures and the constant relative volatility. At atmospheric pressure, normal boiling points are used; for other pressures, the boiling points at the system pressure are required. A way of extending the proposed method to non-

atmospheric pressures was also developed in § 7.3.6, and shown to maintain similar accuracy to the base atmospheric-pressure case.

The intended use of the proposed approach is principally for high-level distillation calculations, at the synthesis or conceptual design stage when alternatives are being screened to discard unfavourable ones. At this phase of distillation design, it is convenient to simplify the problem to use only boiling points and constant relative volatility (and perhaps some other rudimentary information), which is why the proposed equations have been designed to use this minimal information only. Unlike in rigorous calculations, the vapour pressure as a function of temperature is not required.

The temperature-explicit nature of the equation makes the computation of bubble- and dew-point temperatures non-iterative. This has the advantage of easy application in spreadsheet calculations and direct inclusion in other equations which may require the equilibrium temperature.

Using the proposed equations, the largest relative error (compared to rigorously calculated values) in the equilibrium temperature estimates for 5 797 mixtures (with $\alpha < 30$) was 2.46%. The average relative error across the entire composition did not exceed 0.81%. For the purposes of high-level estimates, this margin of error is entirely acceptable, especially given that the errors are typically much lower than these maximum values.

The accuracy of the proposed equations is appreciably better—especially at higher α values—than that of the standard approach that uses the same inputs to estimate the equilibrium temperatures. However, that method retains the advantage of being applicable to multicomponent systems as well.

The proposed equations are designed to estimate the results of rigorous ideal binary calculations, using basic information only; however, it is still the role of the engineer to determine the suitability of the ideality assumption for a given problem.

Chapter 8

Conclusions

8.1 Overview

The work in this thesis has been developed to facilitate understanding of limitations in distillation, as well as the design of efficient distillation columns, by introducing useful methods, techniques, tools, and novel process configurations.

Inherent to all processes is the limit imposed by entropy generation, which, according to the second law of thermodynamics, must always be positive. Through the use of a new function, δS , the entropy generation in a column section can be assessed between any two cross-sections in the column. It was shown mathematically in Chapter 2 that the stationary points of δS correspond to pinch points in the column, the implication of which is that maximum entropy generation and traditional pinch points are, in fact, the same limitation in distillation columns. The pinch types were also characterised by the type of stationary point: it was found that maximum δS corresponds to a stable node and minimum δS to an unstable one, while an inflection in δS is a saddle point or a tangent pinch.

The correspondence between extrema in the δS function and pinch points was exploited to derive a novel minimum reflux equation for binary systems based solely on entropy generation. This equation is drastically different from previous approaches. Although it is not an elegant solution—indeed, it is a more complicated approach than minimum reflux using McCabe–Thiele diagrams—it is a strong demonstration of the usefulness of entropy analysis, and of its intricate link to pinch points and minimum reflux. Perhaps most interestingly, the entropy analysis finds pinch points without VLE calculations, which further strengthens this argument.

Pinch points are an integral feature (and limitation) of distillation in their own right, and are critical for designing distillation systems, since they often dictate the approach that needs to be taken for a particular problem. Some design techniques, such as the column profile method, require the knowledge of all pinch point locations; there was previously no method that could fulfil this requirement, and that was solvable using common (non-specialised) numerical techniques. In order to provide such a method, the work in Chapter 3 was developed, and then extended to some key areas that were lacking for the column profile map (CPM) method. The proposed algorithm can find all of the pinch points in a given search space; thereafter, with the knowledge of these pinch point locations, finite reflux distillation boundaries (FRDBs) were introduced. FRDBs are simply a non-ideal analogue for the transform triangles used in the CPM method. This allows for one of the most powerful features of the CPM method to be applied to more realistic, non-constant relative volatility systems. Such an application was presented as a distributed-feed example to demonstrate this approach, and the usefulness of finding all pinch points.

By taking a radically different approach from that in Chapter 3, a very efficient method of constructing pinch point curves was presented in Chapter 4. Not only is it faster than continuation algorithms, but it also does not experience branch-switching like the latter, and it is directly parameterised by a relevant design variable (reflux ratio), whereas continuation methods are parameterised by arc length, with reflux ratio as a dependent variable. Another major advantage of the method proposed in this chapter is that it can be implemented using standard tools in common mathematical software, whereas continuation methods require specialised, non-standard solvers. Additionally, the proposed method can locate azeotropes during the course of its run (identified at infinite reflux), whereas continuation methods, being parameterised by arc length, have no way of demarcating azeotropes.

Having addressed pinch points and FRDBs in non-ideal systems—thereby providing a tool for the CPM method to design realistic complex columns—attention was turned to other ways of reducing energy requirements in distillation systems. A relatively simple, and potentially under-utilised, option that was considered in Chapter 5 was standard vapour recompression (SVRC). A high-level analysis was performed to compare the behaviour of conventional columns and SVRC; the main finding from this analysis was that as feed purity increases in either direction, the disparity between minimum theoretical and

practical work/energy input increases. An explanation for this was deduced: as feed composition tends to the composition of a product, the required work of separation tends to zero, as less and less separation must take place; however, the column requires vapour reboil to operate, and even if the feed impurity is infinitesimally small, reboil must still take place. In this case, the energy input goes solely to vapour generation (and hence entropy generation), even if effectively no separation is taking place.

Through the use of thermodynamics at the fundamental level, a comparison was made between SVRC and conventional distillation, and a region was derived to indicate which is more thermodynamically efficient, based solely on the two product temperatures. It was found that the SVRC-favoured region was surprisingly wide, and included many systems to which vapour recompression had not been applied. To investigate this further, a practical constraint was analysed, in the form of the required pressure ratio in the compressor. Overlaying isobars onto the thermodynamic criterion resulted in a synthesis tool, in the form of a single chart, which allows the designer to obtain a first-pass estimate of whether or not SVRC is worthy of further consideration for the specific problem, with no calculations whatsoever. In this way, the proposed tool can be used for rapid assessment of SVRC, and saves substantial time and effort that could otherwise be wasted on rigorous simulation in cases where no possible benefit could be derived from the use of SVRC. The synthesis tool itself was validated using a number of rigorously simulated examples, each of which deviated from the inherent assumptions in the derivation of the tool, in order to test its applicability and robustness.

In terms of general insight afforded by the tool, it showed that the practical implementation of SVRC systems is determined almost exclusively by the required pressure ratios, and thus limits it to close-boiling systems, even though thermodynamic favourability extends far beyond that constraint.

When SVRC is applicable, the energy savings are significant; however, very few systems fall into this category. In Chapter 6, a parametric study was performed on the effects of preconditioning in conventional columns (taking into account the change in minimum reflux caused by the preconditioning), with specific focus on total energy input, and total entropy generation. From this study, two opportunities were identified for energy integration, by means of a vapour recompression heat pump (since energy needed to be transferred from a cold vapour to a hot liquid), which led to two novel vapour recompression configurations: Feed–Distillate Vapour Recompression (FDVRC) and

Feed–Bottoms Vapour Recompression (FBVRC). Through a series of numerical experiments, it was determined that these configurations are applicable to much wider-boiling systems than SVRC, and that they always have lower compression ratios than SVRC. Where SVRC is limited to the types of system to which it is applicable, the novel configurations are limited to the type of feed they can accept: FDVRC is used for light liquid feeds, and FBVRC for heavy vapour feeds. For feeds that are applicable, the novel configurations can yield significant energy-saving benefits with respect to SVRC and conventional distillation, which was verified with a number of rigorously simulated examples.

Finally, Chapter 7 presented two simple shortcut methods for high-level distillation analysis, which were developed during the course of this thesis, since methods in the literature were not satisfactory. One of these methods is used to estimate whether a saturated vapour will condense or become superheated on compression, using only the vapour's latent heat and ideal gas heat capacity at the saturation temperature. For cases where condensation occurs, a simple method was derived for estimating the minimum compressor suction superheating required to avoid condensation in the compressor. This is also useful as an initial guess for the iterative procedure that is needed to calculate the minimum inlet superheating rigorously with process simulators.

A second shortcut method was presented in the same chapter for the non-iterative estimation of bubble- and dew-point temperatures in ideal binary systems, using only the pure-component boiling points, and the constant relative volatility. If the latter is unavailable, Melpolder and Headington's (1947) correlation given in Eq. (7.44) can estimate it very well, such that only the boiling points are required. The method was also extended to non-atmospheric pressures. Only one other method for this appears to exist (Halvorsen and Skogestad, 2000), and the method proposed in this work was found to incur about half the error of the former across 5 797 mixtures with $\alpha < 30$.

Overall, this thesis has presented original research that focuses on pinch points and entropy generation, with particular emphasis on supporting and developing techniques and insights that facilitate the design of efficient distillation systems.

8.2 Recommendations for future research

There are a number of ways in which the work presented in this thesis can be built upon in future research, some of which are more ambitious than others.

The entropy generation analysis could be extended to multicomponent systems easily; particularly, contour maps of δS can be overlaid on column profile maps, such that various profiles' reversibility can be compared graphically. However, extension is required to fully integrate it with the CPM, to allow the entropy generation between column sections, at feed points, and at reboilers and condensers to be assessed with the same process.

It may also be possible to derive a multicomponent minimum reflux equation based on entropy generation, which would be particularly useful, since a simple, satisfactory way of finding multicomponent minimum reflux for all splits has not yet been found.

For the FRDB modification to the CPM method, an improved algorithm is required for the construction of these distillation boundaries; one particular suggestion would be to use eigenvectors at saddle points as initial guesses for the boundary profiles.

It is also possible that the pinch point curve algorithm in Chapter 4 could be improved further, using a hybrid approach, where arc length continuation is used at high reflux ratio values to overcome slow pinch point movement, and then switched over to the proposed ODE-based method at lower reflux ratios.

For the SVRC synthesis tool, an excellent addition would be a way of graphically assessing the economic impact on the capital and operating expenditure of SVRC in comparison with conventional distillation.

Regarding the novel FDVRC and FBVRC configurations, a generalised synthesis tool, such as the one for the SVRC, would be extremely useful. This was not possible at this phase, due to the fact that energy loads can be split between the compressor and reboiler somewhat arbitrarily, and more information is required than for SVRC. Nevertheless, the use of properties correlations as functions of boiling points could go some way towards removing that obstacle.

Furthermore, some characteristics of the novel configurations remain to be determined; namely, the controllability and start-up must be assessed, and an industrial case study should be performed to ascertain the economics (operating and capital expenditure, payback period, etc.) of the novel configurations in relation to conventional distillation and SVRC.

References

- Abbas, R., 2011. *Utilisation of Column Profile Maps for the Design and Optimisation of Complex Distillation Processes*. PhD thesis, University of the Witwatersrand, Johannesburg, South Africa.
- Abbott, M.M., Van Ness, H.G., 1989. *Schaum's Outlines: Thermodynamics with Chemical Applications*, 2nd Edition. McGraw-Hill, New York.
- Acrivos, A., Amundson, N.R., 1955. On the steady state fractionation of multicomponent and complex mixtures in an ideal cascade. Part 5. The extension to packed columns. *Chem. Eng. Sci.* 4 (5), 206–208.
- Agrawal, R., 2000. Multieffect distillation for thermally coupled configurations. *AIChE J.* 46 (11), 2211–2224.
- Agrawal, R., 2003. Synthesis of multicomponent distillation column configurations. *AIChE J.* 49 (2), 379–401.
- Agrawal, R., Herron, D.M., 1997. Optimal thermodynamic feed conditions for distillation of ideal binary mixtures. *AIChE J.* 43 (11), 2984–2996.
- Agrawal, R., Herron, D.M., 1998. Intermediate reboiler and condenser arrangement for binary distillation columns. *AIChE J.* 44 (6), 1316–1324.
- Aguirre, P., Espinosa, J., 1996. A robust method to solve mass balances in reversible column sections. *Ind. Eng. Chem. Res.* 35 (2), 559–572.
- Aguirre, P., Espinosa, J., Tarifa, E., Scenna, N., 1997. Optimal thermodynamic approximation to reversible distillation by means of interheaters and intercoolers. *Ind. Eng. Chem. Res.* 36 (11), 4882–4893.
- Al-Elg, A.H., Palazoglu, A., 1989. Modeling and control of a high-purity double-effect distillation column. *Comp. Chem. Eng.* 13 (10), 1183–1187.

- Amale, A.S., Lucia, A., 2008. Non-pinchd, minimum energy distillation designs. *Chem. Eng. Res. Des.* 86 (8), 892–903.
- Annakou, O., Mizsey, P., 1995. Rigorous investigation of heat pump assisted distillation. *Heat Recov. Syst. CHP* 15 (3), 241–247.
- Aspen Technology, Inc., 2007. Aspen Plus 2006.5 [computer software].
- Ayotte-Sauvé, E., Sorin, M., 2010. Energy requirements of distillation: Exergy, pinch points, and the reversible column. *Ind. Eng. Chem. Res.* 49 (11), 5439–5449.
- Bandyopadhyay, S., 2002. Effect of feed on optimal thermodynamic performance of a distillation column. *Chem. Eng. J.* 88 (1-3), 175–186.
- Bandyopadhyay, S., 2007. Thermal integration of a distillation column through side-exchangers. *Chem. Eng. Res. Des.* 85 (1), 155–166.
- Bandyopadhyay, S., Malik, R.K., Shenoy, U.V., 2003. Feed preconditioning targets for distillation through invariant rectifying–stripping curves. *Ind. Eng. Chem. Res.* 42 (26), 6851–6861.
- Barttfeld, M., Aguirre, P.A., 2002. Optimal synthesis of multicomponent zeotropic distillation processes. 1. Preprocessing phase and rigorous optimization for a single unit. *Ind. Eng. Chem. Res.* 41 (21), 5298–5307.
- Baur, R., Krishna, R., Taylor, R., 2005. Influence of mass transfer in distillation: Feasibility and design. *AIChE J.* 51 (3), 854–866.
- Bausa, J., v. Watzdorf, R., Marquardt, W., 1996. Minimum energy demand for nonideal multicomponent distillations in complex columns. *Comp. Chem. Eng.* 20, S55–S60.
- Bausa, J., v. Watzdorf, R., Marquardt, W., 1998. Shortcut methods for non-ideal multicomponent distillation: I. Simple columns. *AIChE J.* 44 (10), 2181–2198.
- Bellows, M., Lucia, A., 2007. The geometry of separation boundaries: Four-component mixtures. *AIChE J.* 53 (7), 1770–1778.
- Beneke, D.A., Hildebrandt, D., Glasser, D., 2011a. On column profile maps: An analysis of sharp splits. *Ind. Eng. Chem. Res.* 50 (10), 6331–6342.

- Beneke, D.A., Kim, S.B., Linninger, A.A., 2011b. Pinch point calculations and its implications on robust distillation design. *Chin. J. Chem. Eng.* 19 (6), 911–925.
- Bogacki, P., Shampine, L.F., 1989. A 3(2) pair of Runge–Kutta formulas. *Appl. Math. Lett.* 2 (4), 321–325.
- Bonilla-Petriciolet, A., Iglesias-Silva, G.A., Hall, K.R., 2009. Calculation of homogeneous azeotropes in reactive and non-reactive mixtures using a stochastic optimization approach. *Fluid Phase Equil.* 281 (1), 22–31.
- Bossen, B.S., Jørgensen, S.B., Gani, R., 1993. Simulation, design, and analysis of azeotropic distillation operations. *Ind. Eng. Chem. Res.* 32 (4), 620–633.
- Boyce, M.P., 2011. *Gas Turbine Engineering Handbook*, 4th Edition. Butterworth–Heinemann, Massachusetts.
- Branan, C. (Ed.), 2005. *Rules of Thumb for Chemical Engineers*, 4th Edition. Gulf Professional Publishing, Houston.
- Brankin, R.W., Gladwell, I., 1997. Algorithm 771: rksuite_90: Fortran 90 software for ordinary differential equation initial-value problems. *ACM Trans. Math. Softw.* 23 (3), 402–415.
- Brankin, R.W., Gladwell, I., Shampine, L.F., 1992. RKSUITE: A suite of Runge–Kutta codes for the initial value problem for ODEs. Softreport 92-S1, Department of Mathematics, Southern Methodist University, Dallas, Texas, USA.
- Brousse, E., Claudel, B., Jallut, C., 1985. Modelling and optimization of the steady state operation of a vapour recompression distillation column. *Chem. Eng. Sci.* 40 (11), 2073–2078.
- Brüggemann, S., Marquardt, W., 2004. Shortcut methods for nonideal multi-component distillation: 3. Extractive distillation columns. *AIChE J.* 50 (6), 1129–1149.
- Burri, J.F., Manousiouthakis, V.I., 2004. Global optimization of reactive distillation networks using IDEAS. *Comp. Chem. Eng.* 28, 2509–2521.

- Caballero, J.A., Grossmann, I.E., 2003. Thermodynamically equivalent configurations for thermally coupled distillation. *AIChE J.* 49 (11), 2864–2884.
- Caballero, J.A., Grossmann, I.E., 2013. Synthesis of complex thermally coupled distillation systems including divided wall columns. *AIChE J.* 59 (4), 1139–1159.
- Campanella, E.A., 1997. A vapor pressure equation for heavy compounds. *Chem. Eng. Technol.* 20 (2), 101–107.
- Carta, R., Kovacic, A., Tola, G., 1982. Separation of ethylbenzene–xylenes mixtures by distillation: A possible application of the vapour recompression concept. *Chem. Eng. Commun.* 19 (1-3), 157–165.
- Castillo, F.J.L., Thong, D.Y.C., Towler, G.P., 1998a. Homogeneous azeotropic distillation. 1. Design procedure for single-feed columns at nontotal reflux. *Ind. Eng. Chem. Res.* 37 (3), 987–997.
- Castillo, F.J.L., Thong, D.Y.C., Towler, G.P., 1998b. Homogeneous azeotropic distillation. 2. Design procedure for sequences of columns. *Ind. Eng. Chem. Res.* 37 (3), 998–1008.
- Chapman, R.G., Goodwin, S.P., 1993. A general algorithm for the calculation of azeotropes in fluid mixtures. *Fluid Phase Equil.* 85, 55–69.
- Chen, H., Huang, K., Wang, S., 2010. A novel simplified configuration for an ideal heat-integrated distillation column (ideal HIDiC). *Sep. Purif. Technol.* 73 (2), 230–242.
- Cheng, H.C., Luyben, W.L., 1985. Heat-integrated distillation columns for ternary separations. *Ind. Eng. Chem. Proc. Des. Dev.* 24 (3), 707–713.
- Chiang, T.P., Luyben, W.L., 1983. Comparison of energy consumption in five heat-integrated distillation configurations. *Ind. Eng. Chem. Proc. Des. Dev.* 22 (2), 175–179.
- de Koeijer, G., Røsjorde, A., Kjelstrup, S., 2004. Distribution of heat exchange in optimum diabatic distillation columns. *Energy* 29 (12), 2425–2440.

- de Koeijer, G.M., Kjelstrup, S., Salamon, P., Siragusa, G., Schaller, M., Hoffmann, K.H., 2002. Comparison of entropy production rate minimization methods for binary diabatic distillation. *Ind. Eng. Chem. Res.* 41 (23), 5826–5834.
- Demirel, Y., 2004. Thermodynamic analysis of separation systems. *Separ. Sci. Technol.* 39 (16), 3897–3942.
- Deshmukh, B.F., Malik, R.K., Bandyopadhyay, S., 2005. Efficient feed preheat targeting for distillation by feed splitting. *Comput. Aided Chem. Eng.* 20, 751–756.
- Dhole, V.R., Linnhoff, B., 1993. Distillation column targets. *Comp. Chem. Eng.* 17 (5-6), 549–560.
- Dodge, B.F., Huffman, J.R., 1937. Calculation of the number of theoretical plates for a rectifying column. *J. Ind. Eng. Chem.* 29 (12), 1434–1436.
- Doedel, E.J., Champneys, A.R., Fairgrieve, T.F., Kuznetsov, Yu. A., Sandstede, B., Wang, X., 1998. AUTO 97: Continuation and bifurcation software for ordinary differential equations (with HomCont). User's guide, Concordia University, Montreal, Canada.
- Doherty, M.F., Malone, M.F., 2001. *Conceptual Design of Distillation Systems*. McGraw-Hill, New York.
- Drake, J.E., Manousiouthakis, V., 2002. IDEAS approach to process network synthesis: Minimum utility cost for complex distillation networks. *Chem. Eng. Sci.* 57 (15), 3095–3106.
- Durandet, J., 1983. *Vapour compression heat pump fluids – properties and selection*. In: Berghmans, J. (Ed.), *Heat Pump Fundamentals*. Martinus Nijhoff Publishers, The Hague.
- Emami, F.S., Vahid, A., Elliott, Jr., J.R., Feyzi, F., 2008. Group contribution prediction of vapor pressure with statistical associating fluid theory, perturbed-chain statistical associating fluid theory, and Elliott–Suresh–Donohue equations of state. *Ind. Eng. Chem. Res.* 47 (21), 8401–8411.
- Engelien, H.K., Skogestad, S., 2005. Minimum energy diagrams for multieffect distillation arrangements. *AIChE J.* 51 (6), 1714–1725.

- Everett, D.H., 1960. 519. some correlations between thermodynamic properties and the structure of liquids. *J. Chem. Soc.*, 2566–2573.
- Felbab, N., 2012. An efficient method of constructing pinch point curves and locating azeotropes in nonideal distillation systems. *Ind. Eng. Chem. Res.* 51 (20), 7035–7055.
- Felbab, N., 2013. Condensation of saturated vapours on compression and estimation of minimum suction superheating. *Appl. Therm. Eng.* 52 (2), 527–530.
- Felbab, N., Hildebrandt, D., Glasser, D., 2011. A new method of locating all pinch points in nonideal distillation systems, and its application to pinch point loci and distillation boundaries. *Comp. Chem. Eng.* 35 (6), 1072–1087.
- Felbab, N., Patel, B., El-Halwagi, M. M., Hildebrandt, D., Glasser, D., 2013. Vapor recompression for efficient distillation. 1. A new synthesis perspective on standard configurations. *AIChE J.* 59 (8), 2977–2992.
- Ferré, J.A., Castells, F., Flores, J., 1985. Optimization of a distillation column with a direct vapor recompression heat pump. *Ind. Eng. Chem. Proc. Des. Dev.* 24 (1), 128–132.
- Fidkowski, Z. T., Malone, M. F., Doherty, M. F., 1991. Nonideal multicomponent distillation: Use of bifurcation theory for design. *AIChE J.* 37 (12), 1761–1779.
- Fidkowski, Z. T., Malone, M. F., Doherty, M. F., 1993. Computing azeotropes in multicomponent mixtures. *Comp. Chem. Eng.* 17 (12), 1141–1155.
- Fien, G.J.A.F., Liu, Y.A., 1994. Heuristic synthesis and shortcut design of separation processes using residue curve maps: A review. *Ind. Eng. Chem. Res.* 33 (11), 2505–2522.
- Fitzmorris, R.E., Mah, R.S.H., 1980. Improving distillation column design using thermodynamic availability analysis. *AIChE J.* 26 (2), 265–273.
- Flores, J., Castells, F., Ferré, J.A., 1984. Recompression saves energy. *Hydrocarb. Process.* 63, 59–62.

- Flower, J. R., Jackson, R., 1964. Energy requirements in the separation of mixtures by distillation. *Trans. Instn Chem. Engrs* 42, T249–T258.
- Fonyó, Z., 1974. Thermodynamic analysis of rectification I. Reversible model of rectification. *Int. Chem. Eng.* 14 (1), 18–27.
- Fonyó, Z., Benkő, N., 1998. Comparison of various heat pump assisted distillation configurations. *Chem. Eng. Res. Des.* 76 (3), 348–360.
- Freshwater, D. C., 1951. Thermal economy in distillation. *Trans. Instn Chem. Engrs* 29, 149–160.
- Gani, R., Bek-Pedersen, E., 2000. Simple new algorithm for distillation column design. *AIChE J.* 46 (6), 1271–1274.
- Glenchur, T., Govind, R., 1987. Study on a continuous heat integrated distillation column. *Separ. Sci. Technol.* 12 (12), 2323–2338.
- Glinos, K., Malone, M. F., 1989. Net work consumption in distillation—Short-cut evaluation and applications to synthesis. *Comp. Chem. Eng.* 13 (3), 295–305.
- Gmehling, J., Kolbe, B., Kleiber, M., Rarey, J., 2012. *Chemical Thermodynamics for Process Simulation*. Wiley-VCH, Weinheim.
- Gomez-Munoz, A., Seader, J. D., 1985. Synthesis of distillation trains by thermodynamic analysis. *Comp. Chem. Eng.* 9 (4), 311–341.
- Gopichand, S., Devotta, S., Omideyi, T. O., Holland, F. A., 1988. Heat pump assisted distillation. X: Potential for industrial applications. *Int. J. Energy Res.* 12 (4), 569–582.
- Granryd, E., 2001. Hydrocarbons as refrigerants — an overview. *Int. J. Refrig.* 24 (1), 15–24.
- Halvorsen, I. J., 2001. *Minimum Energy Requirements in Complex Distillation Arrangements*. Dr. Ing. thesis, Norwegian University of Science and Technology (NTNU), Trondheim, Norway, available from the webpage of the Department of Chemical Engineering, NTNU (Accessed June 2009: <http://www.chemeng.ntnu.no/thesis/download/2001/halvorsen/>).

- Halvorsen, I.J., Skogestad, S., 2000. *Theory of Distillation*. In: Wilson, I.D., Adlard, E.R., Cooke, M., Poole, C.F. (Eds), *Encyclopedia of Separation Science*. Academic Press, Massachusetts, pp. 1117–1134.
- Halvorsen, I.J., Skogestad, S., 2004. Shortcut analysis of optimal operation of Petlyuk distillation. *Ind. Eng. Chem. Res.* 43 (14), 3994–3999.
- Halvorsen, I.J., Skogestad, S., 2011. Energy efficient distillation. *J. Nat. Gas. Sci. Eng.* 3 (4), 571–580.
- Harding, S.T., Maranas, C.D., McDonald, C.M., Floudas, C.A., 1997. Locating all homogeneous azeotropes in multicomponent mixtures. *Ind. Eng. Chem. Res.* 36 (1), 160–178.
- Hauan, S., Westerberg, A.W., Lien, K.M., 2000. Phenomena-based analysis of fixed points in reactive separation systems. *Chem. Eng. Sci.* 55 (6), 1053–1075.
- Henley, E.J., Seader, J.D., 1981. *Equilibrium-Stage Separation Operations in Chemical Engineering*. John Wiley & Sons, New York.
- Hernández-Gaona, C.G., Cárdenas, J.C., Segovia-Hernández, J.G., Hernández, S., Rico-Ramírez, V., 2005. Second law analysis of conventional and nonconventional distillation sequences. *Chem. Biochem. Eng. Q.* 19 (23), 235–241.
- Hoffmaster, W.R., Hauan, S., 2002. Sectional and overall reachability for systems with S-shaped distillation lines. *AIChE J.* 48 (11), 2545–2556.
- Hoffmaster, W.R., Hauan, S., 2004. Difference points in reactive and extractive cascades. III—Properties of column section profiles with arbitrary reaction distribution. *Chem. Eng. Sci.* 59 (17), 3671–3693.
- Holland, F.A., Watson, F.A., Devotta, S., 1982. *Thermodynamic Design Data for Heat Pump Systems*. Pergamon Press, Oxford.
- Holland, S.T., 2005. *Column Profile Maps: A Tool for the Design and Analysis of Complex Distillation Systems*. PhD thesis, University of the Witwatersrand, Johannesburg, South Africa.

- Holland, S.T., Abbas, R., Hildebrandt, D., Glasser, D., 2010. Complex column design by application of column profile map techniques: Sharp-split Petlyuk column. *Ind. Eng. Chem. Res.* 49 (1), 327–349.
- Holland, S.T., Tapp, M., Hildebrandt, D., Glasser, D., 2004a. Column profile maps. 2. Singular points and phase diagram behaviour in ideal and nonideal systems. *Ind. Eng. Chem. Res.* 43 (14), 3590–3603.
- Holland, S.T., Tapp, M., Hildebrandt, D., Glasser, D., Hausberger, B., 2004b. Novel separation system design using “moving triangles”. *Comp. Chem. Eng.* 29 (1), 181–189.
- Huang, K., Matsuda, K., Iwakabe, K., Takamatsu, T., Nakaiwa, M., 2006. Interpreting design of an ideal heat-integrated distillation column through exergy analysis. *J. Chem. Eng. Jpn* 39 (9), 963–970.
- Huang, K., Shan, L., Zhu, Q., Qian, J., 2008. A totally heat-integrated distillation column (THiDiC) – the effect of feed pre-heating by distillate. *Appl. Therm. Eng.* 28 (8), 856–864.
- Humphrey, J.L., 1995. Separation processes: Playing a critical role. *Chem. Eng. Prog.* 91 (10), 31–45.
- Humphrey, J.L., Siebert, A.F., 1992. Separation technologies: An opportunity for energy savings. *Chem. Eng. Prog.* 88 (3), 32–41.
- Itoh, J., Niida, K., Shiroko, K., Umeda, T., 1980. Analysis of the available energy in a distillation system. *Int. Chem. Eng.* 20, 379–385.
- Jana, A.K., 2010. Heat integrated distillation operation. *Appl. Energy* 87 (5), 1477–1494.
- Jones, D.R., Perttunen, C.D., Stuckman, B.E., 1993. Lipschitzian optimization without the Lipschitz constant. *J. Optim. Theory Appl.* 79 (1), 157–181.
- Julka, V., Doherty, M.F., 1990. Geometric behavior and minimum flows for nonideal multicomponent distillation. *Chem. Eng. Sci.* 45 (7), 1801–1822.
- Kaiser, V., Gourlia, J.P., 1985. The ideal-column concept: Applying exergy to distillation. *Chem. Eng.* 92 (17), 45–53.

- Kayihan, F., 1980. Optimum distribution of heat load in distillation columns using intermediate condensers and reboilers. *AIChE Symp. Ser.* 192 (76), 1–5.
- Kim, S.B., Ruiz, G.J., Linninger, A.A., 2010. Rigorous separation design. 1. Multicomponent mixtures, nonideal mixtures, and prefractionating column networks. *Ind. Eng. Chem. Res.* 49 (14), 6499–6513.
- King, C.J., 1980. *Separation Processes*. McGraw-Hill, New York.
- Koehler, J., Aguirre, P., Blass, E., 1991. Minimum reflux calculations for nonideal mixtures using the reversible distillation model. *Chem. Eng. Sci.* 46 (12), 3007–3021.
- Köhler, J., 1991. *Struktursynthese und minimaler Energiebedarf nichtidealer Rektifikationen*. PhD dissertation, Technische Universität München, Munich, Germany.
- Kooijman, H., Taylor, R., 2013. ChemSep LITE v6.94 [computer software].
- Kossack, S., Kraemer, K., Marquardt, W., 2006. Efficient optimization-based design of distillation columns for homogenous azeotropic mixtures. *Ind. Eng. Chem. Res.* 45 (25), 8492–8502.
- Krolikowski, L.J., 2006. Determination of distillation regions for non-ideal ternary mixtures. *AIChE J.* 52 (2), 532–544.
- Kudchadker, A.P., Zwolinski, B.J., 1966. Vapor pressures and boiling points of normal alkanes, C₂₁ to C₁₀₀. *J. Chem. Eng. Data* 11 (2), 253–255.
- Le Goff, P., Cachot, T., Rivero, R., 1996. Exergy analysis of distillation processes. *Chem. Eng. Technol.* 19 (6), 478–485.
- Levy, S.G., Doherty, M.F., 1986. A simple exact method for calculating tangent pinch points in multicomponent nonideal mixtures by bifurcation theory. *Chem. Eng. Sci.* 41 (12), 3155–3160.
- Levy, S.G., Van Dongen, D.B., Doherty, M.F., 1985. Design and synthesis of homogeneous azeotropic distillations. 2. Minimum reflux calculations for nonideal and azeotropic columns. *Ind. Eng. Chem. Fundam.* 24 (5), 463–474.

- Lewis, W.K., 1922. The efficiency and design of rectifying columns for binary mixtures. *J. Ind. Eng. Chem.* 14 (6), 492–496.
- Liley, P.E., Thomson, G.H., Friend, D.G., Daubert, T.E., Buck, E., 1997. *Physical and Chemical Data*. In: Perry, R.H., Green, D.W. (Eds), *Perry's Chemical Engineers' Handbook*, 7th Edition. McGraw-Hill, New York.
- Linnhoff, B., Dunford, H., Smith, R., 1983. Heat integration of distillation columns into overall processes. *Chem. Eng. Sci.* 38 (8), 1175–1188.
- Linninger, A.A., 2009. Industry-wide energy saving by complex separation networks. *Comp. Chem. Eng.* 33 (12), 2018–2027.
- Lucia, A., Amale, A., 2006. Energy efficient hybrid separation processes. *Ind. Eng. Chem. Res.* 45 (25), 8319–8328.
- Lucia, A., Amale, A., Taylor, R., 2008. Distillation pinch points and more. *Comp. Chem. Eng.* 32 (6), 1342–1364.
- Lucia, A., Taylor, R., 2006. The geometry of separation boundaries: I. Basic theory and numerical support. *AIChE J.* 52 (2), 582–594.
- Lundberg, B.N., Poore, A.B., 1991. Variable-order Adams–Bashforth predictors with an error-stepsize control for continuation methods. *SIAM J. Sci. Stat. Comput.* 12 (3), 695–723.
- Macknick, A.B., Prausnitz, J.M., 1979. Vapor pressures of heavy liquid hydrocarbons by a group-contribution method. *Ind. Eng. Chem. Fundam.* 18 (4), 348–351.
- Maier, R.W., Brennecke, J.F., Stadtherr, M.A., 1988. Reliable computation of homogeneous azeotropes. *AIChE J.* 44 (8), 1745–1755.
- Mane, A., Jana, A.K., 2010. A new intensified heat integration in distillation column. *Ind. Eng. Chem. Res.* 49 (19), 9534–9541.
- Maranas, C.D., McDonald, C.M., Harding, S.T., Floudas, C.A., 1996. Locating all azeotropes in homogeneous azeotropic systems. *Comp. Chem. Eng.* 20, S413–S418.
- McLinden, M.O., Radermacher, R., 1987. Methods for comparing the performance of pure and mixed refrigerants in the vapour compression cycle. *Int. J. Refrig.* 10 (6), 318–325.

- Meili, A., Stuecheli, A., 1987. Distillation columns with direct vapor recompression. *Chem. Eng.* 94 (2), 133–143.
- Melpolder, F.W., Headington, C.E., 1947. Calculation of relative volatility from boiling points. *Ind. Eng. Chem.* 39 (6), 763–766.
- Mészáros, I., Fonyó, Z., 1986. Design strategy for heat pump assisted distillation system. *Heat Recov. Syst.* 6 (6), 469–476.
- Mészáros, I., Meili, A., 1994. 1-Butene separation processes with heat pump assisted distillation. *Heat Recov. Syst. CHP* 14 (3), 315–322.
- Mix, T.W., Dweck, J.S., Weinberg, M., Armstrong, R.C., 1978. Energy conservation in distillation. *Chem. Eng. Prog.* 74 (4), 49–55.
- Modise, T.S., Tapp, M., Hildebrandt, D., Glasser, D., 2005. Can the operating leaves of a distillation column really be expanded? *Ind. Eng. Chem. Res.* 44 (19), 7511–7519.
- Moon, J., Linninger, A.A., 2009. A hybrid sequential niche algorithm for optimal engineering design with solution multiplicity. *Comp. Chem. Eng.* 33 (7), 1261–1271.
- Muhrer, C.A., Collura, M.A., Luyben, W.L., 1990. Control of vapor recompression distillation columns. *Ind. Eng. Chem. Res.* 29 (1), 59–71.
- Mullins, O.C., Berry, R.S., 1984. Minimization of entropy production in distillation. *J. Phys. Chem.* 88, 723–728.
- Nakaiwa, M., Huang, K., Endo, A., Ohmori, T., Akiya, T., Takamatsu, T., 2003. Internally heat-integrated distillation columns: A review. *Chem. Eng. Res. Des.* 81 (1), 162–177.
- Nakaiwa, M., Huang, K., Naito, K., Endo, A., Owa, M., Akiya, T., Nakane, T., Takamatsu, T., 2000. A new configuration of ideal heat integrated distillation columns (HIDiC). *Comp. Chem. Eng.* 24 (2), 239–245.
- Nash, L.K., 1984. Trouton and the T–H–E rule. *J. Chem. Educ.* 61 (11), 981–984.
- Nelder, J.A., Mead, R., 1965. A simplex method for function minimization. *Comp. J.* 7 (4), 308–313.

- Null, H. R., 1976. Heat pumps in distillation. *Chem. Eng. Prog.* 72 (7), 58–64.
- Ognisty, T. P., 1995. Analyze distillation columns with thermodynamics. *Chem. Eng. Prog.* 91 (2), 40–46.
- Ohe, S., 2007. Energy-saving distillation through internal heat exchange (HIDiC): Overview of a Japanese national project. Presented at AIChE Spring Meeting & 3rd Global Congress on Process Safety, San Francisco.
- Olujić, Ž., Fakhri, F., de Rijke, A., de Graauw, J., Jansens, P. J., 2003. Internal heat integration – the key to an energy-conserving distillation column. *J. Chem. Technol. Biotechnol.* 78 (2-3), 241–248.
- Omideyi, T. O., Kasprzycki, J., Watson, F. A., 1984. The economics of heat pump assisted distillation systems—I. A design and economic model. *J. Heat Recov. Syst.* 4 (3), 187–200.
- Patwardhan, V. S., 1987. Condensation of saturated vapours on isentropic compression: A simple criterion. *Heat Recov. Syst. CHP* 7 (5), 395–399.
- Perry, R. H., Green, D. W. (Eds), 1999. *Perry's Chemical Engineers' Handbook*, 7th Edition. McGraw-Hill, New York.
- Petlyuk, F. B., 2004. *Distillation Theory and Its Application to Optimal Design of Separation Units*. Cambridge University Press, New York.
- Petlyuk, F. B., Danilov, R. Yu., 2001a. Few-step iterative methods for distillation process design using the trajectory bundle theory: Algorithm structure. *Theor. Found. Chem. Eng.* 35 (3), 239–251.
- Petlyuk, F. B., Danilov, R. Yu., 2001b. Theory of distillation trajectory bundles and its application to the optimal design of separation units: Distillation trajectory bundles at finite reflux. *Chem. Eng. Res. Des.* 79 (7), 733–746.
- Petlyuk, F. B., Danilov, R. Yu., 2002. Few-step iterative methods for distillation process design using trajectory bundle theory: Rigorous minimum-reflux calculation. *Theor. Found. Chem. Eng.* 36 (1), 34–47.
- Petlyuk, F. B., Danilov, R. Yu., Serafimov, L. A., 2007. Minimum-reflux regime of simple distillation columns. *Theor. Found. Chem. Eng.* 41 (4), 372–385.

- Petlyuk, F.B., Danilov, R. Yu., Serafimov, L. A., 2008. Trees of reversible distillation trajectories and the structure of trajectory bundles for sections of adiabatic columns. *Theor. Found. Chem. Eng.* 42 (6), 795–804.
- Petlyuk, F.B., Danilov, R. Yu., Serafimov, L. A., 2009. Feasible variants of separation in distillation of multicomponent azeotropic mixtures. *Theor. Found. Chem. Eng.* 43 (1), 26–36.
- Petlyuk, F.B., Platonov, V.M., Slavinskii, D.M., 1965. Thermodynamically optimal method for separating multicomponent mixtures. *Int. Chem. Eng.* 5 (3), 555–561.
- Petlyuk, F.B., Serafimov, L. A., Avet'yan, V.S., Vinogradova, E.I., 1981. Trajectories of reversible rectification when one of the components completely disappears in each section. *Theor. Found. Chem. Eng.* 15, 185–192.
- Poellmann, P., Blass, E., 1994. Best products of homogeneous azeotropic distillations. *Gas Sep. Purif.* 8 (4), 194–228.
- Poling, B.E., Prausnitz, J.M., O'Connell, J.P., 2001. *The Properties of Gases and Liquids*, 5th Edition. McGraw-Hill, New York.
- Prausnitz, J.M., Anderson, T.F., Grens, E.A., Eckert, C.A., Hsieh, R., O'Connell, J.P., 1980. *Computer Calculations for Multicomponent Vapor–Liquid and Liquid–Liquid Equilibria*. Prentice–Hall, New Jersey.
- Quadri, G.P., 1981a. Use heat pump for P–P splitter. Part 1: Process design. *Hydrocarb. Process.* 60, 119–126.
- Quadri, G.P., 1981b. Use heat pump for P–P splitter. Part 2: Process optimization. *Hydrocarb. Process.* 60, 147–151.
- Radermacher, R., Hwang, Y., 2005. *Vapor Compression Heat Pumps with Refrigerant Mixtures*. CRC Press, USA.
- Ratkje, S.K., Sauar, E., Hansen, E. M., Lien, K.M., Hafskjold, B., 1995. Analysis of entropy production rates for design of distillation columns. *Ind. Eng. Chem. Res.* 34 (9), 3001–3007.
- Ray, S., Sengupta, S.P., 1996. Irreversibility analysis of a sieve tray in a distillation column. *Int. J. Heat Mass Tran.* 39 (7), 1535–1542.

- Redlich, O., Kwong, J.N.S., 1949. On the thermodynamics of solutions. V. An equation of state. Fugacities of gaseous solutions. *Chem. Rev.* 44 (1), 233–244.
- Reid, R.C., Prausnitz, J.M., Sherwood, T.K., 1977. *The Properties of Gases and Liquids*, 3rd Edition. McGraw-Hill, New York.
- Renon, H., Prausnitz, J.M., 1968. Local compositions in thermodynamic excess functions for liquid mixtures. *AIChE J.* 14 (1), 135–144.
- Rév, E., Emtir, M., Szitkai, Z., Mizsey, P., Fonyó, Z., 2001. Energy savings of integrated and coupled distillation systems. *Comp. Chem. Eng.* 25 (1), 119–140.
- Rheinboldt, W., Burkardt, J., 1983. Algorithm 596: A program for a locally parameterized continuation process. *ACM Trans. Math. Softw.* 9 (2), 236–241.
- Rivero, R., 2001. Exergy simulation and optimization of adiabatic and diabatic binary distillation. *Energy* 26 (6), 561–593.
- Robinson, J.C., 2004. *An Introduction to Ordinary Differential Equations*. Cambridge University Press, Cambridge.
- Sandler, S.I., 2006. *Chemical, Biochemical, and Engineering Thermodynamics*, 4th Edition. John Wiley & Sons, New Jersey.
- Sauar, E., Rivero, R., Kjelstrup, S., Lien, K.M., 1997. Diabatic column optimization compared to isoforce columns. *Energy Convers. Mgmt* 38 (15-17), 1777–1783.
- Serafimov, L.A., Timofeev, V.S., Balashov, M.I., 1973a. Distillation of multi-component mixtures: 3. Local characteristics of the trajectories continuous distillation process at finite reflux ratios. *Acta Chim. Acad. Sci. Hungar.* 75, 235–254.
- Serafimov, L.A., Timofeev, V.S., Balashov, M.I., 1973b. Distillation of multicomponent mixtures: 4. Non-local characteristics of the continuous distillation, trajectories for ternary mixtures at finite reflux ratios. *Acta Chim. Acad. Sci. Hungar.* 75, 255–270.

- Seydel, R., Hlaváček, V., 1987. Role of continuation in engineering analysis. *Chem. Eng. Sci.* 42 (6), 1281–1295.
- Shampine, L.F., Gordon, M.K., 1975. *Computer Solution of Ordinary Differential Equations: the Initial Value Problem*. W.H. Freeman, San Francisco.
- Shenvi, A.A., Shah, V.H., Agrawal, R., 2013. New multicomponent distillation configurations with simultaneous heat and mass integration. *AIChE J.* 59 (1), 272–282.
- Shinskey, F.G., 1977. *Distillation Control: For Productivity and Energy Conservation*. McGraw-Hill, New York.
- Skogestad, S., 2009. *Chemical and Energy Process Engineering*. CRC Press, Florida.
- Smith, J.M., Van Ness, H.C., Abbott, M.M., 2001. *Introduction to Chemical Thermodynamics*, 6th Edition. McGraw-Hill, New York.
- Smith, R., Jobson, M., Chen, L., Farrokhpahan, S., 2010. Heat integrated distillation system design. *Chem. Eng. Trans.* 21, 19–24.
- Soares Pinto, F., Zemp, R., Jobson, M., Smith, R., 2011. Thermodynamic optimisation of distillation columns. *Chem. Eng. Sci.* 66 (13), 2920–2934.
- Soave, G., Feliu, J.A., 2002. Saving energy in distillation towers by feed splitting. *Appl. Therm. Eng.* 22 (8), 889–896.
- Srinivasan, K., 1991. Certain aspects of the behaviour of saturated-fluid phases. *Chem. Phys. Lett.* 179 (3), 268–270.
- Suphanit, B., 2011. Optimal heat distribution in the internally heat-integrated distillation column (HIDiC). *Energy* 36 (7), 4171–4181.
- Tapp, M., Holland, S.T., Hausberger, B., Hildebrandt, D., Glasser, D., 2003. Expanding the operating leaves in distillation column sections by distributed feed addition and sidestream withdrawal. *Comp. Aided Chem. Eng.* 15, 1050–1057.
- Tapp, M., Holland, S.T., Hildebrandt, D., Glasser, D., 2004. Column profile maps. 1. Derivation and interpretation. *Ind. Eng. Chem. Res.* 43 (2), 364–374.

- Taprap, R., Ishida, M., 1996. Graphic exergy analysis of processes in distillation column by energy-utilization diagrams. *AIChE J.* 42 (6), 1633–1641.
- Taylor, R., Kooijman, H., 1991. Composition derivatives of activity coefficient models (for the estimation of thermodynamic factors in diffusion). *Chem. Eng. Commun.* 102 (1), 87–106.
- Terranova, B.E., Westerberg, A.W., 1989. Temperature–heat diagrams for complex columns. 1. Intercooled/interheated distillation columns. *Ind. Eng. Chem. Res.* 28 (9), 1374–1379.
- Tian, W., Sun, S., Guo, Q., 2009. Stage difference equation and its application in distillation synthesis. *Ind. Eng. Chem. Res.* 48 (14), 6715–6722.
- Tiller, F.M., Tour, R.S., 1944. Stagewise operations — applications of the calculus of finite differences to chemical engineering. *Trans. Am. Inst. Chem. Engrs* 40, 317–332.
- Underwood, A.J.V., 1948. Fractional distillation of multicomponent mixtures. *Chem. Eng. Prog.* 44, 603–614.
- Van Dongen, D.B., Doherty, M.F., 1985. Design and synthesis of homogenous azeotropic distillations. 1. Problem formulation for a single column. *Ind. Eng. Chem. Fundam.* 24 (4), 454–463.
- von Watzdorf, R., Bausa, J., Marquardt, W., 1999. Shortcut methods for non-ideal multicomponent distillation: 2. complex columns. *AIChE J.* 45 (8), 1615–1628.
- Wahnschafft, O.M., Koehler, J.W., Blass, E., Westerberg, A.W., 1992. The product composition regions of single-feed azeotropic distillation columns. *Ind. Eng. Chem. Res.* 31 (10), 2345–2362.
- Wahnschafft, O.M., Köhler, J.W., Westerberg, A.W., 1994. Homogeneous azeotropic distillation: Analysis of separation feasibility and consequences for entrainer selection and column design. *Comp. Chem. Eng.* 18, S31–S35.
- Wahnschafft, O.M., Westerberg, A.W., 1992. The product composition regions of azeotropic distillation columns. 2. Separability in two-feed columns and entrainer selection. *Ind. Eng. Chem. Res.* 32 (6), 1108–1120.

- Wankat, P.C., Kessler, D.P., 1993. Two-feed distillation: Same-composition feeds with different enthalpies. *Ind. Eng. Chem. Res.* 32 (12), 3061–3067.
- Wasykiewicz, S.K., Doherty, M.F., Malone, M.F., 1999. Computing all homogeneous and heterogeneous azeotropes in multicomponent mixtures. *Ind. Eng. Chem. Res.* 38 (12), 4901–4912.
- Westerberg, A.W., Wahnschafft, O., 1996. Synthesis of distillation-based separation systems. *Adv. Chem. Eng.* 23, 63–170.
- Zhang, L., Linninger, A.A., 2004. Temperature collocation algorithm for fast and robust distillation design. *Ind. Eng. Chem. Res.* 43 (12), 3163–3182.

Appendix A

A.1 Important thermodynamic relations

Perry and Green (1999) give the well-known equations for calculating changes in enthalpy and entropy with readily available information:

$$d\hat{H} = \hat{C}_p dT + \left[\hat{V} - T \left(\frac{\partial \hat{V}}{\partial T} \right)_P \right] dP \quad (\text{A-1})$$

$$d\hat{S} = \frac{\hat{C}_p}{T} dT - \left(\frac{\partial \hat{V}}{\partial T} \right)_P dP \quad (\text{A-2})$$

From Sandler (2006), the following thermodynamic relations are given directly or can be deduced:

$$\Delta\hat{H}_{\text{mix}} = \hat{H}^E \quad (\text{A-3})$$

$$\hat{H}^E = -RT^2 \sum_{i=1}^N x_i \left(\frac{\partial \ln \gamma_i}{\partial T} \right)_{P,x} \quad (\text{A-4})$$

$$\Delta\hat{S}_{\text{mix}} = \hat{S}^E - R \sum_{i=1}^N x_i \ln x_i \quad (\text{A-5})$$

$$\hat{S}^E = \frac{\hat{H}^E - \hat{G}^E}{T} \quad (\text{A-6})$$

$$\hat{G}^E = \sum_{i=1}^N x_i \bar{G}_i^E \quad (\text{A-7})$$

$$\bar{G}_i^E = RT \ln \gamma_i \quad (\text{A-8})$$

In the above equations, a caret represents a molar property, whereas an overbar represents a partial molar property. The former is a per-mole value, and the latter is defined by Abbott and Van Ness (1989) as:

$$\bar{M} \equiv \left(\frac{\partial(nM)}{\partial n_i} \right)_{T,P,n_j}$$

where M is an extensive property.

In order to evaluate the $\Delta\hat{H}_{\text{mix}}$ and $\Delta\hat{S}_{\text{mix}}$ terms as functions of composition and temperature using readily available information, the following can be deduced from Eqs (A-3)–(A-8):

$$\Delta\hat{H}_{\text{mix}} = -RT^2 \sum_{i=1}^N x_i \left(\frac{\partial \ln \gamma_i}{\partial T} \right)_x \quad (\text{A-9})$$

$$\Delta\hat{S}_{\text{mix}} = -R \left[T \sum_{i=1}^N x_i \left(\frac{\partial \ln \gamma_i}{\partial T} \right)_x + \sum_{i=1}^N x_i \ln(x_i \gamma_i) \right] \quad (\text{A-10})$$

Finally, for expressions to calculate the enthalpy and entropy of vaporisation, the former of which is also referred to as λ_i :

$$\Delta\hat{H}_{\text{vap},i} = \lambda_i = -R \frac{d \ln P_i^{\text{vap}}}{d(1/T)} \quad (\text{A-11})$$

$$\Delta\hat{S}_{\text{vap},i}(T_{b,i}) = \frac{\Delta\hat{H}_{\text{vap},i}(T_{b,i})}{T_{b,i}} \quad (\text{A-12})$$

Note that $T_{b,i}$ (the boiling point of pure component i) is used rather than an arbitrary T , since Eq. (A-12) is only valid when $\Delta\hat{G}_{\text{vap}} = 0$, i.e. at equilibrium of the vapour and liquid, which occurs at saturation or boiling.

A.2 Full derivation of entropy equations

As the thermodynamic basis, pure liquids at 101 325 Pa and 298.15 K have zero enthalpy and entropy; these will be referred to as P_0 and T_0 , respectively.

The equations that follow are founded on the common assumption of constant molar overflow (CMO). The condition of CMO is based on four underlying assumptions (Perry and Green, 1999):

- 1 The latent heat of each component in the system is the same.
- 2 There is no heat of mixing.
- 3 Sensible heat is negligible in comparison with the latent heat.
- 4 The column is adiabatic, i.e. there are no heat losses to the environment.

The main implication of CMO is that liquid and vapour flows, L and V respectively, remain constant throughout a column section.

Figure 2.2 is a useful reference for the nomenclature used in this section. Equation (2.4) gave an expression for the entropy generation in a generalised column section; the terms on the right-hand side can be evaluated as follows:

$$S_{\text{liq}}^n = L^n \left[\sum_{i=1}^N x_i^n \hat{S}_i^{\text{liq}} + \Delta \hat{S}_{\text{mix,liq}}^n \right] \quad (\text{A-13})$$

$$\begin{aligned} S_{\text{vap}}^n &= V^n \left[\sum_{i=1}^N Y_i^n \hat{S}_i^{\text{vap}} + \Delta \hat{S}_{\text{mix,vap}}^n \right] \\ &= V^n \left[\sum_{i=1}^N Y_i^n \left(\int_{T_0}^{T_{\text{b},i}} \frac{\hat{C}_{p,i}^{\text{liq}}}{T} dT + \frac{\lambda_i}{T_{\text{b},i}} + \int_{T_i}^{T_{\text{vap}}^n} \frac{\hat{C}_{p,i}^{\text{vap}}}{T} dT \right) + \Delta \hat{S}_{\text{mix,vap}}^n \right] \end{aligned} \quad (\text{A-14})$$

Incorporating the CMO assumption leads to a number of simplifications:

- The liquid and vapour flows remain constant throughout the column section, such that $L^n = L$ and $V^n = V$.
- The latent heats of all of the components are considered to be equal, such that $\lambda_1 = \lambda_2 = \dots = \lambda_N = \lambda$.
- $\lambda_i \gg \hat{C}_{p,i}$, such that $\hat{C}_{p,i}$ can be considered to be negligible in terms where it is added to or subtracted from λ_i . Moreover, since the basis states that liquids at 298.15 K and 1 atm have zero entropy, the entropy of a liquid at any other temperature would be found with the use of $\hat{C}_{p,i}$. However, the entropy of a vapour would, from that basis, require both a $\hat{C}_{p,i}$ term (see Eq. (A-2)) and a λ term (see Eq. (A-12)). As a result, $\hat{S}_i^{\text{vap}} \gg \hat{S}_i^{\text{liq}}$, such that the entropy of a *pure* liquid is considered to be negligible compared to that of a *pure* vapour.

Finally, when comparing the sum of pure liquid entropies to the entropy of mixing—such as in Eq. (A-13)—the former is considered to be negligible in relation to the latter, since $\hat{C}_{p,i}/T_{\text{b},1}$ (see Eq. (A-2)) is much smaller than the gas constant ($R \approx 8.314 \text{ J/mol}\cdot\text{K}$) (see Eq. (A-10)).

Using the above simplifications, Eqs (A-13) and (A-14) become:

$$S_{\text{liq}}^n = L\Delta\hat{S}_{\text{mix,liq}}^n \quad (\text{A-15})$$

$$S_{\text{vap}}^n = V \left[\lambda \sum_{i=1}^N \frac{Y_i^n}{T_{b,i}} + \Delta\hat{S}_{\text{mix,vap}}^n \right] \quad (\text{A-16})$$

The δS^n variable, defined in Eq. (2.5), becomes the following with Eqs (A-15) and (A-16):

$$\delta S^n = L\Delta\hat{S}_{\text{mix,liq}}^n - V \left[\lambda \sum_{i=1}^N \frac{Y_i^n}{T_{b,i}} + \Delta\hat{S}_{\text{mix,vap}}^n \right] \quad (\text{A-17})$$

When Eq. (A-17) is divided through by Δ , with an underbar used to denote a ‘per- Δ ’ quantity, the following is obtained:

$$\delta \underline{S}^n = r_{\Delta}\Delta\hat{S}_{\text{mix,liq}}^n - (1 + r_{\Delta}) \left[\lambda \sum_{i=1}^N \frac{Y_i^n}{T_{b,i}} + \Delta\hat{S}_{\text{mix,vap}}^n \right] \quad (\text{A-18})$$

Finally, substituting Eq. (2.3) into Eq. (A-18) gives the final form of the $\delta \underline{S}^n$ equation:

$$\delta \underline{S}^n = r_{\Delta}\Delta\hat{S}_{\text{mix,liq}}^n - \left[\lambda \sum_{i=1}^N \left(\frac{X_{\Delta,i} + r_{\Delta}x_i^n}{T_{b,i}} \right) + (1 + r_{\Delta})\Delta\hat{S}_{\text{mix,vap}}^n \right] \quad (\text{A-19})$$

The vapour is assumed to be ideal, such that its entropy of mixing is simply:

$$\Delta\hat{S}_{\text{mix,vap}}^n = -R \sum_{i=1}^N Y_i^n \ln(Y_i^n) \quad (\text{A-20})$$

The CMO assumption allows for simplification of the liquid entropy of mixing given in Eq. (A-10). As shown in Eq. (A-6), the first term is \hat{H}^E , or equivalently $\Delta\hat{H}_{\text{mix}}$, which CMO sets to zero. Therefore, the liquid entropy of mixing simplifies to:

$$\hat{S}_{\text{mix,liq}}^n = -R \sum_{i=1}^N x_i^n \ln(x_i^n \gamma_i^n) \quad (\text{A-21})$$

A.3 Derivative of $\delta \underline{S}$ with respect to n

It is quite straightforward to show that differentiating Eq. (2.8) with respect to n results in:

$$\begin{aligned} \frac{d}{dn}(\delta S) = & -r_{\Delta}R \sum_{i=1}^N \left[(\ln(x_i \gamma_i) + 1) \frac{dx_i}{dn} + \frac{d \ln \gamma_i}{dn} \right] - \lambda r_{\Delta} \sum_{i=1}^N \left[\left(\frac{1}{T_{b,i}} \right) \frac{dx_i}{dn} \right] + \\ & r_{\Delta}R \sum_{i=1}^N \left[\left(\ln \left(\frac{X_{\Delta,i} + r_{\Delta} x_i}{1 + r_{\Delta}} \right) + 1 \right) \frac{dx_i}{dn} \right] \quad (\text{A-22}) \end{aligned}$$

In order to change dy_i/dn in Eq. (A-22) to a more convenient form, it is important to recognise the variable dependence of γ_i . Generally, γ_i is a function of $N - 1$ mole fractions (since the N^{th} is fixed by mole fraction summation to unity) and T . However, in VLE problems such as distillation, for a set system pressure P , T is fixed by the bubble point calculation. Therefore, γ_i is only a function of x_1, x_2, \dots, x_{N-1} . Taking the total derivative of γ_i gives:

$$d \ln \gamma_i = \sum_{j=1}^{N-1} \left[\left(\frac{\partial \ln \gamma_i}{\partial x_j} \right) dx_j \right] \quad (\text{A-23})$$

Equation (A-23) can be divided through by dn to give the required result:

$$\frac{d \ln \gamma_i}{dn} = \sum_{j=1}^{N-1} \left[\left(\frac{\partial \ln \gamma_i}{\partial x_j} \right) \frac{dx_j}{dn} \right] \quad (\text{A-24})$$

Finally, substituting Eq. (A-24) into Eq. (A-22) gives Eq. (2.11).

A.4 Latent heat derivatives

For a fixed system pressure, P , bubble point temperature is an implicit function of liquid composition, which may be represented as follows:

$$T = f_b(x_1, x_2, \dots, x_{N-1}) \quad (\text{A-25})$$

If the total derivative of Eq. (A-25) is taken:

$$\begin{aligned} df_b &= \left(\frac{\partial f_b}{\partial x_1} \right) dx_1 + \left(\frac{\partial f_b}{\partial x_2} \right) dx_2 + \dots + \left(\frac{\partial f_b}{\partial x_{N-1}} \right) dx_{N-1} \\ df_b &= \sum_{i=1}^{N-1} \left(\frac{\partial f_b}{\partial x_i} \right) dx_i \quad (\text{A-26}) \end{aligned}$$

To obtain the derivative of bubble-point temperature with stage number, Eq. (A-26) is simply divided through by dn :

$$\frac{df_b}{dn} = \sum_{i=1}^{N-1} \left(\frac{\partial f_b}{\partial x_i} \right) \frac{dx_i}{dn} \quad (\text{A-27})$$

Latent heat is a function of temperature only; therefore, using the chain rule, the following can be deduced:

$$\frac{d\lambda_i}{dn} = \frac{d\lambda_i}{dT} \frac{df_b}{dn} \quad (\text{A-28})$$

Upon substitution of Eq. (A-27) into Eq. (A-28), it is found that:

$$\frac{d\lambda_i}{dn} = \frac{d\lambda_i}{dT} \sum_{i=1}^{N-1} \left[\left(\frac{\partial f_b}{\partial x_i} \right) \frac{dx_i}{dn} \right] \quad (\text{A-29})$$

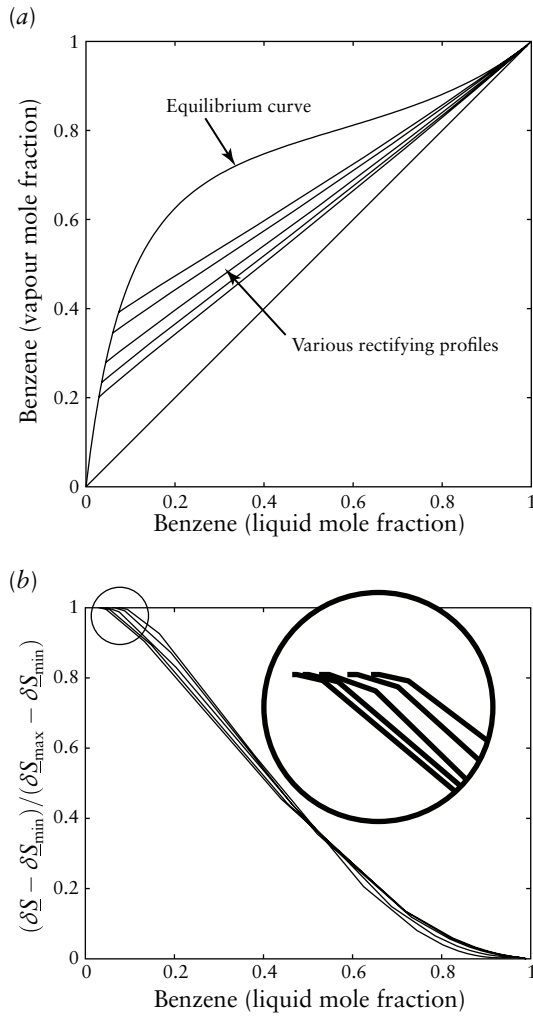
It is noteworthy that each term in Eq. (A-29) has a factor of dx_i/dn , such that, at a pinch point, $d\lambda_i/dn = 0$.

A.5 Rigorous McCabe–Thiele and $\delta\underline{S}$

To definitively assess the correspondence between pinch points encountered in rectifying sections on a McCabe–Thiele diagram, and the points of maximum $\delta\underline{S}$ as a function of x_1 , both must be treated with thermodynamic rigour. For this, the rectifying section was modelled using mass and energy balances, and was ‘stepped down’ plate by plate from the top of the column, once a reflux ratio had been chosen. The stepping down procedure was stopped once the rectifying section was very close to the equilibrium curve, and effectively pinched. Unfortunately, this procedure, which does not assume CMO, cannot extend the rectifying section beyond the pinch, such that hypothetical parts of the rectifying section (those past the equilibrium curve) cannot be examined.

For rigorous $\delta\underline{S}$, the entropy equations without simplifications were used, i.e. Eqs (A-13) and (A-14). These make use of the compositions and flow rates from the McCabe–Thiele calculations, in order to make sure that the two approaches correspond exactly. As such, the $\delta\underline{S}$ curve must terminate where the rectifying section in the McCabe–Thiele diagram ends. Because the $\delta\underline{S}$ values vary so much between the different r_Δ values, the only way to show them clearly on the same plot is as a normalised $\delta\underline{S}$, defined as $(\delta\underline{S} - \delta\underline{S}_{\min})/(\delta\underline{S}_{\max} - \delta\underline{S}_{\min})$. This ensures that all of the curves are bound between 0 and 1 on the vertical axis.

Figure A.1 gives these two plots for the benzene–ethylenediamine system first discussed in § 2.4.4; a distillate with composition $x_D = (0.99, 0.01)$. A magnification is provided for the $\delta\underline{S}$ values, which shows a clear local maximum ($d(\delta\underline{S})/dx_1 = 0$) at the pinch points.

**Figure A.1**

(a) McCabe–Thiele diagram showing rectifying profiles at various reflux ratios; and (b) normalised $\delta\underline{S}$ curves corresponding to the rectifying profiles for the benzene–ethylenediamine system with $x_D = (0.99, 0.01)$. Magnification is provided for the $\delta\underline{S}$ in the vicinity of the pinches.

A.6 Derivation of minimum reflux equation based on S_{gen} for binary separations

The derivation requires $d(\delta\underline{S})/dx_1 = 0$ to be calculated. By using $N = 2$, substituting the definition of $\Delta\hat{S}_{\text{mix}}$ into Eq. (2.8), and expanding the summation, the following is obtained:

$$\begin{aligned} \delta\underline{S} &= -r_{\Delta}R \sum_{i=1}^2 x_i \ln(x_i y_i) - \lambda \sum_{i=1}^2 \left(\frac{X_{\Delta,i} + r_{\Delta}x_i}{T_{b,i}} \right) - \\ &\quad R(1 + r_{\Delta}) \sum_{i=1}^2 Y_i \ln(Y_i) \\ &= -r_{\Delta}R x_1 \ln(x_1 y_1) - r_{\Delta}R x_2 \ln(x_2 y_2) - \lambda \left(\frac{X_{\Delta,1} + r_{\Delta}x_1}{T_{b,1}} \right) - \\ &\quad \lambda \left(\frac{X_{\Delta,2} + r_{\Delta}x_2}{T_{b,2}} \right) + R(1 + r_{\Delta})(Y_1 \ln(Y_1)) + \end{aligned}$$

$$R(1 + r_\Delta)(Y_2 \ln(Y_2)) \quad (\text{A-30})$$

Substituting Eq. (2.3) into Eq. (A-30), with some manipulation (recognising that $x_2 = 1 - x_1$), gives:

$$\begin{aligned} \delta \underline{S} = & -r_\Delta R x_1 \ln(x_1 \gamma_1) - r_\Delta R (1 - x_1) \ln((1 - x_1) \gamma_2) - \\ & \lambda \left(\frac{X_{\Delta,1} + r_\Delta x_1}{T_{b,1}} \right) - \lambda \left(\frac{X_{\Delta,2} + r_\Delta (1 - x_1)}{T_{b,2}} \right) + \\ & R \left[(X_{\Delta,1} + r_\Delta x_1) \ln \left(\frac{X_{\Delta,1} + r_\Delta x_1}{1 + r_\Delta} \right) \right] + \\ & R \left[(X_{\Delta,2} + r_\Delta (1 - x_1)) \ln \left(\frac{X_{\Delta,2} + r_\Delta (1 - x_1)}{1 + r_\Delta} \right) \right] \quad (\text{A-31}) \end{aligned}$$

The differentiation of Eq. (A-31) with respect to x_1 is a lengthy procedure, and is impractical to show here in detail. The result is:

$$\begin{aligned} \frac{d(\delta \underline{S})}{dx_1} = & -r_\Delta R \left[\ln \left(\frac{x_1 \gamma_1}{(1 - x_1) \gamma_2} \right) + \frac{x_1}{\gamma_1} \left(\frac{\partial \gamma_1}{\partial x_1} \right)_{T,P} + \frac{(1 - x_1)}{\gamma_2} \left(\frac{\partial \gamma_2}{\partial x_1} \right)_{T,P} + \right. \\ & \left. \frac{\lambda(T_{b,2} - T_{b,1})}{RT_{b,1}} + \ln \left(\frac{X_{\Delta,2} + r_\Delta (1 - x_1)}{X_{\Delta,1} + r_\Delta x_1} \right) \right] \quad (\text{A-32}) \end{aligned}$$

In Eq. (A-32), $d(\delta \underline{S})/dx_1$ can be set to zero and divided through by $-R$ to obtain the following:

$$r_\Delta \left[\Psi + \ln \left(\frac{X_{\Delta,2} + r_\Delta (1 - x_1)}{X_{\Delta,1} + r_\Delta x_1} \right) \right] = 0 \quad (\text{A-33})$$

where

$$\begin{aligned} \Psi = & \ln \left(\frac{x_1 \gamma_1}{(1 - x_1) \gamma_2} \right) + \frac{x_1}{\gamma_1} \left(\frac{\partial \gamma_1}{\partial x_1} \right)_{T,P} + \\ & \frac{(1 - x_1)}{\gamma_2} \left(\frac{\partial \gamma_2}{\partial x_1} \right)_{T,P} + \frac{\lambda(T_{b,2} - T_{b,1})}{RT_{b,1} T_{b,2}} \quad (\text{A-34}) \end{aligned}$$

From Eq. (A-33), it is apparent immediately that one solution to the equation is $r_\Delta = 0$, for any x and any X_Δ . The other solution is found by equating the contents of the bracket to zero:

$$\Psi + \ln \left(\frac{X_{\Delta,2} + r_\Delta (1 - x_1)}{X_{\Delta,1} + r_\Delta x_1} \right) = 0$$

$$\frac{X_{\Delta,1} + r_\Delta x_1}{X_{\Delta,2} + r_\Delta (1 - x_1)} = \exp(\Psi)$$

$$X_{\Delta,1} + r_\Delta x_1 = X_{\Delta,2} \exp(\Psi) + r_\Delta (1 - x_1) \exp(\Psi)$$

$$r_{\Delta}x_1 - r_{\Delta}(1 - x_1) \exp(\Psi) = X_{\Delta,2} \exp(\Psi) - X_{\Delta,1}$$

$$r_{\Delta} = \frac{X_{\Delta,2} \exp(\Psi) - X_{\Delta,1}}{x_1 - (1 - x_1) \exp(\Psi)} \quad (\text{A-35})$$

For minimum reflux in a conventional binary column, the variables in Eqs (A-34) and (A-35) can be replaced with traditional variables: $r_{\Delta} = r_{\min}$, $x_1 = x_{F,1}$, $X_{\Delta,1} = x_{D,1}$, $X_{\Delta,2} = x_{D,2} = (1 - x_{D,1})$, $\gamma_1 = \gamma_{F,1}$, and $\gamma_2 = \gamma_{F,2}$.

Appendix B

B.1 Relationship between $X_{\Delta,2}$ and $r_{\Delta,2}$ for the distributed-feed example

Consider the part of the column where the bottom-most feed enters, as shown in Figure B.1.

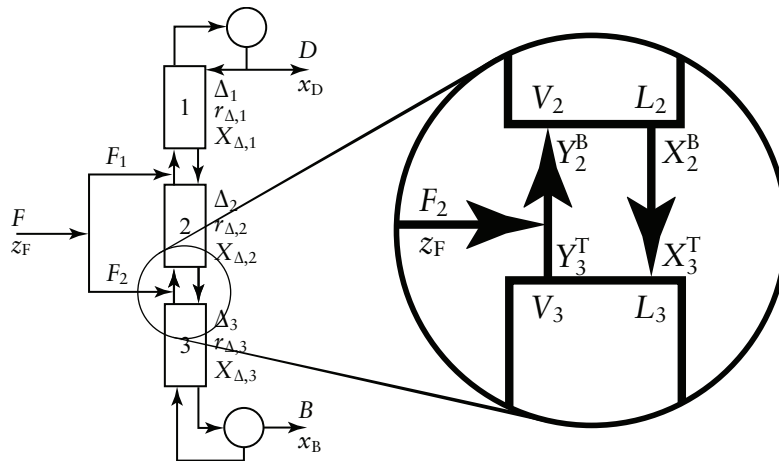


Figure B.1 The nomenclature required for the derivation of the relationship between $X_{\Delta,2}$ and $r_{\Delta,2}$.

An overall mass balance around this part of the column gives:

$$F_2 + L_2 + V_3 = L_3 + V_2$$

$$F_2 = (V_2 - L_2) - (V_3 - L_3)$$

$$F_2 = \Delta_2 - \Delta_3 \tag{B-1}$$

Similarly, a component mass balance on the same section, where X and Y represent liquid and vapour composition vectors, gives:

$$\begin{aligned}
F_2 z_F + L_2 X_2^B + V_3 Y_3^T &= L_3 X_3^T + V_2 Y_2^B \\
F_2 z_F &= (V_2 Y_2^B - L_2 X_2^B) - (V_3 Y_3^T - L_3 X_3^T) \\
F_2 z_F &= \Delta_2 X_{\Delta,2} - \Delta_3 X_{\Delta,3}
\end{aligned} \tag{B-2}$$

Substituting Eq. (B-1) into Eq. (B-2) gives:

$$\begin{aligned}
(\Delta_2 - \Delta_3) z_F &= \Delta_2 X_{\Delta,2} - \Delta_3 X_{\Delta,3} \\
\Delta_2 z_F - \Delta_3 z_F &= \Delta_2 X_{\Delta,2} - \Delta_3 X_{\Delta,3} \\
\Delta_2 X_{\Delta,2} &= \Delta_3 (X_{\Delta,3} - z_F) + \Delta_2 z_F \\
X_{\Delta,2} &= \frac{\Delta_3}{\Delta_2} (X_{\Delta,3} - z_F) + z_F
\end{aligned} \tag{B-3}$$

From the definition of r_Δ and the fact that, because of the vapour feed, all of the liquid flows in the column are equal, it can easily be deduced that:

$$\begin{aligned}
r_{\Delta,2} &= \frac{L_2}{\Delta_2} \\
r_{\Delta,2} &= \frac{L_1}{\Delta_2} \\
r_{\Delta,2} &= r_{\Delta,1} \left(\frac{\Delta_1}{\Delta_2} \right) \\
\Delta_2 &= \Delta_1 \left(\frac{r_{\Delta,1}}{r_{\Delta,2}} \right)
\end{aligned} \tag{B-4}$$

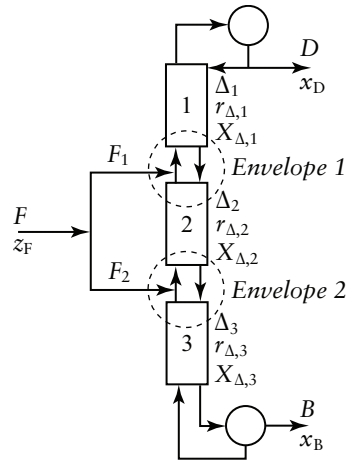
Finally, substituting Eq. (B-4) into Eq. (B-3) gives the relationship between $X_{\Delta,2}$ and $r_{\Delta,2}$:

$$X_{\Delta,2} = \left(\frac{\Delta_3}{\Delta_1} \right) \left(\frac{r_{\Delta,2}}{r_{\Delta,1}} \right) (X_{\Delta,3} - z_F) + z_F$$

B.2 Limitations on valid $r_{\Delta,2}$ values for the distributed-feed example

Consider the two envelopes shown in Figure B.2.

By a similar procedure to Eq. (B-1), using the definition of r_Δ and the

**Figure B.2**

Two envelopes around which mass balances must be performed to deduce the limiting values of $r_{\Delta,2}$.

equivalence of all the liquid flows in the column (due to the saturated vapour feed and CMO assumption), an overall mass balance around envelope 1 gives:

$$F_1 = \Delta_1 - \Delta_2 \quad (\text{B-5})$$

and for envelope 2:

$$F_2 = \Delta_2 - \Delta_3 \quad (\text{B-6})$$

If it is assumed that the middle section (CS 2) is in rectifying mode, $\Delta_2 > 0$. Since $F_1 \geq 0$, it stands to reason by Eq. (B-5) that $\Delta_1 - \Delta_2 \geq 0$, which can only be true if $\Delta_1 \geq \Delta_2$. From the definition of r_{Δ} and the equivalence of L_1 and L_2 , it is easy to show that:

$$r_{\Delta,2} = \left(\frac{\Delta_1}{\Delta_2} \right) r_{\Delta,1} \quad (\text{B-7})$$

Since $\Delta_1 \geq \Delta_2$, it means that $\Delta_1/\Delta_2 \geq 1$, in which case, the constraint imposed on CS 2 by CS 1 is that $r_{\Delta,2}$ must always be greater than or equal to $r_{\Delta,1}$. The two constraints on Δ_2 can be expressed more succinctly as $0 < \Delta_2 \leq \Delta_1$. As such, by Eq. (B-7), $r_{\Delta,2}$ has no upper limit (as $\Delta_2 \rightarrow 0$, so $r_{\Delta,2} \rightarrow \infty$). CS 3 imposes no additional constraint on CS 2, since $F_2 \geq 0$, $\Delta_2 > 0$ and $\Delta_3 < 0$, meaning that both sides of Eq. (B-6) are always positive.

If CS 2 is assumed to be in stripping mode, that is, $\Delta_2 < 0$, it can be shown in a similar fashion that CS 1 imposes no constraint on CS 2, but CS 3 dictates that $r_{\Delta,2} \leq r_{\Delta,3}$ always in order to satisfy the mass balance.

Appendix C

C.1 Full ODE derivation

First, the variable dependencies must be recognised: by setting r_Δ and X_Δ , the pinch points on a CPM are set, such that $x_{p,i} = \mathcal{F}(r_\Delta, X_\Delta)$. Because bubble point calculations fix T , and because liquid mole fractions sum to one, the vapour in equilibrium with a pinch point is a function of $N-1$ liquid mole fractions only, i.e. $y_{p,i} = \mathcal{H}(x_{p,1}, x_{p,2}, \dots, x_{p,N-1})$. For this derivation, neither X_Δ nor r_Δ will not be considered to be constant. However, having two entirely independent and variable parameters is not suitable for PPCs, but is also unlikely to arise; there will usually, if not always, be a known relationship between the two. For example, Appendix B.1 gives a derivation of the relationship between the X_Δ and r_Δ in a distributed-feed column. Since X_Δ is a vector and r_Δ is a scalar, it is more convenient to express X_Δ as a function of r_Δ , i.e. $X_\Delta = \mathcal{J}(r_\Delta)$.

The derivation of the ODE begins at the definition of the pinch point, that is, setting $dx_i/dn = 0$ at $x_{p,i}$ in Eq. (4.3).

$$\begin{aligned} \left(1 + \frac{1}{r_\Delta}\right)(x_{p,i} - y_{p,i}) + \frac{1}{r_\Delta}(X_{\Delta,i} - x_{p,i}) &= 0 \\ x_{p,i} - y_{p,i} + \frac{1}{r_\Delta}x_{p,i} - \frac{1}{r_\Delta}y_{p,i} + \frac{1}{r_\Delta}X_{\Delta,i} - \frac{1}{r_\Delta}x_{p,i} &= 0 \\ x_{p,i} - y_{p,i} - \frac{1}{r_\Delta}y_{p,i} + \frac{1}{r_\Delta}X_{\Delta,i} &= 0 \end{aligned} \quad (\text{C-1})$$

Differentiating Eq. (C-1) with respect to r_Δ yields:

$$\begin{aligned} \frac{dx_{p,i}}{dr_\Delta} - \frac{dy_{p,i}}{dr_\Delta} - \frac{1}{r_\Delta} \frac{dy_{p,i}}{dr_\Delta} + \frac{1}{r_\Delta^2} y_{p,i} - \frac{1}{r_\Delta^2} X_{\Delta,i} + \frac{1}{r_\Delta} \frac{dX_{\Delta,i}}{dr_\Delta} &= 0 \\ \frac{dx_{p,i}}{dr_\Delta} - \left(1 + \frac{1}{r_\Delta}\right) \frac{dy_{p,i}}{dr_\Delta} + \frac{1}{r_\Delta^2} (y_{p,i} - X_{\Delta,i}) + \frac{1}{r_\Delta} \frac{dX_{\Delta,i}}{dr_\Delta} &= 0 \end{aligned} \quad (\text{C-2})$$

With the knowledge that y_i is a function of $N-1$ liquid mole fractions, the total derivative can be taken, and divided through by dr_Δ :

$$\begin{aligned}
dy_i &= \left(\frac{\partial y_i}{\partial x_1} \right) dx_1 + \left(\frac{\partial y_i}{\partial x_2} \right) dx_2 + \cdots + \left(\frac{\partial y_i}{\partial x_{N-1}} \right) dx_{N-1} \\
\frac{dy_i}{dr_\Delta} &= \left(\frac{\partial y_i}{\partial x_1} \right) \frac{dx_1}{dr_\Delta} + \left(\frac{\partial y_i}{\partial x_2} \right) \frac{dx_2}{dr_\Delta} + \cdots + \left(\frac{\partial y_i}{\partial x_{N-1}} \right) \frac{dx_{N-1}}{dr_\Delta} \\
\frac{dy_i}{dr_\Delta} &= \sum_{j=1}^{N-1} \left(\frac{\partial y_i}{\partial x_j} \right) \frac{dx_j}{dr_\Delta} \tag{C-3}
\end{aligned}$$

Substituting Eq. (C-3) into Eq. (C-2) gives:

$$\frac{dx_{p,i}}{dr_\Delta} - \left(1 + \frac{1}{r_\Delta} \right) \sum_{j=1}^{N-1} \left(\frac{\partial y_{p,i}}{\partial x_{p,j}} \right) \frac{dx_{p,j}}{dr_\Delta} = \frac{1}{r_\Delta^2} (X_{\Delta,i} - y_{p,i}) - \frac{1}{r_\Delta} \frac{dX_{\Delta,i}}{dr_\Delta} \tag{C-4}$$

Equation (C-4) can be seen as a non-homogeneous system of linear equations in $dx_{p,i}/dr_\Delta$, as given in Eqs (4.9)–(4.14), except with \vec{b} defined as follows for the non-constant X_Δ case:

$$\vec{b} = \frac{1}{r_\Delta} \begin{bmatrix} \frac{1}{r_\Delta} (X_{\Delta,1} - y_{p,1}) - \frac{dX_{\Delta,1}}{dr_\Delta} \\ \frac{1}{r_\Delta} (X_{\Delta,2} - y_{p,2}) - \frac{dX_{\Delta,2}}{dr_\Delta} \\ \vdots \\ \frac{1}{r_\Delta} (X_{\Delta,N-1} - y_{p,N-1}) - \frac{dX_{\Delta,N-1}}{dr_\Delta} \end{bmatrix} \tag{C-5}$$

The evaluation of $dX_{\Delta,i}/dr_\Delta$ should usually be straightforward, because it is likely that it will be an algebraic expression, such that a simple analytical derivative will be readily available; if the function that relates X_Δ to r_Δ is more complicated, numerical derivatives can be used.

For constant X_Δ , $dX_{\Delta,i}/dr_\Delta = 0$, such that Eq. (C-5) collapses to Eq. (4.14).

C.2 Evaluation of the Jacobian

The Jacobian matrix \mathbf{J} , defined as Eq. (4.11), can either be evaluated numerically directly with $N - 1$ bubble point calculations, or with derivatives evaluated without using the bubble point.

At each step of the integration, y_p must be calculated for the evaluation of the vector \vec{b} ; \mathbf{J} is also required.

If, for the benefit of programming ease, some computational efficiency is sacrificed, \mathbf{J} can be calculated by direct numerical differentiation, noting that

the increase in computational effort is roughly proportional to the number of components when using this approach. The best way of doing this is by forward differences. For calculation of perturbed y_i , note that the perturbation in x_i must be accompanied by an equal and opposite shift in x_N to ensure mole fraction summation to unity.

A much better—albeit somewhat more complex—approach is to reduce the problem analytically to a non-iterative one, at least to the point of obtaining expressions involving $\partial y_i/\partial x_j$, $\partial y_i/\partial T$, and dP_i^{vap}/dT , which can be computed numerically, but without iteration. The procedure is described by Poellmann and Blass (1994), and is reproduced below, with some minor modifications for generality. Prausnitz et al. (1980) give a function that describes the bubble point condition, which, for set P , is given by:

$$\mathcal{G}_b(T = T_b, x_1, \dots, x_{N-1}) = \ln \left(\frac{1}{P} \sum_{i=1}^N x_i \gamma_i(x_1, \dots, x_{N-1}, T = T_b) P_i^{\text{vap}}(T = T_b) \right) = 0 \quad (\text{C-6})$$

with

$$x_N = 1 - \sum_{i=1}^{N-1} x_i$$

Poellmann and Blass (1994) explain how the bubble point criterion implicitly defines a function $T_b = f_b(x_1, \dots, x_{N-1})$ for fixed P .

Differentiating Eq. (C-6) with respect to liquid mole fraction yields:

$$\frac{\partial \mathcal{G}_b}{\partial T} \frac{\partial f_b}{\partial x_i} + \frac{\partial \mathcal{G}_b}{\partial x_i} = 0 \quad (\text{C-7})$$

Equation (C-7) can be rearranged to give:

$$\frac{\partial f_b}{\partial x_i} = - \frac{\partial \mathcal{G}_b / \partial x_i}{\partial \mathcal{G}_b / \partial T} \quad (\text{C-8})$$

The necessary expressions for evaluating the right-hand side of Eq. (C-8) are given as follows:

$$\frac{\partial \mathcal{G}_b}{\partial x_i} = \frac{P_i^{\text{vap}} \gamma_i - P_N^{\text{vap}} \gamma_N + \sum_{j=1}^N \left(P_j^{\text{vap}} x_j \frac{\partial \gamma_j}{\partial x_i} \right)}{\sum_{j=1}^N x_j \gamma_j P_j^{\text{vap}}} \quad (\text{C-9})$$

and

$$\frac{\partial \mathcal{G}_b}{\partial T} = \frac{\sum_{i=1}^N \left(x_i \gamma_i \frac{dP_i^{\text{vap}}}{dT} + x_i \frac{\partial \gamma_i}{\partial T} P_i^{\text{vap}} \right)}{\sum_{i=1}^N x_i \gamma_i P_i^{\text{vap}}} \quad (\text{C-10})$$

Using Eqs (C-9) and (C-10), $\partial f_b / \partial x_i$ can be evaluated. Finally, using $\partial f_b / \partial x_i$ and the required derivatives of $\partial \gamma_i / \partial x_j$, $\partial \gamma_i / \partial T$, and dP_i^{vap} / dT (evaluated analytically or numerically), the elements of the Jacobian can be computed with the following equation, which originates from the differentiation of Raoult's modified law ($y_i = x_i \gamma_i P_i^{\text{vap}} / P$) with respect to liquid mole fraction:

$$\frac{\partial y_i}{\partial x_j} = \frac{x_i}{P} \left[\gamma_i \frac{dP_i^{\text{vap}}}{dT} \frac{\partial f_b}{\partial x_j} + P_i^{\text{vap}} \left(\frac{\partial \gamma_i}{\partial x_j} + \frac{\partial \gamma_i}{\partial T} \frac{\partial f_b}{\partial x_j} \right) \right] + \delta_{ij} \left(\frac{P_i^{\text{vap}} \gamma_i}{P} \right) \quad (\text{C-11})$$

where

$$\delta_{ij} = \begin{cases} 1 & \text{if } i = j, \\ 0 & \text{if } i \neq j. \end{cases} \quad (\text{C-12})$$

C.3 Some practical considerations

In this appendix, several practical considerations for the successful and efficient implementation of the proposed method are summarised. Some of these are reiterations from the main text, while others are additional points.

- If required, besides pure components and azeotropes, a known starting point for the integration is at $r_\Delta = -1$, where the pinch point location is exactly at X_Δ .
- The proposed method works well with several integrators, the simplest of which is the 3(2) Runge–Kutta pair due to Bogacki and Shampine (1989). It is available as part of RKSUITE for FORTRAN 77 (Brankin et al., 1992) and Fortran 90 (Brankin and Gladwell, 1997).
- Both of the theoretical bounds for the integration ($r \rightarrow \pm\infty$ and $r = 0$) are impractical; numerical approximations of these must be used, e.g. $r_\Delta = \pm 1 \times 10^{14}$ and $r_\Delta = \pm 1 \times 10^{-14}$, respectively.
- As mentioned earlier, provision needs to be made for when the integration reaches $r_{\Delta, \text{crit}}$; in this work, this was done by stopping integration when the distance between the last two successful solutions is less than 5×10^{-5} and the relative difference between the last two r_Δ or ρ^\pm values (corresponding to the last two points) is less than 1×10^{-5} . The latter quantity is defined as $|\rho^{\pm[i]} - \rho^{\pm[i-1]}| / |\rho^{\pm[i]}|$, where i indicates iteration number.

- Bubble point calculations are required by the proposed method. One such calculation is always required for the evaluation of the vector \vec{b} ; depending on the approach, the evaluation of the Jacobian \mathbf{J} can either require $N - 1$ or zero additional bubble point calculations (see Appendix C.2). For bubble point calculations, the algorithm described by Prausnitz et al. (1980) is recommended. As the integration proceeds, the solutions from step to step are close in composition space, meaning that the difference in bubble point temperature from step to step is small; therefore, the previous step's temperature should be used as a starting point for the current step's temperature for the best efficiency.
- Numerical derivatives are used throughout this work, rather than analytical derivatives, for reasons discussed earlier in § 4.4.1. A simple and efficient method for evaluating these is by forward (or backward) differences. Central differences are not recommended, as they require twice as many calculations.
- After the PPC has been obtained, the stability and type of the pinch points can be determined (see, e.g. p. 301 of Robinson (2004), or Holland et al. (2004a)).
- The proposed method can find azeotropes by means of 'jumping over' turning points using non-linear arc length extrapolation to continue the integration on the adjacent PPC section. Although the approximation of the arc length as multiple linear segments is crude, it is entirely sufficient for this purpose. The non-linear extrapolation can be done by means of either the cubic spline interpolation algorithm or piecewise cubic Hermite interpolation, although the former seems to be more reliable. As with any extrapolation lacking a theoretical model, points far away from the known data set are subject to large uncertainty. In order for the extrapolated point to be meaningful, the extrapolation must be very small. The distance by which to extrapolate the arc length can be a fixed value, say 1×10^{-3} , or a calculated value.
- To find the azeotropes, the method relies, to some extent, on continuity, and hence, on the ability of the activity coefficient model to handle negative mole fractions. Some models, especially those containing logarithms of mole fractions, have limited or no ability to handle negative mole fractions: the Wilson model can extend outside of the positive space to some extent,¹ while UNIQUAC does not permit anything other than positive, non-zero mole fractions. In systems where this is particularly restrictive, it may be necessary to try several X_{Δ} points to discover all of the azeotropes.

1 The distance outside of the MBT that it can 'reach' depends on the parameters for a given system.

- For best efficiency, it is suggested to perform an initial run (or series of runs) to find all of the azeotropes using the arc length extrapolation technique described earlier, and then to initiate integration from the pure components and located azeotropes for subsequent runs.
- A few Newton iterations to determine a more accurate starting point that corresponds to $r_{\Delta} = \pm 1 \times 10^{14}$, which is very near to a pure component or azeotrope, is beneficial, although not strictly necessary for the algorithm. Similarly, a few Newton iterations can help to refine the approximation of an azeotrope that is found by the proposed ODE.

C.4 Custom continuation algorithm

The success of continuation algorithms depends on the quality of the predictor, and on the step-size control. The step-size control here is configured to be applicable to the PPC problem in particular. The vector-valued function that describes the pinch points is $\Phi(\vec{x}, r_{\Delta}, \vec{X}_{\Delta}) = (1 + 1/r_{\Delta})(\vec{x} - \vec{y}) + (\vec{X}_{\Delta} - \vec{x})/r_{\Delta}$ for which the roots must be found. A basic outline of this algorithm follows.

- 1 Start at a known r_{Δ} and \vec{x}_p , and set a target distance away from this point that the next solution is required.
- 2 At the previously known solution, calculate the vector $\partial\Phi/\partial r_{\Delta}$ and the matrix $\partial\Phi/\partial x$. Then find dx/dr_{Δ} by solving the linear system $(\partial\Phi/\partial x)(dx/dr_{\Delta}) = -\partial\Phi/\partial r_{\Delta}$.
- 3 Use the tangent dx/dr_{Δ} to estimate the r_{Δ} and \vec{x} that would give a solution at the target distance.
- 4 Fix the above r_{Δ} , and use Newton's method to correct the estimated \vec{x} back to the solution path.
- 5 If Newton's method fails, decrease the target distance and return to step 1.
- 6 If Newton's method is successful, move forward one step in the solution. If Newton's method took more than two iterations, decrease the target distance by 30%; if it converged in one or two iterations, increase the target distance by 30%.
- 7 Return to step 1 until the full section of the PPC has been calculated.

C.5 Parallel stereoscopic viewing

Stereoscopic images work by giving each of the viewer's eyes a slightly different image to create the illusion of 3-D. To view these images, look at the pair of pictures, and then defocus your eyes (or focus them at a point in the distance), such that you see two somewhat blurry pairs of images, making four images in total. Now, refocus your eyes gradually until the innermost two images overlap and come into focus, which creates the desired 3-D effect. Note that for electronic viewing, the image on-screen should be no larger than the printed version.

Appendix D

D.1 Derivations

Minimum practical energy input in conventional columns

The easiest way of estimating minimum reflux for an ideal mixture is to use Underwood's method (1948). For the split of a binary, saturated liquid feed—with known relative volatility (α)—to pure components, minimum reflux using Underwood's method simplifies to the following (Branan, 2005):

$$r_{\min} = \frac{1}{x_{F,1}(\alpha - 1)} \quad (\text{D-1})$$

Using the mass balance of the column internals, with a saturated liquid feed and the CMO assumption, it can easily be shown that the vapour flow through the column is given by:

$$V = D(r + 1) \quad (\text{D-2})$$

For sharp splits, $D = Fx_{F,1}$; using this fact and Eqs (D-1) and (D-2), the minimum vapour flow in the column can be estimated:

$$V_{\min} = F \left(\frac{1}{\alpha - 1} + x_{F,1} \right) \quad (\text{D-3})$$

The minimum practical heat input at the reboiler can be calculated as follows:

$$Q_{\text{in},\min} = \lambda V_{\min} \quad (\text{D-4})$$

$$Q_{\text{in},\min} = F\lambda \left(\frac{1}{\alpha - 1} + x_{F,1} \right) \quad (\text{D-5})$$

Minimum practical energy input in SVRC

The stream numbers used here are given in Figure 5.4.

The modifications that SVRC makes to the conventional configuration are

external to the column itself; for the same split of the same feed, the internal specifications of the column can remain identical. Consequently, the SVRC has the same minimum vapour flow as the conventional configuration, given in Eq. (D-3).

The energy input into the compressor is found with an energy balance:

$$W_{\text{comp,min}} = V_{\text{min}} \hat{C}_{p,1}^{\text{IG}} (T_3 - T_2) \quad (\text{D-6})$$

The use of the superheater and the temperatures T_2 and T_3 depend on the fluid being compressed. The isentropic compression of an ideal gas is given by:

$$\frac{P_{\text{comp}}}{P_0} = \left(\frac{T_3}{T_2} \right)^{\hat{C}_{p,1}^{\text{IG}}/R} \quad (\text{D-7})$$

If the saturated vapour superheats on compression, then $T_1 = T_2 = T_C$. Assuming isentropic compression, and constant λ (in order to use the Clausius–Clapeyron equation), the minimum T_3 can easily be deduced:

$$T_3 = T_C \exp \left(\frac{\lambda}{\hat{C}_{p,1}^{\text{IG}}} \left(\frac{1}{T_C} - \frac{1}{T_R} \right) \right) \quad (\text{D-8})$$

Consequently, the energy input into the system is given by the compression of the vapour from T_3 to T_2 only, since $Q_{\text{sh}} = 0$ W. Therefore, from Eqs (D-3), (D-6), and (D-8):

$$W_{\text{comp,min}} = F \hat{C}_{p,1}^{\text{IG}} T_C \left(\frac{1}{\alpha - 1} + x_{F,1} \right) \left(\exp \left(\frac{\lambda}{\hat{C}_{p,1}^{\text{IG}}} \left(\frac{1}{T_C} - \frac{1}{T_R} \right) \right) - 1 \right) \quad (\text{D-9})$$

The energy (and work) input into the system in this case is simply equal to $W_{\text{comp,min}}$.

If the saturated vapour condenses, then $T_1 = T_C$ and $T_3 = T_R$, while T_2 is given by:

$$T_2 = T_R \exp \left(\frac{\lambda}{\hat{C}_{p,1}^{\text{IG}}} \left(\frac{1}{T_R} - \frac{1}{T_C} \right) \right) \quad (\text{D-10})$$

In this case, the energy input into the system is the sum of $Q_{\text{sh,min}}$ and $W_{\text{comp,min}}$. The superheater's duty, using Eqs (D-3) and (D-10), is given by:

$$Q_{\text{sh,min}} = F \hat{C}_{p,1}^{\text{IG}} \left(\frac{1}{\alpha - 1} + x_{F,1} \right) \left(T_R \exp \left(\frac{\lambda}{\hat{C}_{p,1}^{\text{IG}}} \left(\frac{1}{T_R} - \frac{1}{T_C} \right) \right) - T_C \right) \quad (\text{D-11})$$

From Eqs (D-3), (D-6), and (D-10), the energy input into the compressor is:

$$W_{\text{comp,min}} = F \hat{C}_{p,1}^{\text{IG}} T_R \left(\frac{1}{\alpha - 1} + x_{F,1} \right) \left[1 - \exp \left(\frac{\lambda}{\hat{C}_{p,1}^{\text{IG}}} \left(\frac{1}{T_R} - \frac{1}{T_C} \right) \right) \right] \quad (\text{D-12})$$

Compression ratio

If the overhead vapour is superheated on isentropic compression, the process is expressed as follows:

$$\frac{P_{\text{comp}}}{P_0} = \left(\frac{T_3}{T_C} \right)^{\hat{C}_{p,1}^{\text{IG}}/R} \quad (\text{D-13})$$

The expression for T_3 is given in Eq. (D-8). Substituting this, along with Eq. (5.24), into Eq. (D-13) ultimately gives:

$$\frac{P_{\text{comp}}}{P_0} = \exp \left([4.0 + \ln(T_C/\text{K})] \left(1 - \frac{T_C}{T_R} \right) \right) \quad (\text{D-14})$$

If the overhead vapour condenses on isentropic compression, the relationship between compression ratio and temperature is as follows:

$$\frac{P_{\text{comp}}}{P_0} = \left(\frac{T_R}{T_2} \right)^{\hat{C}_{p,1}^{\text{IG}}/R} \quad (\text{D-15})$$

T_2 is given in Eq. (D-10). Again, if this is substituted into Eq. (D-15) and used along with Eq. (5.24), the compression ratio can be calculated as follows.

$$\frac{P_{\text{comp}}}{P_0} = \exp \left([4.0 + \ln(T_C/\text{K})] \left(1 - \frac{T_C}{T_R} \right) \right) \quad (\text{D-16})$$

It should be no surprise that Eqs (D-14) and (D-16) are identical; Figure 5.6 illustrates why the compression ratio must be the same in both cases.

Zero superheating of compressor inlet

The vapour enters the superheater at T_C and is heated to T_2 , which is given in Eq. (D-10). No superheating is required when $T_2 = T_C$. From Eq. (D-10), the following can be deduced:

$$T_C = T_R \exp \left(\frac{\lambda}{\hat{C}_{p,1}^{\text{IG}}} \left(\frac{1}{T_R} - \frac{1}{T_C} \right) \right) \quad (\text{D-17})$$

With the use of Eq. (5.24) in Eq. (D-17), the following is obtained:

$$T_C = T_R \exp\left(\frac{R[4.0 + \ln(T_C/K)]}{\hat{C}_{p,1}^{\text{IG}}}\left(\frac{T_C}{T_R} - 1\right)\right) \quad (\text{D-18})$$

D.2 Heat pumps with external working fluid, and bottoms flashing

Heat-pump-assisted distillation with an external working fluid (Figure 5.1*c*) and bottoms flashing (Figure 5.1*d*) and can both be analysed in the same way as SVRC, using the assumptions listed in the § 5.2. In fact, both of these configurations reduce to the same problem, which is the same as SVRC, except with heat rejection at T_C , and not T_R . Energy is added in the compressor as W_{comp} and rejected as Q_{out} at T_C in the trim condensers.

As with SVRC, the energy balance simply reduces to $W_{\text{comp}} = Q_{\text{out}}$.

In order to assess the best theoretical performance, the systems are assumed to be reversible, such that $S_{\text{gen}} = 0$ W/K. Similarly to Eq. (5.12), the entropy analysis then reduces to:

$$F\Delta\hat{S}_{\text{mix}} = \frac{W_{\text{comp}}}{T_C} \quad (\text{D-19})$$

If, as was done with SVRC, Eq. (5.7) is equated to Eq. (D-19), the following result is obtained:

$$\frac{W_{\text{comp}}}{W_{\text{in}}} = \frac{T_R - T_C}{T_R - T_0} \quad (\text{D-20})$$

The implication of this result is that these two configurations are always better than conventional distillation when the condenser temperature is higher than ambient temperature. (If it is sub-ambient, then a heat pump is required to remove the energy from the column, and the analysis changes.) Therefore, it would appear that only practical concerns, not fundamental thermodynamic ones, prevent the widespread implementation of these configurations.

D.3 Aspen Plus simulation settings

Example 1

The feeds in either case (F1 and F2) are at their bubble point, at a pressure of 400 kPa, with a total flow of 1 kmol/h, and a composition of 0.63 1-butene

and 0.37 *n*-butane.

C1 and C2 are identical: they have no reboiler or condenser in the RADFRAC block (these are external). They have 100 stages, with feeds (F1 or F2, respectively) being fed on stage 50. RFL1 and RFL2 are added back on stage 1, and VB1 and VB2 are added on stage 100. The column is isobaric at 400 kPa.

CON1 has zero pressure drop, and cools the stream to its bubble point.

V1 and V2 have zero pressure drop and zero heat duty.

SH1 is set to effect a 12 K temperature increase, with no pressure drop.

K1 has isentropic and mechanical efficiencies of 100%, and a pressure ratio of 1.43.

SPL1 and SPL2 send fractionally 0.9350 of LT1 and LB6 to RFL1 and RFL2, respectively. This results in a reflux ratio of 14.38 in both cases.

REB1 is set to heat LB1 to a vapour fraction of 0.9625. Similarly, HEX1 has its cold outlet stream vapour fraction set to 0.9625, and a minimum approach temperature of 5 K.

SC1 has a heat duty of -5442.8014 W.

PV1 reduces the pressure back to 400 kPa.

Example 2

The following settings were used in the simulation:

F1/F2: 1 kmol/h; 100 kPa; bubble point temperature; composition: 0.71 hydrogen cyanide, 0.29 acrylonitrile.

C1/C2: 20 stages; no condenser; no reboiler; RFL1/RFL2 on stage 1; F1/F2 on stage 10; VB1/VB2 on stage 20; 100 kPa condenser pressure.

CON1: zero pressure drop; bubble point.

V1/V2: zero pressure drop; zero heat duty.

SH1: zero pressure drop; zero heat duty.

K1: pressure ratio 6.42; 100% isentropic and mechanical efficiency.

SPL1/SPL2: fractionally 0.3165 of LT1/LB6 sent to RFL1/RFL2.

REB1: zero pressure drop; vapour fraction 0.765.

HEX1: cold stream outlet vapour fraction 0.765; 5 K minimum temperature approach.

SC1: zero pressure drop; heat duty -1287.8069 W.

PV1: 100 kPa outlet pressure.

Example 3

The following settings were used in the simulation:

F1/F2: 1 kmol/h; 100 kPa; bubble point temperature; composition: 0.23 1-propanol, 0.77 *n*-octane.

C1/C2: 6 stages; no condenser; no reboiler; RFL1/RFL2 on stage 1; F1/F2 on stage 3; VB1/VB2 on stage 6; 100 kPa condenser pressure.

CON1: zero pressure drop; bubble point.

V1/V2: zero pressure drop; zero heat duty.

SH1: zero pressure drop; 65 K temperature change.

K1: pressure ratio 2.6; 100% isentropic and mechanical efficiency.

SPL1/SPL2: fractionally 0.3536 of LT1/LB6 sent to RFL1/RFL2.

REB1: zero pressure drop; vapour fraction 0.43.

HEX1: cold stream outlet vapour fraction 0.43; 5 K minimum temperature approach.

SC1: zero pressure drop; heat duty -513.51014 W.

PV1: 100 kPa outlet pressure.

Example 4

The following settings were used in the simulation:

F1: 1 kmol/h; 100 kPa; bubble point temperature; composition: 0.13 methanol, 0.22 2-propanol, 0.24 2,6,8-trimethyl-4-nonanone, 0.41 1-undecanal.

C1: 10 stages; no condenser; no reboiler; RFL1 on stage 1; F1 on stage 5; VB1 on stage 10; 100 kPa condenser pressure.

CON1: zero pressure drop; bubble point.

V1: zero pressure drop; zero heat duty.

SPL1: fractionally 0.3 of LT1 sent to RFL1.

REB1: zero pressure drop; vapour fraction 0.5.

Appendix E

E.1 Properties for rigorous calculations

For the detailed calculations in Chapter 6, the distillation columns and auxiliary equipment are modelled using rigorous mass and energy balances, although heat of mixing is excluded, as it is not significant in the near-ideal systems used here. Although the systems chosen in Chapter 6 are intentionally close to ideal, the slight non-idealities are modelled with the non-random two-liquid (NRTL) activity coefficient model (Renon and Prausnitz, 1968). Moreover, the gas is assumed to be ideal; this is not a perfectly accurate representation in all cases, since high compression ratios will deviate from ideality. However, only low compression ratios are of practical interest, in which case, the ideal gas assumption is generally reasonable.

All pure-component properties were obtained from Liley et al. (1997), except where unavailable, in which case they were obtained from Aspen Plus (Aspen Technology, Inc., 2007), along with all of the NRTL parameters. All temperatures (T) are in K.

$$P^{\text{vap}} = \exp\left(C1 + \frac{C2}{T} + C3 \ln T + C4 T^{C5}\right) \quad (\text{E-1})$$

$$\hat{C}_p^{\text{IG}} = C1 + C2\left(\frac{C3/T}{\sinh(C3/T)}\right)^2 + C4\left(\frac{C5/T}{\cosh(C5/T)}\right)^2 \quad (\text{E-2})$$

$$\lambda = C1\left(1 - \frac{T}{C5}\right)^{C2+C3 T/C5+C4 (T/C5)^2} \quad (\text{E-3})$$

The coefficients for these models are given in Table E.1.

In order to maintain thermodynamic consistency, a separate model for liquid heat capacity was not used; instead, it can easily be shown that \hat{C}_p^{liq} is related to the already specified quantities as follows:

$$\hat{C}_p^{\text{liq}} = \hat{C}_p^{\text{IG}} - \frac{d\lambda}{dT} \quad (\text{E-4})$$

Table E.1 Coefficients for pure-component property models for vapour pressure, ideal gas heat capacity, liquid heat capacity, and enthalpy of vaporisation, Eqs (E-1)–(E-3).

Prop.	Component	C1	C2	C3	C4	C5
P^{vap} (Pa)	acetonitrile	58.302	−5385.6	−5.4954	5.3634 E−6	2
	nitromethane	57.278	−6089	−4.9821	1.2154 E−17	6
	benzene	83.918	−6517.7	−9.3453	7.1182 E−6	2
	toluene	80.877	−6902.4	−8.7761	5.8034 E−6	2
	1-heptanal	107.17	−9070.3	−12.503	7.4446 E−6	2
	1-decanal	201.64	−15133	−26.264	1.4625 E−5	2
	<i>n</i> -hexane	104.65	−6995.5	−12.702	1.2381 E−5	2
	<i>n</i> -nonane	109.35	−9030.4	−12.882	7.8544 E−6	2
\hat{C}_p^{IG} (J/mol·K)	acetonitrile	41.91	88.76	1581.80	50.32	699.80
	nitromethane	42.267	108.42	1488.5	68.603	683.57
	benzene	44.42	232.05	1494.60	172.13	−678.15
	toluene	58.14	286.30	1440.60	189.80	−650.43
	1-heptanal	140.40	259.07	831.50	131.20	2201.00
	1-decanal	196.41	514.12	1898.90	412.78	862.51
	<i>n</i> -hexane	104.40	352.30	1694.60	236.90	761.60
	<i>n</i> -nonane	151.75	491.50	1644.80	347.00	749.60
λ (J/mol)	acetonitrile	43511	0.34765	0	0	545.5
	nitromethane	47417	0.3062	0	0	588.15
	benzene	47500	0.45238	0.0534	−0.1181	562.16
	toluene	50144	0.3859	0	0	591.8
	1-heptanal	61299	0.37999	0	0	617.0
	1-decanal	79073	0.4129	0	0	674.2
	<i>n</i> -hexane	44544	0.39002	0	0	507.6
	<i>n</i> -nonane	60370	0.38522	0	0	594.6

For the activity coefficients, the NRTL model (Renon and Prausnitz, 1968) was used, which is expressed as (Aspen Technology, Inc., 2007):

$$\ln \gamma_i = \frac{\sum_{j=1}^N x_j \tau_{ji} G_{ji}}{\sum_{k=1}^N x_k G_{ki}} + \sum_{j=1}^N \frac{x_j G_{ij}}{\sum_{k=1}^N x_k G_{kj}} \left(\tau_{ij} - \frac{\sum_{m=1}^N x_m \tau_{mj} G_{mj}}{\sum_{k=1}^N x_k G_{kj}} \right) \quad (\text{E-5})$$

where

$$G_{ij} = \exp(-c_{ij} \tau_{ij}) \quad (\text{E-6})$$

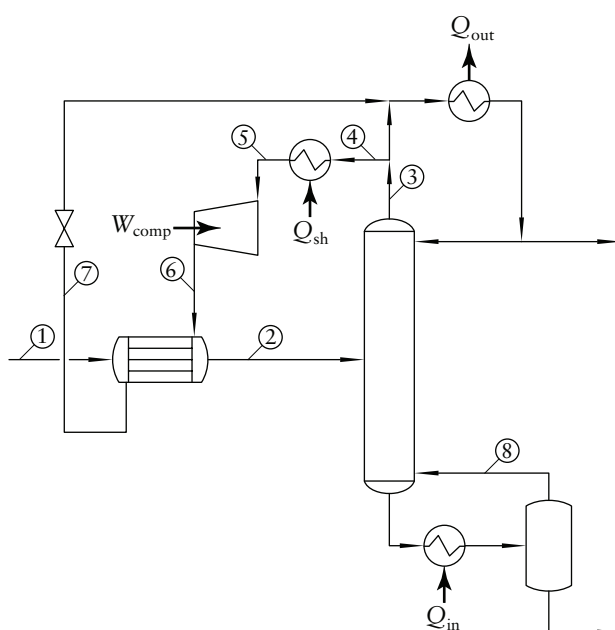
$$G_{ii} = 1 \quad (\text{E-7})$$

$$\tau_{ij} = a_{ij} + \frac{b_{ij}}{T} \quad (\text{E-8})$$

$$\tau_{ii} = 0 \quad (\text{E-9})$$

Table E.2 Binary interaction parameters for the NRTL activity coefficient model.

System	a_{12}	a_{21}	b_{12}	b_{21}	$c_{12} = c_{21}$
benzene (1) toluene (2)	-2.8852	2.1911	1123.9501	-863.7308	0.3
acetonitrile (1) nitromethane (2)	0.2239	-0.0946	31.1015	-75.5778	0.3
1-heptanal (1) 1-decanal (2)	0	0	84.2969	-78.0471	0.3
<i>n</i> -hexane (1) <i>n</i> -nonane (2)	0	0	-222.5504	261.3854	0.3

**Figure E.1** FDVRC configuration with stream labels for relevant streams.

The coefficients for Eqs (E-6)–(E-9) are given in Table E.2. These parameters were obtained from Aspen Plus’s database, or, where unavailable, estimated by means of UNIFAC with Aspen Plus.

E.2 High-level FDVRC equations

Figure E.1 should be used as a reference for the stream numbers that are used in the following derivations.

Heat and work input at reboiler

The feed enters the system as a saturated liquid, which is then vaporised completely. This vaporised feed joins with the vapour rising through the

stripping section to produced the vapour in the rectifying section. Owing to the constant molar overflow (CMO) assumption, the flow rate of the overhead vapour is equal to this sum of vapour feed and vapour from the reboiler, which mathematically amounts to the following:

$$V_3 = F + V_8 \quad (\text{E-10})$$

The column is (theoretically) operated at minimum reflux, which can be estimated using Underwood's method, assuming constant relative volatility. For a binary, saturated vapour feed, separated to pure components, minimum reflux using Underwood's method simplifies to the following (Branan, 2005):

$$r_{\min} = \frac{\alpha}{z_{F,1}(\alpha - 1)} - 1 \quad (\text{E-11})$$

It can be shown through mass balance that:

$$V_3 = Fz_{F,1}(r_{\min} + 1) \quad (\text{E-12})$$

$$V_3 = F\left(\frac{\alpha}{\alpha - 1}\right) \quad (\text{E-13})$$

Therefore, using Eqs (E-10) and (E-13), the following is obtained:

$$V_8 = F\left(\frac{1}{\alpha - 1}\right) \quad (\text{E-14})$$

Thus, the minimum heat input at the reboiler is estimated as follows:

$$Q_{\text{in,min}} = \lambda V_8 \quad (\text{E-15})$$

$$Q_{\text{in,min}} = F\lambda\left(\frac{1}{\alpha - 1}\right) \quad (\text{E-16})$$

Heat and work input at compressor and superheater

The energy input at the compressor and superheater is a somewhat more complex consideration than in the reboiler.

The feed enters the system at T_1 , which is its bubble point. In the heat exchanger, the feed is vaporised fully to its dew point, T_2 . This dew point can be estimated using only the relative volatility and pure-component boiling points by means of the following equation (see Chapter 7):

$$T_2 = \left[\left(\frac{\frac{1}{T_{b,2}} - \frac{1}{T_{b,1}}}{\ln(\alpha^{1.206})} \right) \ln(z_{F,1} + \alpha^{1.206}(1 - z_{F,1})) + \frac{1}{T_{b,1}} \right]^{-1} \quad (\text{E-17})$$

The compressor and superheater must be considered together, since their operation is linked. First, the minimum compression ratio must be determined. In the limit of operation, the condensing temperature of the vapour leaving the compressor, T_6 , should be equal to T_2 ; no heat transfer can take place if $T_6 < T_2$. An easy way of estimating this with rudimentary information is using the Clausius–Clapeyron equation:

$$P_6 = P_0 \exp \left[\frac{\lambda}{R} \left(\frac{1}{T_{b,1}} - \frac{1}{T_6} \right) \right] \quad (\text{E-18})$$

Since $T_6 = T_2$, the former can be estimated from Eq. (E-17).

The minimum degrees of superheating prior to compression, ΔT , can be estimated using the following equation (Felbab, 2013), which ensures that the outlet of the compressor is a saturated vapour (i.e. at the lowest possible temperature before it condenses):

$$\Delta T = \max \left\{ \frac{T_{b,1} \left[\frac{v}{\lambda - v} + \sigma \right]}{1 - \sigma}, 0 \right\} \quad (\text{E-19})$$

where

$$v = RT_{b,1} \ln \left(\frac{P_6}{P_0} \right) \quad (\text{E-20})$$

$$\sigma = 1 - \left(\frac{P_6}{P_0} \right)^{R/\hat{C}_{p,1}^{\text{IG}}} \quad (\text{E-21})$$

If $\Delta T = 0$ K, it means that no superheating is required, and as such, $Q_{\text{sh}} = 0$ W. In this case, the compression is merely an isentropic compression from $T_4 (= T_{b,1})$ and P_0 to T_6 and P_6 . The compression work required for this is calculated for this isentropic compression of an ideal gas with constant \hat{C}_p^{IG} as follows:

$$W_{\text{comp}} = V_4 \hat{C}_{p,1}^{\text{IG}} T_{b,1} \left(\left(\frac{P_6}{P_0} \right)^{\hat{C}_{p,1}^{\text{IG}}/R} - 1 \right) \quad (\text{E-22})$$

If it is assumed that λ is constant throughout the system, as per the CMO assumption, then to vaporise F completely, the required energy input to the feed stream is λF . Since λ is constant, and the energy input for vaporisation is provided by condensing the compressed vapour, it follows that $V_4 = F$. Thus, using this fact, and substituting Eq. (E-18) into Eq. (E-22), the energy/work

input into the compressor, when no superheating is required, is:

$$W_{\text{comp,min}} = F \hat{C}_{p,1}^{\text{IG}} T_{b,1} \left(\left(\exp \left[\frac{\lambda}{R} \left(\frac{1}{T_{b,1}} - \frac{1}{T_6} \right) \right] \right)^{\hat{C}_{p,1}^{\text{IG}}/R} - 1 \right) \quad (\text{E-23})$$

However, if $\Delta T > 0$ K, then the superheater is required. Therefore, since the diverted overhead vapour has a flow rate equal to F , and the superheater heats the vapour by ΔT , the heat input is simply:

$$Q_{\text{sh,min}} = F \hat{C}_{p,1}^{\text{IG}} \Delta T \quad (\text{E-24})$$

Using Eq. (6.5), the virtual work associated with $Q_{\text{sh,min}}$ is estimated by the following equation:

$$W_{\text{sh,min}} = F \hat{C}_{p,1}^{\text{IG}} \Delta T \left(1 - \frac{T_0}{T_{b,1} + \Delta T} \right) \quad (\text{E-25})$$

Finally, the energy/work input to the compressor is calculated using an energy balance. In cases where superheating is required, the minimum compression results in a saturated vapour outlet, as mentioned earlier. Since the limit of operation in the heat exchanger is being considered, this compressor outlet is at T_2 , and the inlet temperature must be at $T_{b,1} + \Delta T$. Thus, the minimum work input in the compressor is:

$$W_{\text{comp,min}} = F \hat{C}_{p,1}^{\text{IG}} (T_2 - T_{b,1} - \Delta T) \quad (\text{E-26})$$

E.3 Aspen Plus simulation settings

The following settings were selected in the Aspen Plus simulations. The nomenclature for the conventional column and the SVRC can be found in Figures 5.12 and 5.13, respectively.

Example 1

F1/F2/F3: 100 kPa; bubble point; 1 kmol/h; 0.85 1-heptanal, 0.15 1-decanal.

C1/C2: no condenser; no reboiler; 12 stages; F1/F2 on stage 6; VB1/VB2 on stage 12; RFL1/RFL2 on stage 1; 100 kPa column pressure.

CON1: bubble point; zero pressure drop.

SPL1/SPL2: fractionally 0.264667 of LT1/LT2 sent to RFL1/RFL2.

REB1: vapour fraction 0.874381; zero pressure drop.

HEX1: cold stream outlet vapour fraction 0.874381; zero pressure drop; 5 K temperature approach.

V1/V2/V3: zero heat duty; zero pressure drop.

SH1: zero pressure drop; 65 K temperature change.

K1: discharge pressure 456.282 kPa; isentropic efficiency 0.85.

SC1: zero pressure drop; heat duty -7137.0784 W.

PV1: adiabatic; outlet pressure 100 kPa.

C3: 12 stages; F3B on stage 7; VB3 on stage 12; RFL3 on stage 1; no condenser; no reboiler; 100 kPa column pressure.

HEX2: cold stream outlet at dew point; zero pressure drop; 5 K temperature approach.

SPL3: fractionally 0.67 of VT6 to VT7;

SH2: zero pressure drop; 14 K temperature change.

K2: 155 kPa discharge pressure; isentropic efficiency 0.85.

PV2: 100 kPa outlet pressure.

CON2: zero pressure drop; bubble point.

SPL4: fractionally 0.404716 of LT5 to RFL3.

REB2: zero pressure drop; vapour fraction 0.804686.

Example 2

F1/F2/F4: 100 kPa; bubble point; 1 kmol/h; 0.09 benzene, 0.91 toluene.

C1/C2: 18 stages; F1/F2 on stage 12; VB1/VB2 on stage 18; RFL1/RFL2 on stage 1; no condenser; no reboiler; 100 kPa column pressure.

CON1/CON3/CON4: bubble point; zero pressure drop.

SPL1/SPL2: fractionally 0.967859 of LT1/LB6 to RFL1/RFL2.

REB1: vapour fraction 0.628033; zero pressure drop.

HEX1: cold stream outlet vapour fraction 0.628033; zero pressure drop; 5 K temperature approach.

V1/V2/V4: zero heat duty; zero pressure drop.

SH1: 6 K temperature change; zero pressure drop.

K1: 266.851 kPa discharge pressure; 0.85 isentropic efficiency.

SC1: zero pressure drop; heat duty -12320.387 W.

PV1: adiabatic; 100 kPa outlet pressure.

SPL4: all of F4 to F5.

SH3: 45 K temperature change; zero pressure drop.

K3: 130 kPa discharge pressure; 0.85 isentropic efficiency.

HEX3: cold stream outlet vapour fraction 0.562124; approach temperature 5 K; zero pressure drop.

PV3: adiabatic; 100 kPa outlet pressure.

C4: 22 stages; F12 on stage 14; RFL4 on stage 1; VB4 on stage 22; no condenser; no reboiler; 100 kPa column pressure.

SPL5: fractionally 0.931042 of LT6 to RFL4.

Example 3

F1/F2/F3: 100 kPa; bubble point; 1 kmol/h; 0.89 water, 0.03 monoethanolamine, 0.08 diethylene glycol.

C1/C2: no condenser; no reboiler; 30 stages; F1/F2 on stage 20; VB1/VB2 on stage 30; RFL1/RFL2 on stage 1; 100 kPa.

CON1: bubble point; zero pressure drop.

SPL1/SPL2: fractionally 0.10207 of LT1/LT2 sent to RFL1/RFL2.

REB1: vapour fraction 0.87077535; zero pressure drop.

HEX1: cold stream outlet vapour fraction 0.87077535; zero pressure drop; 5 K temperature approach.

V1/V2/V3: zero heat duty; zero pressure drop.

SH1: zero pressure drop; 0 K temperature change.

K1: discharge pressure 2353.259 kPa; isentropic efficiency 0.85.

SC1: zero pressure drop; heat duty -3753.3505 W.

PV1: adiabatic; outlet pressure 100 kPa.

C3: 15 stages; F3B on stage 9; VB3 on stage 15; RFL3 on stage 1; no condenser; no reboiler; 100 kPa column pressure.

HEX2: cold stream outlet at dew point; zero pressure drop; 5 K temperature approach.

SPL3: all of VT6 to VT7;

SH2: zero pressure drop; 47 K temperature change.

K2: 350 kPa discharge pressure; isentropic efficiency 0.85.

PV2: 100 kPa outlet pressure.

CON2: zero pressure drop; bubble point.

SPL4: fractionally 0.3157 of LT5 to RFL3.

REB2: zero pressure drop; vapour fraction 0.57757286.

Example 4

F1/F2/F4: 100 kPa; bubble point; 1 kmol/h; 0.05 *n*-pentane, 0.05 *n*-hexane, 0.90 *n*-heptane.

C1/C2: 23 stages; F1/F2 on stage 8; VB1/VB2 on stage 23; RFL1/RFL2 on stage 1; no condenser; no reboiler; 100 kPa column pressure.

CON1/CON3/CON4: bubble point; zero pressure drop.

SPL1/SPL2: fractionally 0.9623848 of LT1/LB6 to RFL1/RFL2.

REB1: vapour fraction 0.589; zero pressure drop.

HEX1: cold stream outlet vapour fraction 0.589; zero pressure drop; 5 K temperature approach.

V1/V2/V4: zero heat duty; zero pressure drop.

SH1: 21 K temperature change; zero pressure drop.

K1: 420.0 kPa discharge pressure; 0.85 isentropic efficiency.

SC1: zero pressure drop; heat duty -14413.671 W.

PV1: adiabatic; 100 kPa outlet pressure.

SPL4: all of F4 to F5.

SH3: 20 K temperature change; zero pressure drop.

K3: 135.0 kPa discharge pressure; 0.85 isentropic efficiency.

HEX3: cold stream outlet vapour fraction 0.53153456; approach temperature 5 K; zero pressure drop.

PV3: adiabatic; 100 kPa outlet pressure.

C4: 25 stages; F12 on stage 8; RFL4 on stage 1; VB4 on stage 25; no condenser; no reboiler; 100 kPa column pressure.

SPL5: fractionally 0.91212059 of LT6 to RFL4.